

Synthesis and Evaluation of Lung Tissue Retentive Prodrugs



The University of
Nottingham

UNITED KINGDOM • CHINA • MALAYSIA



Jack Raymond Ayre

MChem

Thesis submitted to the University of Nottingham
for the degree of Doctor of Philosophy

December 2021

Acknowledgements

I would firstly like to thank my family, for without their continued support throughout my education none of this would have been possible. From an early age I showed an interest in science and I want to thank you for your encouragement to grow into the person (and scientist) that I am today.

Studying away from home, none of the incredible experiences I have had throughout my 8 years at university would have been possible without the greatest set of friends imaginable. From my 'Sheffield friends' with whom I took my first steps as a chemist, to my 'Nottingham friends' who made my postgraduate just as enjoyable, I am so grateful for the experiences we have shared. I would also like to thank my housemates throughout my time at Nottingham, in particular Ryan Cairns, Joe Andrews, Josh Drewitt and Ryan Gangloff.

I would like to thank all members of C30 lab and C floor corridor past and present for enabling a fun and enjoyable place to work. In particular Ruiling Liu, Scott Grossman, Matt Allison, Eleonora Comeo, Bianca Casella, and Dr. Aimie Garces for their support and friendship over the years. In addition, I would like to thank Paulyna Magaña Gomez for her help with the confocal microscopy.

Next, I must thank my colleagues and friends at GSK, in particular Laura Thomlinson, James Wood, Molly Harrison and David Fallon for the incredible help I received

during my placement at GSK. My placement at GSK would not have been enjoyable if it wasn't for incredible 'IP friends' with whom I can't wait to share more memories with.

I would next like to thank my supervisors Prof. Michael Stocks, Prof. Cynthia Bosquillon and Dr. Jo Redmond for their incredible support and mentorship during my PhD. It is definitely true that without your wisdom and kindness, none of this would have been possible or enjoyable.

Finally, I must thank the University of Nottingham, the School of Pharmacy, the EPSRC and GSK, for their support and funding throughout my PhD.

COVID 19 Impact Statement:

Due to the events of the 2020 COVID-19 global respiratory pandemic the research in this thesis was significantly affected. In particular, 6 months of research time was lost due to closure of the university during the nationwide lockdown. In-addition, implementation of working rotas/shift patterns to minimise transmission of the virus resulted in a further staggered loss of 3 months of research time.

The following is a list of alterations to the intended research program in response to COVID-19.

Chapter 1: Prior to the events of the pandemic, GSK had committed to perform a full scale *in-vivo* PK study on the two most promising candidates from chapter 1, alongside the original drug candidate. This would have allowed for the generation of drug and prodrug concentration data in both the lung and blood, at multiple time points. Unfortunately, despite funding this research, the project was deemed ‘Non-essential’ and GSK was unable to perform any PK analysis. Ultimately, the research was dramatically scaled down and performed by an external company across multiple studies, which, due to funding difficulties, lead to a drastic reduction in the research results and quality. In addition, it was not possible to determine the potency of the chosen drug molecule or final prodrug which entered the PK study and thus use of the phrase ‘inactive prodrug’ is assumed.

Chapter 2: Due to synthetic difficulties and reduced research time, chapter 2 was terminated early. Prior to the pandemic, it was agreed that a second DMPK industrial placement at GSK would take place based on the development of intracellular PI3K prodrugs. Unfortunately, GSK was unable to accommodate for a second placement due to the ongoing COVID restrictions, and thus the decision to close the chapter early was taken, due to the unobtainability of DMPK data for any compounds produced. Due to the dramatic loss of time, the opportunity to undertake any mechanistic studies within cells was also lost.

Chapter 3: Due to the dramatic loss of time, chapter 3 was heavily reduced. Chapter 3 was intended to be a collaboration with fellow student, Paulyna Magaña Gomez, focussing on the confocal microscopy of a range of dibasic fluorescent probes. This work would have incorporated several iterations of chemical synthesis followed by subsequent confocal microscopy. In addition, a series of cellular assays were intended to investigate the transporter protein substrate potential of the synthesised probes. Unfortunately, only one round of synthesis and subsequent confocal microscopy was achieved, in a heavily reduced manner to that what was intended.

Abstract

In the time of a global respiratory pandemic, there has never been a more pertinent time to improve the current medications responsible for relieving the symptoms of respiratory diseases such as COPD and Asthma. Administration of drugs directly to the site of action through the pulmonary drug delivery route can give significant benefits over other traditional routes of administration i.e. oral. Avoidance of first pass metabolism in the liver, reduced drug dosage and significant reduction of compound exposure to other organs, ultimately leading to fewer side effects, are all benefits of the pulmonary delivery route. However, rapid drug elimination from lung tissue into the pulmonary vein, combined with the pan antagonistic nature of receptor antagonists and heavy presence of muscarinic receptors in other tissues, often leads to increased side effects in other organs, such as the heart.

Aims: The aim of this thesis was to design and evaluate a novel, self-activating, dibasic prodrug system as a possible method of achieving sustained delivery post inhalation. Evaluation of the method of increased lung tissue retention would then be explored using confocal microscopy to probe the lysosomal trapping potential of dibasic compounds. This system, if successful would represent a remarkable achievement in that the prodrug design could be developed to suit a wide range of chemical structures, and thus has the potential improve the inhaled PK profile of a wide variety of inhaled pharmaceuticals and thus massively expedite the development of novel-long acting treatments.

Chapter 1: Outlines the advantages of inhaled administration as a route for targeted drug delivery. In addition, it details the common mechanisms for achieving sustained drug delivery to the lung, alongside describing the pertinent need for new long acting muscarinic receptor antagonists in order to improve the current prevention and treatment of breathing difficulties in COPD and asthmatic patients.

Chapter 2: Describes the use of prodrug systems as mechanisms for improving drug delivery. In addition, it follows the development and implementation of a novel cleavable prodrug system from initial design stages, through to final *in-vivo* PK studies, as a method of efficaciously delivering an active muscarinic agent over a sustained period in attempt to increase the duration of action of an existing muscarinic receptor drug. It outlines the discovery of compound **24** as a novel, dibasic, pH-sensitive, self-cleaving, muscarinic prodrug capable of withstanding enzymatic cleavage in order to liberate an active muscarinic receptor antagonist at a sustained rate over 24 hours. The subsequent *in-vivo* pharmacokinetic studies demonstrate that when inhaled independently, over 99% of the active drug was eliminated from the lung tissue within 3 hours, but when delivered as a prodrug, sustained prodrug activation meant that the drug was present in the lung at a pharmaceutically relevant concentration for over 24 hours, with no detected exposure of the drug to blood plasma.

Chapter 3: Develops further the prodrug system introduced in chapter 1, this time focusing on an intracellular PI3K δ target. It follows an attempt to improve an intermediate drug candidate which suffered from poor physiochemical properties and

thus did not progress to clinical trials. Included is the design and attempted synthesis of a series of prodrugs, which based on the results of chapter 1, would be interesting candidates for an *in-vivo* PK study to determine their duration of action relative to the parent drug candidates, and thus feasibility as sustained release delivery agents.

Chapter 4: Investigates how the dibasic moiety of the prodrug design affects the distribution of the prodrug in lung tissue. By taking a lysosome-targeting fluorescent probe, replacing the functionality responsible for its lysosome targeting nature with the dibasic prodrug moiety, a distribution comparison can be created. This chapter attempted to visualise the effect of incorporating a dibasic moiety into the prodrug design on the distribution and organelle sequestration.

Conclusion: A dibasic, self-activating prodrug (**Compound 24**) has been created which displays a much-increased lung tissue retention relative to the parent drug (**Compound 1**). Post intratracheal dosing, sustained release of **1** from **24** resulted in a high, pharmaceutically relevant concentration of **1** in the lung tissue for over 24 hours all from a single dose. Thus, the unique approach of using a prodrug system which incorporates lung tissue retentive chemical moieties to extend the lung residency time of a muscarinic antagonist has been successful. Further studies will determine whether an extended pharmacodynamic response has also been achieved and will help to elucidate the mechanism of lung retention.

Table of Contents

Acknowledgements	3
Abstract	7
Table of Contents.....	10
List of Abbreviations	14
1. Introduction	16
1.1 The Pulmonary Drug Delivery Route	17
1.1.1 Structure of the Lungs	17
1.1.2 Drug Administration via the Pulmonary System	20
1.1.2.1 Drug Administration Devices	20
1.1.2.2 Drug Absorption Post Inhalation	22
1.1.2.2.1 Membrane Transport Systems	23
1.1.2.2.1.1 Organic Cationic Transporters	24
1.1.2.2.1.2 Peptide Transporters.....	24
1.1.3 Limitations of Pulmonary Drug Delivery	26
1.1.3.1 Characterising Lung Retention	28
1.1.3.2 Strategies for Improving Lung Retention	29
1.1.3.2.1 Improving Non-Specific Binding.....	30
1.1.3.2.2 Optimising Basicity.....	32
1.1.3.2.2.1 Lysosomal Trapping.....	34
1.1.3.2.2.2 Mechanism of Lysosomal Trapping.....	35
1.1.3.2.3 Optimising Lipophilicity.....	36
1.1.3.2.4 PEG linkers	42
1.1.3.2.5 Organic Ion-Pairing.....	43
1.1.3.2.6 Inorganic Ion Coupling	44
1.1.3.2.7 Drug Carriers.....	45
1.1.3.2.8 Insolubility	46
1.2 Chronic Obstructive Pulmonary Disease and Asthma	47
1.2.1 COPD and Asthma Treatment.....	48
1.2.1.1 β_2 Adrenoceptors	48
1.2.1.2 Anticholinergics.....	52
1.2.1.2.1 Development of New Long-Acting Anticholinergics.....	55
1.2.1.3 Theophylline	56
1.2.1.4 Glucocorticoids.....	57
1.3 Background Work Supporting this Thesis	58

Thesis Aims and Objectives	62
2. Design and Synthesis of Novel Muscarinic Receptor Antagonist Prodrugs...	63
2.1 Introduction.....	64
2.1.1 Prodrug Techniques.....	64
2.1.2 Prodrug Design.....	64
2.1.2.1 Administration	65
2.1.2.2 Permeability	65
2.1.2.3 Distribution	67
2.1.2.4 Metabolism	68
2.1.3 Sustained Release Prodrug Systems.....	68
2.1.4 Prodrug application to inhaled administration	71
2.2 Aims.....	75
2.3 Results and Discussion.....	76
2.3.1 Design and Synthesis of Prodrug Scaffold.....	76
2.3.1.1 Muscarinic Drug Selection	76
2.3.1.2 Linker Group Design	79
2.3.1.3 Dibasic Amino Acid Design.....	82
2.3.1.3.1 Potential Prodrug Cleavage Mechanism	82
2.3.2 Synthesis and Evaluation of Monobasic Prodrugs	84
2.3.2.1 Amine Position	85
2.3.2.1.1 Monobasic Prodrug Cleavage Mechanism	86
2.3.2.2 Amine Alkylation	88
2.3.2.3 C-1 Substitution.....	90
2.3.3 Synthesis and Evaluation of Dibasic Prodrugs.....	91
2.3.3.1 Biological Evaluation:	93
2.3.3.1.1 Phosphate Buffer Solution Stability Determination:	93
2.3.3.1.2 Rat Lung Homogenate Stability Determination:	96
2.3.3.1.3 Enzymatic Cleavage Pathway	97
2.3.3.1.4 Rat Blood Stability Determination:.....	100
2.3.3.1.5 Binding Determination.....	101
2.3.3.1.6 Pharmacokinetic Studies – Performed by Signature Discoveries	102
2.3.3.1.6.1 Pharmacokinetic Study Design – Drug (1).....	103
2.3.3.1.6.2 Pharmacokinetic Study Results – Drug (1)	103
2.3.3.1.6.3 Pharmacokinetic Study Design – Prodrug (24).....	104
2.3.3.1.6.4 Pharmacokinetic Study Results – Prodrug (24)	104

2.3.3.1.6.5 Limitations of the Pharmacokinetic Studies.....	106
2.3.3.1.6.6 Conclusions and Future Work Based on the Pharmacokinetic Studies	106
2.4 Chapter Conclusion	112
2.5 Future Work.....	114
3. Design and Synthesis of Novel PI3K Prodrugs	116
3.1 Introduction.....	117
3.1.1 Phosphoinositide 3-kinase	117
3.1.1.1 Class I PI3Ks	117
3.1.2 PI3K Inhibition.....	119
3.1.3 PI3K Involvement in COPD Treatment	121
3.1.3 Development of Nemiralisib and GSK22927675	123
3.2 Aims.....	130
3.3 Results and Discussion.....	131
3.3.1 PI3K Prodrug Design	131
3.3.2 Model Cleavage Studies	133
3.3.3 Prodrug Synthesis.....	135
3.3.4 Synthesis of Compound E	136
3.3.5 Identification of New Drug Candidates.....	143
3.3.6. Discovery of Compound F	143
3.3.7. Synthesis of Compound G.....	146
3.3.7.1 Route Optimisation	148
3.3.8. Synthesis of Compound G Prodrugs	150
3.3.9. Identification of Pictilisib	152
3.3.10 Synthesis of Pictilisib	153
3.3.11 Synthesis of Pictilisib Prodrugs.....	153
3.4 Reflections from Failed Prodrug Synthesis	154
3.5 Chapter Conclusion	156
3.6 Future Work.....	158
4. Quantification of the Lysosomal Trapping Potential of Dibasic Prodrugs ..	160
4.1 Introduction.....	161
4.1.1 Lysosomal Trapping of Basic Drugs.....	161
4.1.2 Predicting/Quantifying Lysosomal Uptake/Trapping	162
4.1.3 Lysosome Visualisation using Fluorescence Microscopy.....	165
4.1.4 Intracellular Ion Concentration Monitoring	167
4.1.4.1 Development of 1,8-Naphthalimide Probes	167

4.1.4.3 Development of Lyso-NHS	168
4.1.4.2 1,8-Napthalimide Probes Design	169
4.1.5 Application of Lyso-NHS to Lysosome Visualisation.....	171
4.2 Aims.....	172
4.3 Results and Discussion.....	173
4.3.1 Experimental Lysosomotropism Determination	173
4.3.2 Adaptation of the 1,8-Napthalimide Probe.....	174
4.3.3 Fluorescent Probe Synthesis.....	175
4.3.2.1 Fluorescent Probe Prodrug Stability.....	178
4.3.4 Fluorescent Probe Prodrug Characterisation	178
4.3.3.1 pH Dependent Fluorescence	179
4.3.3.3 Confocal Microscopy – Performed by Paulyna Magaña Gomez	181
4.4 Chapter Conclusion	187
4.5 Future Work.....	188
5. Discussion	190
6. Experimental.....	196
Preamble	197
5.1 Chapter 1	209
5.2 Chapter 2	276
5.3 Chapter 3	329
7. Appendix.....	344
7.1 Structural characterization of compound 1.....	345
7.2 Structural characterization of compound 24.....	347
7.3 Structural characterization of compound 95.....	350
7.4 Structural characterization of compound 102.....	352
8. References.....	354

List of Abbreviations

AcOH – Acetic Acid	EtOAc – Ethyl Acetate
AcOK – Potassium Acetate	EtOH - Ethanol
ADHD – Attention Deficit Hyperactivity Disorder	FDA – Food and Drug Administration
ADME – Absorption, Distribution, Metabolism, Elimination	GPCR – G-Protein Coupled Receptor
ASDT – Apical Sodium-Dependent Bile Acid Transporter	H ₂ O – Water
ATP – Adenosine Triphosphate	HATU - Hexafluorophosphate Azabenzotriazole Tetramethyl Uronium
β ₂ – Beta 2 Adrenoceptor	HCl – Hydrochloric Acid
bd – Broad Doublet	hERG - human Ether-à-go-go-Related Gene
BEP – 2-Bromo-1-ethyl Pyridinium Tetrafluoroborate	HPLC – High Performance Liquid Chromatography
Boc ₂ O – Di-tert-butyl dicarbonate	Hr – Hour
Bs – Broad Singlet	ITPK – Intratracheal Pharmacokinetic
cAMP – Cyclic Adenosine Monophosphate	LABA – Long Acting β ₂ Adrenoceptor Agonists
CCR5 – C-C Chemokine Receptor	LAMA – Long Acting Muscarinic receptor antagonists
COPD – Chronic Obstructive Pulmonary Disease	LCMS – Liquid Chromatography Mass Spectrometry
d - Doublet	LDX – Lisdexamfetamine
D ₂ – Dopamine Receptor	LLOQ – Lower Level of Quantification
DCM - Dichloromethane	M ₃ – Muscarinic M ₃ Receptor
dd – Doublet of Doublets	MDI – Metered Dose Inhaler
DIPEA – Diisopropylethylamine	MeCN - Acetonitrile
DKP – Diketopiperazine	MeSO ₂ Cl – Methane Sulfonyl Chloride
DMAP – Dimethylaminopyridine	MWt – Molecular Weight
DMF – Dimethylformamide	NGP – Neighbouring Group Participation
DPI – Dry Powder Inhaler	
DPP4 – Dipeptidyl Peptidase	
dt – Doublet of Triplets	

NMI – N-Methyl Imidazole	q – Quartet
NMR – Nuclear Magnetic Resonance	QSAR – Quantitative Structure Activity Relationship
OCT – Organic Cation Transporter	S – Singlet
PBS – Phosphate Buffer Solution	SABA – Short Acting β 2 Agonist
PD – Pharmacodynamic	SAMA – Short Acting Muscarinic receptor antagonist
PEPT – Peptide Transporter	SLC – Solute Carrier
PI – Inorganic Phosphate	t - Triplet
PI3K – Phosphoinositide 3-kinase	THF – Tetrahydrofuran
PK – Pharmacokinetic	Tol – Toluene
Py – Pyridine	

1. Introduction

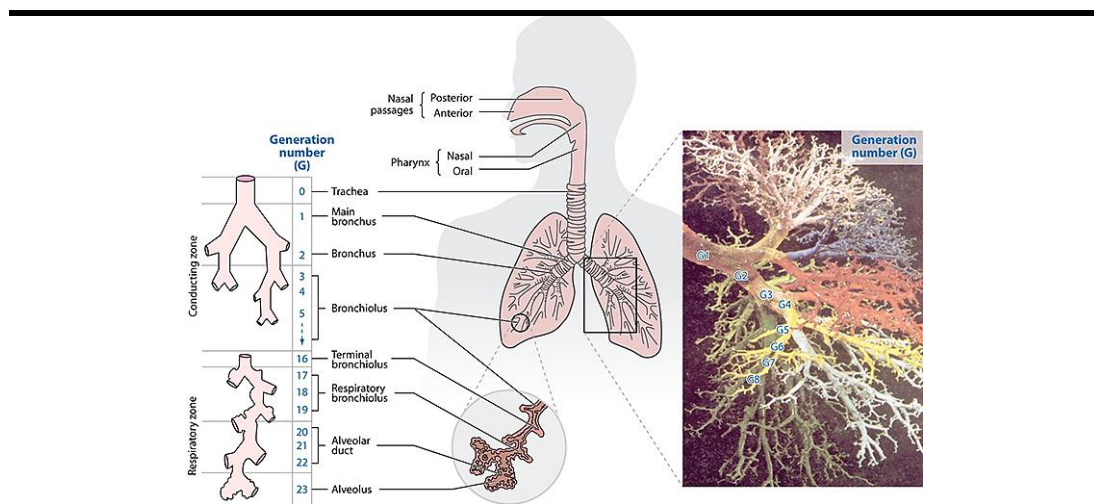
1.1 The Pulmonary Drug Delivery Route

From ancient hieroglyphs depicting the Egyptians inhaling ‘medicinal vapours’ around 3500 years ago¹; the introduction of the first metered dose inhaler in 1956,² or the revolutionary development of the first inhaled insulin treatment, *Exubera*, in 2006,³ the pharmaceutical industry has seen a significant growth in the interest of drug administration *via* pulmonary delivery route. The lungs have become an increasingly attractive organ for drug administration and thus the pulmonary delivery route is now widely regarded as the most efficient method of treatment for diseases such as chronic obstructive pulmonary disease (COPD), asthma and respiratory tract infections.

1.1.1 Structure of the Lungs

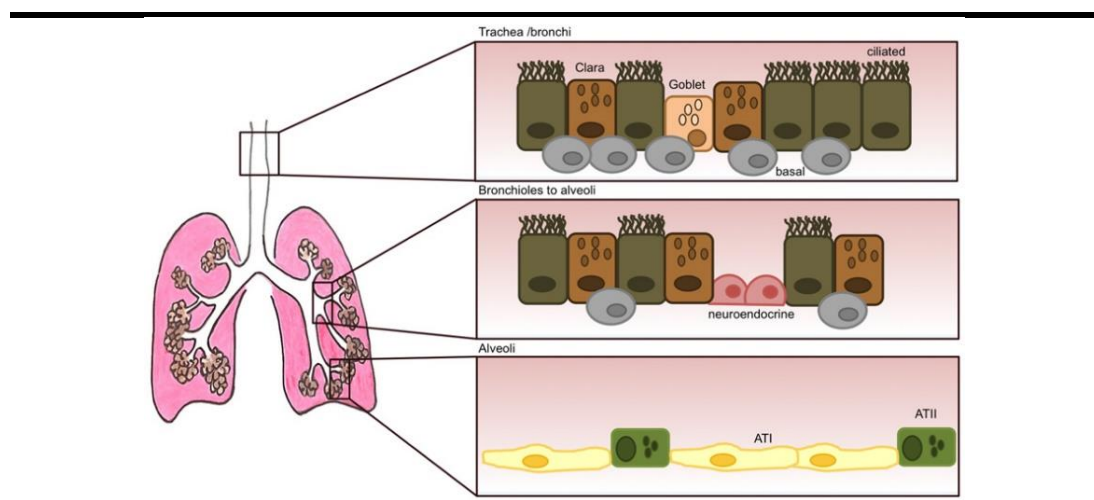
The airways are comprised of the trachea, bronchi and bronchioles which form a complex tree-like structure reducing in size until reaching the sac-like alveoli which act as a vast gaseous exchange surface, much like that of the leaves on a tree.¹ As the airway size decreases, the surface area increases greatly, with the alveoli having a surface of over 100m².⁴ This huge exchange surface allows for the rapid exchange of gas molecules during respiration and when targeted during drug administration, leads to the rapid absorption of drug molecules resulting in a quick, high drug concentration in the surrounding tissue.

Figure 1: Structure of Mammalian Lungs, Taken from Feng *et al*⁵



In order to enter systemic circulation, gases during respiration or drug formulations inhaled during drug administration must first cross the lung epithelium. Epithelium acts as the main barrier between the internal and external environment of the body, and as the lung is traversed, epithelial cell type differs greatly with each tissue, (**Figure 2**).

Figure 2: Epithelium Composition Throughout the Lungs, Taken from Camelo *et al*⁶



The trachea and large bronchi are lined with a pseudostratified array of columnar cells, predominantly ciliated cells which are interspersed with goblet and undifferentiated

basal cells.⁷ The main functions of these cells are to transport air to the gaseous exchange surface in the alveoli, and to protect the lungs from debris during inhalation. The goblet cells secrete a thick substance called mucus, which consists of negatively charged mucins and inorganic salts suspended in water.⁸ Mucus traps any debris particulates which enter the lung during inhalation and then ciliated cells direct the mucus up the trachea where it is then swallowed and eliminated.⁹ The small bronchi and bronchioles largely consist of a cuboidal array of ciliated cells and club cells (Clara cells) which metabolise toxic compounds inhaled during respiration such as hydrocarbons, naphthalene, and components of tobacco smoke: a particular problem in eastern cities, in which a high percentage of the population smoke.¹⁰ Finally, the squamous epithelium of the alveoli consists of type I cells (ATI) which facilitate gaseous exchange and cuboidal type II cells (ATII) which secrete pulmonary surfactant.¹¹

Both the airways and alveoli have lung lining fluids in order to help aid the function of the epithelium. The upper airways have a biphasic, viscoelastic mucus layer which consists of water and mucin produced by goblet cells, which acts a preventative barrier for inhaled particulates.¹² The alveoli contains a layer of isotonic fluid containing mainly macrophages with low levels of plasma proteins approximately (10%).¹³ It is coated by the lung surfactant secreted by type II pneumocytes which acts as a solubilising agent for small particulates which arrive at the alveoli, with any insoluble particles such as silica, viruses or asbestos being engulfed and destroyed by macrophages, protecting the integrity of the gaseous exchange surface.^{11,14} In addition, by lowering the surface tension of the alveoli, the lung surfactant prevents the alveoli from collapsing during respiration.^{15,16}

1.1.2 Drug Administration via the Pulmonary System

Drug delivery *via* the pulmonary system is the administration of aerosolized drug molecules to the lower airways *via* inhalation through the nose or mouth. Depending on the treatment, administration takes place using one of three devices: nebulisers, pressurised metered dose inhalers (pMDI) or dry powder inhalers (DPI).

1.1.2.1 Drug Administration Devices

One of the main problems with drug administration via inhalation is the improper use of the delivery device by the patient, due to poor training. Nebulisers use compressed air or ultrasound to deliver an aqueous drug solution/suspension aerosolised into 1-5 μM droplets. Due to the cumbersome equipment and noise generated, are commonly used by elderly and immobile patients, who would otherwise have difficulties using an inhaler.¹⁷ pMDI's are pressurised gaseous formulations of a drug delivered as an aerosol through gas evaporation, and are the most common form of delivery device. They deliver approximately 20-100 μL per actuation and rely on good patient coordination between device activation and inhalation to achieve an appropriate dose.² DPI's deliver a dry powder drug formulation, aerosolised by patient inhalation into 1-5 μm particles.¹⁸ These devices rely less on a patient's ability to coordinate breathing alongside device activation, and tend to have greater chemical stability of the solid formulation.¹⁹ In general, drug administration via any of these devices is still relatively poor, with only 20% of the administered dose being deposited in the lungs.²⁰ This is due to high deposition of the drug in the oro-pharynx which leads to a large portion of the dose (circa 80%) being swallowed instead of inhaled. If the drug has any oral bioavailability then this presents further issues in relation to observed side effects.²¹

Once successfully administered to the lungs via one of the above devices, a drug molecule must then embark on a complex journey through the lungs and relevant tissues in order to reach its biological target. Depending on the location of the receptors required for a pharmacological response, different drugs require different areas of the lungs to be targeted. As previously mentioned, the differing cell epithelial types alongside the presence of lung lining fluids, and the reducing size of the lung regions presents a challenge for drug administration. In order for an inhaled drug to be quickly absorbed into systemic circulation, the ideal target is the lung alveoli where the exchange surface is greatest, lung surfactant is present to help solubilise particulates and where the contact with blood vessels is at its maximum.²² However, the requirement of drug particulates to be $<3\ \mu\text{m}$ in size means that most commonly, the formulated drug molecule is unable to reach the alveoli, and the drug is deposited in the bronchi and bronchioles.²³

Drug administration to the bronchi and bronchioles is not without its own challenges however, depending on the mucus binding potential of a drug, mucociliary clearance could greatly increase the rate of drug elimination from the lung, preventing a high portion of the drug from reaching its biological target.²⁴ In general, the ability of a drug formulation to be successfully delivered to the lung results from a combination of the patient's anatomy, inhalation device and technique and the aerodynamic diameter of the drug particle.

Due to the convoluted structure of the lungs, and the various metabolic and elimination mechanisms present in the lungs, improving the efficacy of drug delivery

relies on having an appreciable understanding of the structure of the lungs and the targeted receptor and indeed incorporating this into the design and formulation of the drug itself.

1.1.2.2 Drug Absorption Post Inhalation

Once inhaled and deposited to the appropriate section of the lung, the drug molecule must then embark on a cellular journey in order to reach its intended target and exhibit a pharmacological response. Usually, the drug molecule will need to be absorbed across the epithelial cell membrane in order to enter the lung tissue, and various mechanisms are present to facilitate this translocation. The lipophilicity ($\log P$) of the drug plays a key role in its ability to penetrate through the cell plasma membrane by simple transcellular diffusion, in which drug molecules passively diffuse into cells following their concentration gradient.²⁵ If a compound's lipophilicity is too high (>5), it is likely the compound will be insoluble in aqueous media and too hydrophobic to cross the cell membrane, if lipophilicity is too low (<1) the compound will be unable to pass through the hydrophobic region of the membrane. For inhaled drugs the desired $\log p$ value is between 1.7-2.5.²⁶ In addition, it is important to also control the $\log D$ value of the compound, as the degree of ionisation will directly affect its ability to cross hydrophobic components of the cell membrane (**Table 1**).

Table 1: Comparison of Lipophilicity with Drug-Like Properties, Taken from Stocks *et al*²⁷

Lipophilicity (Log D _{7.4})	Common Impact on Drug-Like Properties	Common Impact <i>In-vivo</i>
<1	High solubility Low permeability Low metabolism	Low volume of distribution Low absorption and bioavailability Possible renal clearance
1-3	Moderate solubility Moderate permeability Low metabolism	Balanced volume of distribution Potential for good absorption and bioavailability
3-5	Low solubility High permeability Moderate to high metabolism	Variable oral absorption
>5	Poor Solubility High Permeability High Metabolism	Very high volume of distribution Poor oral absorption

Simple transcellular diffusion is not the only option for drug absorption however. Molecules which are unable to permeate the lipid bilayer may enter tissue via paracellular transportation through intercellular junctions, or through transporter mediated processes.

1.1.2.2.1 Membrane Transport Systems

Besides the more common transcellular diffusion of molecules through the plasma membrane into lung tissue, various carrier mediated transport mechanisms occur.²⁸ Several transporter proteins such as organic cationic transporter (OCT)²⁹ and peptide transporter (PEPT)³⁰ have been identified as possible transporters responsible for the active uptake of basic (drug like) molecules into the lung epithelial cells.

1.1.2.2.1.1 Organic Cationic Transporters

Organic cation transporters (OCTs) are membrane-bound solute carrier proteins responsible for the translocation of both endogenous and exogenous cationic substances across the plasma membrane into cells. Owing to their inherent permanent positive charge and resultant hydrophilicity, highly cationic organic molecules are unable to cross the cell membrane *via* passive diffusion.³¹ Instead, mammalian cells have evolved to contain complex transport systems including OCT 1-3 from the solute carrier family SLC 22. These carrier proteins utilise the plasma membrane's permanent negative potential (-40 to -90mV), as generated by diffusional K⁺ ions, to actively uptake electrogenic organic cations. This process allows for OC intracellular concentrations of up to 10-15 times that of extracellular concentrations.³²

Mukherjee *et al* and Koepsell *et al* determined that OCT's are very strongly expressed in lung epithelium, particularly in the case of asthma patients with epithelial damage and thus play a crucial role in cell uptake of organic cations such as drug molecules which are cationic at physiological pH.^{33,34} Whilst there are only a few known OCT substrates, these happen to include formoterol, tiotropium bromide and ipratropium bromide, displaying the associative potential that inhaled bronchodilators can have for OCTs.³⁵

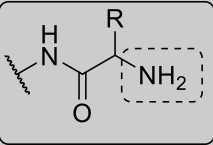
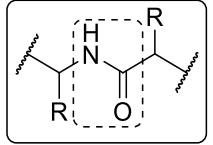
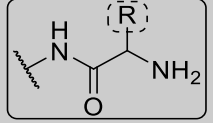
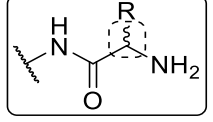
1.1.2.2.1.2 Peptide Transporters

In addition to OCTs, peptide transporters PEPT1 and PEPT2 are proton coupled solute carrier proteins responsible for the facilitated uptake of peptidomimetic substrates including dipeptide and tripeptide species with a broad substrate specificity.^{36,37}

PEPT1 has mainly been located in the intestinal and bile duct tissue and is commonly targeted for use by oral (pro)drugs,³⁸ whilst PEPT2 is highly expressed in the bronchial and tracheal epithelial amongst other tissues.³⁹ PEPT2 possesses an almost 15x higher substrate affinity compared to PEPT1, transporting over 8000 tripeptides and 400 dipeptides. Substrate structures have been highly explored for PEPT2, and several key observations have been made and summarised by Biegel *et al* in 2005 (**Table 2**).⁴⁰

A free α -amino group able to bind to a histidine residue on the peptides recognition site is important for affinity as N/C terminal groups play important roles in recognition of the substrate.⁴¹⁻⁴³ A peptide bond is not essential for substrate recognition as several replacements have been successfully trialled with maintained affinity.⁴⁴ Amino acid side chains with large aromatic groups or bulky hydrophobic groups such as aliphatic chains lead to high PEPT2 affinity.^{45,46} Finally, PEPT2 affinity relies on the 3D structure of the substrate, and it has been observed (although not fully understood) that use of D-chiral amino acids in di/tripeptides and prodrugs leads to a loss of affinity, with the order of affinity in dipeptides being LL>LD>DL>>DD.⁴⁷⁻⁴⁹

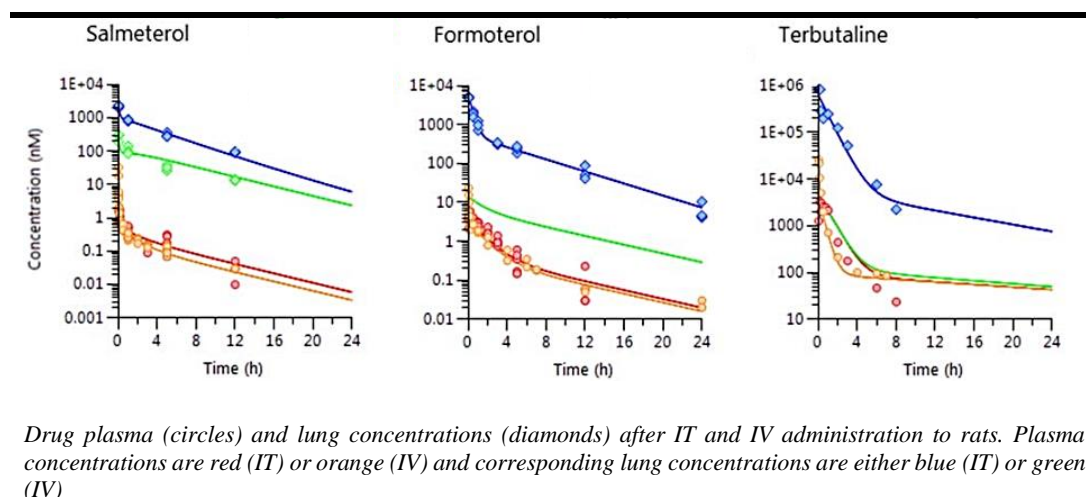
Table 2: Summary of PEPT2 Substrate Requirements

Structural Characteristic	Example	Effect
Free N-Terminus Group		Important for substrate affinity/recognition
Peptide Bond		Not essential for recognition
Amino Acid Side Chain		Bulky/Aromatic R groups have higher substrate affinity
Chirality		Chirality effects 3D structure, altering affinity LL>LD>DL>>DD

1.1.3 Limitations of Pulmonary Drug Delivery

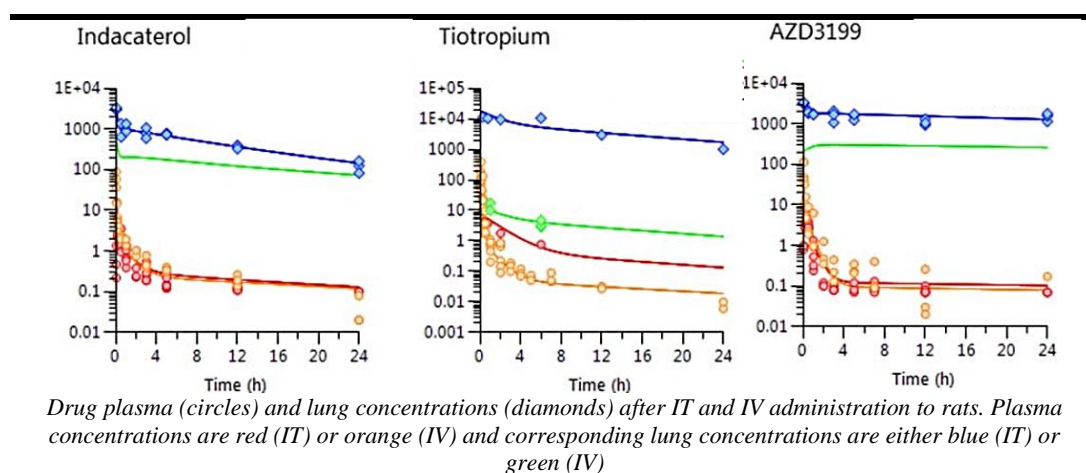
As previously mentioned, current advances in the development of new inhaled therapeutic agents are often stalled due to the lack of pharmacokinetic knowledge of the drug candidate, causing a bottleneck within the drug discovery process. In addition to poor therapy adherence, one pertinent issue with inhaled drug delivery is poor lung retention of the inhaled compound. This mainly arises due to the highly lipophilic nature of inhaled drug candidates which ensures they are able to readily cross the plasma membrane and enter the lung tissue. Unfortunately, this also means that the compound is freely able to diffuse out of the lung tissue and into the adjacent pulmonary vein. This results in an inhaled drug PK profile with a quick high concentration of compound in the lung which rapidly reduces, followed by a subsequent high concentration in the blood which is maintained for a much longer period dependant on the drugs plasma stability (**Figure 3**).

Figure 3: Inhaled PK Profile for Salmeterol, Formoterol and Terbutaline, Taken from Hendrickx *et al*⁵⁰



This data shows that with short acting compounds Salmeterol, Formoterol and Terbutaline less than 1% of the initial dose remains after a few hours, and hence their pharmaceutical effect is short lived. The preferred PK profile is that of long acting compounds Indacaterol, Tiotropium Bromide and AZD3199 (discussed in more detail later), where after 24 hours a considerable amount of drug remains in the lung tissue, and the concentration in the blood does not exceed unwanted levels (**Figure 4**).

Figure 4: Inhaled PK Profile for Indacaterol, Tiotropium and AZD3199, Taken from Hendrickx *et al*⁵⁰



To reduce the number of failed compounds and thus expedite the drug development process, one must be able to accurately predict the behaviour of the compound in its biological environment. This allows for improved critical analysis of *in vitro* and *in silico* data such that an accurate *in vivo* prediction can be made, relating all observed PK data to the structure and physiochemical properties of the compound.

1.1.3.1 Characterising Lung Retention

In response to the observation that poor lung retention can stall the development of novel inhaled therapeutics, several attempts have been made to characterise and improve the lung retention of inhaled compounds.

In 2018, Bäckstrom *et al*⁵¹ sought to uncover the regional and histological distribution of isotopically-labelled salmeterol post inhalation through mass spec imaging (MSI). Their work established that inhaled salmeterol was homogeneously distributed in the alveolar and bronchiolar regions at the 5-minute time point but was more preferentially retained in the bronchioles from the 15-minute time point onwards, indicating that lung retention occurs in the bronchioles. When analysing at a cellular level, they found that salmeterol retention in bronchial structures could be correlated to high drug concentrations in the bronchial epithelium, and cited non-specific binding and lysosomal trapping as possible causes.

In 2020, Hamm *et al* followed up this research with a further *ex-vivo* analysis of the spatial lung distribution of salmeterol, salbutamol and fluticasone propionate (FP) post IV or IT administration to identify the targeting within lung substructures of drugs

with very different physiological properties.⁵² These results demonstrated that inhaled salbutamol and salmeterol concentrated within the bronchial regions with good retention after 30 mins, whilst FP, owing to its increased hydrophobicity, was distributed throughout the whole lung tissue with good retention also. Interestingly when administered systemically, the distribution patterns for salbutamol and salmeterol were reversed, with an observed high concentration in the peripheral alveolar regions but with reduced lung retention after 30 mins. FP concentrations in the distal alveolar regions were reportedly higher when administered systemically but with poorer retention.

In summary, these two studies demonstrate the application of high-resolution mass spectrometry imaging in elucidating the tissue distribution of inhaled compounds. They also highlight the importance of incorporating considerations regarding the intended targeted tissue and route of administration into drug formulation designs.

1.1.3.2 Strategies for Improving Lung Retention

As previously mentioned, Bäckstrom *et al* cited non-specific binding and lysosomal trapping as possible causes for the increased lung retention of salmeterol in lung epithelium. Optimising compounds to increase their propensity for these interactions are just two of many methods employed by medicinal chemists to increase the lung retention and thus duration of action of inhaled therapeutics.

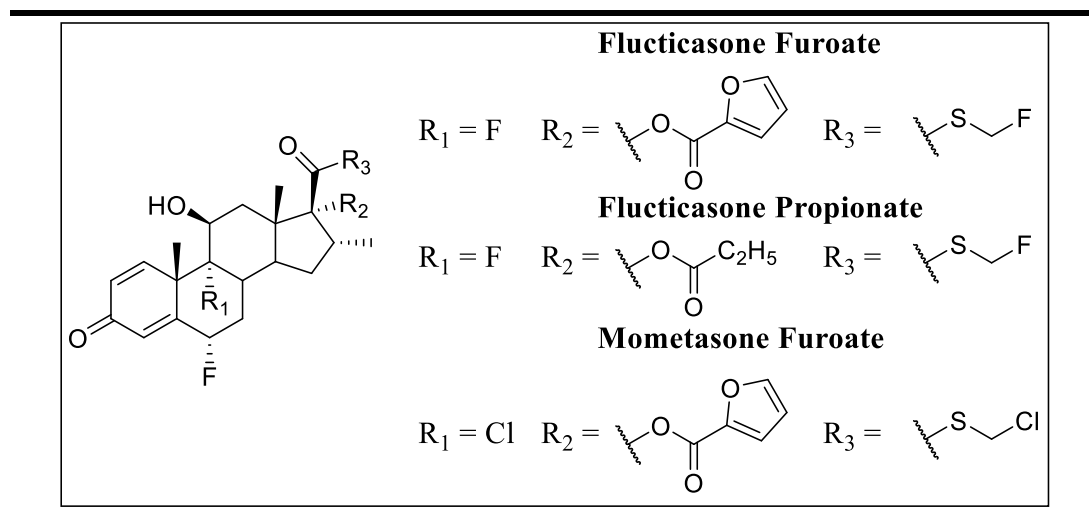
1.1.3.2.1 Improving Non-Specific Binding

Non-specific tissue binding is described as the binding affinity of a drug molecule to sites other than the target receptor including binding to proteins, plasma, and tissue and is a major factor that affects both the pharmacokinetic and pharmacodynamic profile of the drug molecule.⁵³ Binding may occur through Van der Waals or dipole-dipole interactions, or in the case of charged drug molecules, the electrostatic potential of cationic moieties provides an opportunity for the drug to interact with negatively charged species such as mucins or phospholipids.⁵⁴ Once bound, the drug-protein complex is then usually too large to pass out of the extracellular space, or for the ligand to interact with the target receptor, and thus it is the unbound, free ligand that is able to exhibit the intended pharmacological response.⁵⁵ Binding is however normally reversible and thus the bound and unbound fraction of the drug exist in equilibrium, the position of which is dictated by the binding kinetics of the drug to the protein.

When considering inhaled administration, increased non-specific binding can have positive effects on the pharmacokinetic profile of a drug when trying to reduce the volume of distribution and localise the drug molecule to one specific area of the lung. By binding to various components in the lung such as mucus or phospholipids, the percentage of drug which passes through the epithelium is reduced, resulting in an increased drug residency within the lung tissue. Providing the drug being administered is highly potent such that only a low concentration is required for pharmacological activity, then an increased non-specific binding could provide a drug depot from which sustained release of the active drug could be achieved.⁵⁶

This is indeed what was observed by Valotis *et al* when they compared the *in-vitro* receptor and lung tissue binding affinities of novel inhaled glucocorticoid fluticasone furoate (FF), to similar steroids fluticasone propionate (FP) and mometasone furoate (MF) (**Figure5**).⁵⁷

Figure 5: Structure of Fluticasone Furoate, Fluticasone Propionate and Mometasone Furoate



Though only differing by subtle changes in chemical structure, FF demonstrated an increased receptor affinity alongside the highest lung tissue binding affinity of the three compounds and thus was predicted to display the most controlled rate of distribution from lung tissue into systemic circulation *in-vivo*. Indeed, this hypothesis was confirmed by Salter *et al*, who demonstrated that a high cellular accumulation of FF alongside a slow rate of receptor dissociation lead to a pharmacokinetic profile indicative of a sustained pharmacological response.⁵⁸

This study represents the potential of improved tissue binding as a mechanism for improving lung retention. By optimising the compound structure such that tissue

binding potential is increased, it is possible to create a depot of bound drug in close proximity to the target receptor. Of course, this method requires an understanding of the intended receptor, the receptors proximity to the targeted tissue, and site of deposition of the drug post inhalation, and thus it can be a difficult to achieve improved pharmacology from this method alone.

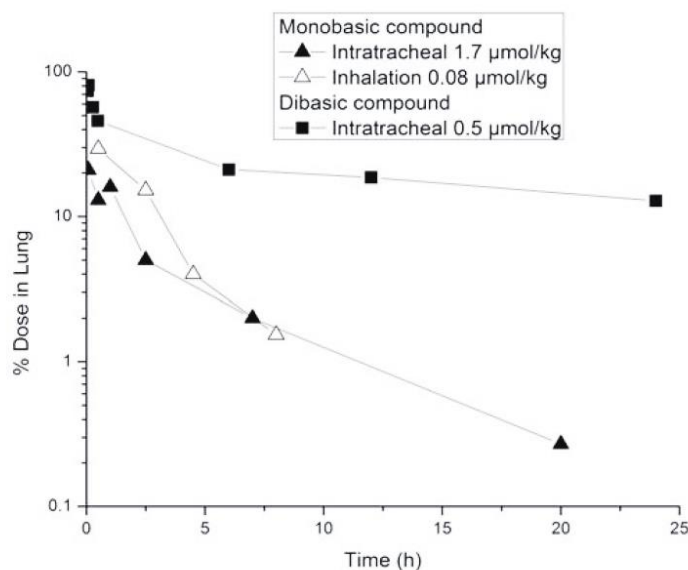
1.1.3.2.2 Optimising Basicity

The acid-base properties of a drug compound have direct consequences on the PK characteristics of the drug, by influencing physiochemical properties such as protein binding, membrane permeability, lipophilicity and solubility. As previously mentioned, protein binding can be an important characteristic in determining the retention of the drug in the desired tissue as well as determining the percentage of unbound 'free' drug available to interact with the target receptor. In most cases, protein binding between a drug molecule and phospholipids is electrostatic, the phosphate groups present in the plasma membrane are negatively charged and thus there is potential for electrostatic interaction with positive cations. At physiological pH (7.4), basic groups with a $pK_a > 7$ will be protonated and thus cationic. However, in the absence of transporter proteins such as OCT's, protonated species will have a reduced ability to cross plasma membranes due their inherent hydrophilicity and thus if not carefully managed, the absorption and thus distribution of the drug could be negatively impacted. This is especially relevant for intracellular targets.

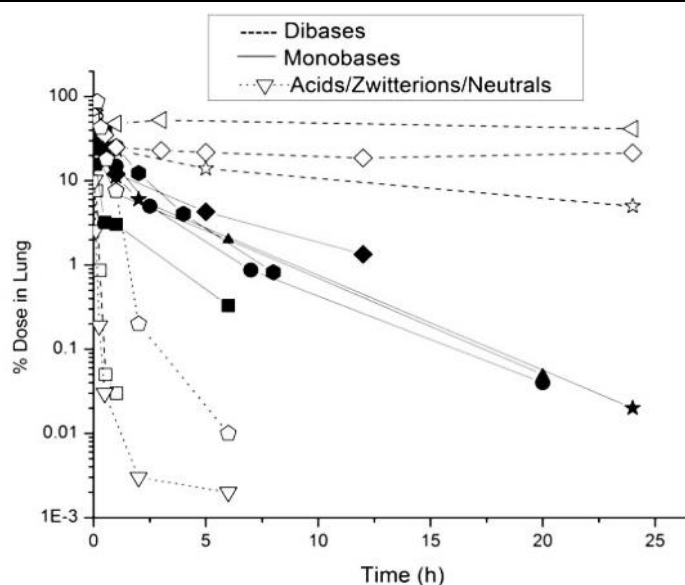
In 2012, Cooper *et al* reviewed how the extent of basicity can affect both absorption and lung retention of inhaled compounds.⁵⁹ They demonstrated how when

administered, dibasic compounds display an increased retention in the lung compared to monobasic compounds, which they suggested was a result of reduced rate of absorption, due to reduced membrane permeability (**Figure6**).

Figure 6: Comparison of the Lung Retention of a Monobasic and Dibasic Compound post IV or IT Administration, Taken from Cooper *et al*⁵⁹



This relationship was explored further, when they explored how the ion class of a range of drugs affected the lung duration following intratracheal dosing in rats (**Figure7**). Their results demonstrated how dibasic compounds had a far superior lung retention relative to monobasic, acidic, zwitterionic and neutral compounds.

Figure 7: Comparison of Acidity/Basicity on Lung Retention taken from Cooper *et al*⁵⁹

They rationalised that this increase in retention could be due to lysosomal trapping of the dibasic compounds, preventing elimination of the drug into systemic circulation.

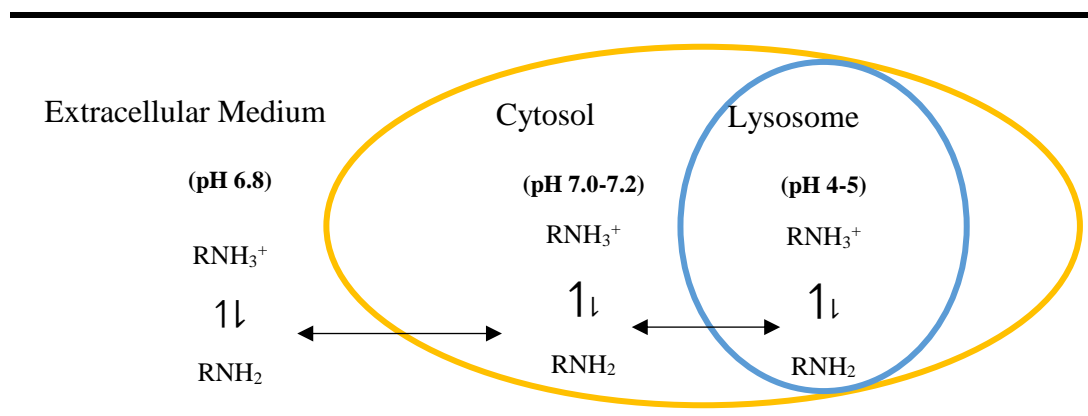
1.1.3.2.2.1 Lysosomal Trapping

Lysosomes are acidic, membrane bound organelles, which are responsible for apoptosis, phospholipid turnover, autophagy and the breakdown of endogenous waste products.⁶⁰ Optimal activity of the digestive enzymes held within lysosomes is maintained due to the acidity of the lysosomal lumen, in which an internal pH of 4-5 is maintained due to the lysosomal proton pump, V-H⁺-ATPase.⁶¹ This proton pump actively pumps hydrogen ions against their concentration gradient from the cell cytosol into the lumen.

1.1.3.2.2 Mechanism of Lysosomal Trapping

Lysosomes are in abundance in tissues such as the liver, lung, kidney and spleen, and present an opportunity for sequestration of lipophilic and amphiphilic weakly basic compounds based on their physiochemical properties, in a process known as lysosomal trapping.⁶² There are various mechanisms by which compounds can be compartmentalised by lysosomes, however the greatest volume of lysosomal trapping occurs due to the passive diffusion of neutral molecules through the plasma membrane.⁶³ At physiological pH (7.2-7.4), lipophilic drug compounds containing a basic protonatable group, such as amines with a $pK_a > 7$, will be only partially protonated and thus the neutral component will be capable of crossing the cell membrane and cytosol, diffusing into the lysosome *via* simple passive diffusion, acting as a sink for basic drugs (**Figure 8**).⁶⁴⁻⁶⁶

Figure 8: Lysosomal Trapping of Neutral Amines



Once inside the lysosome, the acidic environment will protonate the drug, restricting its ability to cross back through the cell membrane due to the membrane's integral hydrophobic nature.⁶⁷ Depending on the concentration of basic amine, the internal pH of the lysosome will begin to rise as the increasing base concentration exceeds that of

proton uptake. Depending on the stability of the compound in this environment, the neutral component of unbound active drug molecules may either diffuse back out of the lysosome and bind to their target receptor or decompose due to the lysosome's highly metabolic enzymatic environment.

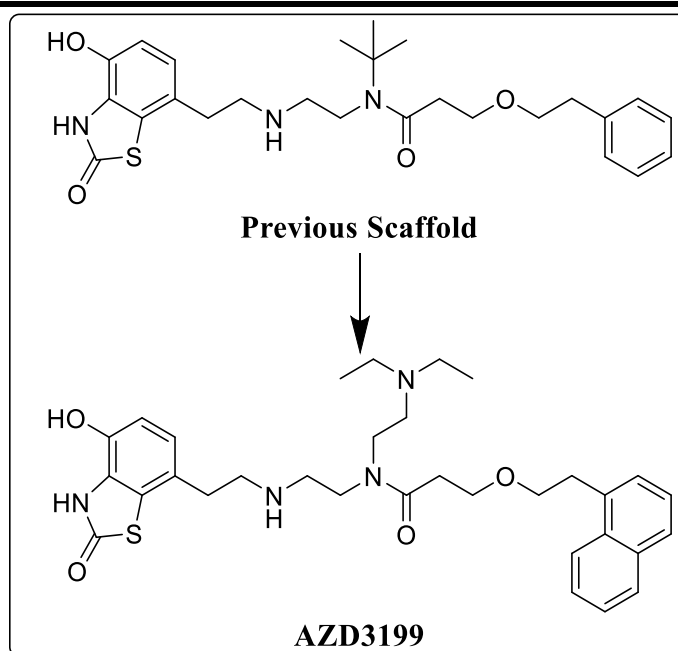
This concept presents an opportunity for increasing the lung retention of poorly retained and highly potent inhaled drug candidates. If the structure and resulting physiochemical properties could be altered such that the potency of a drug candidate was maintained whilst the opportunity for lysosomal sequestration was increased, then perhaps a novel long acting inhaled therapy could be achieved. It is clear therefore that optimising basicity can be an important factor in increasing the tissue retention of administered drugs, but must be carefully managed depending on the desired terminal location of the drug. This is especially relevant for inhaled compounds which must cross the epithelial cells in order to enter the lung tissue.

1.1.3.2.3 Optimising Lipophilicity

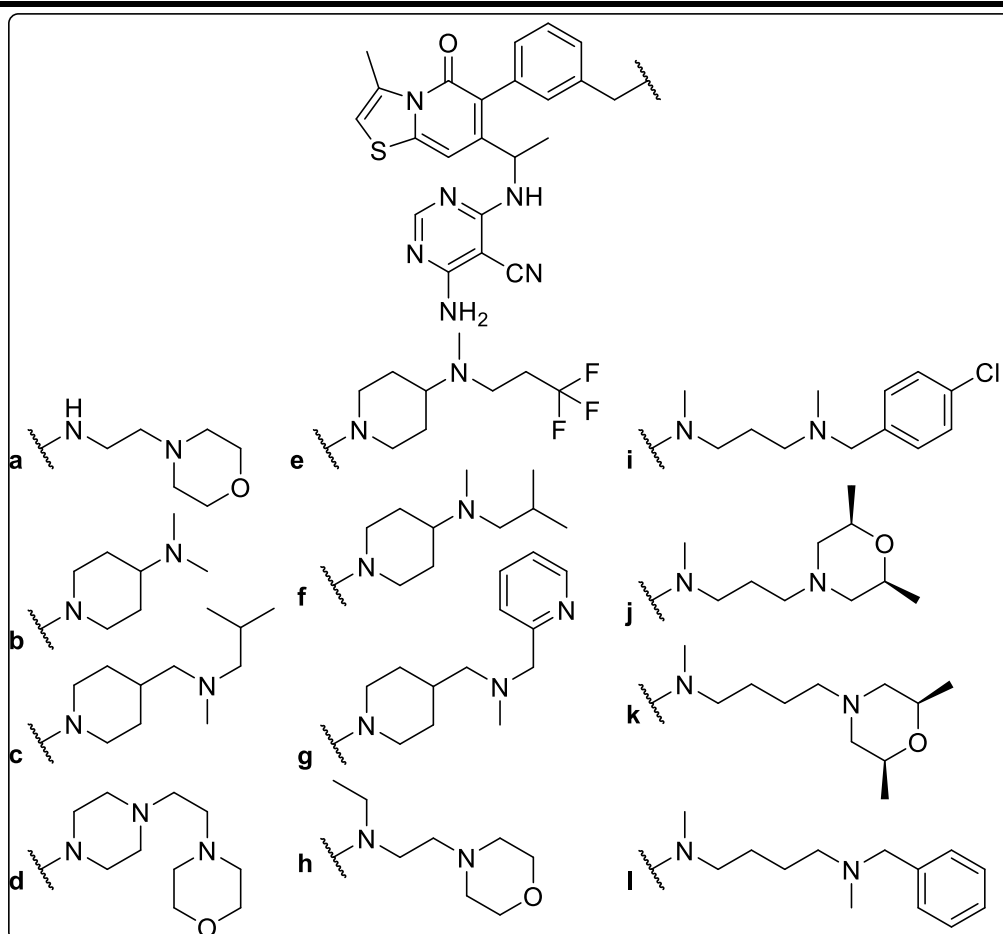
As previously mentioned, lipophilicity is an important physiochemical property with the ability of affecting multiple pharmacokinetic 'ADME' properties. Optimising lipophilicity in combination with the incorporation of a dibasic pharmacophore into candidate design can drive lung retention either through association with acidic phospholipids, or through lysosomal trapping.^{59,60,68,69} In particular, Stocks *et al* used this hypothesis as the basis for achieving sustained duration of action when creating a range of lipophilic, dibasic, ultralong acting, β_2 agonists.⁷⁰ They aimed to determine whether the compounds could display a short onset of action alongside the retention

of a once-a-day profile, whilst reducing observed side effects through monitoring of the blood plasma potassium concentrations post IT administration, as precursor for hypokalaemia. The study built on previous work which had demonstrated how incorporation of a second basic component increases membrane partitioning resulting in increased duration of action.^{71,72}

They took their previous β_2 scaffold and made structural modifications such to introduce a second basic moiety from the amide group (**Scheme 1**). Gratifyingly, after several rounds of quantitative structure-activity relationship (QSAR) exploration, their work yielded AZD 3199 as a novel, selective β_2 agonist. They noted that after incorporation of the dibasic pharmacophore, binding selectivity for β_2 had reached greater than 1000-fold higher than for β_1/β_3 , as well as high selectivity over α -adrenoceptor and D_2 dopamine receptor. AZD 3199 was found to have similar or improved onset time compared to existing β_2 therapies indacaterol, formoterol and salmeterol. Interestingly, onset time was increased proportional to lipophilicity for monobasic compounds, whilst a much-reduced onset time was achieved for dibasic compounds with similar lipophilicities. In Addition, AZD 3199 achieved plasma terminal half-lives greater than 11 hours in rats, guinea pigs, and dogs, and resulted in a much smaller reduction in plasma potassium, signalling less observed side effects than previous efforts.

Scheme 1: Evolution of Previous β 2 Scaffold to Discovery of AZD3199

Further to this, in 2017, Perry *et al* followed a similar approach in the design and synthesis of novel dibasic, PI3K antagonists for inhaled delivery. PI3 kinases (discussed in more detail in Chapter 2), are intracellular receptors often targeted for symptom relief of inflammatory responses such as those present in asthma and COPD patients. Interestingly, Perry *et al* demonstrated how lipophilicity and basicity directly affected the lung retention and cell absorption (**Figure 9**).⁷³

Figure 9: Dibasic Compound Evaluation, Reproduced from Perry *et al*⁷³

Cmpd	PI3K δ pIC ₅₀ ^a	PI3K β pIC ₅₀ ^a	PI3K δ cell pIC ₅₀	LogD	CLogP	pKa B1 ^b	pKa B2 ^b	Lung t _{1/2}	Residual Dose at 24 h (%)
a	9.2	7.7	7.9	0.6	2.7	9.6	4.7	4.2	0.1
b	9.3	7.2	8.0	0.5	2.7	9.5	6.5	23.2	4.8
c	9.2	7.3	8.6	2.1	4.8	9.8	8.0	12.0	3.3
d	9.1	7.0	9.0	2.5	3.5	8.4	5.4	4.5	0.2
e	8.8	6.6	7.9	1.1	2.6	7.3	6.0	8.7	3.5
f	9.2	7.1	8.9	1.7	4.2	9.7	6.8	9.9	2.8
g	9.1	7.2	8.7	2.0	3.8	9.0	7.0	10.9	5.2
h	9.1	6.6	8.9	1.4	3.8	8.0	4.0	0.0	0.0
i	9.2	7.9	8.5	3.2	6.1	8.8	7.5	13.0	3.3
j	8.9	6.9	8.3	1.5	4.4	8.5	5.7	5.9	0.8
k	8.9	7.1	8.2	1.5	4.3	8.9	6.3	7.6	3.9
l	9.3	7.8	8.7	2.2	5.1	9.1	7.0	17.6	7.4

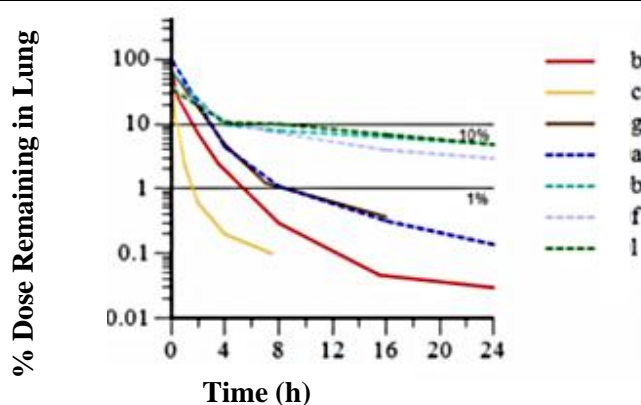
^apIC₅₀ values for PI3K α and γ not shown; these were consistently low ($\alpha \leq 6.2$, $\gamma \leq 6.7$). All biological values are means of ≥ 3 replicates.

^bB1 and B2 are defined as the first and second base (left to right) in the structures as drawn above

Initially, it was seen that compound **a** and **b** displayed very different retention profiles, with **b** having a much higher percentage remaining in the lung after 24 hours (4.8%

and 0.1% for **b** and **a** respectively) and a more favourable base-driven PK profile (**Figure 10**).

Figure 10: Rat ITPK Time course of selected examples, Taken from Perry *et al*⁷³

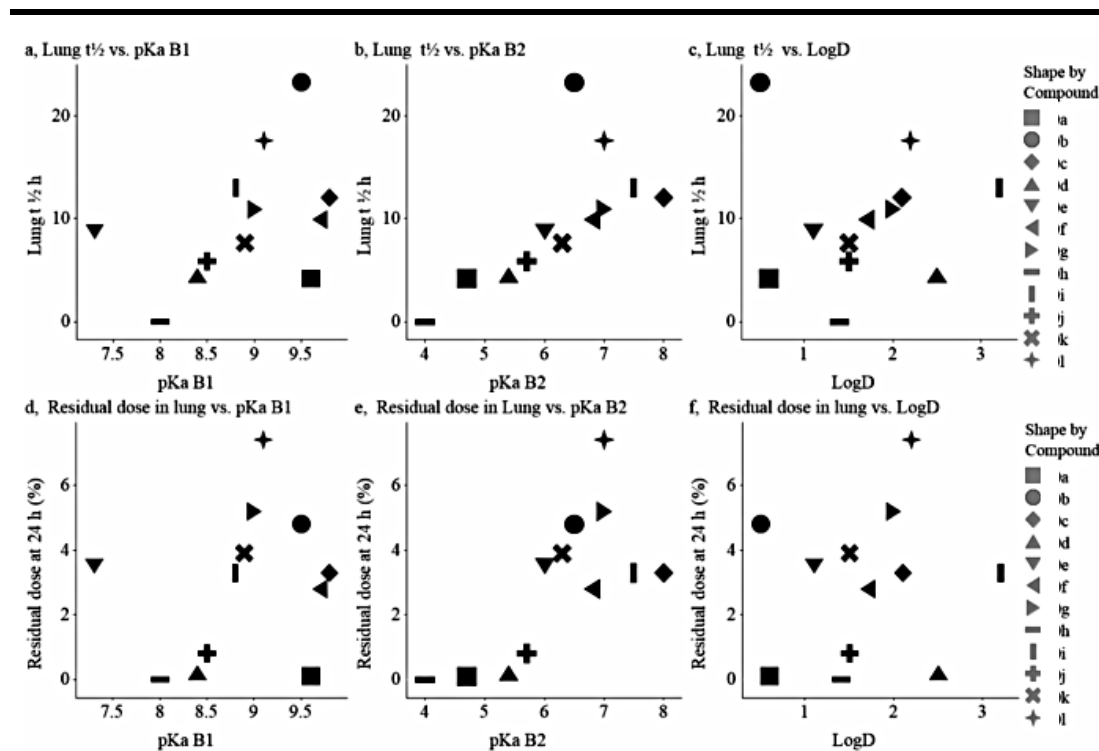


With the uncertainty of why **b** and not **a** had led to an increased lung retention, they turned their attention to the exact basicities of each amine in the dibases. They found that the second amine in each structure had very different pKa values (4.7 and 6.5 for **a** and **b** respectively). They then investigated further by synthesising analogues **c-l** and discovered that second basic pKa was indeed the most important factor determining compound half-life and thus lung retention (see **a, h, j**). It was clear that until the second basic pKa was at least 6, there would be little to no residual compound remaining in the lung. When the pKa is less than 6, changes in lipophilicity had little effect on the lung retention (see **a** vs **h**; **d** vs **j**). Conversely, increasing the pKa beyond 6 increases the lung retention, albeit in a less definable pattern.

Interestingly, the pKa of the first base displayed no effect on the lung retention for the range of pKa used in this study (7.3-9.6), whilst lipophilicity, as shown through Log D

values, displayed no effect on the residual dose remaining, it did contribute to the half-life of the compound (see **c**) (**Figure 11**).

Figure 11: Comparison of Physicochemical Properties and Lung Retention, taken from Perry *et al*⁷³



The last study they performed was a comparison of cell potency and enzyme inhibition as a consequence of compound lipophilicity. They concluded that if a compound's lipophilicity (Log D) is greater than 1.6 then a compound which exhibits good PI3K enzyme inhibition will also attain good cell half-life.

These results were rationalised using the lysosomal trapping model as a method of sequestering dibases (based on their lipophilicity and thus membrane permeability of the neutral compound) creating a di-cationic species. The half-life therefore is driven by the pKa of the terminal amine which determines the percentages of mono- and di-cationic species, and thus sequestering potential due to organic cation transportation.

Based on this work, there are some clear observations that should be considered when designing dibasic compounds for an inhaled administration: Lipophilicity should be monitored to achieve a value of between 1.7-2.5, whilst the pKa of basic amines should be maximised to ensure a favourable IT-PK time course.

1.1.3.2.4 PEG linkers

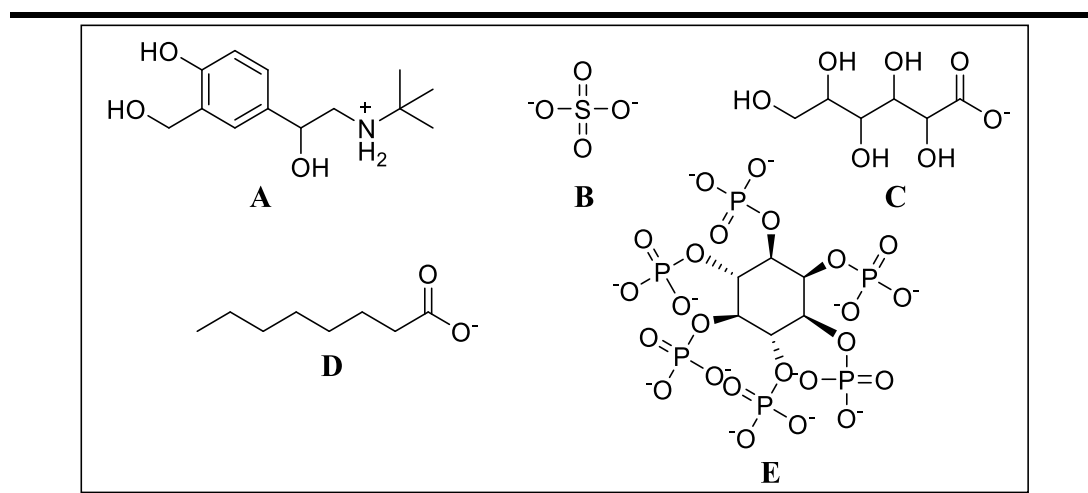
Another interesting method for increasing the lung residency time is the synthesis of high molecular weight drug-polymer conjugates through conjugation of a drug molecule to polymers such as polyethylene glycol (PEG) using a linker which is bioactivated to the release the drug *in-situ*.⁷⁴ This approach extends the lung residency by increasing the hydrophilicity and thus aqueous solubility of the drug, and delaying the lung absorption of the molecule due to its size, requiring a slower, paracellular route of epithelial absorption.⁷⁵

In 2009, Gursahani *et al* studied the how the size of the PEG conjugate effected the rate of permeability and thus lung retention of a range of fluorescently tagged polymer conjugates.⁷⁶ Their results demonstrated that without any PEG conjugate, the half-life of the sodium fluorescein was incredibly poor at 0.52 hours, but that this could be increased through PEG conjugation from 2.36 hours in a 0.55 kDa conjugate to 12.02 hours for a 5 kDa polymer. This result certified the relationship that larger molecular weight PEG polymer conjugates could achieve extended lung residency times and formed the basis for various PEGylated drug conjugates for inhaled delivery.⁷⁷⁻⁷⁹

1.1.3.2.5 Organic Ion-Pairing

The use of ion-pairing is an established method of improving pharmacokinetic properties, and has found significant application in topical⁸⁰, ocular⁸¹ and oral⁸² routes of delivery. Ion-pairing is the electrostatic association of counterions to charged drug molecules, as a method of overcoming physiochemical properties and improving absorption across cellular membranes.⁸³ Once administered, the increased proportion of drug molecules able to cross the plasma membrane as ion pairs can improve the pharmacological activity of the drug, meaning lower doses can be administered, resulting in less systemic exposure and fewer adverse effects.

Interestingly, the opposite result can be achieved by creating hydrophilic organic ion-pairs with reduced rates of absorption to achieve an increased residency time, although this has yet to be extensively explored in the literature. Indeed, this hypothesis was demonstrated by Dutton *et al*, in which a series of organic, salbutamol ion-pairs were created and evaluated to determine their rate of transport across respiratory epithelium in Calu-3 human bronchial cells (**Figure 12**).⁸⁴

Figure 12: Structures of Salbutamol (A) and Ion-Pair Partners (B-E), Taken from Dutton *et al*⁸⁴

By selecting ion-pairs with differing molecular weights, lipophilicity and polar surface areas, they were able to extensively compare how different physiological properties would affect the cellular absorption of salbutamol. Their results demonstrated that formation of salbutamol ion-pairs significantly impaired cell permeability relative to the free base, and suggested the increase in polar surface as the cause of reduced membrane permeability. This result supported previous literature that observed a reduced Calu-3 epithelial cell permeability for salbutamol sulfate compared with the free base.⁸⁵

As previously mentioned, application of organic ion-pairing to inhaled delivery is still under-researched and further investigation is required to determine whether extended pharmacological activity post inhalation of ion-pair formulations can be achieved.

1.1.3.2.6 Inorganic Ion Coupling

One similar alternative to organic ion-pairing, is the coordination of a drug molecule to metal centres such as Ca^{2+} , Mg^{2+} , Zn^{2+} or Al^{3+} , forming complexes which vary in

stoichiometry and molecular weight. As with organic ion-pairing, these large, charged, complexes possess slower rates of epithelial absorption and thus display potential for increasing lung residency times of inhaled therapeutics. Across two studies, Lamy *et al* and Brillault *et al* have demonstrated that by inhaling an aerosolized nanoparticle formulation of an 80% copper complex of the antibiotic ciprofloxacin, it is possible to retard the cellular absorption across lung epithelium, increasing the lung residency of ciprofloxacin compared to direct administration.^{86,87} Gratifyingly, the efficacy of ciprofloxacin-copper complex against two *Pseudomonas aeruginosa* strains was determined to match that of free ciprofloxacin, but use of the copper complex meant that higher lung concentrations were achievable, without an increased toxicity or occurrence of side effects.⁸⁸

1.1.3.2.7 Drug Carriers

The use of drug carriers to aid the delivery of inhaled therapeutics shows promise within sustained drug release. Through encapsulation of the drug molecule within large carrier structures such as micelles, polymeric nanoparticles and liposomes etc, the pharmacokinetic properties of the drug at the intended delivery site can be improved. Release of the drug from the carrier is dependent on the rate of diffusion of the drug through the carrier matrix and the rate of degradation of the carrier itself, and thus through careful design of the carrier, and the therapeutic goal, a sustained rate of release of the active drug can be achieved.

Although presenting opportunity for improved drug characteristics, liposomes are the only sustained release carrier systems for inhaled administration to reach clinical

trials. Liposomes encapsulate drug molecules inside lipid bilayers, the composition and thus permeability of which drives their sustained release potential, by restricting the diffusion of the drug from the carrier. They have demonstrated their potential with a wide range of inhaled therapeutics including, bronchodilators for COPD treatment⁸⁹, immunosuppressants⁹⁰ and various antibiotics⁹¹.

1.1.3.2.8 Insolubility

A final method employed in the delivery of inhaled therapeutics is to exploit low aqueous solubility as mechanism of increasing lung retention. By reducing the solubility of the inhaled agent, the rate of absorption across the epithelial membrane is reduced due to the requirement of the drug to be in solution for transcellular absorption. This method has found application in the administration of estradiol as a hormone replacement therapy. Owing to its low aqueous solubility, estradiol was originally administered as a subcutaneous injection as an aqueous suspension. However, through inhalation of large porous particle formulations of estradiol, Wang *et al* were able to exploit the low solubility of estradiol as a method of sustained delivery, and were able to produce elevated systemic concentrations for up to 5 days post inhalation.⁹²

Unfortunately, inhalation of insoluble particles is not always a practical solution for increasing the duration of action of inhaled therapeutics. Deposition of insoluble drug molecules in the lungs while extending duration of action, can often lead to increased airway inflammation causing side effects such as breathing difficulties and severe exacerbation.⁹³ For patients with breathing difficulties, such as asthma and COPD

patients, in which inhalation is quickest method of symptom relief, provoking an inflammatory response in the airways can be counter intuitive.

1.2 Chronic Obstructive Pulmonary Disease and Asthma

Drug administration through inhalation is employed in the treatment of chronic obstructive pulmonary disease (COPD) and Asthma. COPD is defined as a preventable, progressive disease state caused by limited air flow to the lungs as an inflammatory response to gases and particulates such as those encountered while smoking.⁹⁴ Smoking is the main prevalent risk factor, with 20% of all smokers having COPD, with this number raising to 50% for lifelong smokers. In 2015, the Global Burden of Disease Study found that COPD was responsible for over 5% of deaths that year, totalling almost 3.2 million people, and predicted COPD to become the fourth highest cause of death by 2030.⁹⁵

In addition to a persistent cough, the other major symptom of COPD is shortness of breath caused by a combination of obstructive bronchiolitis and emphysema.⁹⁶ Collectively these conditions cause the degradation of the walls of the alveoli resulting in a reduced surface area for gas exchange and thus poor airflow and shortness of breath. In addition to this, inflammatory responses from neutrophils and macrophages caused by inhalation of irritants causes a narrowing of the airways preventing a patient's ability to breathe out.⁹⁷

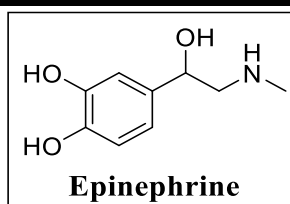
In contrast, asthma is defined as chronic inflammation caused by airway hyperresponsiveness affecting over 300 million people worldwide, and results in breathlessness, wheezing and coughing, particularly in the early morning or late at night.^{98,99} Some of the main causes of asthma is hyperresponsiveness to allergens such as dust, animal fur and pollen.¹⁰⁰ Whilst exacerbations can be severe, and in a small percentage of cases, fatal, the reactions can be reversible with effect symptom management/prevention.

1.2.1 COPD and Asthma Treatment

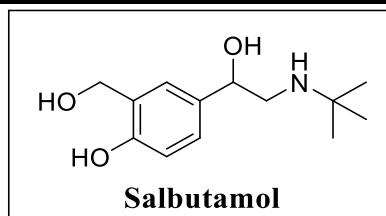
The most prevalent treatment for the management of COPD and asthma symptoms is the inhalation of bronchodilators (sometimes in combination with glucocorticoids) to remove resistance in the airways by targeting receptors responsible for the dilation of the bronchi and bronchioles.¹⁰¹ Bronchodilators are broken down into three main types of prescribed medication; short, long and ultra-long acting β_2 adrenoceptor agonists, short and long acting anticholinergics, and the phosphodiesterase inhibitor, theophylline, the former options usually being taken in combination with anti-inflammatory glucocorticoid steroids.

1.2.1.1 β_2 Adrenoceptors

β_2 adrenergic receptor agonists mimic the natural receptor ligand epinephrine (**Figure 13**) causing an increased production of cAMP, stimulating muscle relaxation in the bronchi.¹⁰²

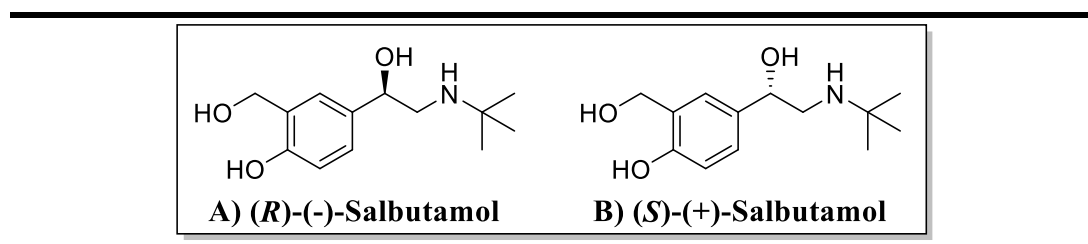
Figure 13: Structure of Epinephrine

Targeting of the β_2 adrenoceptors is the most effective bronchodilation method as they are natural agonists for the dilation of smooth airway muscle, and are located along the entire bronchial tree.¹⁰³ Short acting β_2 agonists (SABA) are used to provide temporary, quick relief from asthma symptoms and flare ups by relieving bronchospasms. These typically take effect in under 20 minutes, and the effect lasts for around 4-6 hours.

Figure 14: Structure of Salbutamol

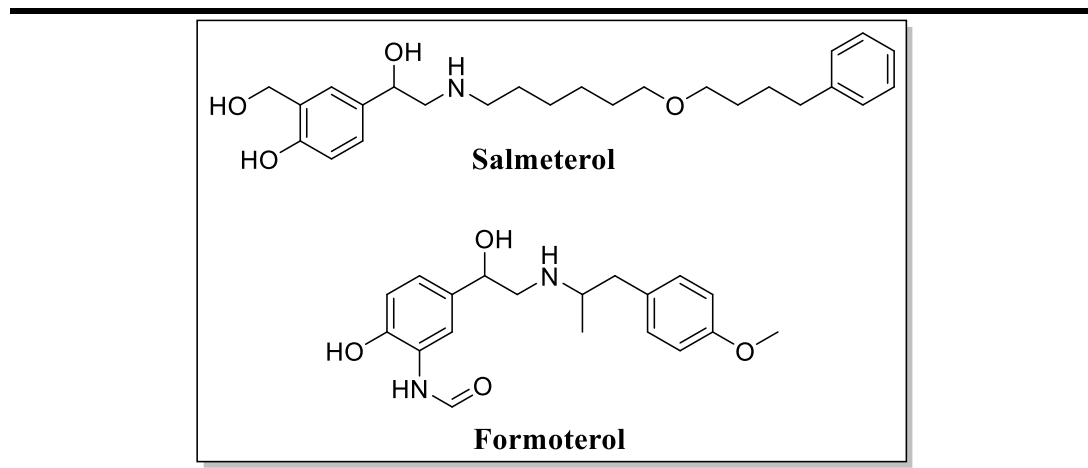
First marketed in the UK in 1969,¹⁰⁴ salbutamol (**Figure 14**) is the most commonly prescribed SABA and was listed as the 10th most prescribed drug in the US in 2016.¹⁰⁵ Although it can be synthesised stereospecifically, Salbutamol is sold as a racemic mixture due to the complementary effects of each enantiomer. The (R)-(-)-enantiomer (**Figure 15 A**) is required for the pharmacologic activity, whilst the (S)-(+)-enantiomer (**Figure 15 B**) blocks metabolism pathways which lead to the elimination of the active (R) enantiomer. However, due to its slow metabolism, an accumulation of the (S) enantiomer often occurs, leading to an inflammatory response.¹⁰⁶⁻¹⁰⁹

Figure 15: Structures of A) (R)-(-)-Salbutamol and B) (S)-(+)-Salbutamol



Long acting β_2 agonists (LABA's) are taken routinely, ahead of flare ups in order to prevent and control bronchospasms: they do not help with an in-progress flare up. Although much longer acting, these are still taken at least twice a day, often alongside an inhaled steroid, to provide airway constriction relief for up to 12 hours. Although both salmeterol and formoterol (**Figure 16**), are under the same classification, they function in completely different ways due to their differing physiochemical properties.¹¹⁰

Figure 16: Structures of Salmeterol and Formoterol



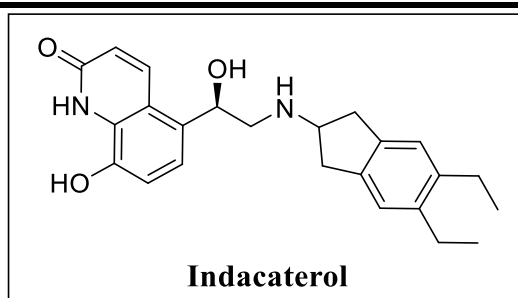
Due to formoterol's higher aqueous solubility and only moderate lipophilicity (2.2 for formoterol compared to 4.2 for salmeterol)^{111,112}, it often concentrates in extracellular space, possibly relying on the action of transporters to ensure a rapid delivery to the β_2 adrenoceptor present on the surface of smooth muscle. Salmeterol however is

highly lipophilic and only sparsely water soluble meaning a much slower onset of action is observed, but cell uptake occurs passively without the need for active transport.¹⁰³

In contrast to salbutamol, where its' aqueous solubility ensures a rapid elimination from lung tissue, the lipophilicity of formoterol and salmeterol allows for their storage within cell membranes, acting as an agonist source for the β_2 receptors.¹¹³ Formoterol acts as a full agonist due to the additional side chain methoxy group which completely changes the shape of the receptor when binding. Salmeterol however only partially changes the receptor shape leading to inefficient signal transduction.

Indacaterol (**Figure 17**) was introduced to the market in 2009 as the first once daily inhaled ultra LABA. Early research found it to have quick onset of bronchodilatory action of under 5 minutes, which was then sustained over 24 hours, all from a single 300 μg dose.¹¹⁴

Figure 17: Structure of Indacaterol



Developing new ultra LABA's is of current research interest with the intent of eliminating the need for dosing more than once per day in attempt to reduce the

observed side effects, such as inflammation, alterations to patients' blood pressure and heartrate, headaches and tremors¹¹⁵.

1.2.1.2 Anticholinergics

Muscarinic receptors are acetylcholine receptors, which together with G-proteins, form G protein-coupled-receptor (GPCR) complexes in neuronal cell membranes.^{116,117} Consisting of 7 transmembrane regions, these metabotropic receptors use G-proteins as their signalling method: acetylcholine is the natural agonist ligand, binding to the receptor, causing the G-protein to initiate an information cascade within the cell.^{118,119} Split into 5 isoforms (M1-M5) with different regulatory roles (**Table 3**), knockout-mice studies have shown the M3 isoform to be primarily involved in airway smooth muscle contraction such as that observed in chronic obstructive pulmonary disease (COPD).^{120–122}

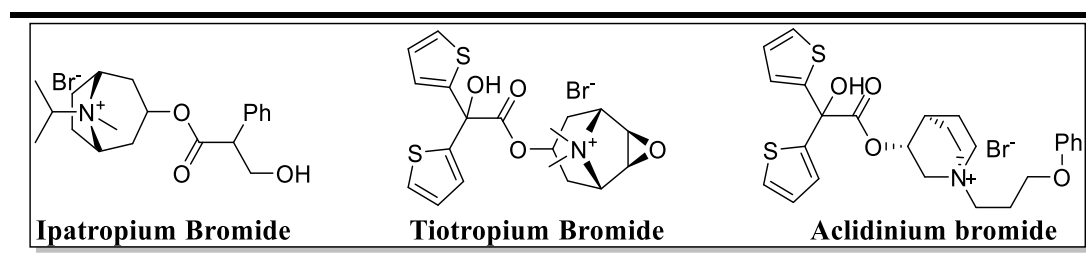
Table 3: Distribution and Cardiovascular Effect of Muscarinic Receptors, summarised from Saternos *et al*¹²³

Receptor	Main Tissue Distribution	Cardiovascular Effect
M ₁	Brain, prostate, salivary gland	Heart: Increases contractile force and heart rate. Vasculature: Vasodilation and Vasoconstriction.
M ₂	Gallbladder, heart muscle, lung	Heart: Regulates pacemaker, atrioventricular conduction, contractile force. Vasculature: Vasodilation.
M ₃	Salivary gland, lung, bladder	Heart: Dilation of coronary artery, regulates heart rate and repolarization, activation of survival pathways. Vasculature: Vasodilation, Vasoconstriction and endothelial barrier function.
M ₄	Spleen	Heart: Atrial neurotransmitter release, regulation of K ⁺ channels.
M ₅	Brain, placenta, testis	N/A

There are two types of muscarinic receptor antagonists currently available, termed short acting and long acting muscarinic receptor antagonists (SAMA and LAMA respectively).¹²⁴ Ipratropium bromide (**Figure 18**) is the most widely prescribed SAMA and acts by non-selectively blocking all muscarinic receptors. Onset of action is typically observed after 1 minute, reaching peak activity after about 1 hour and lasting on average 3-6 hours.^{125,126} As shown above, the non-specific blocking of all muscarinic receptors can invoke a wide ranging pharmacological response in a wide variety of tissues and thus depending on the drug stability in the blood, occurrence of side effects is expected.¹²⁷

Despite providing quick relief from Asthma and COPD symptoms, less than 10% of the inhaled dose reaches the lung tissue at which point it is able to exhibit a short lived pharmaceutical response.¹²⁸ Unfortunately, due to short lived receptor antagonism, ipratropium bromide exhibits a high volume of secondary tissue distribution (3 and 15 l kg⁻¹) post absorption into the pulmonary vein, and exhibits high stability in both rat blood and urine (21-24 hours and 6-8 hours respectively).¹²⁹ The high potency and poor pharmacokinetics of ipratropium bromide provide ample opportunity for secondary pharmacology and thus patients regularly experience multiple side effects including heartburn, pain when urinating, fast or pounding heartbeat and chest pain.

Figure 18: Structure of Ipratropium Bromide and Tiotropium Bromide



Tiotropium bromide was the first LAMA licensed for use in 2005, its prolonged pharmacodynamic response is a consequence of its kinetic selectivity for M₁ and M₃ receptors, with the latter providing an extended reversing of vagally induced bronchoconstriction.¹³⁰ Tiotropium was found to be approximately 20 times more potent than ipratropium bromide, achieving sustained bronchodilation for over 24 hours from an equipotent dose. Unfortunately, as with ipratropium bromide, high oral bioavailability alongside short-lived lung tissue residency results in maximal plasma concentration within just 5 minutes of inhalation of a single dose, and a plasma half-life (t_{1/2}) of 5-6 days.¹³¹ Fortunately, high receptor off rates for the M₃ receptor and a much-increased potency relative to ipratropium bromide meant that a much lower dosage was required (40µg – 2mg vs 10-18 µg)¹³², and thus concerns regarding plasma stability are much reduced. Despite the reduced dosage and improved bronchodilatory response, significant side effects are observed including unstable or life-threatening arrhythmia or heart failure regarding hospitalisation.

Indeed, this has been the focus of recent literature surrounding the use of tiotropium bromide. Several groups have noted the increased risk of mortality associated with the use of the tiotropium Respimat inhaler,^{133,134} including Bateman *et al*, who attributed the increased risk of cardiovascular mortality to the devices ability to create a ‘fine mist’, which could lead to higher than accounted for concentrations, although further investigation is required.¹³⁵ Although tiotropium has yet to be withdrawn, its potential withdrawal highlights the pertinent need for novel long acting muscarinic receptor antagonists with improved safety profiles.

Aclidinium bromide is a relatively new LAMA, having only been approved in 2012.¹³⁶ Pharmacologically, aclidinium achieves its long acting response ($t_{1/2} = 29$ h for aclidinium vs $t_{1/2} = 64$ h for tiotropium) in a similar way to tiotropium, having an extended, but inferior, dissociation time from M_3 receptors versus other receptor isoforms.¹³⁷ Interestingly, association of aclidinium with M_3 receptors matched that of ipratropium, meaning that onset of action was much quicker than tiotropium achieving bronchodilation in just 10 minutes from an equipotent dose (versus up to 30 minutes for tiotropium).^{138,139} Aclidinium also demonstrates a much shorter plasma stability half-life of between 1 and 3 hours, but despite this, demonstrates identical side effects to tiotropium, with severe arrhythmia causing widespread concern. Studies are currently underway to determine its superiority over tiotropium.

1.2.1.2.1 Development of New Long-Acting Anticholinergics

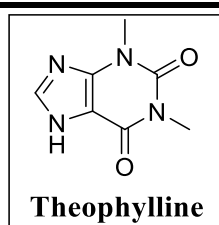
Unfortunately, despite past successes in the development of anticholinergics, new long acting treatments are not forthcoming due to the difficulties of inhaled delivery in combination with high muscarinic receptor expression in surrounding tissue. Most muscarinic receptor antagonists are non-selective and as such, when they are eliminated into the pulmonary vein, high plasma stability can often result in the delivery of the drug directly to the M_2 receptors in the heart leading to severe side effects. It is clear the high expression of all muscarinic isoforms throughout the lungs and heart makes it difficult to achieve the desired pharmacological activity without the prevalence of severe side effects. Even if a completely selective M_3 receptor antagonist was discovered, plasma stability could ensure that cardiac side effects are still observed. Instead a drug delivery approach which either reduces the amount of

active drug entering the blood, or reduces/eliminates its pharmacological potential in the blood may be required.

1.2.1.3 Theophylline

Although its mechanism of action is not completely understood, theophylline has been one of the most prescribed drugs in the treatment of Asthma and COPD since its discovery over 80 years ago (**Figure 19**).¹⁴⁰

Figure 19: Structure of Theophylline

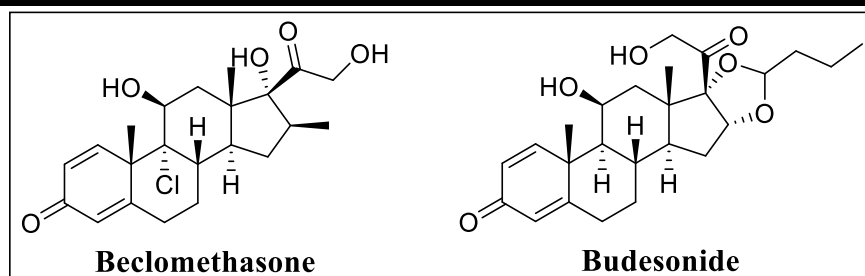


When administered (orally or intravenously) in high concentrations, theophylline acts as a bronchodilator by inhibiting phosphodiester enzymes, causing an increase in intracellular cAMP and ultimately instigating smooth muscle relaxation.¹⁴¹ In low doses, theophylline also exhibits mild anti-inflammatory responses due to multiple mediator inhibition although this response is inferior when compared with the use of inhaled corticoid steroids.¹⁴² Unfortunately, the requirement of high concentrations to achieve pharmacological activity leads to a high prevalence of severe side effects and has resulted in theophylline becoming a third-line treatment, with β_2 agonists much more effective as bronchodilators, and inhaled corticoid steroids being superior anti-inflammatory agents.

1.2.1.4 Glucocorticoids

Glucocorticoids are steroid hormones which bind to the glucocorticoid receptor reducing the effects of the inflammatory immune response.¹⁴³ Upon binding, the receptor complex translocates into the cell nucleus where it binds to the promoter region causing the regulation of lipocortin-1, which ultimately results in an anti-inflammatory response.^{144,145} When nebulised and inhaled using MDI's, glucocorticoids alongside bronchodilators are recommended for the management of acute exacerbations caused by COPD as they have been found to improve the lung function and oxygenation, whilst also reducing the occurrence of treatment failure, relapse risk and hospitalization length.¹⁴⁶ Two of the most commonly prescribed glucocorticoids include beclomethasone and budesonide (**Figure 20**).

Figure 20: Structure of Beclomethasone and Budesonide



Unfortunately, as glucocorticoids do not offer symptom relief and are simply administered to prevent worsening exacerbation severity, adherence to strict dosing regimens is usually very poor (circa 30%).^{147,148} This leads to over-reliance of β_2^- agonists for symptom relief which unfortunately increases a patient's chance of more severe exacerbations and ultimately death.¹⁴⁹ Recent clinical studies have investigated the potential of as-needed combined β_2 agonists with glucocorticoids such as budesonide-formoterol. Across two studies, it was found that when used as needed,

budesonide-formoterol was just as effective at preventing severe exacerbations as twice daily budesonide maintenance therapy but at approximately 70% of the dose, with a much higher dosing regimen adherence.^{150,151}

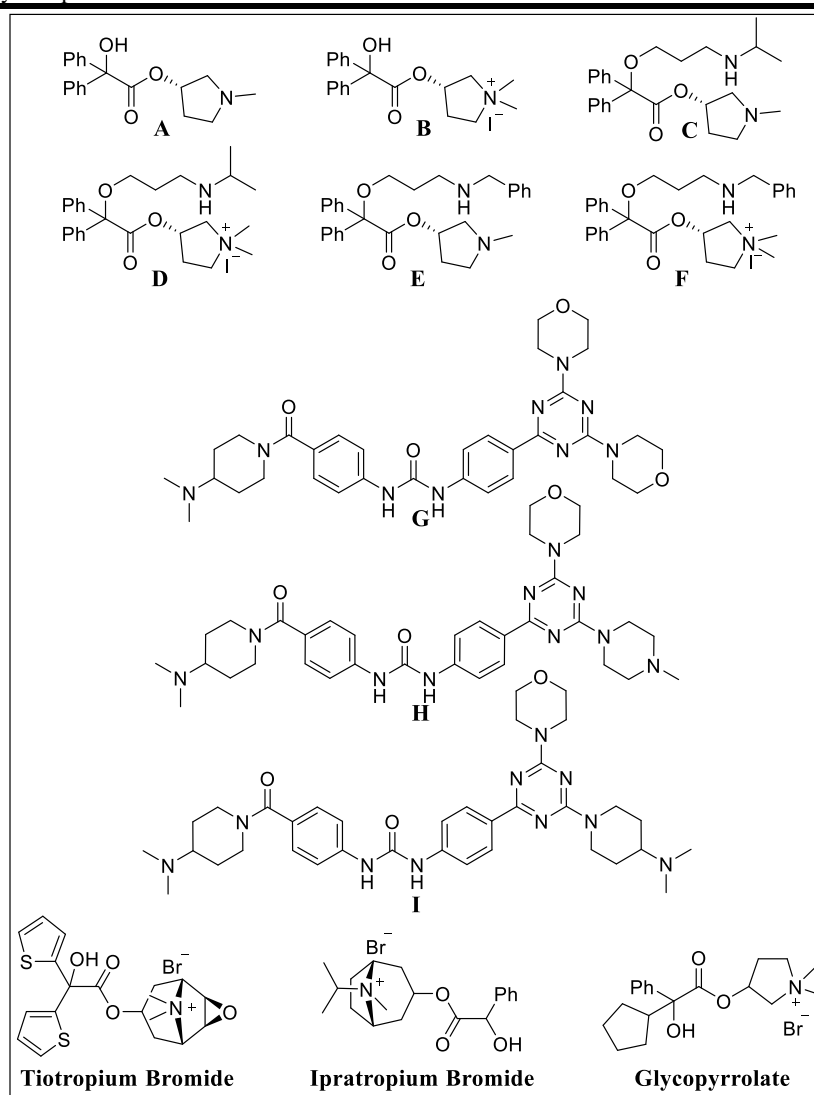
1.3 Background Work Supporting this Thesis

Some recent work within the Stock's group aimed to apply the concept of extended lung residency due to incorporation of a dibasic pharmacophore by applying it to the design of a novel long acting muscarinic receptor antagonist. By taking a known active muscarinic receptor antagonist (**1**) and creating quaternary (**2**), dibasic (**3, 4**) and basic quaternary (**5, 6**) analogues, they were able to compare lung retention post intratracheal dosing in rats (**Figure 21, Table 4**). Their aim was to create an analogue which maintained potency and selectivity but lead to an increased duration of action due to increased membrane binding and acidic organelle sequestering potential.

To understand the effects observed, the compounds' stability in rat lung homogenate and blood plasma were studied post IT dosing. The following compounds (**A-F**) were synthesized, and the results compared to those of clinically used anticholinergics tiotropium bromide, ipratropium bromide and glycopyrrolate.¹⁵² In addition, to test the hypothesis further, a small range of PI3 kinase inhibitors analogues were prepared (**H-I**) as dibasic analogues of **G**, to again examine the lung retention with and without a dibasic group in another therapeutically useful series of compounds.

Their data demonstrated that dibasic (**C, E, H-I**) and quaternary (**B, D, F**) compounds have an increased lung retention and plasma stability over their monobasic equivalents (**A, G**). Unfortunately, for the muscarinic compounds, whilst these modifications

improved the compound's lung retention, any modification to the original potent monobase, led to pharmaceutically inactive compounds due to the binding requirements of the alcohol and heterocyclic amine in the receptor. Whilst this proved that the extended lung retention can be a physicochemical consequence of the dibasic nature of the compounds rather than a receptor-mediated process, it unfortunately meant that no significant direct improvement could be made to the compound that would both maintain potency and selectivity whilst increasing the lung retention. In addition, insolubility of compounds (**A-I**) in the aqueous dosing media created uncertainty as to the amount of inhaled compound that was administered.

Figure 21: Structures of Compounds (1-9), Ipratropium and Tiotropium Bromide and Glycopyrrolate
-Performed by D. Speed**Table 4: PK Data for Compounds (1-9), Ipratropium and Tiotropium Bromide and Glycopyrrolate**

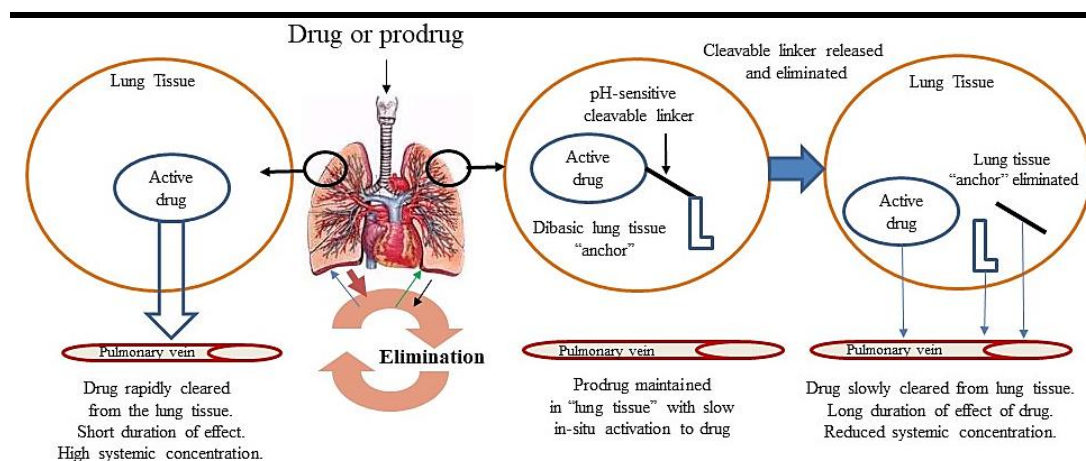
Compound	Type	cLogD ^a	LogD	cLogP ^a	Rat Lung T _{1/2} (hr) ^b	Rat Plasma T _{1/2} (hr) ^c
<i>A</i>	Basic	2.11	1.69	2.67	1	0.3
<i>B</i>	Quat	-1.49	-0.65	-1.49	13	7
<i>C</i>	Dibasic	0.37	0.47	3.78	19	9
<i>D</i>	Quat-Basic	-3.23	-2.23	-0.38	42	4
<i>E</i>	Dibasic	1.89	2.01	4.7	27	3
<i>F</i>	Quat-Basic	-1.26	-1.71	0.6	69	16
<i>G</i>	Basic	1.58	ND	3.65	28	0
<i>H</i>	Dibase	1.44	ND	3.77	66	2.2
<i>I</i>	Dibase	-0.45	ND	3.91	67	1.9
<i>Tiotropium</i>	Quat	-1.76	ND	-1.76	10	ND
<i>Ipratropium</i>	Quat	-1.82	ND	-1.82	6	ND

^a Calculated using Marvin Sketch^b Terminal half-life after intratracheal dosing in rats (n=2);^c Plasma half-life after intratracheal dosing (n=2)

N/D – Not Determined.

This work supported the hypothesis for the work presented in this thesis. Since an improved PK profile without the loss of potency could not be achieved by direct chemical derivatisation, it is hypothesised that a prodrug system could resolve these issues. By chemically attaching an active muscarinic antagonist to a dibasic, potentially lung tissue retentive moiety via a cleavable linker (**Figure 22**), the application of a prodrug sustained delivery system is evaluated.

Figure 22: Cleavable Prodrug Concept



Prodrug design concept. Directly inhaled drug compounds distribute into lung tissue where they are poorly retained, leading to a high clearance and subsequent high blood/systemic concentration. The prodrug hypothesis would result in a longer lung tissue residence time due to increased propensity for plasma membrane binding and acid organelle sequestration. The prodrug would then activate in-situ to release the drug at a controlled rate. Non-toxic breakdown products resulting from activation would then be cleared from the lung by diffusion into the blood.

It is hoped that the incorporation of the dibasic moiety would optimise the prodrug towards an increased propensity for non-specific binding and lysosomal trapping, such that a high lung tissue retention for the prodrug at the intended muscarinic site action would be achieved. Controlled activation of the cleavable linker would then release the active drug *in-situ* directly at the site of action, such that an extended duration of pharmacological activity is achieved, alongside a final PK profile comparable to that of tiotropium or AZD3199.

Thesis Aims and Objectives

Herein, this thesis aims to test the hypothesis that incorporation of a potent muscarinic antagonist into a dibasic chemical prodrug scaffold can achieve a sustained drug lung residency time post intratracheal administration. If successful, this system should be adapted to incorporate a drug candidate with an intracellular receptor target to assess the applicability of the prodrug system to intracellular targets. Finally, through evaluation of the prodrug's physiochemical properties alongside the determination of its *in-vitro* and *in-vivo* pharmacokinetic profile, this thesis also aims to elucidate the mechanism by which any basicity driven, lung retention is obtained.

In order to test these hypotheses, the following objectives must be completed:

1. A prodrug success criterion must be created in order to identify key objectives and requirements of the prodrug system.
2. A chemical series of prodrugs must then be designed, synthesised and evaluated in a range of *in-vitro* DMPK stability and binding assays in order to accurately determine the suitability of the prodrug system.
3. Ultimately, if a successful candidate is identified, the final prodrug must then be evaluated in an *in-vivo* PK study to determine whether the initial aim of increasing lung residency has been achieved.
4. Adapt the prodrug design to incorporate a drug with an intracellular target
5. Following successful *in-vivo* PK results, a series of cell-based confocal microscopy assays should be undertaken to elucidate the mechanism of lung retention.

2. Design and Synthesis of Novel Muscarinic Receptor Antagonist Prodrugs

2.1 Introduction

2.1.1 Prodrug Techniques

Absorption, distribution and metabolism are amongst just some of the variables which can be improved through use of a prodrug strategy. Prodrugs are inactive forms of a pharmaceutical agent which, upon administration activate to release an active agent.¹⁵³

Prodrugs are highly regarded as an important technique of delivering targeted therapeutics, with prodrugs making up almost 10% of all currently marketed medicines, and 20% of all small molecules approved by the Food and Drug Administration (FDA) in the past 20 years.¹⁵⁴ Use of a prodrug strategy allows for the development of 'ADME' properties to avoid unfavourable drug characteristics which may reduce the PK/PD properties. Additionally, prodrugs may be employed to increase selectivity and thus efficacy or to reduce systemic side effects, by creating an inactive species which becomes bio-activated to generate the active drug in a much-reduced concentration than if the drug were directly administered. Hence, use of pro-drugging strategies are becoming more common when overcoming problematic drug candidates with poor PK profiles.

2.1.2 Prodrug Design

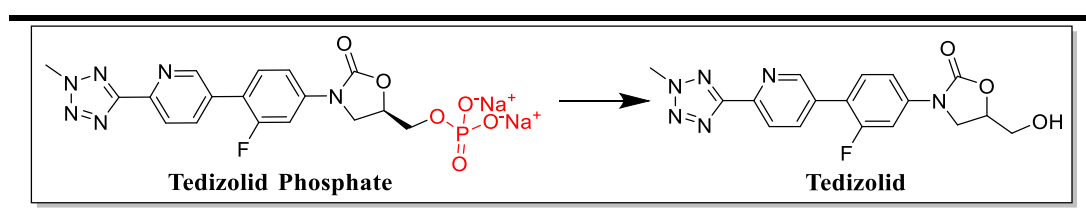
Depending on the rationale for pro-drugging and the ADME property being optimised, the prodrug design can vary considerably. A common approach is to include a chemically or enzymatically unstable component which degrades *in-vivo* liberating the active drug.¹⁵⁵ These prodrugs tend to have a linker or synthetic handle between the promoiety and active component which spontaneously cleaves in an appropriate biological/chemical environment. Other prodrugs are chemically stable until

biological oxidation or reduction reactions take place, and these are termed bio-precursors.¹⁵⁶

2.1.2.1 Administration

Improving drug administration by improving physicochemical properties such as solubility is a common motif in many prodrug systems. Incorporation of polarizable or ionizable groups such as amino acids or phosphates into the prodrug design can lead to an increased aqueous solubility relative to the parent drug.¹⁵⁷ This strategy is demonstrated in the development of the prodrug, tedizolid phosphate. Incorporation of the phosphate moiety on the free hydroxyl group led to the prodrug having both an increased aqueous solubility and potency of between 4-16 times that of the original drug, allowing for its use as an orally administered drug (**Scheme 2**).¹⁵⁸ Incorporation of ionizable amino acid esters to compensate poor aqueous solubility leads to a similar outcome, however high amide stability can sometimes lead to incomplete enzyme bioconversion *in-vivo* resulting in a reduced bioavailability.^{159,160}

Scheme 2: Metabolism of tedizolid sodium phosphate to Tedizolid by phosphatase activity

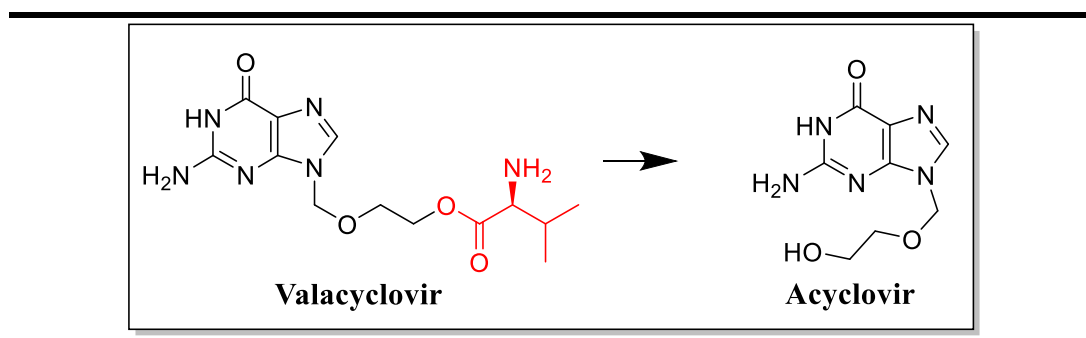


2.1.2.2 Permeability

Despite the risk of poor enzyme bioconversion, amino ester prodrugs can increase the permeability of the prodrug relative to the parent. This is because transport of the drug through the plasma membrane often relies on the use of transporter proteins.¹⁶¹ As

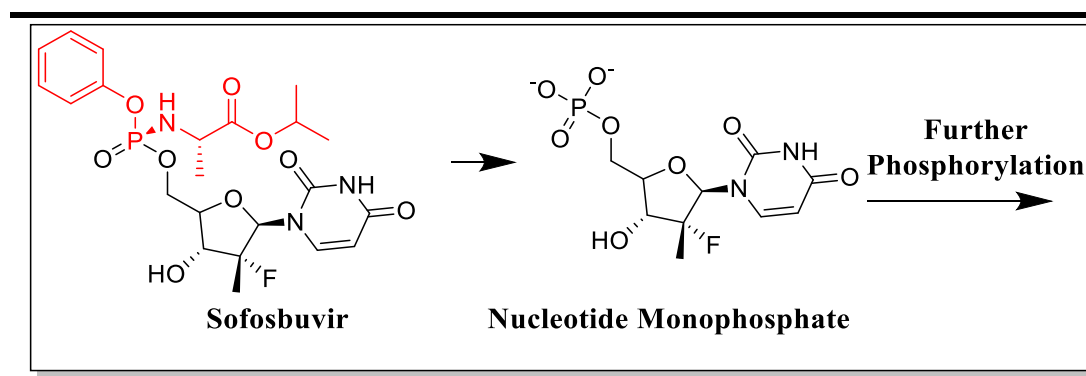
previously discussed, transporters such as OCTs and peptide transporters play a vital role in the distribution of peptidic drug molecules, and thus, by increasing a compound's affinity for these proteins through incorporation of amino acid/dipeptide moieties, one can increase the permeability and thus distribution of a (pro)drug candidate. Beauchamp *et al* used this method in the development of ester prodrug valacyclovir, a herpes virus treatment.¹⁶² By using the L-valyl ester of acyclovir (**Scheme 3**), they found the bioavailability to be 20 to 35% better than the parent drug due to increased uptake by peptide transporter PEPT1.¹⁶³

Scheme 3: Structures of Acyclovir and Valacyclovir



In addition, masking polarizable groups such as carboxyl groups with an ester alternative can lead to increased membrane permeability and distribution. This was achieved in the development of hepatitis C prodrug sofosbuvir. The strongly polar, negatively charged phosphate group in the parent drug was masked creating a prodrug with increased absorption upon oral administration, which was quickly converted to the active monophosphate during metabolism before being phosphorylated further (**Scheme 4**).¹⁶⁴

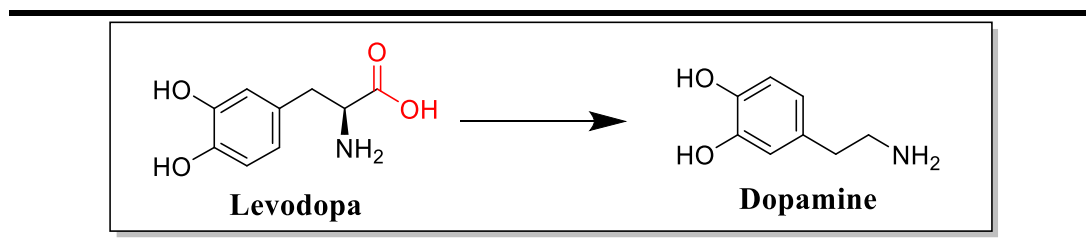
Scheme 4: Structures of sofosbuvir and its active metabolite



2.1.2.3 Distribution

The distribution of a drug upon administration can be altered through employment of a prodrug strategy. Prodrugs can be designed to target/accumulate in tissues which the parent drug would otherwise not associate with. A common example of this is the development of the dopamine anti-Parkinson's prodrug, Levodopa (**Scheme 5**). Dopamine is a neurotransmitter which is unable to cross the blood-brain barrier due to its inherent hydrophilicity.¹⁶⁵ Use of an amino acid analogue of dopamine creates a prodrug which is a substrate for a brain amino acid transporter proteins, and upon decarboxylation causes dopamine accumulation in otherwise unreachable dopaminergic nerves.^{159,166}

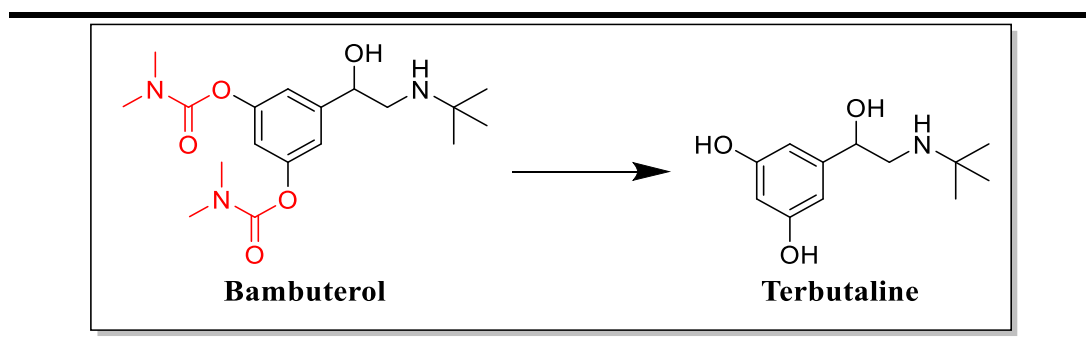
Scheme 5: Structure of Dopamine and it's Prodrug Levodopa



2.1.2.4 Metabolism

Concealing functional groups through development of a prodrug can lead to increased stability towards first pass metabolism. This is because the prodrug itself can be designed to be slowly metabolised instead of its concealed active component. This results in a higher concentration of the active drug reaching the desired location. In the case of terbutaline, conversion of its phenol moieties to more stable carbamate groups, creates a prodrug (bambuterol) with an increased resilience to metabolism and longer lung residency (**Scheme 6**).^{167,168} This prodrug strategy has converted a multiple daily dosed drug into a once daily administered prodrug with reduced side effects.¹⁶⁹

Scheme 6: Structure of terbutaline and bambuterol

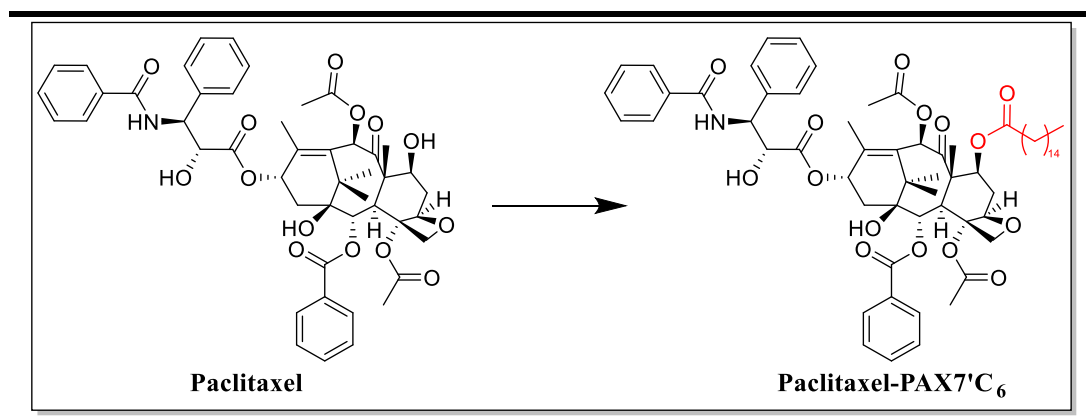


2.1.3 Sustained Release Prodrug Systems

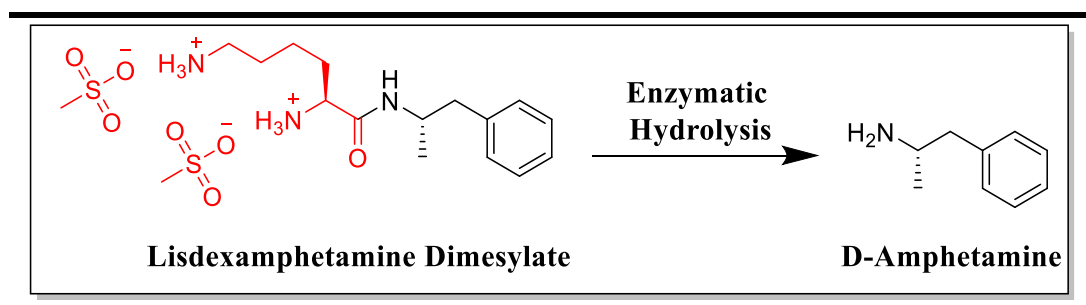
An interesting application of prodrug systems is the development of slow or sustained release systems. These aim to lower the dosage requirements of the initial drug to reduce both the administration frequency and occurrence/severity of adverse side effects present in higher drug concentrations. Typically, these systems involve the derivatisation of drug candidates into highly amphiphilic alky derivatives which then self-assemble into highly soluble micellar structures with internalised hydrophobic

compartments containing drug molecules. Micelle formation possess many advantages including increased gastrointestinal absorption and reduced metabolic degradation which leads to a sustained release of the active drug over time, and thus a prolonged plasma half-life concentration.¹⁷⁰ Recently this idea has been utilised in the development of a paclitaxel acyl ester prodrug for use in cancer treatment (**Scheme 7**). Micelle assembly of this prodrug led to a sustained release delivery system with increased plasma duration for a more effective, sustained delivery of paclitaxel over 24 hours.¹⁷¹

Scheme 7: Structure of paclitaxel and its prodrug paclitaxel-Pax7'C6

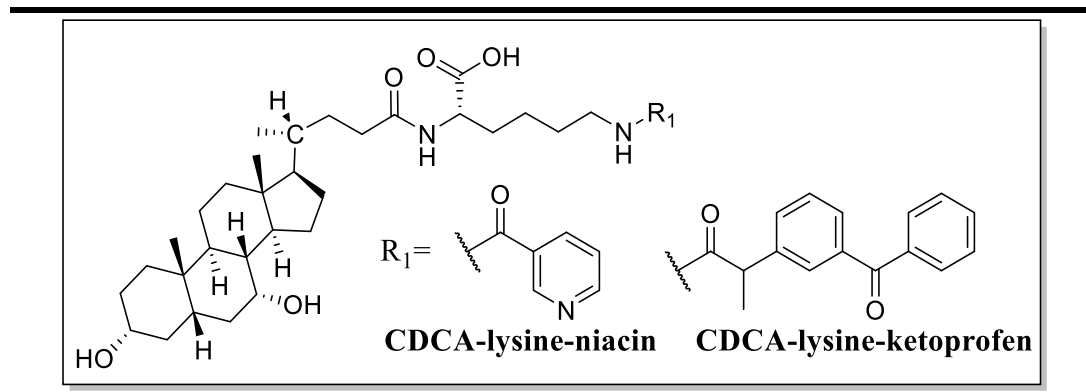


Other forms of sustained release prodrugs include the use of amino acids as pro-moieties which are hydrolysed at a sustained rate to release the drug over an extended period of time. Lisdexamfetamine dimesylate (LDX) is a lysine prodrug of D-amphetamine used in the treatment of Attention Deficit/Hyperactivity Disorder (ADHD) as a psychostimulant (**Scheme 8**).¹⁷²

Scheme 8: Structure of D-amphetamine and its prodrug Lisdexamphetamine Dimesylate

LDX is a sustained release prodrug, absorbed by PEPT1 and other amino acid transporters, designed to be chemically stable until enzymatically cleaved in red blood cells.¹⁷³ Through use of this prodrug approach, the otherwise rapidly metabolised D-amphetamine was converted into a once-daily administered prodrug with extended duration of action of almost 24 hours. This resulted in no abuse potential for the final prodrug and fewer observed side effects due to the lower administered dose.¹⁷⁴

Xiaowan Zheng *et al*¹⁷⁵ applied a similar prodrug approach in their development of sustained release prodrugs of niacin and ketoprofen to improve parent drug availability (**Scheme 9**).

Scheme 9: Structure of Niacin and Ketoprofen Chenodeoxycholate Lysine Linked Prodrugs

Through conjugation of the parent drug to a known bile acid (Chenodeoxycholate) *via* an enzyme hydrolysable linker, they managed to target the apical sodium-dependent bile acid transporter (ASDT) as a mechanism for improving the cellular uptake of the original parent drug, and avoiding extensive first pass metabolism. The prodrugs were then slowly cleaved *via* enzymatic amide hydrolysis during enterohepatic circulation, increasing the cell residency time of the drug.

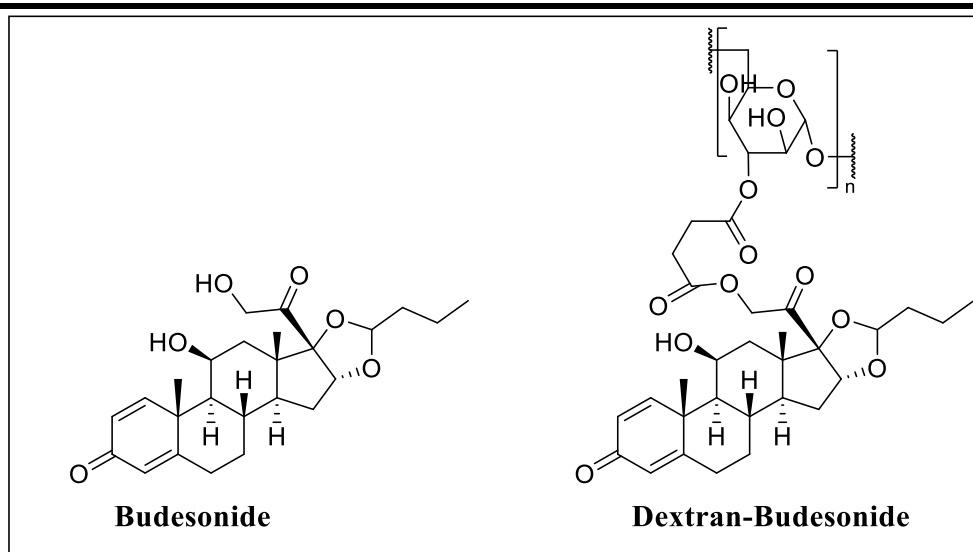
2.1.4 Prodrug application to inhaled administration

Application of prodrug strategies to inhaled delivery provides further opportunity to improve the pharmacokinetic profile of the parent drug. Administration of drugs directly to the site of action through the pulmonary drug delivery route can give significant benefits over other traditional routes of administration: most of which generally rely on obtaining a high plasma concentration of the drug for distribution to the site of action. As well as the administration of the drug directly to the target lung, further benefits arise through the avoidance of first pass metabolism in the liver, reduced drug dosage and thus significant reduction of compound exposure to other organs, ultimately leading to fewer side effects due to less competing secondary pharmacology away from the intended site of action.

As previously mentioned, budesonide is a glucocorticoid with rapid absorption into systemic circulation post inhalation, routinely prescribed to asthma patients as a method of severe exacerbation prevention.¹⁷⁶ Whilst effective, budesonide exhibits a short elimination half-life from the lung tissue (2-3.6 hours) and thus is usually

prescribed as a twice daily inhaled medication. Unfortunately, adherence to the dosing schedule is usually poor,¹⁷⁷ especially in older patients, and thus in 2019 Waters *et al* investigated the potential of dextran-budesonide ester conjugates as slow release prodrugs in attempt to reduce the dosing schedule (**Figure 23**).¹⁷⁸

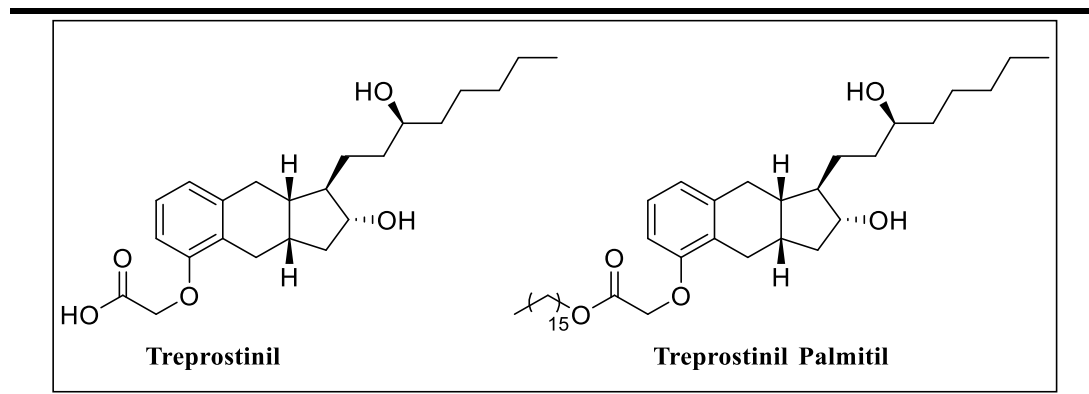
Figure 23: Structure of Budesonide and Dextran-Budesonide Conjugates



As oral agents, dextranase enzymes located in microflora present in the colon are known to hydrolyse the conjugates, rapidly releasing budesonide.¹⁷⁹ However, as inhaled agents, the lack of dextranase enzymes in the lung results in only a slow chemical activation of the prodrug conjugate, meaning a much slower release profile is exhibited. This, in combination with increased hydrophobicity and molecular weight lead to a much slower absorbance across the plasma membrane, and allowed for a depot of inactive prodrug to be created *in-situ* from which the active budesonide was slowly generated.

Treprostinil is another example of an inhaled therapeutic which has benefitted from improved pharmacokinetic properties upon employment of a prodrug strategy. Owing to its short half-life (4.6 Hours)¹⁸⁰, and thus requirement of constant infusion/dosing,¹⁸¹ treprostinil suffers from exacerbated side effects when administered as a pulmonary vasodilator. In order to alleviate the issue, Chapman *et al* sought to apply a prodrug strategy to in order to increase the drug half-life, and reduce the dosing frequency/side effects severity (**Figure 24**).¹⁸²

Figure 24: Structure of Treprostinil and its Prodrug Treprostinil Palmitil

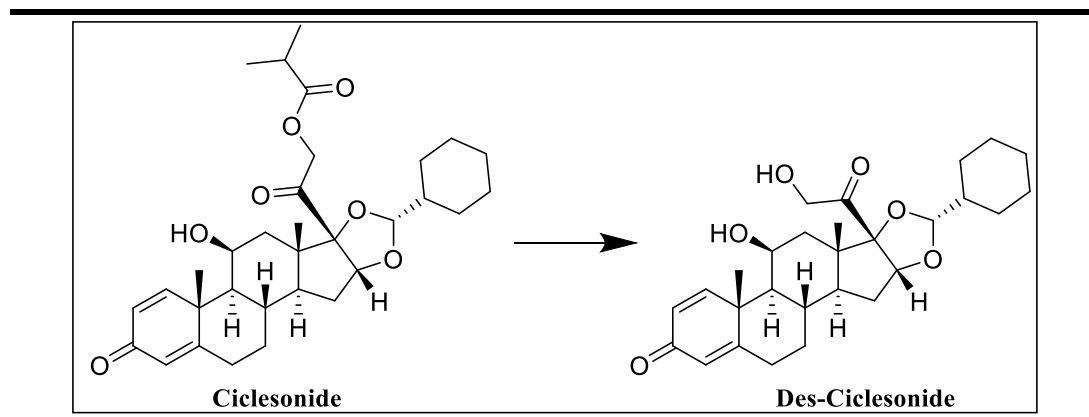


Various esters were synthesised, with longer alkyl chains prodrugs providing the slowest rate of conversion to treprostinil.¹⁸³ It was observed that by inhaling the prodrug treprostinil palmitil, a formylated liquid nanoparticle, as a nebulised suspension, it was possible to achieve a PK profile in which the concentration of treprostinil remained high in the lungs, with minimal exposure to blood plasma.¹⁸⁴

A similar ester prodrug approach was applied to the inhaled corticosteroid ciclesonide for the treatment of pulmonary asthma (**Scheme 10**).¹⁸⁵ When inhaled using an MDI, esterases present in the upper airways convert ciclesonide into the active metabolite

des-ciclesonide which demonstrates a 100x higher receptor binding affinity than ciclesonide.^{186,187}

Scheme 10: Structure of Prodrug Ciclesonide and its Active Metabolite des-Ciclesonide



Despite the recent advances in prodrug systems designed for inhaled administration, there is still a considerable lack of sustained release prodrug systems capable of increasing the duration of action of existing asthma and COPD treatments. As previously mentioned, it is also clear that there is a pertinent need for new, long acting, muscarinic anticholinergics /bronchodilators, and thus application of a prodrug system based upon the inherent lung retention of dibasic compounds may offer a method of converting current short-acting drugs into longer acting treatments.

2.2 Aims

The aims of this first chapter were to investigate the potential of a novel prodrug system to efficaciously deliver an active muscarinic M₃ receptor antagonist over a sustained period. In order to have a longer duration of action relative to the parent drug, the prodrug would incorporate a dibasic component to increase the propensity of both membrane retention and lysosomal trapping.

In order to achieve a sustained delivery with reduced side effects, the final prodrug must adhere to the following requirements:

- The prodrug must be pharmaceutically inactive.
- The prodrug must display an increased aqueous solubility such that the insolubility dosing issues witnessed in **Figure 21** were removed.
- The prodrug must have a high blood stability (> 4 hours) in order to reduce systemic exposure to the active drug.
- The prodrug must be pH-dependently cleaved, i.e. slowly cleaved ($t_{1/2} > 6$ hours) in slightly acidic to neutral conditions (pH 6-7) whilst stable ($t_{1/2} > 10$ hours) at lower pH (pH <6). This pH dependency would ensure that a controlled release of the prodrug at the targeted tissue is achieved through sustained *in-situ* chemical release of the active drug.
- The prodrug system should also be easily amenable to a wide range of drug candidates. i.e. have a chemical structure which is adaptable to different chemotypes.

2.3 Results and Discussion

2.3.1 Design and Synthesis of Prodrug Scaffold.

As previously discussed, general prodrug designs incorporate an active therapeutic agent often tethered by a linker group to a promoiety. When applied to this system, it was decided that an active muscarinic receptor antagonist would be tethered to a potentially lung tissue retentive, dibasic moiety *via* a pH-sensitive, cleavable linker (**Figure 22**). It is theorised that by improving the lung residency time of the drug, this prodrug system could have the capacity to turn a short acting therapeutic into a much longer acting therapeutic through an extended IT-PK profile similar to AZD3199.

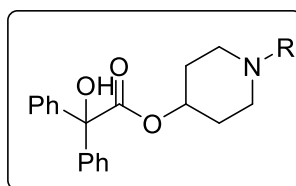
2.3.1.1 Muscarinic Drug Selection

As previously discussed, the recent calls for the withdrawal of tiotropium bromide, alongside a pressing need for novel long acting muscarinic receptor antagonists with improved PK profiles, solidified the decision to incorporate a muscarinic receptor antagonist into the prodrug design. The first step in prodrug design was to select and synthesize a suitable muscarinic receptor antagonist which although highly potent, suffered from poor lung retention and thus was rapidly cleared from the lung. Based on previous work within the Stocks group, a compound with similar chemical structure to compound **A** (page 56) was identified based on the results of various potency and quantitative structure-activity-relationship studies performed initially by TeJani-Butt *et al*¹⁸⁸ in 1990 then further explored by Rong Xu *et al*¹⁸⁹ in 1998.

Initial drug development studies sought to examine the improved anticholinergic response observed by *N*-substituted benzilate esters of quinuclidine and piperidine.

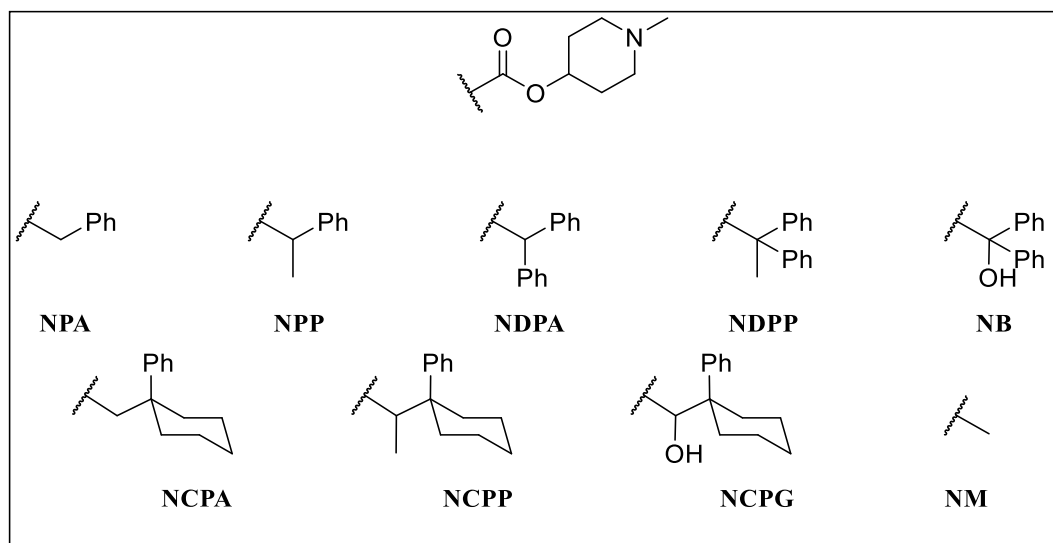
TeJani-Butt *et al* found that small alkyl or aralkyl substitutions onto the nitrogen atom of the piperidyl ring improved the inhibitory constant, K_i , almost 100-fold, citing a small hydrophobic pocket adjacent to the piperidinyll nitrogen as the source of the increased affinity.

Table 5: Structure Activity Relationship of Inhibitory Constant K_i for Benzilate Esters of Piperidine, Reproduced from TeJani-Butt *et al*



R	K_i (nM)
H	2.0 ± 0.2
Me	0.3 ± 0.01
Et	0.5 ± 0.08
n-Pr	36.0 ± 8
i-Pr	8.0 ± 2
$\text{CH}_2\text{C}_6\text{H}_5$	0.2 ± 0.06
$\text{CH}_2\text{C}_6\text{H}_4\text{NO}_2$	13.0 ± 6
$\text{CH}_2\text{C}_6\text{H}_4\text{F}$	3.0 ± 1.0
$(\text{CH}_2)_2\text{C}_6\text{H}_5$	8.0 ± 2.7
$(\text{CH}_2)_2\text{C}_6\text{H}_4\text{NO}_2$	15 ± 2.7

Later, in 1998, Rong Xu *et al* sought to improve the antimuscarinic activity and M2/M3 selectivity of a range of piperidinyll esters (**Table 6**).

Table 6: Physicochemical and Pharmacological Data for *N*-methylpiperidinyl esters, reproduced from Rong Xu *et al*¹⁸⁹

R	pEC ₅₀ (M ₂) ^a	pEC ₅₀ (M ₃) ^b	pEC ₅₀ (M ₃) - pEC ₅₀ (M ₂)
NPA	4.40	5.65	1.25
NPP	5.86	7.32	1.46
NDPA	6.81	7.03	0.22
NDPP	7.87	7.96	0.09
NB	7.58	8.52	0.94
NCPA	7.20	7.61	0.41
R	pEC ₅₀ (M ₂) ^a	pEC ₅₀ (M ₃) ^b	pEC ₅₀ (M ₃) - pEC ₅₀ (M ₂)
NCPP	7.92	8.97	1.05
NCPG	9.07	9.22	0.15
NM	2.48	4.47	1.99

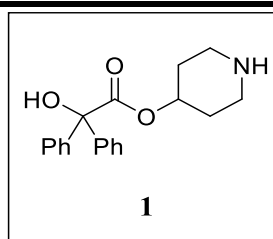
- a) The receptor inhibition is expressed as $-\log EC_{50} (\pm S.E)$ for $n=9-12$ determinations, in which the EC_{50} is the concentration required for 50% inhibition of the ACh-induced contraction of the norepinephrine-induced precontracted endothelium-denuded rabbit aortic rings. The muscarinic receptors in the denuded endothelium have been proposed to belong to the M₂ subtype¹⁹⁰.
- b) The receptor inhibition is expressed as $-\log EC_{50} (\pm S.E)$ for $n=5-6$ determinations, in which the EC_{50} is the concentration required for 50% inhibition of the ACh-induced contraction of the phenylephrine induced precontracted endothelium (intact) of rat aortic rings. The muscarinic receptors in the intact endothelium have been proposed to belong to the M₃ subtype¹⁹¹.

Their results demonstrated the dependency of lipophilicity on antimuscarinic activity, as **NDPP** was almost 1000 times more potent than **NPA** at the muscarinic M₂ receptor and 100 times more potent at M₃. Replacing the methyl group in **NDPP** with the hydroxy group in **NB** increased both the potency and selectivity of the drug at the M₃ receptor whilst also improving the drug solubility. Increasing the lipophilicity further (**NCPA**, **NCPP** and **NCPG**) was found to have no further improvement on the

potency or selectivity; whilst substitution of the bulky phenyl groups for a methyl group (NM) drastically increased the selectivity but reduced the potency 1000-fold.

From both of these studies, the free amino analogue (**Figure 26**) was chosen as the active drug component as it was highly potent, ($K_i 2.0 \pm 0.2$)¹⁸⁸, synthetically achievable without the need for chiral synthesis and contained functionality which allowed for prodrug synthesis. As previously discussed, the steric hinderance surrounding the alcohol group meant that acylation and subsequent prodrug creation would not be possible and hence the amine was identified as an appropriate handle for prodrug development. In addition, due to the widely recognised binding requirement of a basic amine for high affinity, any acylation at this point would remove any pharmacological activity creating an inactive prodrug species.^{192,193}

Figure 26: Structure of the Active Muscarinic Drug



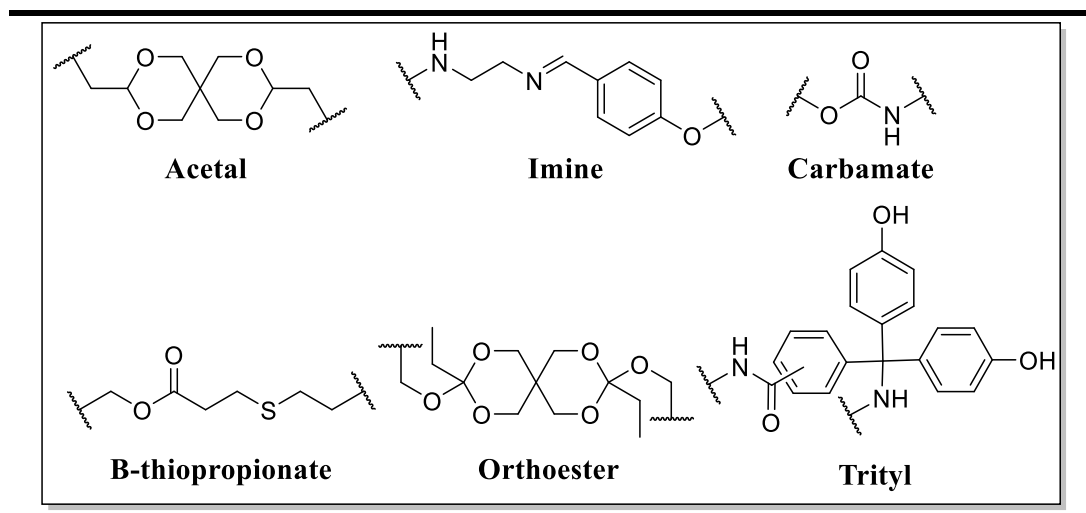
2.3.1.2 Linker Group Design

The linker component of the prodrug is perhaps the most important part of the prodrug design. If the linker breaks down too quickly, then the original active drug will be released too rapidly before the prodrug system is able to achieve an increase in lung retention. Instead, the linker group should be pH activated such that the speed at which

the linker group collapses can be controlled by the external pH, ensuring that the prodrug is able to accumulate within lung tissue (through either membrane binding or accumulation within acidic organelles).

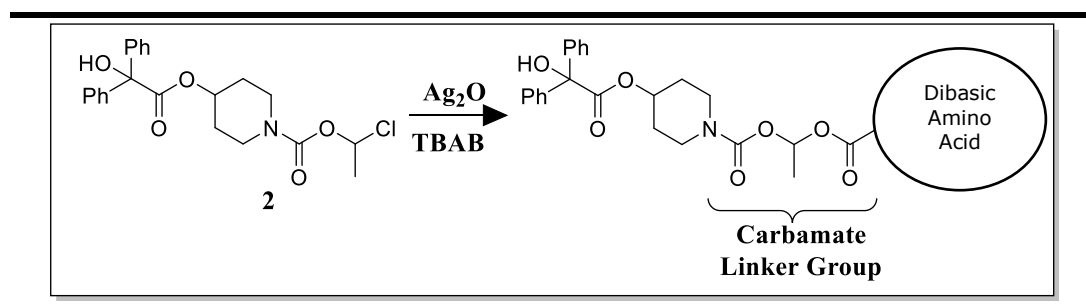
The use of pH sensitive, cleavable linkers has been previously employed in drug delivery systems, including the use of: acetals¹⁹⁴, imines¹⁹⁵, carbamates¹⁹⁶, β -thiopropionates¹⁹⁷, orthoesters¹⁹⁸ and trityls¹⁹⁹, amongst others (**Figure 27**). However, the majority of these linkers decompose rapidly at low pH and are therefore utilised to release the drug in one quick burst.

Figure 27 : pH Sensitive Linkers



Based on unpublished work within the Stocks' group, a carbamate linker group (derived from on 2-chloroethyl chloroformate) was chosen. The use of 2-chloroethyl chloroformate is important as it allows dibasic amino acid moieties to be coupled to the linker group using silver (I) oxide coupling at the chlorine atom (**Scheme 11**).

Scheme 11: Development of Prodrug Scaffold



Importantly, the combination of the carbamate linker group and a dibasic (amino) group allows the cleavage of the linker group to be pH activated. This is because activation of the linker group depends on the availability of a neutral amine group to instigate the cleavage of the prodrug (see 2.3.2.1.1 Monobasic Prodrug Cleavage Mechanism). Thus, by controlling the pKa of the amine group, it is possible to create a prodrug scaffold which is stable at a lower pH.

For this muscarinic prodrug system in which the target receptor for the active drug is located on the plasma membrane, membrane binding is perhaps the most important way of increasing lung residency, as a high membrane binding would ensure a release of active drug in close proximity to the target receptor. This meant that the prodrug must display an appropriate stability in the extracellular medium (approx. pH 7) to ensure a slow activation, allowing the prodrug concentration to build. This is especially relevant, as the lung pH of COPD and asthma patients is made more acidic due to the increased presence of carbon dioxide and thus carbonic acid resulting from the damage caused from the inflammatory response to particulates.^{200,201}

Furthermore, it was also important that the breakdown products from the linker were non-toxic, and rapidly cleared from the lung. The use of the carbamate linker meant

that only carbon dioxide and ethanal would be produced as by products from activation of the prodrugs, both of which are naturally occurring. Whilst the presence of aldehydes is a cause for concern due to their carcinogenic properties²⁰², it should be noted that the incredibly low dose of the administered prodrug ensured that the concentration of ethanal would be negligible compared to that which is consumed during moderate alcohol consumption.

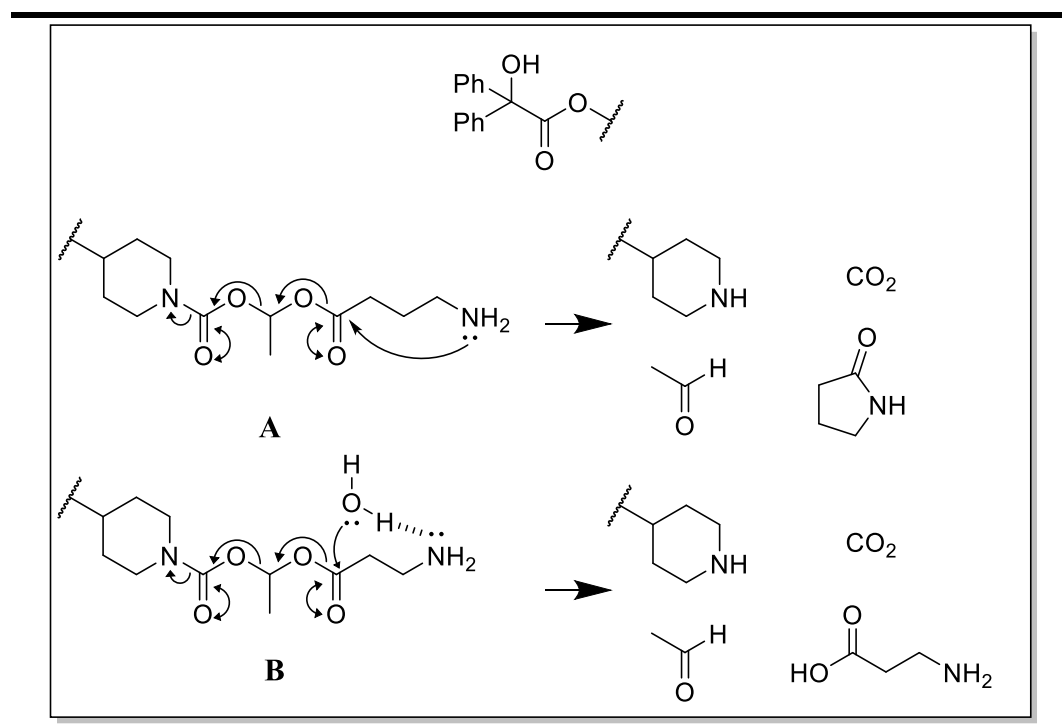
2.3.1.3 Dibasic Amino Acid Design

By selecting/synthesising dibasic amino acids, it was possible to create an overall dibasic species. Utilisation of amino acids in the dibasic moiety, not only optimises the prodrug as potential substrates for peptide transporters, thus increasing the cell permeability of the prodrug, but also ensures that any breakdown products are non-toxic due to the natural occurrence of amino acids in human biology.

2.3.1.3.1 Potential Prodrug Cleavage Mechanism

In order to aid the design of dibasic amino acids, it was first necessary to discover how factors such as pKa and chemical structure would influence the cleavage of the prodrug. When covalently linked to an amino acid, the ester group of the linker would be susceptible to nucleophilic attack, triggering activation of the prodrug. There are two possible mechanisms by which this could occur; direct nucleophilic attack from the neutral component of the deprotected terminal amine forming a strained lactam structure (**Scheme 12A**), or through anchimeric water delivery from the same respective amine, yielding the original amino acid (**Scheme 12 B**).

Scheme 12: Suggested prodrug cleavage mechanisms

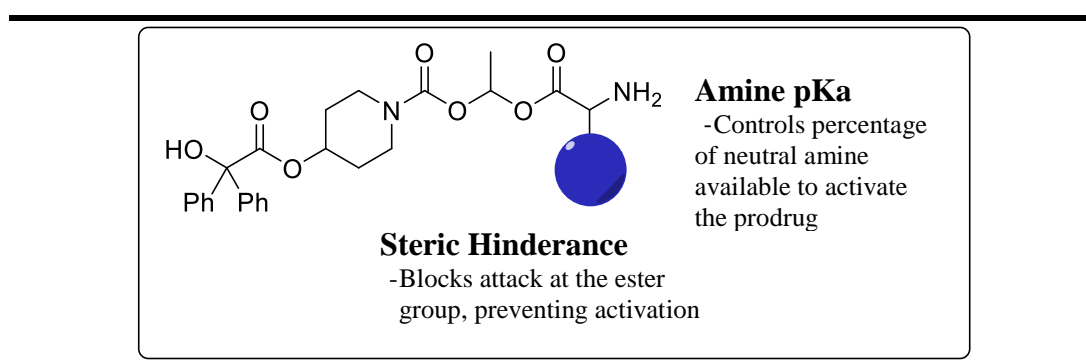


Anchimeric assistance or neighbouring group participation (NGP), is defined as the interaction between a neighbouring, non-conjugated sigma or pi bond within the parent molecule to a reaction centre within the same molecule.²⁰³ In this prodrug system, the neutral portion of the terminal amine is able to coordinate to a water molecule, anchoring it in close proximity to the reactive ester carbonyl, aiding its attack. The requirements and conditions for each possible mechanism were unknown and needed to be investigated in order to fully understand the prodrug activation.

Both cleavage mechanisms are inherently pH dependant due to the requirement of a neutral amine to direct the cleavage. It was therefore important to ensure the final pKa of the basic components were close to physiological pH (7.4), to ensure the presence of neutral amine and to achieve high lung retention based on Perry *et al's* criteria (See Section 1.7). This also presents a method of cleavage rate control, as the smaller the

percentage of neutral amine, the less amine available to cleave the molecule, and thus by controlling the pKa of the amine it is possible to reduce the rate at which the prodrug cleaves. Further to amine pKa, it was also theorized that by using a dibasic amino acid which places a large amount of steric bulk next to the reacting partners, a slower cleavage rate would also be achieved due to steric hinderance, and thus a second method of controlling the cleavage rate would be introduced (**Figure 28**).

Figure 28: Potential Rate Controlling Factors



2.3.2 Synthesis and Evaluation of Monobasic Prodrugs

In order to determine the variables and optimum conditions for a sustained prodrug breakdown, a small library of monobasic prodrugs was first synthesized. This allowed a structure activity relationship (SAR)-like analysis to be performed to discover how the pH, pKa, amine position and substitution, and steric bulk should be balanced to ensure an appropriate rate of prodrug activation.

The decomposition of the deprotected prodrugs in phosphate buffer at 37°C was monitored by LCMS to determine the half-life of the prodrug. Cleavage was stalled by addition of acetic acid to the LCMS sample, and the sample frozen until characterization. This preliminary method was recognised as being limited in terms of

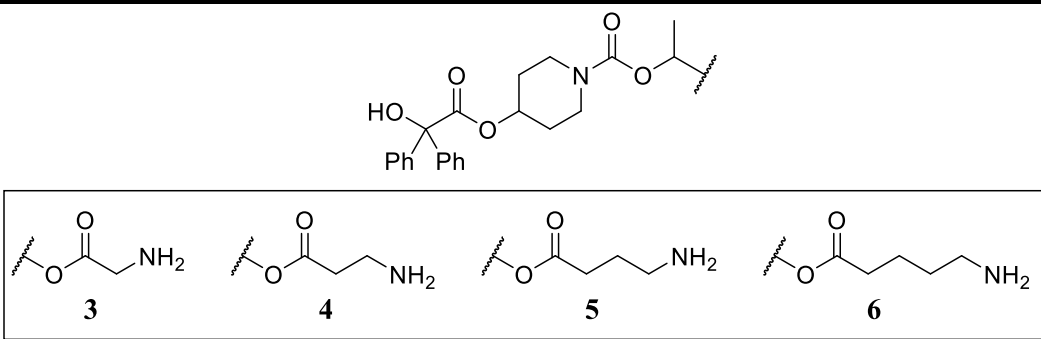
its accuracy, as the acid quench only partly slowed the cleavage. By freezing the samples, cleavage was prevented, however the LCMS samples were not cooled whilst inside the LCMS, and did need to be in solution (not frozen) in order to be tested and hence a degree of inaccuracy was introduced depending on machine availability.

Although subject to some inaccuracy, for this stage of the prodrug design, the results achieved gave a rank order to determine which parameters were more important to achieve a delayed drug release. This data was then used to aid the design of dibasic prodrugs, which would then be tested more rigorously, in triplicate using a high throughput temperature controlled system, calibrated to an internal standard.

2.3.2.1 Amine Position

The first parameter explored was the position of the amine, and how this might affect the rate and mechanism by which the prodrug cleaves (**Table 7**).

Table 7: Exploration of Amine Position on Stability



Compound	Buffer $T_{1/2}$ (Hr) pH 6.5 ^a	cpKa ^b
3	0.52	7.1
4	7.31	9.3
5	0.07	10.1
6	<0.01	10.2

^a Buffer stability was determined using **Biological Assay Procedure 3** using pH 6.5 phosphate buffer solution as the reaction matrix.

^b Predicted using Marvin Sketch

Sequentially moving the amino group one carbon further away from the ester group (**3-6**) raises basicity of the nitrogen and hence the calculated pKa rises to a predicted value of 10.2. It was expected that, as the pKa rose and thus the degree of amine protonation increased, the rate of cleavage should decrease. This trend was observed by the α - and β -substituted prodrugs (**3** and **4** respectively), but was not continued in the γ - and δ -substituted prodrugs (**5** and **6** respectively). The fact that the cleavage rate was increased for these prodrugs suggested that a change in cleavage mechanism had occurred.

2.3.2.1.1 Monobasic Prodrug Cleavage Mechanism

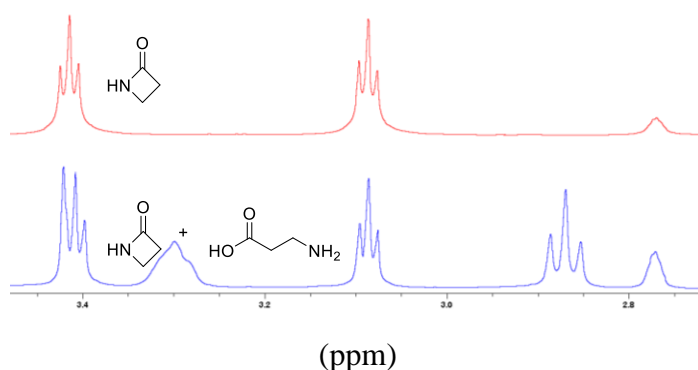
It was predicted that the shorter, α and β positioned amine prodrugs (**3-4**) would cleave *via* an intramolecular water delivery mechanism due to the unfavourable, strained 3- and 4-membered lactams that would form in the case of an intramolecular nucleophilic attack of the amine. The final cleavage products from this reaction would be that of the original carboxylic acid, the free drug, ethanal and carbon dioxide.

In the case of γ and δ positioned amines (**5-6**), it is thought that the unfavourable 7- and 8- membered transition states that would be present through anchimeric assistance, coupled with the reacting groups being positioned further apart, results in an intramolecular nucleophilic attack rather than an anchimeric-assisted delivery of water. This intramolecular reaction would be thermodynamically driven as the final amide is of lower energy than the ester and comprises of an unstrained ring structure. A change in reaction mechanism results in different cleavage products meaning that a 5- or 6- membered lactam would be formed instead of the original carboxylic acid.

Due to the fact that it was only possible to analyse the cleavage products once the prodrug had fully cleaved, one possibility that was considered when debating the reaction mechanism, was whether a strained α or β lactam in an abundance of water would be able to ring open and reform the original carboxylic acid. If this were possible then the reaction may appear concerted, following an anchimeric delivery mechanism, when in fact it was an intramolecular nucleophilic attack but then the intermediate heterocycle formed by this was unstable under the cleavage conditions and thus the cyclic lactam reopened to form the original amino acid.

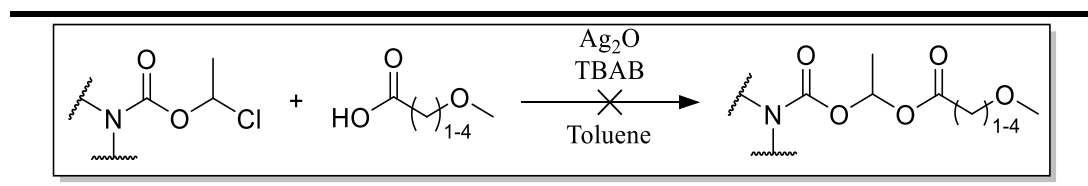
To test this hypothesis, a sample of the beta lactam (azitidin-2-one) was placed into the equivalent deuterated cleavage conditions, and the NMR spectra monitored overtime. The corresponding amino acid (3-aminopropanoic acid) was then subsequently added to the cleavage products to see if the NMR peaks for each species overlapped (**Figure 29**). The results of this showed that the spectra did not change over time, nor did the amino acid NMR peaks align with the lactam peaks proving that this species is not present during the cleavage of the prodrugs.

Figure 29: NMR Spectra of azitidin-2-one with and without 3-aminopropanoic acid



In order to test this hypothesis further, the synthesis of a range of α - δ ether containing prodrugs was attempted, to compare their stabilities to the equivalent amine analogues (**Scheme 13**). This would have provided further evidence for anchimeric water delivery, as the alkylated oxygen would be able to deliver the water molecule, but wouldn't be able to participate in a nucleophilic attack. Unfortunately, during the silver-oxide assisted coupling, the oxygen atom coordinates to the silver precipitating out of the reaction, and no prodrug was observed. Due to the reactive electrophilic nature of the linker, any reaction involving a nucleophile could not be attempted and thus it was not possible to synthesize this range of prodrugs.

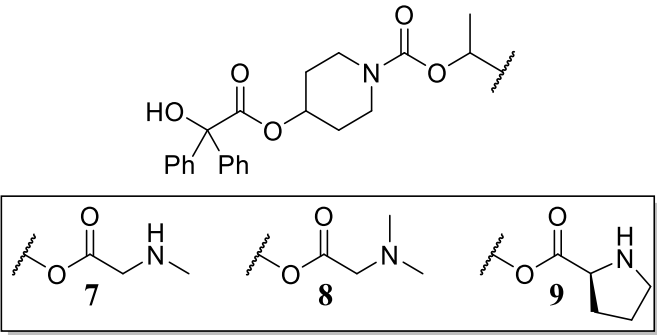
Scheme 13: Attempted Synthesis of Ether Prodrugs



2.3.2.2 Amine Alkylation

With the cleavage mechanism investigated, attention turned to how alkylation of the amine would affect the rate of cleavage (**Table 8**). It was expected that alkylation of the terminal amine would have a less pronounced effect on pKa than the position of the amine. Instead, addition of steric bulk may hinder the anchimeric assistance and delay activation of the prodrug.

Table 8: Exploration of Amine Substitution on Stability



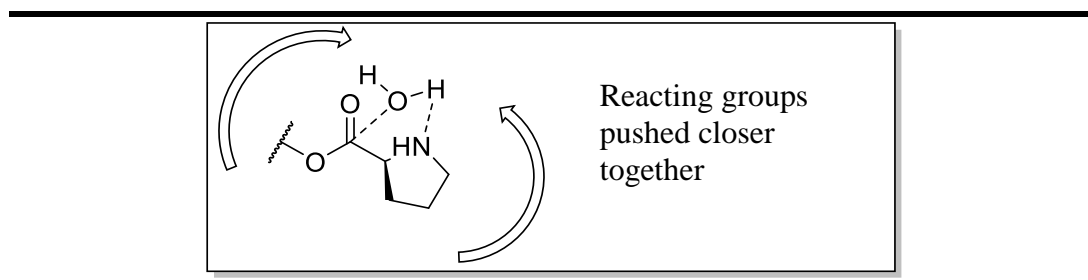
Compound	Buffer Stability pH 6.5 $T_{1/2}$ (hr) ^a	cpKa ^b
7	0.39	6.44
8	3.53	6.57
9	0.14	7.45

^a Buffer stability was determined using **Biological Assay Procedure 3** using pH 6.5 phosphate buffer solution as the reaction matrix.

^b Predicted using Marvin Sketch

As expected, direct mono *N*-alkylation (**7**) reduced the pKa of the amine which dramatically increased the cleavage rate (compared to **3**). Dialkylation (**8**), whilst again reducing the pKa, lead to a slower cleavage rate presumably for increased steric reasons and loss of H-bond donor properties. The use of proline (**9**) caused the cleavage rate to increase rapidly despite raising the pKa. This was rationalised due to Thorpe-Ingold effects which pushes the two reactive components together to relieve steric strain (**Figure 30**).^{204,205}

Figure 30: Thorpe-Ingold effect exerted by the proline side chain



2.3.2.3 C-1 Substitution

As previously mentioned, the size of the amino acid R group is another method by which the rate of prodrug activation can be controlled. By placing a large sterically hindering group next to the carbonyl group, attack at this carbon would be sterically hindered and thus it was important to investigate how the size of the C-1 side chain affects its potential to sterically hinder nucleophilic attack of the carbonyl (**Table 9**).

Table 9: Exploration of C-1 Substitution on Stability

Compound	Buffer $T_{1/2}$ (hr) pH 6.5 ^a	cpKa ^b
10	1.71	7.3
11	3.05	7.6
12	2.93	7.4
13	5.09	7.4
14	15.84	7.5
15	12.16	7.2
16	13.92	7.5

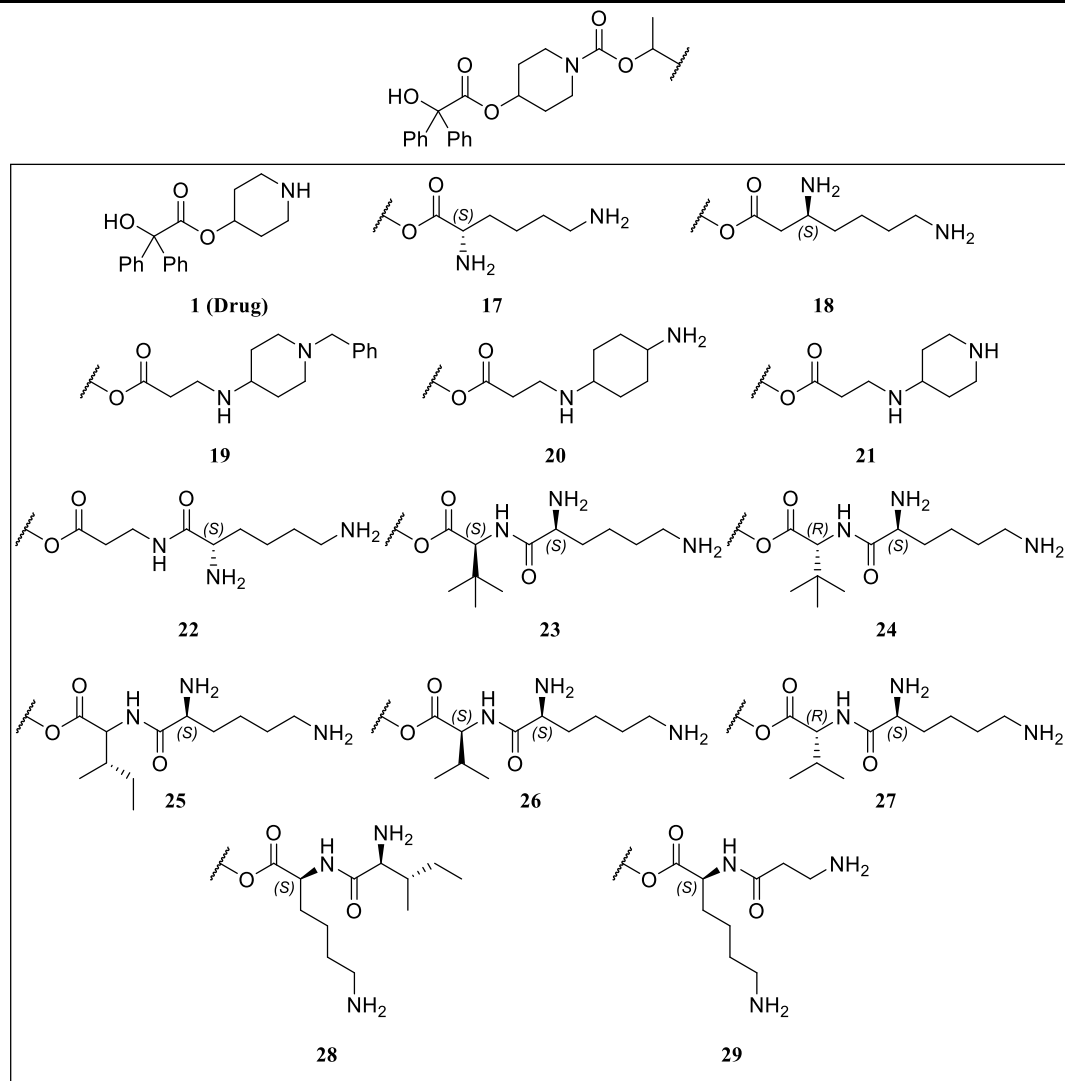
^a Buffer stability was determined using **Biological Assay Procedure 3** using pH 6.5 phosphate buffer solution as the reaction matrix.

^b Predicted using Marvin Sketch

This data demonstrated how bulkier amino acid side chains slow the cleavage of the prodrug by sterically hindering the delivery of water. This resulted in slower cleavage rates in prodrugs (**10-16**) compared to **3**.

2.3.3 Synthesis and Evaluation of Dibasic Prodrugs

From the monobasic prodrug cleavage data, it was clear that there were two possible design approaches when designing dibasic amino acids. One route was to have an α -positioned amino acid with a large bulky side group to reduce the rate of cleavage, while the other approach had a β -positioned amino acid which would rely on the higher amine pKa to reduce cleavage rate. Once incorporated, these α and β amino groups could then be derivatised to contain a second basic component, in which the cleavage mechanism relies solely on anchimeric assistance (**Table 10**)

Table 10: Exploration of Dibasic Prodrug Stability and Binding (performed at GSK)

Cmpd	Buffer $T_{1/2}$ (hr) pH 6.5 ^a	Buffer $T_{1/2}$ (hr) pH 7.4 ^a	cpKa ^b B1	cpKa ^b B2	Rat Lung Homogenate $T_{1/2}$ (hr) ^c pH 6.8	Rat Blood $T_{1/2}$ (hr) ^d pH 7.2	Rat Lung Homogenate Binding (% Free) ^e
1 (Drug)	-	-	10.0	-	Stable	Stable	18.3 ± 1.70
17	3.9 ± 0.05	1.1 ± 0.02	7.4	10.1	- ^f	- ^f	- ^f
18	29.1 ± 1.49	5.9 ± 0.13	9.4	10.2	3.1 ± 0.38	0.3 ± 0.02	- ^f
19	7.9 ± 1.28	1.8 ± 0.02	10	7.4	- ^f	- ^f	- ^f
20	11.1 ± 1.39	1.9 ± 0.08	9.8	10.5	3.5 ± 0.15	0.1 ± 0.00	- ^f
21	9.7 ± 1.11	1.8 ± 0.06	7.9	10.3	- ^f	- ^f	- ^f
22	54.5 ± 3.16	44.8 ± 0.88	8.4	10.1	0.6 ± 0.04	- ^f	- ^f
23	186 ± 0.79	67 ± 0.23	8.4	10.1	2.5 ± 0.07	0.2 ± 0.01	- ^f
24	58.6 ± 4.91	36.6 ± 1.70	8.4	10.1	25.4 ± 1.94	7.0 ± 0.82	0.5 ± 0.10
25	17.6 ± 1.26	8.7 ± 0.69	8.4	10.1	0.8 ± 0.08	- ^f	- ^f
26	14.4 ± 1.68	4.4 ± 0.39	8.4	10.1	0.6 ± 0.09	- ^f	- ^f
27	8.7 ± 1.06	1.8 ± 0.20	8.4	10.1	3.4 ± 0.08	0.6 ± 0.07	- ^f
28	4.9 ± 0.06	0.9 ± 0.04	10.1	8.5	- ^f	- ^f	- ^f
29	102.2 ± 3.86	11.5 ± 0.73	10.1	9.0	0.7 ± 0.21	- ^f	- ^f

a) Buffer stability was determined in triplicate at 37°C using **Biological Assay Procedure 2** using pH 6.5 or 7.4 phosphate buffer solution as the reaction matrix. The mean determined value is displayed ± standard deviation. Quantified using mass spec analysis quantifying against internal standards Labetalol and Reserpine.

b) Predicted using Marvin Sketch

- c) Rat lung homogenate stability was determined in triplicate at 37°C, using **Biological Assay Procedure 2** using a 1 in 4 aqueous dilution of rat lung homogenate as the reaction matrix. The mean determined value is displayed \pm standard deviation. Quantified using mass spec analysis quantifying against internal standards Labetalol and Reserpine.
- d) Rat blood stability was determined in triplicate at 37°C using **Biological Assay Procedure 2** using rat blood as the reaction matrix. The mean determined value is displayed. Quantified using mass spec analysis quantifying against internal standards Labetalol and Reserpine.
- e) Rat lung homogenate Binding was determined in triplicate at 37°C, using a 1 in 4 aqueous dilution using **Biological Assay Procedure 3** using a 1 in 4 aqueous dilution of rat lung homogenate as the reaction matrix. The mean determined value is displayed. Quantified using mass spec analysis quantifying against internal standards Labetalol and Reserpine.
- f) Not determined as previous biological stability was unacceptable.

2.3.3.1 Biological Evaluation:

The compounds were tested systematically for their phosphate buffer, rat lung homogenate and rat blood stability and rat lung homogenate binding.

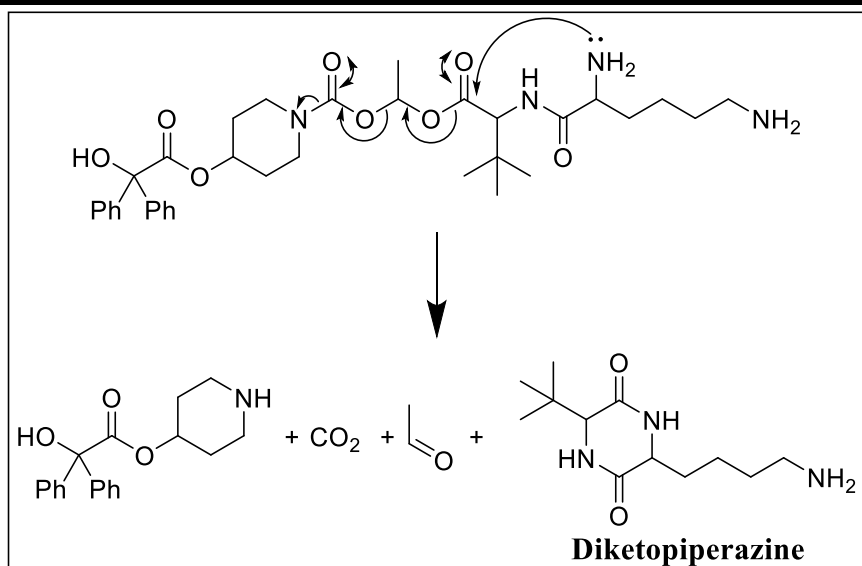
2.3.3.1.1 Phosphate Buffer Solution Stability Determination:

The buffer stability was determined to provide the maximum possible stability the prodrugs would have in the complete absence of enzymatic activity, i.e. the cleavage rate due to self-activation due to the prodrugs' intrinsic chemical instability. This was tested in triplicate at 37°C at both pH 6.5 and 7.4, representing the estimated (averaged) temperature and pH of the lung lining fluid and blood respectively.

Compounds **17** and **18** displayed the same trend as was witnessed for the monobasic prodrugs, with the α -amino group giving a much faster cleavage rate than the β -amino prodrug. The derivatised β -amino compounds (**19-21**) showed similar results to that of sarcosine (**7**) in the initial monobasic prodrug tests, in that alkylation on the terminal nitrogen lowered the pKa of the amine resulting in a reduced cleavage rate.

Unfortunately, as the mono-amino acid prodrugs (**17-21**) did not have a sufficient stability profile to progress further, an alternative strategy was sourced. In order to incorporate a sterically hindered α -positioned amino group, a series of dibasic dipeptides were created. The sterically hindered ester group would then have increased resilience to nucleophilic attack, and thus the prodrug cleavage would depend less on the terminal amine pKa, and more on the steric bulk blocking the cyclisation. This is because cleavage would now take place *via* an intramolecular diketopiperazine (DKP) formation mechanism (**Scheme 14**), in which the intramolecular cyclisation would occur *via* the nucleophilic attack of the primary amine of the first amino acid to the ester. This would create a 6-membered diketopiperazine, the formation of which would be more heavily influenced by steric hindrance rather than by the pKa of the nucleophilic amine.

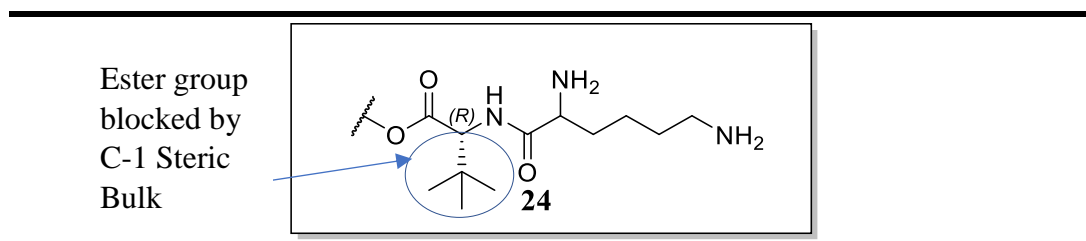
Scheme 14: Dipeptide Breakdown into DKP



Due to the dibasic requirements of the prodrug, lysine was used as one of the amino acids in the dipeptides, as this would provide the second dibasic component. These prodrugs (**22-29**) were found to have a range of stabilities in phosphate buffer. As

previously witnessed, the bulkier the C-1 group the lower the rate of cleavage, and hence the rate increases from compound **28** which has a relatively small α -substituent, to the highly hindered tertiary butyl group in compound **24** (**Figure 31**).

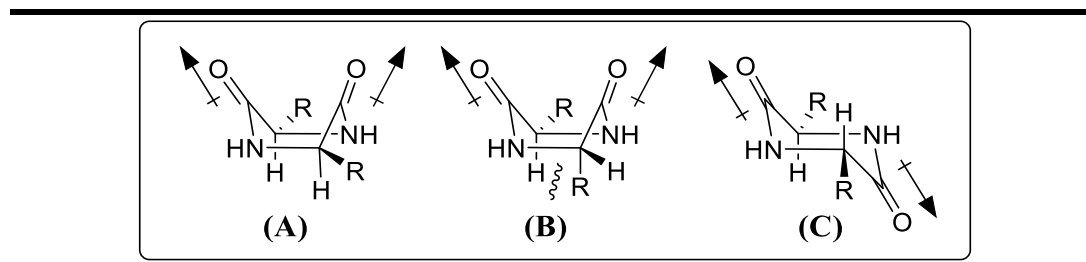
Figure 31: Rate Determining C-1 Steric Hinderance



Both compound **22**, **28** and **29** demonstrated an increased buffer stability due to the formation of an unfavourable 7 membered DKP- like species, however **29** also had the added effect of the higher amine pKa which hindered cleavage further.

The most interesting results came from **24** and **27**. In order to increase chemical stability and reduce internal steric clashes, diketopiperazines place both R groups in pseudo-equatorial positions resulting in a boat shape configuration (**Figure 32A**).^{206,207}

Figure 32: Diketopiperazine Low Energy Conformation; A) Boat Conformation with Natural Isomers, B) Boat Conformation with Unnatural Isomers C) Chair Conformation with Balanced Dipoles



For this reason, it was hypothesized that by inverting the stereochemistry of one of the amino acids in the dipeptide, a destabilising steric clash would be formed (**Figure 32B**) which would make the DKP less likely to form, thus increasing the stability of the prodrug. However, when the stability was tested in compounds **24** and **27**, the prodrug stability in aqueous buffer did not improve relative to compounds **23** and **26**. This could be explained by a shift in the DKP structure to a more chair-like conformation in order to reduce the steric clash between the hydrogen atom and the R group, and to balance the two carbonyl dipoles which would be uneven in the boat conformation for the L, L-dipeptide (**Figure 32C**).

2.3.3.1.2 Rat Lung Homogenate Stability Determination:

The next stability to be determined was the prodrug stability in rat lung homogenate. This would be the first stability determination to incorporate enzymatic activity into the stability estimate. Due to the nature of lung homogenate, it is only an estimated averaged representation of the enzymatic environment within lung tissue, as creating the lung homogenate breaks down membranes of compartmentalized cells and organelles when the organ is ground. This removes enzymes from their natural working environment and instead averages out their concentration, distribution and activity. In addition, the lung homogenate must be diluted 1 in 4 with water in order to be able to sample the matrix. It is therefore likely that the stability value obtained from this experiment is an overestimation of the true metabolic stability. Fortunately, it provided sufficient data to estimate the prodrug stability due to enzymatic cleavage, before advancing to a more accurate *in-vivo* analysis.

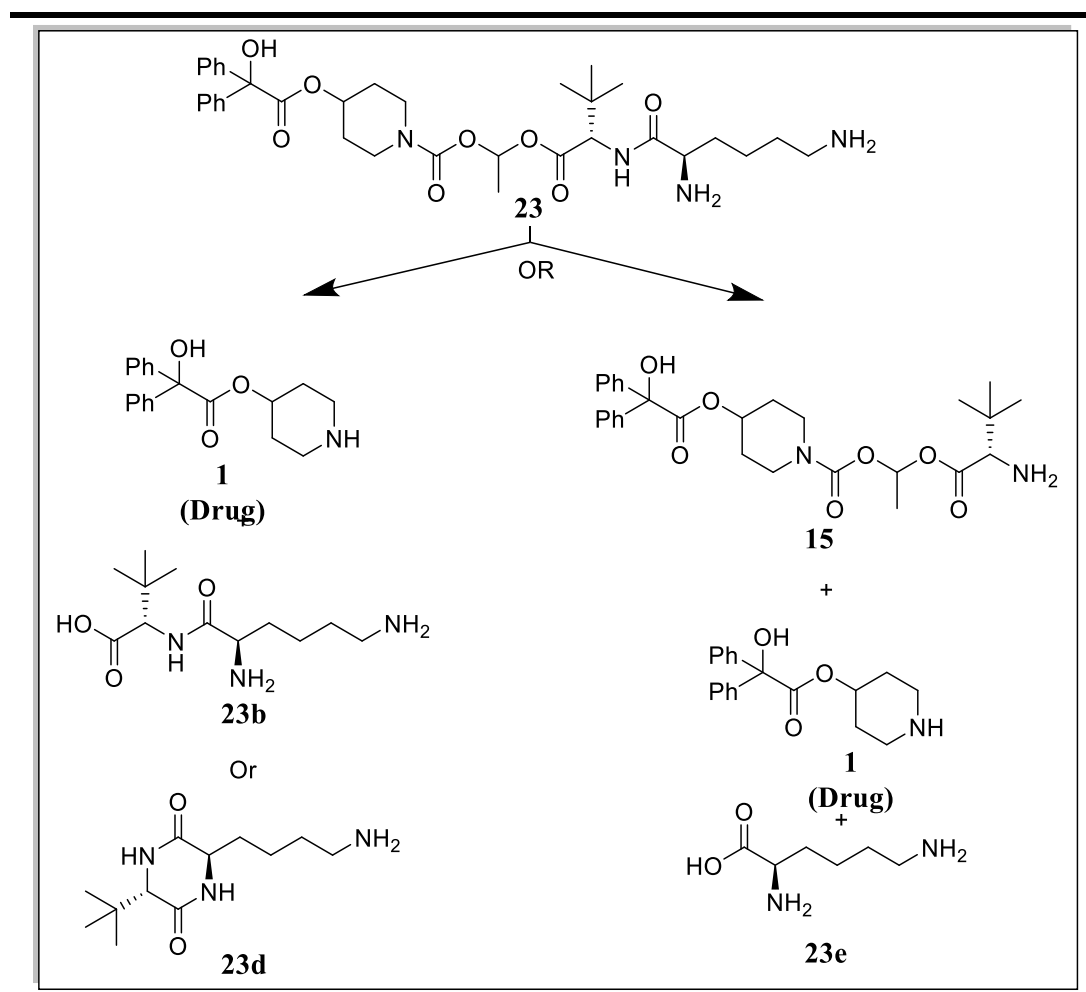
Based on the phosphate stability studies and the prediction that enzymatic activity will increase the cleavage rate, the only compounds that proceeded to rat lung homogenate studies were compounds **18**, **20**, **22-27** and **29**. Wistar Han rat lung homogenate was prepared according to Biological Assay Procedure **2**, and the pH (at a dilution of 1 to 4 in water) was experimentally determined to be 6.8.

The results demonstrated that most of the prodrugs were indeed subjected to a high level of enzymatic metabolism, with the dipeptide prodrugs (**22-29**) being hydrolysed to a greater extent relative to the β -amino prodrugs (**18-21**). The other clear conclusion to be drawn from the lung homogenate stability results was that compounds **24** and **27** in which the chirality of one of the amino acids was inverted from their natural isomer (**23** and **26** respectively), were much more stable relative to their natural isomer matched pair. It is thought that by inverting the chirality, enzymatic cleavage at either the ester or amide bond has been prevented, possibly through removal of the compounds recognition for the enzymes' active site. This could also explain the lack of enzymatic breakdown for compounds **18** and **20**. These compounds also contain unnatural amino acids which are less likely to be recognised by enzymes, reducing their susceptibility to enzymatic cleavage.

2.3.3.1.3 Enzymatic Cleavage Pathway

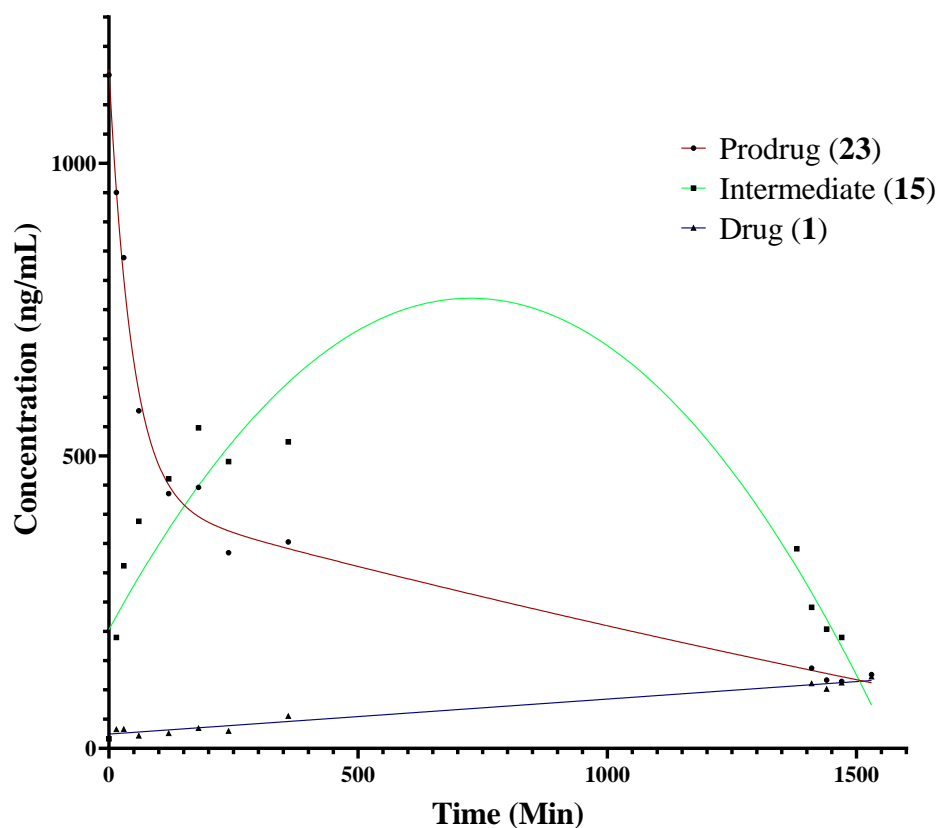
In order to fully understand the enzymatic cleavage that was present (or absent) for compounds **23** and **24**, the lung homogenate stability assay was repeated and the mass spec tuned to detect the intermediate mono-basic species produced if the terminal lysine residue was removed due to peptidic amide bond hydrolysis (**Figure 33**).

Figure 33: Example Dipeptide Enzymatic Pathway



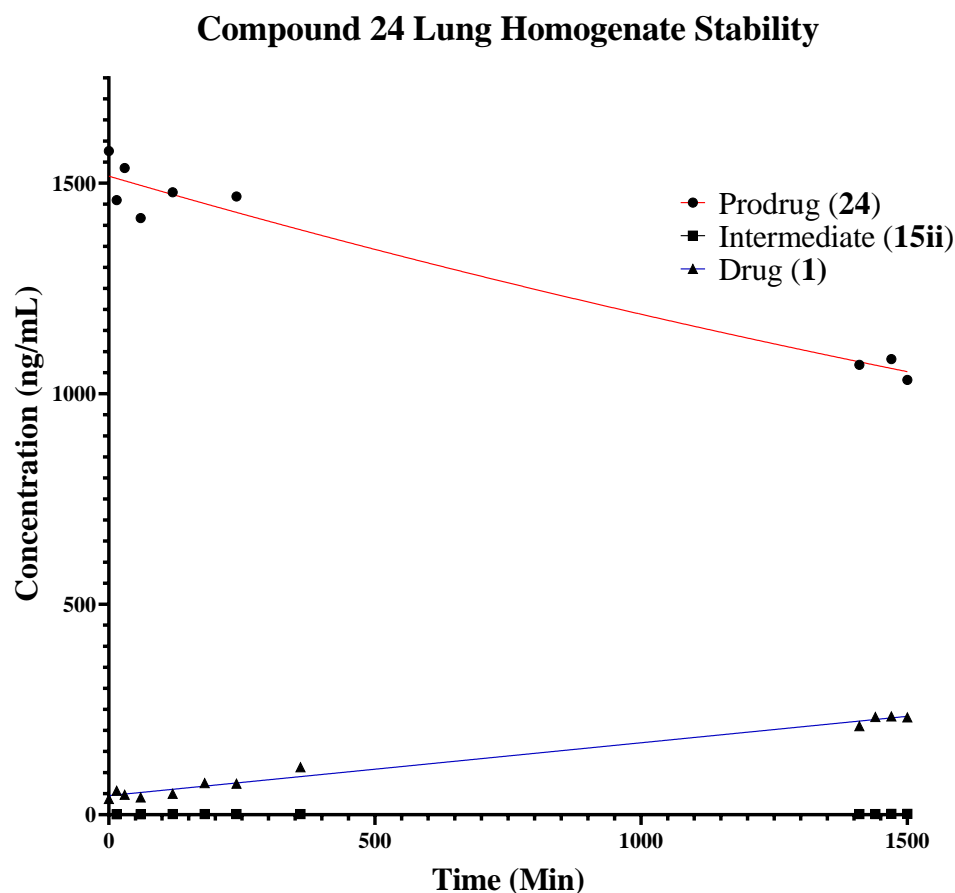
It was concluded that if an enzyme had cleaved the amide bond then there should be a high concentration of the monobasic, tertiary butyl intermediate (15). Theoretically this would have poor lung tissue retention due to the loss of the second basic centre, and thus would be eliminated from the lung tissue. The results demonstrated that the prodrug with natural chirality (23) was subject to high enzymatic amide bond hydrolysis, creating a high concentration of monobasic intermediate (15) (Figure 34). The unnatural isomer (24) did not display any enzymatic amide hydrolysis, thus explaining the increased prodrug stability observed in rat lung homogenate (Figure 35)

Figure 34: Prodrug Cleavage Graphs for Compound 23

Compound 23 Lung Homogenate Stability

Analysis of route of cleavage for compounds 23 in rat lung homogenate demonstrating different hydrolysis routes. Enzymatic cleavage of the natural isomer of prodrug 23 (red) into the monobasic intermediate 15 (green) followed by further chemical cleavage into the parent drug 1 (blue). Compounds were incubated into $n=3$ Wistar Han rat lung homogenate, at a nominal concentration of 1500 ng/mL and breakdown followed over 1500 min using MS/MS analysis against authenticated samples. Lower Limit of Quantification (LLOQs): 1 (20 ng/mL); 15 (0.2 ng/mL); 23 (2 ng/mL) and Data processed using GraphPad PRISM V7.02.

Figure 35: Prodrug Cleavage Graphs for Compound 24



Analysis of route of cleavage for the unnatural amino acid prodrug **24** (red), as indicated by the lack of detection of intermediate **15ii** (green). Instead only chemical cleavage of **24** into parent drug **1** (blue) is detected. Compounds were incubated into $n=3$ Wistar Han rat lung homogenate, at a nominal concentration of 1500 ng/mL and breakdown followed over 1500 min using MS/MS analysis against authenticated samples. Lower Limit of Quantification (LLOQs): **1** (20 ng/mL); **24** (2 ng/mL) and **15ii** (1 ng/mL). Data processed using GraphPad PRISM V7.02.

2.3.3.1.4 Rat Blood Stability Determination:

Rat blood from Wistar Han rats was taken and used undiluted to test the stability of compounds **18**, **20**, **23**, **24** and **27**. The results achieved were consistent with the hypothesis that the increase in pH from rat lung homogenate to rat blood (6.8 and 7.4 respectively) and the higher concentration of enzymes (in their optimum working environment) would lead to a decrease in the prodrug stability. Indeed, most compounds cleaved very rapidly, with compound **24** being the only exception, with a half-life of 7 hours due to increased enzymatic stability. This value for compound **24**

is encouraging as it would mean that any inactive prodrug which leaves the lung tissue would not instantly decompose to the active drug, instead it will remain as the inactive prodrug thus potentially preventing side effects caused by any secondary pharmacology of the active drug in other target organs, such as the heart.

2.3.3.1.5 Binding Determination

In order to determine the compounds tissue affinity, the prodrug must display considerable stability in rat lung homogenate. To comply with the GSK standard assay procedure, the incubation period in this experiment is a minimum of 4 hours and thus only prodrugs which displayed a blood stability considerably greater than 4 hours could be tested. For this reason, only compound **24** and the parent drug (**1**) were able to be tested in the rat lung homogenate binding assays.

As previously discussed, the value achieved from the binding assays gives an estimated value of the amount of unbound drug available to interact with the target receptor. For a muscarinic prodrug where the target muscarinic M₃ receptor is membrane bound and a high lung retention is desired, a high lung homogenate binding fraction for the prodrug is required. This increases the possibility that the prodrug will bind to the lung tissue and slowly activate to release the active drug in close proximity to muscarinic M₃ receptors.

It should be noted once again that the lung homogenate binding assay is a 'best case scenario' value as homogenising and diluting a rat lung causes all internalised compartments and pH's to be averaged such that the resulting pH is more or less acidic

than would be expected. As previously mentioned, pH within the lung can vary however, the experimentally determined pH of rat lung homogenate was found to be 6.8. Since the electrostatic binding of a compound to a phospholipid bilayer is known to depend on the extent of ionisation, the determined *in-vitro* binding value may be an over estimation for the cell membrane as the compound could be less ionised *in-vivo*.

The binding value determined for compound (**24**) indicates that the prodrug is very highly bound in lung homogenate (99.5% bound), supporting the hypothesis that a dibasic compound can exhibit increased high lung retention. Pleasingly the parent drug is less highly bound, with approximately 18% of the compound unbound to interact with the target receptor.

2.3.3.1.6 Pharmacokinetic Studies – Performed by Signature Discoveries

From the results of the *in-vitro* stability and binding assays, it was clear that there were several compounds which could proceed to an *in-vivo* pharmacokinetic study. Compounds **18**, **20**, **24** and **27** all possessed interesting lung homogenate stabilities, with compound **24** being of particular interest due to the observed lack of enzymatic cleavage. As the increased stability of compound **24** had led to full characterisation of its binding parameters and demonstration of higher stability in rat blood, this compound was chosen to undergo an *in-vivo* pharmacokinetic study.

When designing the pharmacokinetic study (See below), it was important to ensure that the dosing concentration was high enough to allow for detection of the drug and prodrug at the terminal time point. For this reason, the compounds were dosed at a

high concentration of 0.2 mg/Kg. In the initial PK studies (see page 56) the compounds had suffered from poor solubility in the dosing media, however the prodrug dosed in this study (24) was fully soluble, demonstrating an immediate advantage of the prodrug system as a poor drug physiochemical property such as aqueous insolubility, can easily be overcome to aid delivery. This alleviates a common problem exhibited during inhaled administration, as insolubility can often cause inflammation of the airway, which usually results in more severe exacerbations.

2.3.3.1.6.1 Pharmacokinetic Study Design – Drug (1)

Compound (1) was dosed intratracheally into three Sprague Dawley rats at a concentration of 0.2 mg/kg in ethanol: pH 6.5 Phosphate Buffered Saline (5:95). Blood samples were taken *via* the cannulated jugular vein at, 0.5, 1, and 3-hour time points, and the concentration of drug measured. At 3 hours, the rats were terminated and the lungs harvested to allow quantification of the remaining lung concentration at 3 hours.

2.3.3.1.6.2 Pharmacokinetic Study Results – Drug (1)

The concentration of the drug in the blood was below the lower level of quantification for all time points and thus was not detected. At 3 hours, the percentage of administered drug remaining in the lung was 0.33% (± 0.06), meaning that >99% of the administered dose was eliminated from the lung within the first 3 hours after administration, disregarding any oral bioavailability from active drug being swallowed. This result demonstrates the very poor lung retention of compound 1, which could be translated to a very short observed pharmacodynamic duration of

action. The average concentration of active drug in the lung at 3 hours was determined to be 137 ± 31 ng/g of homogenised lung tissue (0.44 ± 0.1 μ M). Pleasingly, this data demonstrates the poor PK profile associated with short acting muscarinic receptor antagonists, in which a large percentage of the initial dose is eliminated without being able to exhibit a pharmacologic effect. In addition, the potential high concentration of active drug that enters the blood within the first 3 hours demonstrates the potential for unwanted secondary pharmacology away from the lung, causing observed side effects such as increased heart rate etc.

2.3.3.1.6.3 Pharmacokinetic Study Design – Prodrug (24)

Compound **24** was dosed intratracheally into three Sprague Dawley rats at a concentration of 0.2 mg/kg in ethanol: pH 6.5 Phosphate Buffered Saline (5:95). Blood samples were then taken *via* the cannulated Jugular vein at 0.25, 0.5, 1, 2, 3, 5, 8, and 24-hour time points, and the concentration of drug and prodrug measured. At 24 hours, the rats were terminated and the lungs harvested allowing for the determination of terminal total lung concentrations of drug and prodrug.

2.3.3.1.6.4 Pharmacokinetic Study Results – Prodrug (24)

At time points up to and including 2 hours, the prodrug was detected in the blood at very low concentrations (approximately 2 ng/mL). After 2 hours, the prodrug was not detected in blood (below the LLOQ)

The active drug (**1**) was not detected in the blood at any point following IT administration of (**24**). At 24 hours, 54.27 ± 3.28 % of the administered dose remained

in the lung corresponding to a total lung concentration of 20000 ± 611 ng/g of homogenised lung tissue (40.0 ± 1.8 μM) whilst the active drug (**1**) concentration was determined to be 361 ± 31 ng/g of homogenised lung tissue (1.16 ± 0.1 μM) (Table 11).

Table 11: Pharmacokinetic Study Results Summary

Study	Compound	Estimated Initial Lung Tissue Concentration (μM)	Measured Final Lung Tissue Concentration (μM)	% Remaining at T_{end}
Drug	1 (Drug)	151.88 ± 2.61 (t= 0)	0.44 ± 0.10 (t= 3 hrs)	0.033 ± 0.06 % (t= 3 hrs)
Prodrug	1 (Drug)	0 (t= 0)	1.16 ± 0.10 (t= 24 hrs)	-
	24 (Prodrug)	73.8 ± 1.27 (t= 0)	40.0 ± 1.8 (t= 24 hrs)	54 ± 3.28 % (t= 24 hrs)

Measured across two PK studies, one focusing on prodrug stability and elimination rate from lung tissue and one focusing on drug elimination rate from lung tissue. n=3 rats in each case. Initial lung tissue concentration is an estimate based on the mass of the rat and dosing concentration. It does not account for any swallowed dose. Measured final lung tissue concentrations calculated using the experimentally determined mass of species (drug/prodrug) at each time point.

Pleasingly, this result demonstrated the hypothesis that the application of a sustained release, dibasic, prodrug system could prolong the presence of active drug (**1**) in the lung tissue, relative to direct delivery of the active drug. When administered independently, the drug had a poor lung retention, which resulted in a short lived, low drug lung tissue concentration. However, when administered as a prodrug, the active drug was present in the lung tissue, at a pharmaceutically relevant concentration, for in excess of 24 hours. This achievement gives hope that a sustained pharmaceutical response could also be achieved, although this would require further investigation.

2.3.3.1.6.5 Limitations of the Pharmacokinetic Studies

Although the presence of active muscarinic drug (**1**) in the lung tissue has been increased, this study does not guarantee an increased antimuscarinic effect. Unfortunately, the process of homogenising lung tissue in order to quantify drug/prodrug concentration levels prevents any determination of the drug/prodrug localisation, and thus further cellular studies are required to help quantify the increase in lung retention, specifically the mechanism of lung retention (membrane binding or lysosomal trapping for example), as well as a PD study to determine the pharmacological consequence of an increased drug lung residency.

Another crucial limitation of this PK study is the uncertainty of when the concentration of active drug in the lung tissue would reach pharmaceutically relevant levels, as lung tissue concentration data was only collectable at 24 hours. In addition, as a consequence of only determining the lung concentrations of drug and prodrug at the terminal time point of 24 hours, it is not certain whether the high drug concentration witnessed at 24 hours is due to the slow release prodrug mechanism, or whether it is a consequence of the lung homogenisation process.

2.3.3.1.6.6 Conclusions and Future Work Based on the Pharmacokinetic Studies

Pleasingly, the work in these PK studies has proved the hypothesis that the lung residency time of an inhaled muscarinic antagonist can be increased through implementation of a dibasic prodrug system. Despite this, a prodrug half-life of approximately 12 hours does not fit the profile of a once a day inhaled treatment. It is

clear that this prodrug is too stable and would lead to increasing concentrations of both the drug and prodrug in the lung. As COPD is a progressive disease requiring consistent symptom management, use of this prodrug system in its current form could quickly lead to potentially toxic levels of the drug and prodrug in the lung tissue and blood.

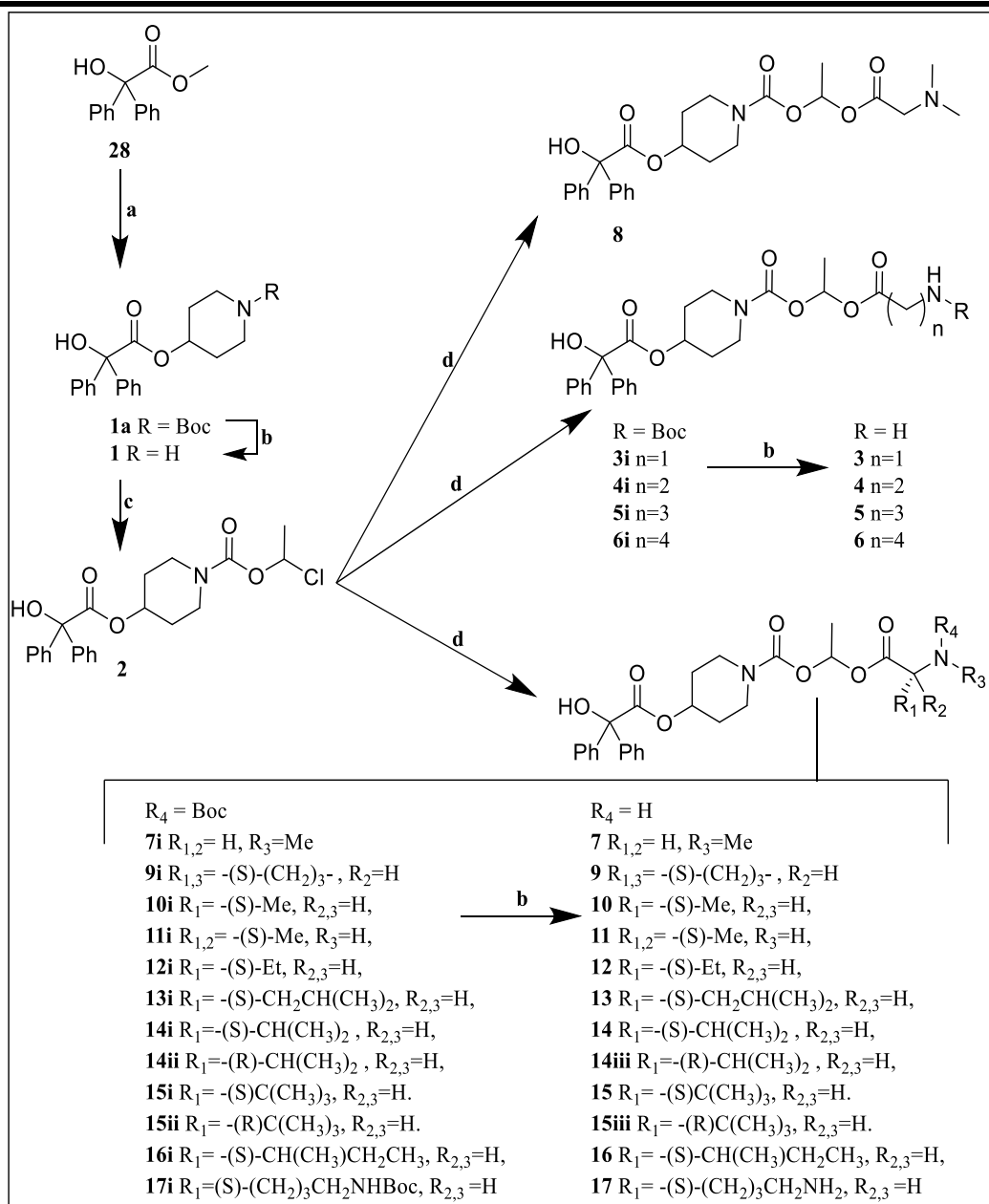
Pleasingly, the simple design of the prodrug system, and easily amendable nature of the dibasic dipeptide, means that a prodrug with a more appropriate half-life is easy to develop. Based on the *in-vitro* assay results, it is possible to estimate the *in-vivo* stability of a prodrug. With the knowledge of how R-chiral amino acids have shown persistent enzymatic stability, alongside the observed stability of unnatural amino acids, a further range of prodrugs could be synthesised. It is hoped that these would achieve stability half-lives consistent with a once a day dosing schedule.

2.3.4 Chemical Synthesis:

All α - and β -amino compounds prepared from methyl benzilate are portrayed in **Scheme 15 - Scheme18**.

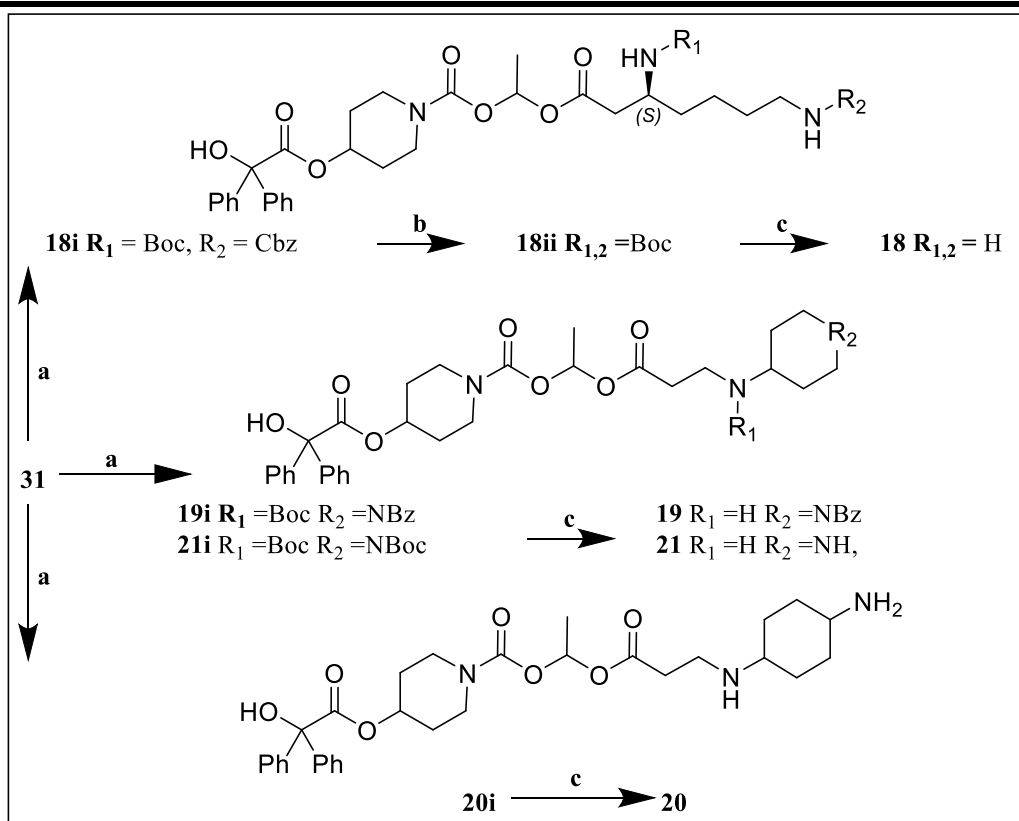
The prodrugs were all synthesized *via* the same initial synthesis, with the derivatisation taking place in the later stages. Methyl benzilate **28** is first transesterified using catalytic amount of sodium, forming the piperidine species **1a**. Standard HCl boc-deprotection gave compound **1**. Subsequent reaction with acetyl chloride attaches the linker group **2**. The linker can then be coupled with derivatised amino acids using silver oxide and tetra-n-butylammonium bromide to form the desired prodrug (**3-29**).

Scheme 15: Synthesis of compounds (3-17)



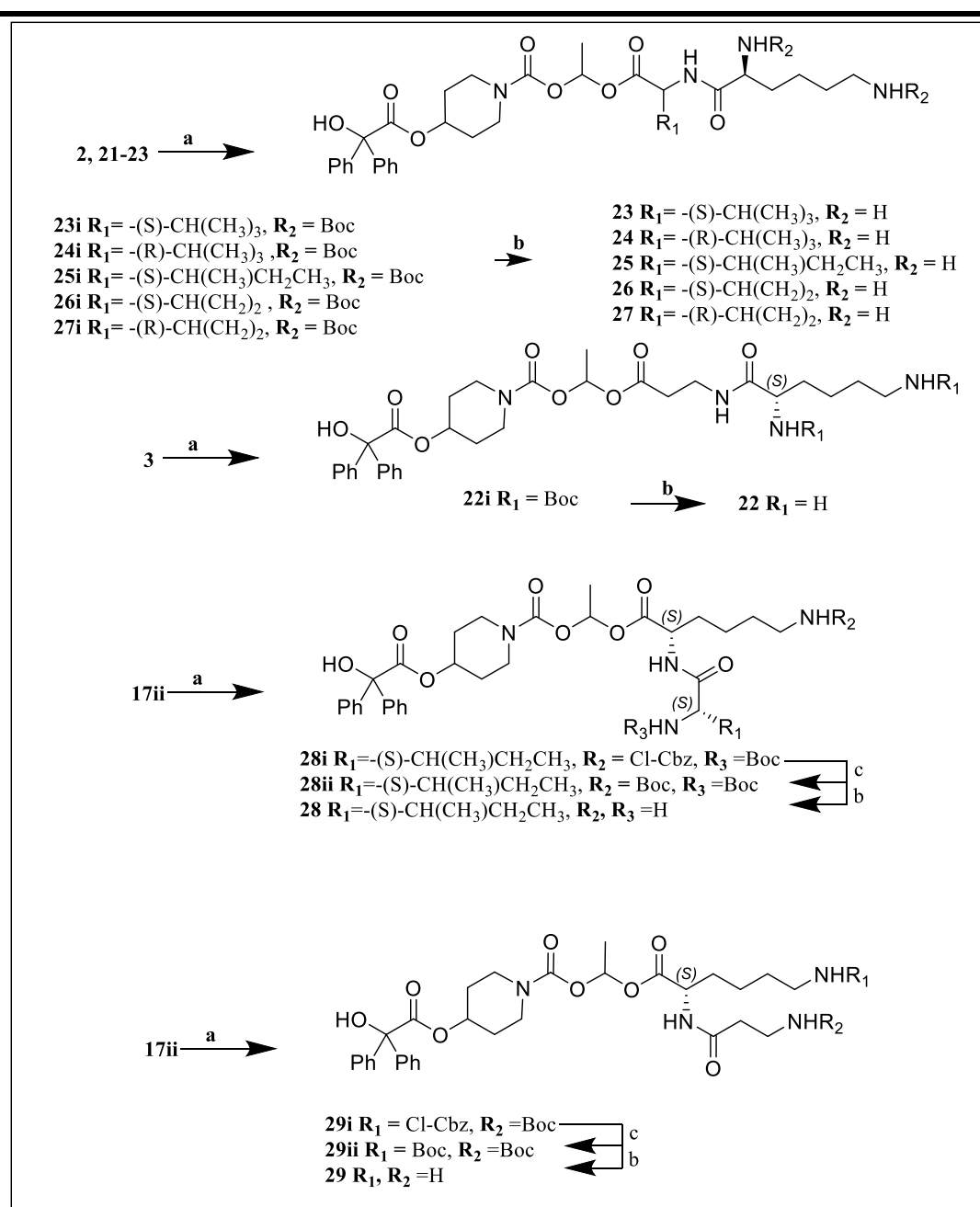
a) 1. *tert*-butyl 4-hydroxypiperidine-1-carboxylate, Na, NEt₃, C₇H₁₆, 60°C; b). HCl, DCM; c) Acetyl Chloride, *N*-methylmorpholine, DCM, -10°C; d) RCOOH, Ag₂O, NBu₄Br, PhMe, 65°C;

Scheme 16: Synthesis of β -amino Compounds (18-20)



a) RCOOH , Ag_2O , NBu_4Br ; b) 1. 10% Pd/C , H_2 , MeOH ; 2. Boc_2O , NEt_3 , DCM ; c) HCl , DCM ;

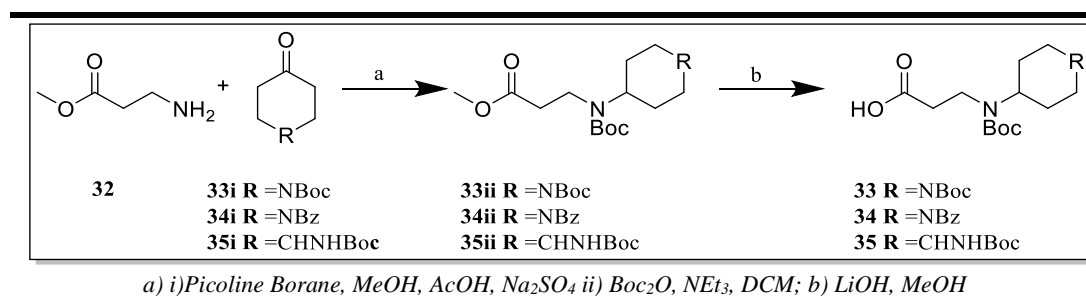
Scheme 17: Synthesis of Dipeptide Compounds (23-29)



a) RCOOH , HATU, DMAP, DIPEA, DCM; b) 4N HCl, DCM; c) 1. 10% Pd/C, H_2 , MeOH; 2. Boc_2O , NEt_3 , DCM;

To synthesise compounds (33-35), 32 was reductively aminated with a variety of piperidinones (33i-35i) using picoline borane to produce a range of protected esters amino esters. The carboxylic acid was then deprotected with LiOH, generating the boc protected dibasic acids. These were then able to undergo silver oxide coupling as per the other carboxylic acids.

Scheme 18: Synthesis of Functionalised Carboxylic Acids (33-35)



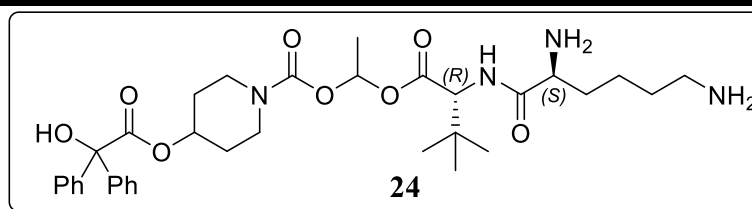
2.4 Chapter Conclusion

This chapter focussed on thesis objectives 1-3 (see **Thesis Aims and Objectives**). The first objective was to create a clear success criterion for the *in-vitro* DMPK studies. It was decided that the prodrug would need to possess a high chemical and enzymatic stability ($t_{1/2} > 6$ hours) in order to ensure that the release of the drug in the lung tissue was controlled and not spontaneous. It was also crucial that the prodrug possessed a high blood stability ($t_{1/2} = > 4$ hours) such that if any prodrug was delivered to the blood, the active drug would not be released and thus the concern of secondary pharmacology thus cardiac side effects was resolved.

In order to achieve this objective, a prodrug system which exploited the reported inherent lung retention of dibasic compounds was designed and developed, such that increased basicity was used as a mechanism for increasing the lung retention of a muscarinic receptor antagonist.

Key prodrug characteristics that would lead to an appropriate prodrug cleavage rate were first identified and evaluated in order to examine the prodrug stability and cleavage mechanism. Once identified using a range of easily synthesised monobasic prodrugs, these characteristics were then developed and incorporated into the design of a range of dibasic prodrugs. These prodrugs were then systematically tested for their stability and binding in phosphate buffer, rat lung homogenate and rat blood. Two candidates (**24** and **27**) displayed pleasing stability and binding values and ultimately, as its homogenate and blood stability matched the success criterion, **24** was chosen to progress further into an *in-vivo* pharmacokinetic study.

Scheme 19: Compound 31 Summary



Cmpd	Buffer T _{1/2} (hr) pH 6.5	Buffer T _{1/2} (hr) pH 7.4	Rat Lung Homogenate T _{1/2} (hr) pH 6.8	Rat Blood T _{1/2} (hr) pH 7.2	Rat Lung Homogenate Binding (% Free) ^e
24	58.6 ± 4.91	36.6 ± 1.70	25.4 ± 1.94	7.0 ± 0.82	0.5 ± 0.1

The *in-vivo* pharmacokinetic study aimed to measure the presence of the prodrug and active muscarinic drug in rat lung tissue and blood at several timepoints following intratracheal dosing. It was theorised that when the prodrug was administered, the concentration of active drug in the blood would be substantially lower than when the drug is directly administered. This reduction in drug blood concentration would then be correlated to a potential decrease in observed side effects through reduction of secondary pharmacology away from the intended site of action

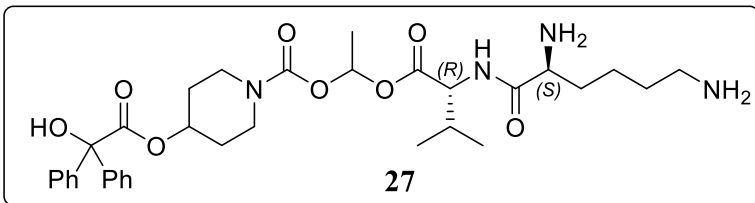
Pleasingly, the PK data demonstrated that 24 hours after IT administration of compound **24**, 54 ± 3.28 % of the prodrug remained in the lung tissue, alongside an active drug lung tissue concentration of 1.16 ± 0.10µM. The drug was not detected at any time point in the blood, and when dosed independently, demonstrated an incredibly poor lung retention of less than 3 hours. This result has proven the hypothesis that application of a dibasic prodrug system to an otherwise poorly retentive muscarinic M₃ inhibitor, can increase the lung retention of the active drug whilst maintaining a possibly therapeutically relevant lung tissue concentration of the active drug. Although further investigation is required to fully quantify the release profile post IT dosing, this result presents a remarkable step forward in the

development of novel long acting muscarinic receptor antagonists. In the next chapter, focus turns to developing a similar prodrug system for use with intracellular PI3K receptors.

2.5 Future Work

As previously mentioned, although the PK data provides a remarkable starting point for improving the lung retention of an inhaled drug candidate, further exploration is required in order to understand the release profile of the drug. In order to acquire this data, it may be beneficial to run a shorter PK study on a compound which demonstrates a shorter chemical stability, such as compound **27** (Scheme 20).

Scheme 20: Compound 34 Summary



27

Compound	Buffer $T_{1/2}$ (hr) pH 6.5	Buffer $T_{1/2}$ (hr) pH 7.4	Rat Lung Homogenate $T_{1/2}$ (hr) pH 6.8	Rat Blood $T_{1/2}$ (hr) pH 7.2
27	8.7 ± 1.06	1.8 ± 0.20	3.4 ± 0.08	0.6 ± 0.07

The PK study in this case would cover a smaller timescale, with more frequent collection of lung and blood drug/prodrug concentration data in order to give a better representation of the drug release profile into lung tissue and blood plasma. This could also help to elucidate whether the lung homogenisation process contributes to the cleavage of the prodrug.

Whilst this PK study would help to understand the release profile of the drug, **27** does not possess the desired requirements as set out in the success criterion; Both the homogenate and rat blood stability values are too low. Whilst the reduced homogenate stability would eliminate the possibility of the lung tissue concentration of (pro)drug reaching toxic levels, after 12 hours and thus almost 4 half-lives, the concentration of the drug released from the prodrug may not reach the therapeutic requirements and thus this prodrug may not fit a once a day dosing schedule. Ultimately this cannot not be fully predicted, and hence an *in-vivo* PD study would be required to determine the longevity of the pharmaceutical response.

Finally, whilst the work in this chapter suffices as proof of concept for the prodrug lung retention rationale, it provides no certainty as to the mechanism of increased lung retention. Whilst the high lung homogenate binding value of the prodrug suggests a high level of retention within the lung tissue, the destructive nature of the assay procedure creates uncertainty as to where the prodrug may bind. Ultimately this location needs to be discovered in order to accurately determine whether the prodrug system is able to achieve a prolonged pharmaceutical response, alongside increased lung tissue retention.

In order to understand the mechanism of lung retention, the prodrug structure could be altered to include a biomarker such as a radio label or fluorescent marker, then the distribution of the prodrug within the lung could be accurately visualised.

3. Design and Synthesis of Novel PI3K Prodrugs

3.1 Introduction

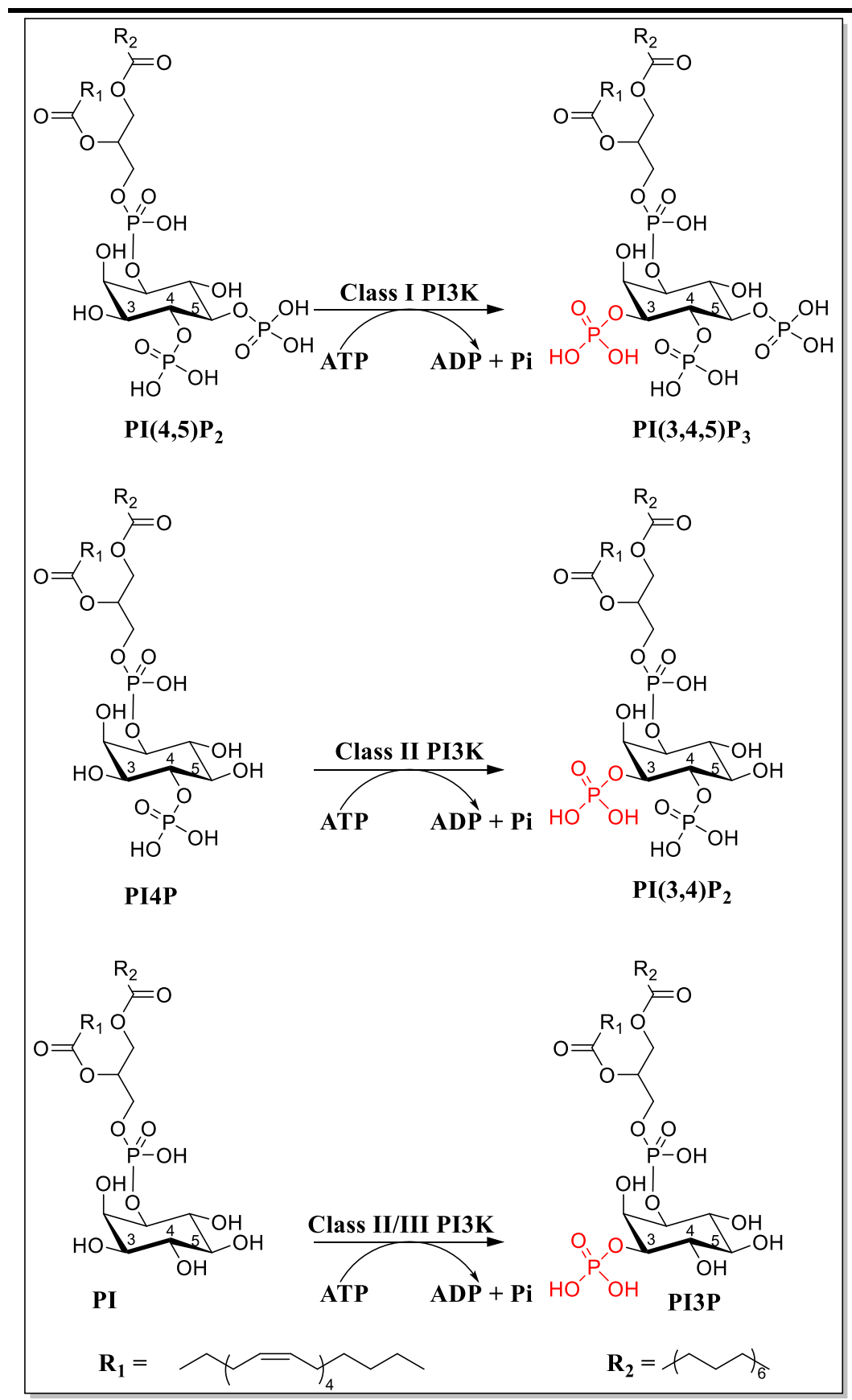
3.1.1 Phosphoinositide 3-kinase

Phosphoinositide 3-kinase (PI3K) is a family of intracellular lipid kinase, signal transducing enzymes responsible for phosphorylation of the 3-OH group of the inositol ring of cell membrane phosphatidylinositol (PI).²⁰⁸ Broadly, these enzymes are responsible for cell signaling, survival, activation, differentiation and senescence and are divided into three main subclasses (Class I, II and III), with Class I being further divided into Class I A and B.²⁰⁹

3.1.1.1 Class I PI3Ks

Distinguished because of their modified approach to receptor transduction pathway regulation, Class IA and IB PI3-kinases exist as heterodimers consisting of a homologous regulatory subunit (p50 α /p55 α /p85 α / p85 β / p55 γ for IA or p101/p84 for IB) bound to a catalytic subunit (p110 α / β / δ for IA or p110/p101 γ for IB) and are termed PI3K α - δ respectively depending on which catalytic subunit is present.²¹⁰ They exist as soluble enzymes which, when activated by tyrosine receptor kinases (Class IA) or GPCRs (Class IB), favourably change conformation and relocate to the cell membrane to catalyse the phosphorylation of phosphatidylinositol 4,5- bisphosphate (PI(4,5)P₂) into phosphatidylinositol 3,4,5-trisphosphate (PI(3,4,5)P₃; PIP₃) (**Scheme 21**).²¹¹ Expression of the Class I PI3Ks varies amongst isoforms, with PI3K α and β being expressed ubiquitously amongst cells and γ and δ being restricted predominantly to leukocytes.^{212,213}

Scheme 21: Phosphorylation reactions performed by Class I-III PI3Ks



3.1.1.2 Class II and III PI3Ks

In comparison to Class I, Class II and III have been relatively understudied, and thus their structure and function is still largely to be determined. Class II PI3Ks consist of only a single catalytic isoform (C2 α /C2 β /C2 γ), with no regulatory protein present, whilst the structure of class III PI3Ks is thought to consist of a single catalytic subunit (Vps34) bound to a protein kinase (Vps15 or p150).^{214,215} Both classes are known to either catalyse the phosphorylation of PI into PIP3 (Class II and III) or phosphatidylinositol 4 phosphate (PI4P) into phosphatidylinositol 3,4- bisphosphate (PI(3,4)P₂) (Class II), although the exact catalytic mechanism for class II is not yet clear.²¹⁶

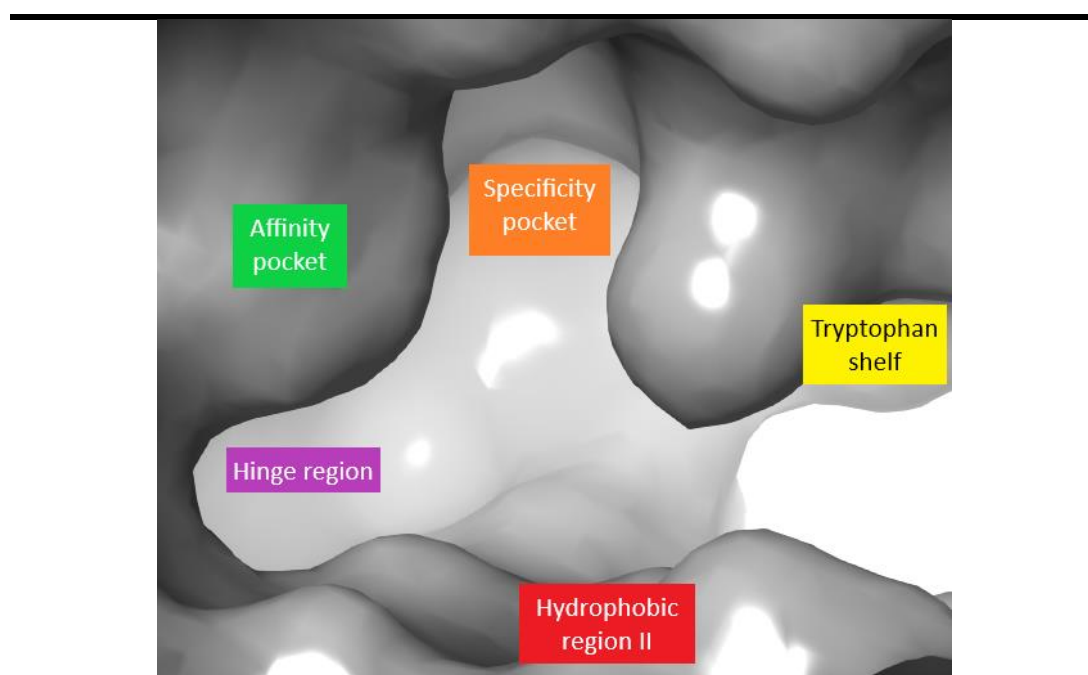
3.1.2 PI3K Inhibition

Inhibition of the PI3K receptors relies on the ability of a drug candidate to competitively bind to the receptor active site, blocking the natural ligand ATP, and preventing a biological response.²¹⁷ Fortunately, the increased acknowledgment of the role of PI3K receptors in various cell processes has resulted in the publication of numerous crystal structures for each isoform, allowing the requirements for isoform selectivity to be identified.

Since the work detailed in this chapter focuses on only PI3K δ inhibitors, only these shall be discussed, and thus from here onwards the term PI3K will refer only to the δ isoform unless stated otherwise.

In 2010 Berndt *et al* published some of the first PI3K crystal structures co-crystallized alongside various selective and non-selective inhibitors, as well as offering structural advice for obtaining isoform selectivity.²¹⁸ The crystal structures demonstrated that a highly selective δ -inhibitor non-covalently binds to 4 different regions termed ‘specificity pocket’, ‘hinge binding region’, ‘affinity pocket’ and ‘hydrophobic region II’ (Figure 36).

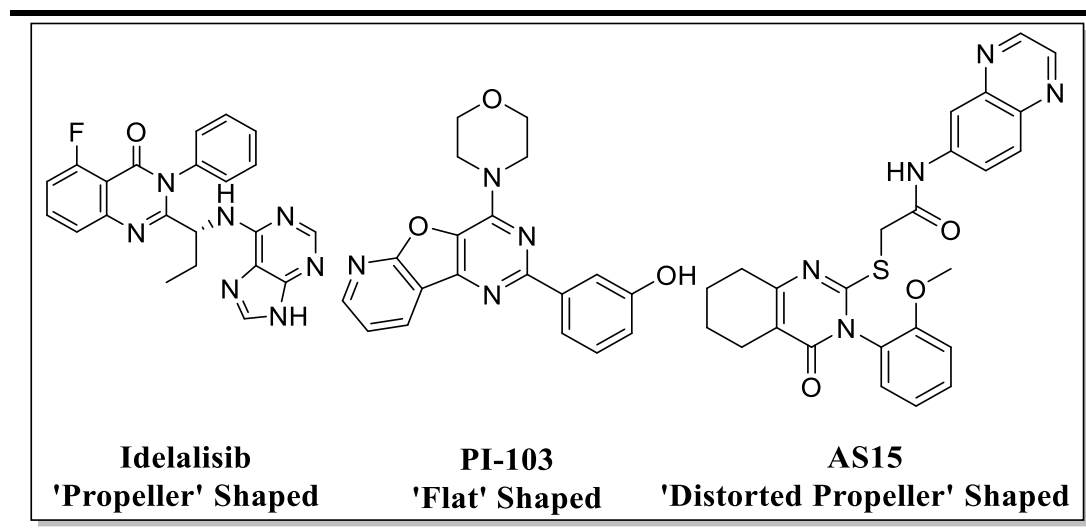
Figure 36: PI3K δ Binding Pocket



They also suggested that inhibitor structure usually follows one of three designs based on their competitive binding (**Error! Reference source not found.** ‘Propeller’ shaped inhibitors adopt such a conformation that causes the kinase to change conformation, opening the hydrophobic ‘specificity pocket’ (commonly referred to as the ‘tryptophan shelf’) which is otherwise inaccessible. These tend to be highly δ -specific inhibitors. ‘Flat’ inhibitors tend to be pan antagonistic and do not offer any accessibility to or interaction with the ‘tryptophan shelf’. Finally, ‘distorted propeller’

shaped inhibitors are mostly δ -selective and bind in a similar way to the ‘propeller’ shaped inhibitors, but without the conformation change leading to the opening of the ‘specificity pocket’.

Figure 37: Examples of Propeller and Flat Shaped PI3K Inhibitors

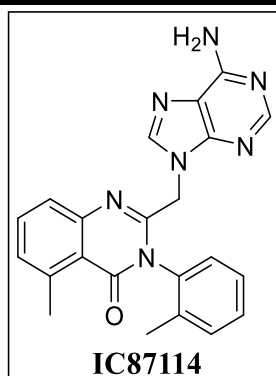


3.1.3 PI3K Involvement in COPD Treatment

As previously discussed, COPD is characterised as a chronic lung inflammatory response to exogenous particulates which results in narrowing of the airways and thus increased difficulty in breathing. Inflammation is a coordinated response to pathogens or damaged cells such as those caused or accelerated by smoking. Upon initiation of an inflammatory response, either an acute or chronic response can be initiated which ultimately results in activation and deployment of immune cells such as leukocytes to the site of infection.²¹⁹ In addition, increased activity of PI3K and its downstream mediators during airway remodelling affects the normal function of airway epithelial cells, leading to heightened inflammatory immune responses, characteristic of COPD.^{220,221}

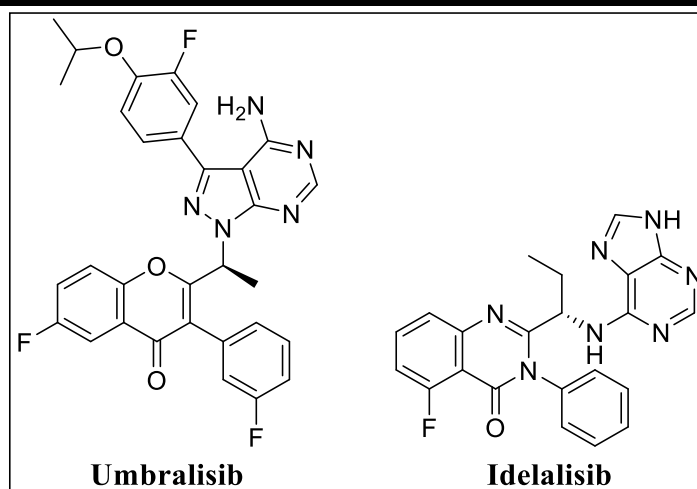
Due to the high expression of PI3K in lung epithelial cells, alongside high expression of γ and δ in leukocytes, and their role in the cell signalling cascade involved in an inflammatory response, targeting of these isoforms represents an opportunity to improve symptom relief in asthma and COPD patients.^{222,223} Indeed, this hypothesis was first proven by Lee *et al* in 2006 who demonstrated that IC87114, a selective PI3K γ and δ inhibitor (**Figure 38**), limited the recruitment of chemokines responsible for the development and maintenance of asthma, suppressing an inflammatory response in lung tissue.^{224,225}

Figure 38: Structure of IC87114



Since 2006, the development of selective PI3K inhibitors has significantly improved, with numerous compounds having recently gained FDA approval including umbralisib and idelalisib (**Figure 39**) as lung cancer therapies and Nemiralisib (**Scheme 22**) as an inhaled COPD treatment.

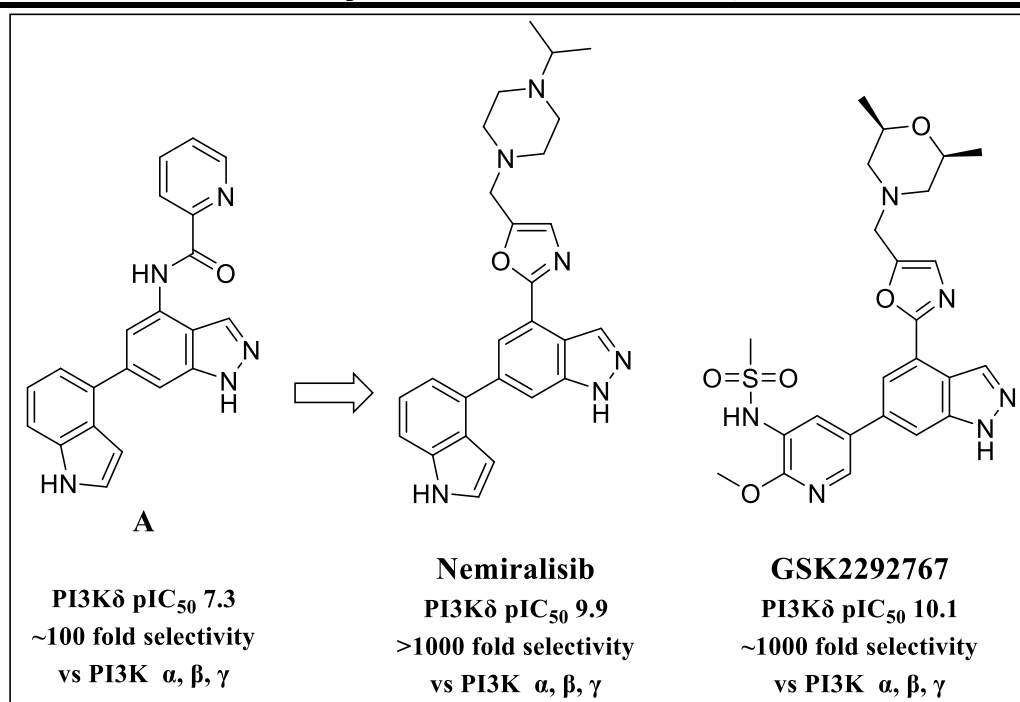
Figure 39: Structures of Umbralisib and Idelalisib



3.1.3 Development of Nemiralisib and GSK22927675

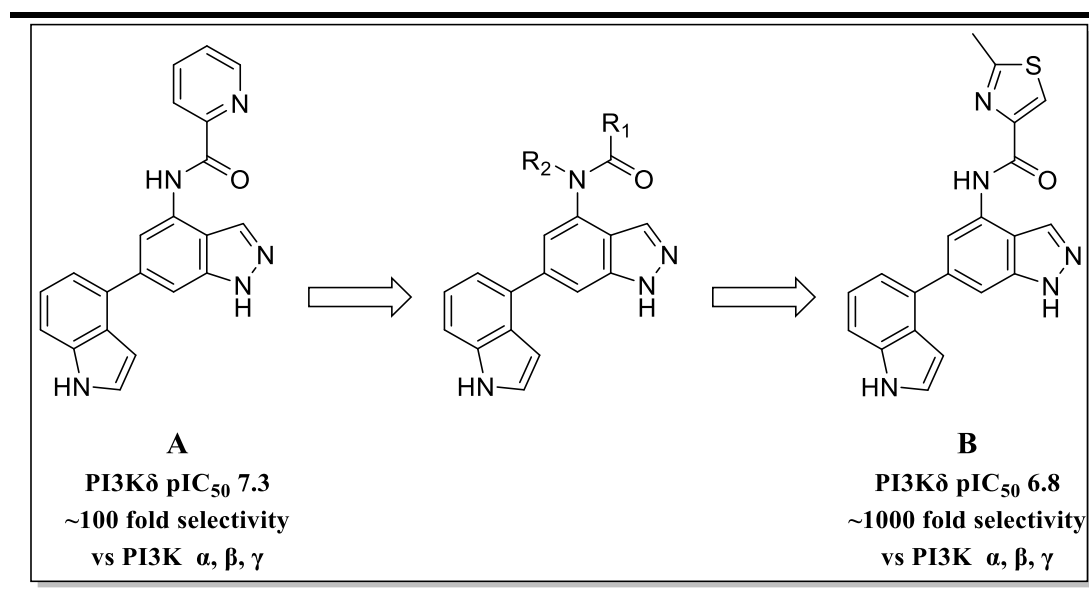
In 2015, GSK published their discovery of 2 novel PI3K δ inhibitors (**GSK2269557**, now known as **Nemiralisib** and **GSK292767**), identified from an SAR investigation from a lead compound identified through a cross-kinase screen for potential novel COPD treatments (**Scheme22**).²²⁶

Scheme 22: Structures of Lead Compound 1 and New Clinical Candidates, Nemiralisib and GSK2292767



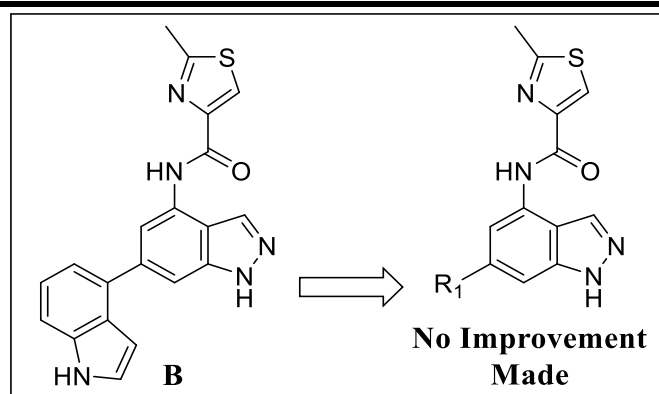
Their aim was to develop lead compound **A** into an inhaled, highly selective (>100-fold for PI3K δ against the other isoforms), highly potent ($pIC_{50} >9$) inhibitor with a moderate to high clearance and low bioavailability of the oral component. Initial SAR investigation aimed at replacing the 4-pyridyl ring with similar substituents (**Scheme 23**). They found that removal of the ortho hetero-atom resulted in a 10-fold reduction in potency, possibly due to loss of an internal hydrogen bond required to maintain planarity. Ultimately, a thiazole moiety (**B**) was selected as it displayed an approximate 10-fold increase in δ -selectivity whilst maintaining potency.

Scheme 23: 4-Position Amide Development



They chose to temporarily settle with the thiazole moiety and turned their focus to the 6-position, trialling various heterocycles in attempt to develop potency and selectivity (**Scheme 24**).

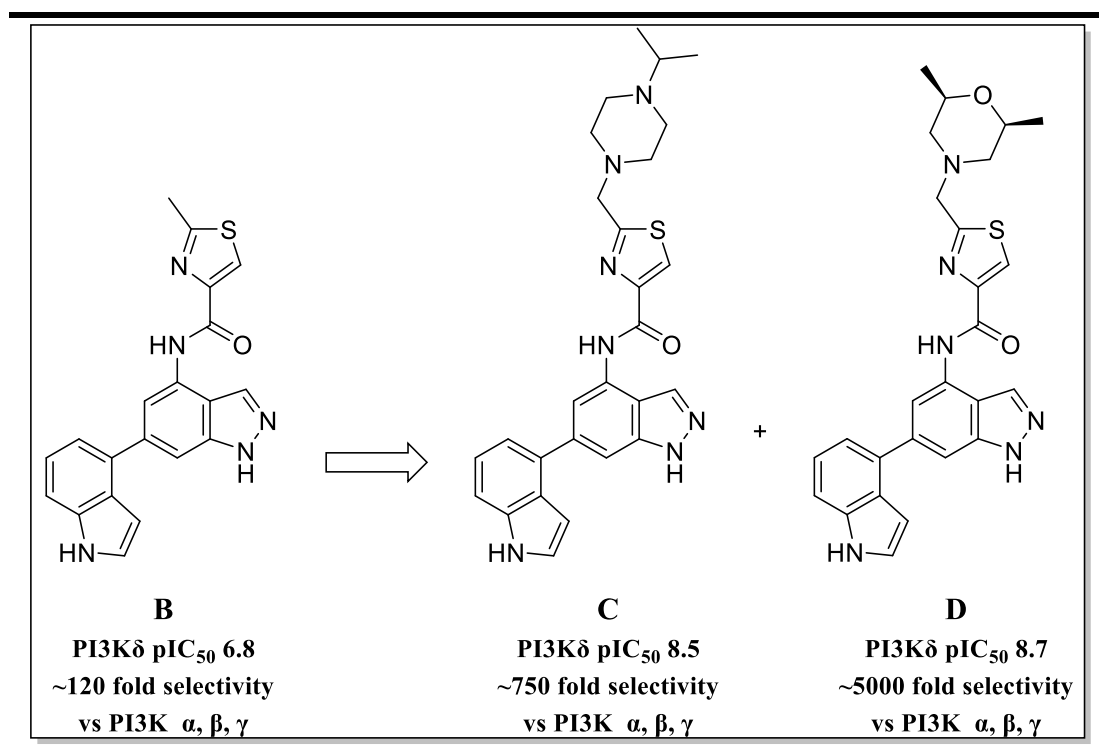
Scheme 24: 6-Position Heterocycle Development



Any monocyclic replacements were met with large drop-offs in potency and any bicyclic indole or indazole replacements were also unfruitful with very little improvement observed.

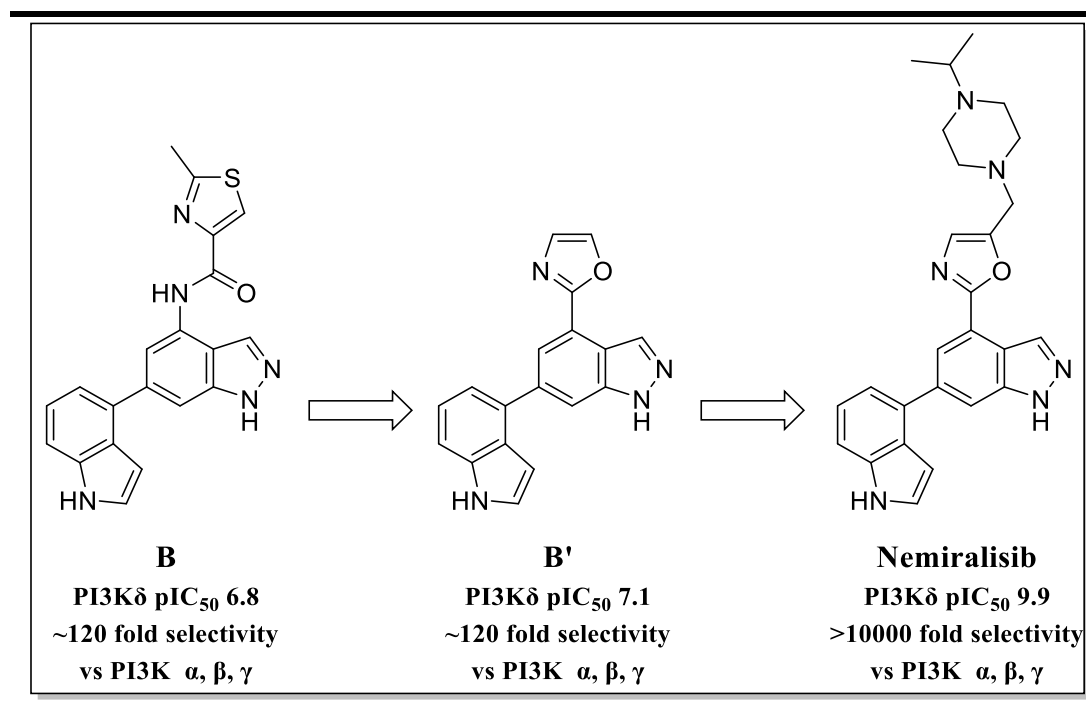
Since no further improvement could be made at the 6-position, they instead trialled various thiazole substitutions in order to utilise all space in the binding pocket (**Scheme 25**). They found that adding a second heterocycle on to the methyl group led to an increase in potency whilst also enhancing selectivity. A range of cyclic substitutions were made with very little difference in selectivity and potency, and thus ultimately, they chose to incorporate a basic (**D**) and dibasic (**C**) component to the compound in order to improve its lipophilicity and basicity: two important physiochemical properties for inhaled candidates.

Scheme 25: Heteroarylamine Development



With the knowledge of how optimization of the heteroarylamine moiety can improve both the potency and selectivity, they decided to try and reduce the molecular weight of the compound through further optimisation of the amide moiety, ensuring to retain the planarity of the molecule (**Scheme 26**). They tested a range of heterocyclic replacements for the amide group and found that the amide hydrogen bond donor was not required for potency, and hence removal of the amide maintained the high intrinsic clearance required.

Scheme 26: Amide Replacement

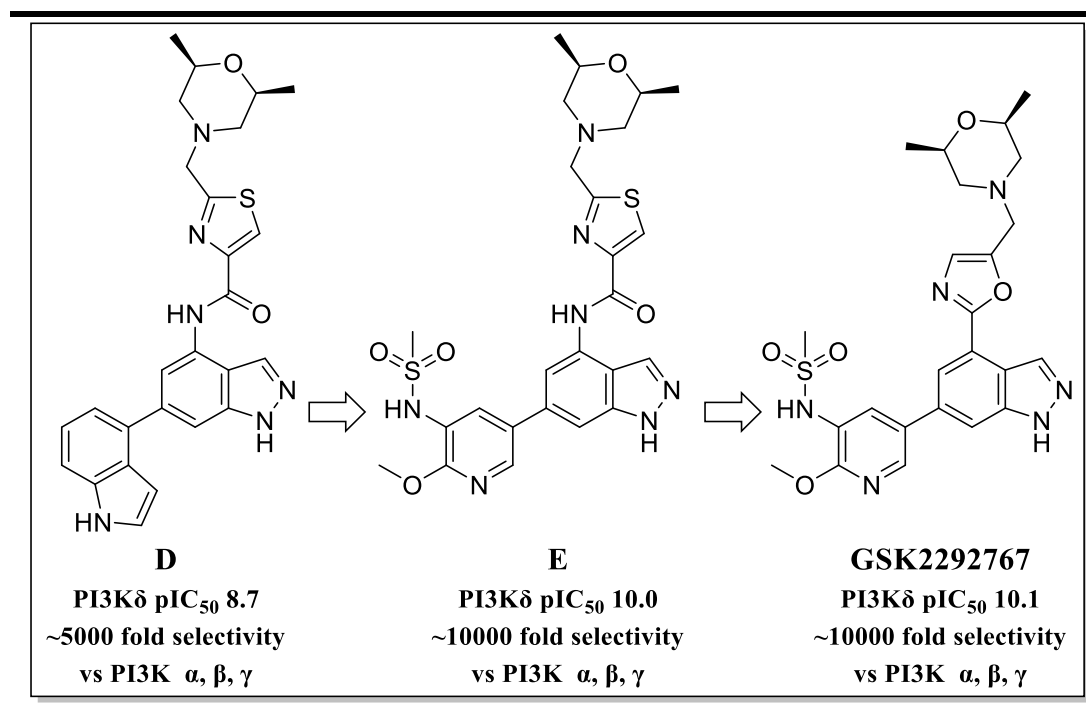


Ultimately an oxazole moiety (**B'**) was found to possess the best characteristics and hence they decided to combine the oxazole moiety with the previously tested lipophilic, basic component creating their first final candidate, Nemiralisib. The second candidate was created in order to find a compound with an improved hERG binding result. hERG is a gene which codes for the α subunit of potassium ion channels ultimately contribute to the electrical activity in the heart. Blockage of this potassium ion channel by drugs can lead to potentially fatal disorders, and thus drug development programs routinely test for hERG binding as a method of estimating drug toxicology.

Due to the highly explored hERG pharmacophore, and knowledge of how controlled amine pKa and lipophilicity denote the hERG binding activity, they embarked upon further SAR to convert compound (**D**) into final candidate **GSK2292767**.²²⁷ Replacement of the indole with a sulfonyl-pyridyl moiety (**E**), followed by

substitution of the thiazole with an oxazole moiety (**GSK2292767**), yielded the second clinical candidate with improved hERG binding profile, high potency and selectivity, and thus both **Nemoralisib** and **GSK2292767** proceeded to clinical trials

Scheme 27: Amide Replacement



Interestingly, compound **E** was found to be almost equally potent and selective as final candidate **GSK2292767**, however poorer aqueous solubility meant that it was unable to progress to clinical trials (solubilities of 114 vs 182 $\mu\text{g}/\text{mL}$ for **E** and **GSK2292767** respectively) due to the airway inflammation potential when dosing insoluble compounds.

This highlights a crucial flaw of the typical SAR drug development processes, as highly potent compounds which have gone through several rounds of structural development and testing are ultimately discarded due to one poor physiochemical

property. Fortunately, compound **E** proved to be a viable target for prodrugging, with the knowledge that poor aqueous solubility can be overcome, such that problems with absorption, distribution and elimination can be avoided.

Utilisation of the compound as the active drug component for pro-drugging as per the design in chapter one, could provide an alternative route to creating a long acting, anti-inflammatory PI3K inhibitor for the treatment of COPD. Herein this chapter attempts to apply the prodrug concept developed in chapter 1 to drug molecules which target intracellular receptors but which exhibit poor ADME properties such that their advancement to clinical trials is prevented.

3.2 Aims

The aims of this chapter were to build on the success of chapter 1 by modifying the structure of the prodrug system such to determine whether the prodrug design would be applicable to intracellular targets. PI3K δ had been identified as an appropriate intracellular target due to its role in COPD airway inflammatory responses, and thus a highly potent and selective PI3K δ compound was to be identified and chosen as the active drug component. Once synthesised, the PI3K prodrug system must incorporate all of the DMPK stability and binding requirements from the previous chapter.

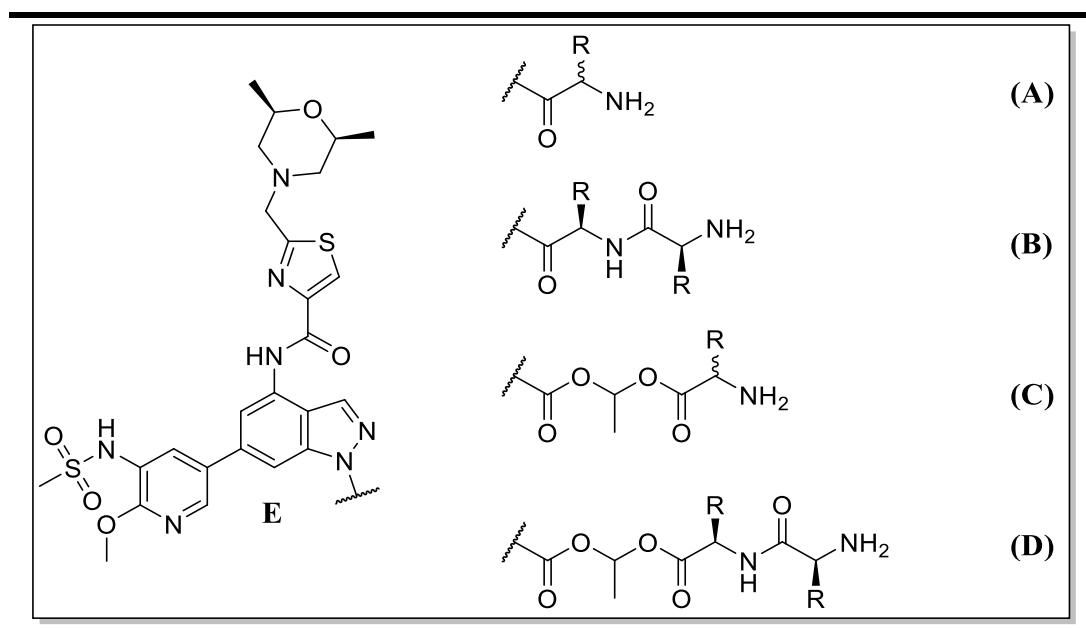
3.3 Results and Discussion

3.3.1 PI3K Prodrug Design

As PI3K δ receptors are intracellular, the focus on this chapter would be on the ability of the created prodrugs to enter the lung epithelial tissue cells and be sequestered inside acidic organelles such as lysosomes. This would create a depot in which the prodrugs would slowly activate to release the active component, which can then diffuse out of the organelle to interact with the target receptor. Membrane binding would be less of an important factor in this chapter, as binding to the external cell membranes would not allow for an appropriate pharmacological response.

As per chapter 1, compound **E** was to be incorporated into a similar prodrug design in which a dibasic dipeptide species is formed (**Figure 40**). The indazole nitrogen was identified as a possible handle from which to create a prodrug as acylation at this point will prevent the drug from creating essential hinge binding interactions with the receptor, thus removing the pharmacology and rendering the prodrug inactive. Four prodrug designs were considered; mono-peptidic prodrugs with (**Figure 40 C**) and without (**Figure 40 A**) the linker unit and di-peptidic prodrugs with (**Figure 40 D**) and without (**Figure 40 B**) the linker unit.

Figure 40: PI3K Prodrug Designs



Since compound **E** already contained a basic nitrogen, it was not necessary for the prodrug component to be dibasic, and instead focus was on steric requirements for a slow cleaving prodrug with high enzymatic stability. The presence of an initial basic site would also allow for single amino acids to be trialled which would cleave through an anchimeric water delivery mechanism similar to compounds **2** and **3** (Chapter 2.3.2.1)

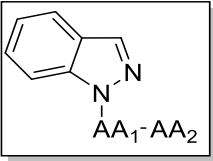
As seen in the previous chapter, the cleavage rate of these prodrugs will vary considerably depending on the activation mechanism. Prodrugs of type B and D would be expected to cleave slower than A and C due to the complex diketopiperazine cyclisation mechanism involved in the drug elimination, and the increased opportunity to control the drug release. In addition, from the SAR-like exploration in chapter 1, it was clear that several structural features should be incorporated into the design of the PI3K prodrug; highly sterically hindering amino acid R groups should be used to ensure a slow DKP formation and thus slow prodrug activation, R-chiral amino acids

should be used for the first amino acid in the dipeptide chain to provide enzymatic stability and the whole molecule should be dibasic to increase the possibility of cation transportation/lysosomal trapping. Organic cation transportation may be a more essential factor for the PI3K prodrugs, as the final target receptor is intracellular, rather than membrane bound and thus cell penetration is key to achieving pharmacology.

3.3.2 Model Cleavage Studies

Before beginning synthesis on compound **E**, it was important to check that the indazole nitrogen was indeed a suitable handle to use for prodrug development, and thus prove prodrug design applicability. A series of indazole dipeptides in the absence of the linker group were created (**Table 12**) to test both the suitability of the indazole nitrogen and to also discover how the steric bulk of each amino acid in the dipeptide affected the activation rate. If indazole elimination is possible without the linker unit, then smaller molecular weight prodrugs could be created, which eliminate to give fewer side products, and require less synthesis overall. The stability of the model prodrugs was then determined according to **Biological Assay procedure 3**, as in chapter 1.

Table 12: Cleavage results for model indazole prodrugs

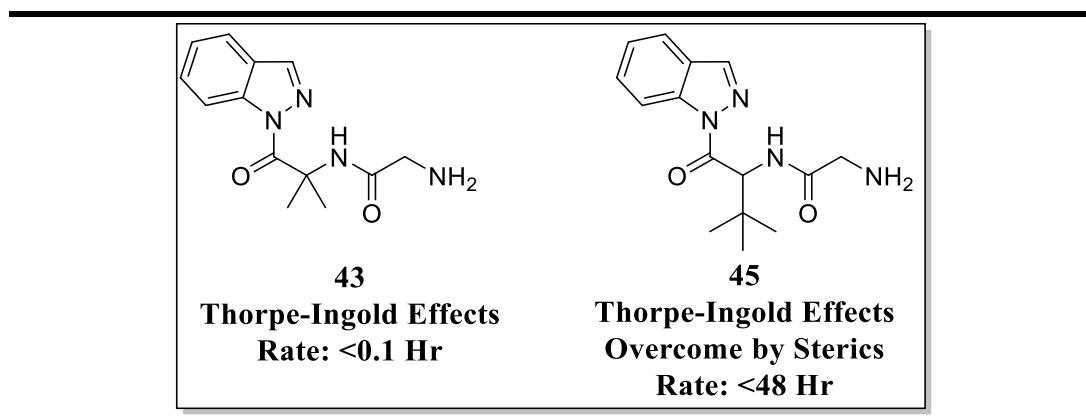


Compound	Amino Acid 1 (AA ₁)	Amino Acid 2 (AA ₂)	Terminal cpKa ^a	pH 6.5 Phosphate Buffer T _{1/2} ^b (Hr)
36	Glycine	Glycine	7.84	0.4
37	Glycine	Alanine	8.09	0.3
38	Glycine	2 Amino Isobutyric Acid	8.34	<48
39	Glycine	Valine	8.21	19.9
40	Glycine	t-Leucine	7.93	44.9
41	Glycine	β-Alanine	9.12	9.9
42	Alanine	Glycine	7.84	<0.1
43	2 Amino Isobutyric Acid	Glycine	7.84	<0.1
44	Valine	Glycine	7.84	0.6
45	t-Leucine	Glycine	7.84	<48
46	β-Alanine	Glycine	8.14	<48

^a Predicted using Marvin Sketch^b Tested according to biological assay procedure 3

The results demonstrated that the indazole nitrogen was indeed an acceptable leaving group to allow the breakdown of the prodrug. The cleavage data followed similar trends to those witnessed in chapter one, such that activation depended heavily on steric bulk and terminal amine pKa, with Thorpe-Ingold interactions causing predictable outliers (**42** and **43**). Compounds **36-41** demonstrated once again how the pKa of the terminal amine can significantly decrease the rate of cyclisation by reducing the percentage of neutral amine present at pH 6.5, whilst compounds **42-46** demonstrated how the size of the steric bulk caused by the amino acid R group can also prevent activation at the carbamate. Interestingly, this data demonstrated how Thorpe-Ingold effects which increase the rate of cyclisation can be overcome by increasing the amount of steric bulk (**Figure 41**).

Figure 41: Comparison of Thorpe-Ingold Effects



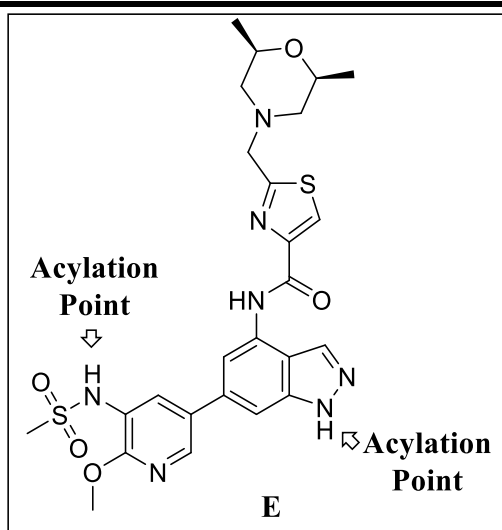
In order to achieve an acceptable stability profile for the prodrug, it was clear that several combinations of amino acids could be used, and providing the first amino acid is of unnatural chirality, the stability should also translate to enzymatic stability *in vivo*.

This model cleavage study also highlighted an improvement to the prodrug system, as the increased leaving group ability of the indazole meant that the linker group could be omitted. This means that less breakdown products would be observed but crucially it meant that the release of ethanal is avoided, preventing any possible side effects observed with intracellular aldehydes.²²⁸ Because of this observation only prodrugs of type (**Figure 41 A**) and (**Figure 41 B**) were considered for synthesis.

3.3.3 Prodrug Synthesis

A small amount of final compound **E** (1g) was supplied from GSK, and thus before embarking on a lengthy drug synthesis, the viability of the compound as a prodrug was trialled. Acylation of the indazole nitrogen proved instantly problematic due to the competing analogous reaction at the sulphonamide (**Figure 42**).

Figure 42: Competing Points of Acylation

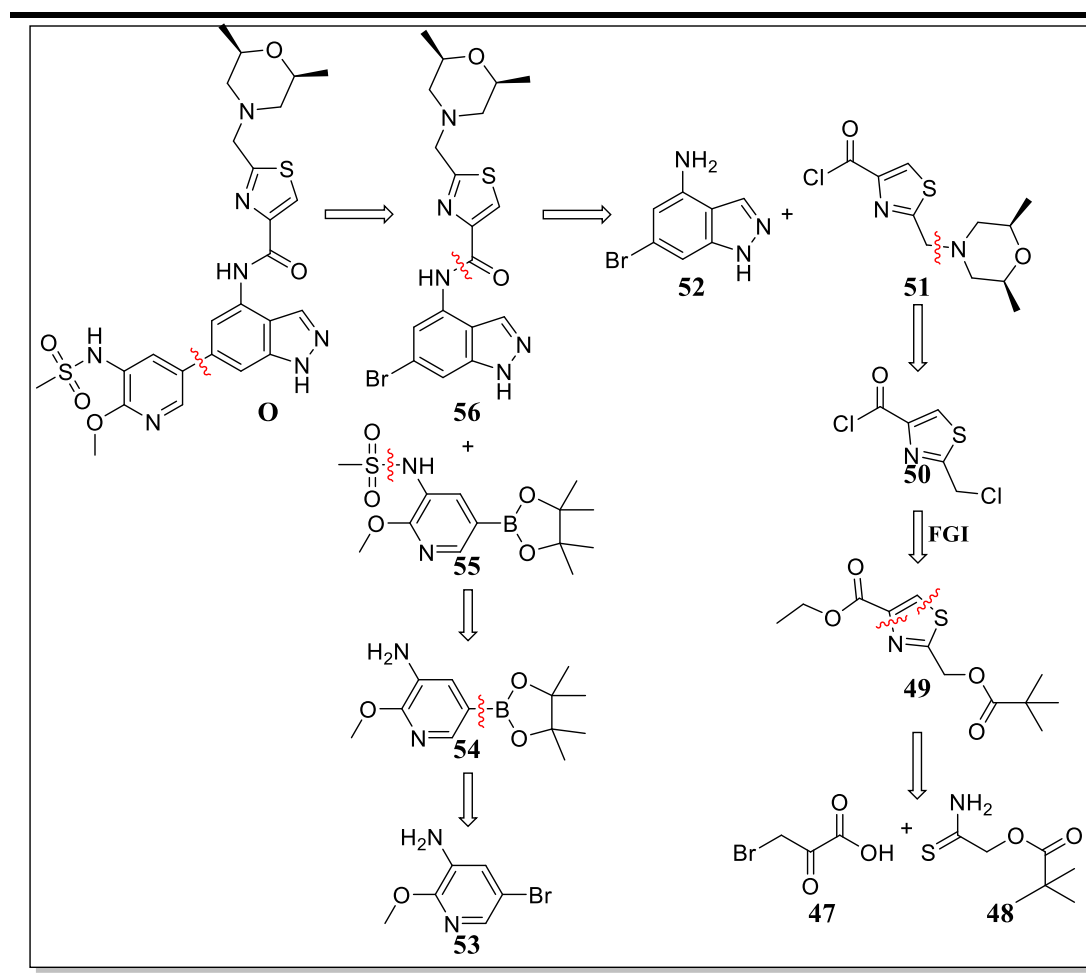


LCMS analysis of the reaction material found 4 separate peaks; 10% remaining starting material, 15% monoacylation (presumably indazole), 15% monoacylation at a second site (presumably sulphonamide) and a final 60% of diacylation. Unfortunately, Separation of these peaks was impossible due to their overlapping chromatography and HPLC retention time. This highlighted an important synthetic obstacle as it meant that prodrug synthesis must be completed before the addition of the sulphonamide moiety, removing any opportunity for competing acylation. This itself provides further complication as the prodrug moiety is susceptible to nucleophilic attack and thus is not stable in all reaction conditions and hence it was uncertain how stable the dipeptides would be in the final Suzuki reaction.

3.3.4 Synthesis of Compound E

Unfortunately, very few intermediates were available from GSK and thus it was necessary to synthesise the final PI3K inhibitor. The full retrosynthetic analysis can be seen below (**Scheme 28**):

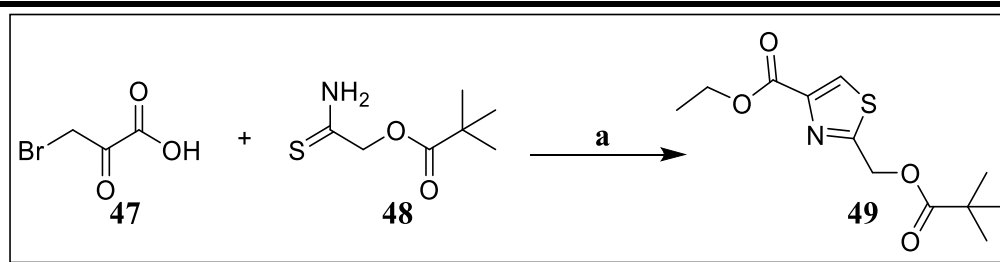
Scheme 28: Retrosynthetic Analysis of Compound E



To synthesis compound **E**, three core components were required; the acid chloride thiazole, the pinacol boronic ester and the core indazole heterocycle. However, based on the results of the trial reactions, the forward synthesis was to be modified such that the prodrug moiety was in place before the Suzuki reaction, in attempt to reduce over-acylation.

The first step to synthesise the acid chloride was a Hantzsch thiazole formation using bromo-pyruvic acid (**47**) and α -Amino-2-thioxoethyl pivalate (**48**). Under reflux conditions using ethanol as a solvent, the ethyl ester product (**49**) is produced in high yield (**Scheme 29**).

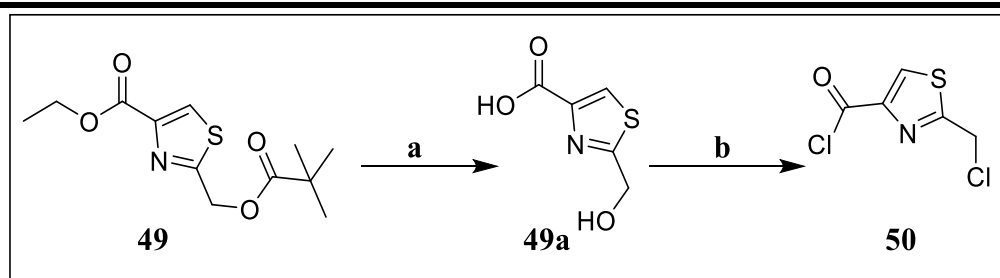
Scheme 29: Synthesis of compound 49



a) EtOH, rf, 24 hr, 68%

Subsequent treatment of **49** with potassium carbonate at 100°C quickly afforded the deprotected thiazole (**49a**) which after work up and separation using amino-functionalised silica, was converted to di-chloro compound (**50**) using thionyl chloride (**Scheme 30**).

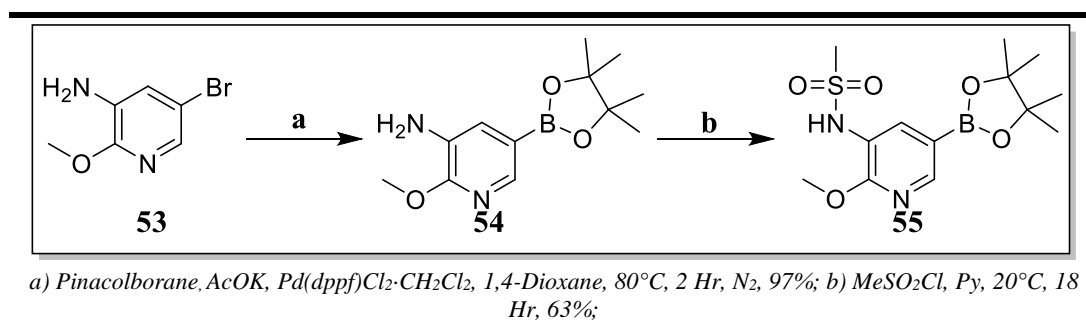
Scheme 30: Synthesis of compounds 49a and 50



a) i) K_2CO_3 , MeOH, H_2O , 100°C, 15 min; ii) 2N HCl, 92%; b) $SOCl_2$, $CHCl_3$ DMF, 2 Hr, quantitative yield;

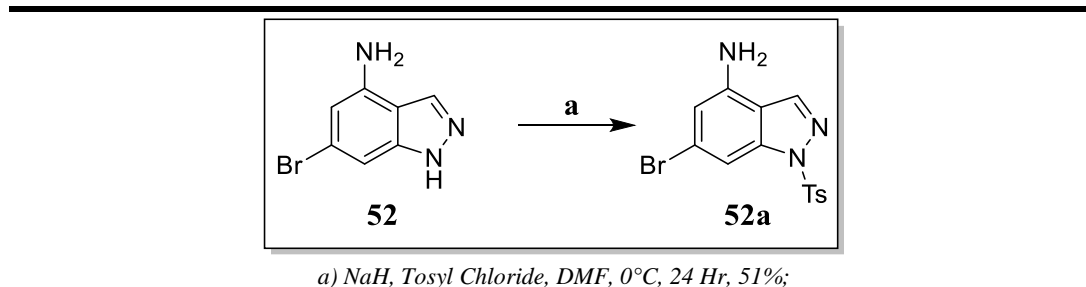
The Sulfonyl pyridine moiety was synthesised from commercially available 5-bromo-2-(methoxy)-3-pyridinamine, using dioxaborolane and potassium acetate in 1,4-dioxane under palladium catalysis to create the pinacol boronate ester (**54**). The pinacol ester was then sulfonated using methanesulphonyl chloride at 20°C overnight to yield the final sulphonamide Suzuki coupling partner **55** (**Scheme 31**).

Scheme 31: Synthesis of compound 54 and 55



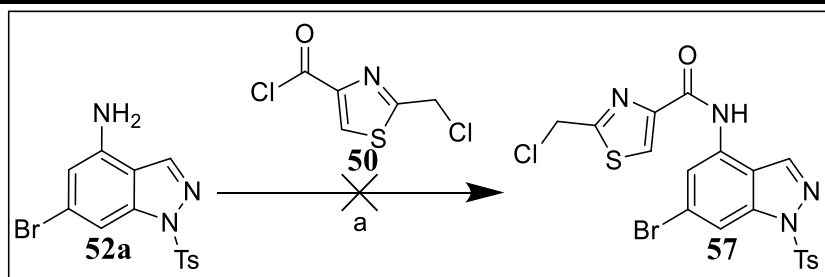
The core indazole heterocycle component **52a** was synthesised from commercially available 6-bromo-1H-indazol-4-amine, using tosyl chloride to protect the indazole nitrogen (Scheme 32).

Scheme 32: Synthesis of compound 52a



With the three components of the final drug synthesised, the next step was to couple the aniline and acid chloride to create amide **57**. Unfortunately, it was at this step where the synthesis failed. Despite following a published patent²²⁹, the aniline appeared to be too unreactive to displace the chlorine atom, and the acid chloride simply degraded to the methyl ester without reacting. Several attempts were made following the published methodology to no avail, with only starting indazole and the methyl ester of the thiazole present after several hours (Scheme 33).

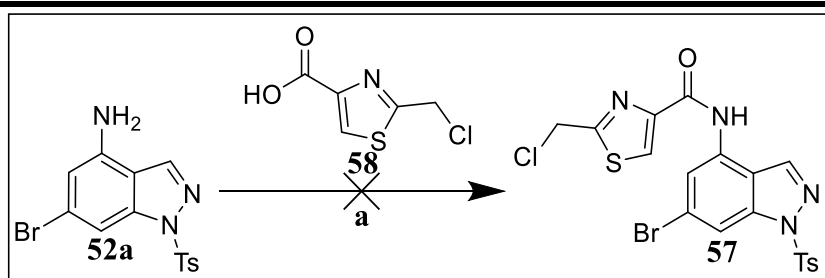
Scheme 33: Unsuccessful Amide Coupling



a) Dry DCM, pyridine or DIPEA, -10°C , N_2

Further attempts were then made to couple the aniline with the more stable thiazole acid (**58**) using various amide coupling methods (**Scheme 34**). Unfortunately, the aniline nitrogen did not participate in the reaction and only starting materials were detectable after several hours.

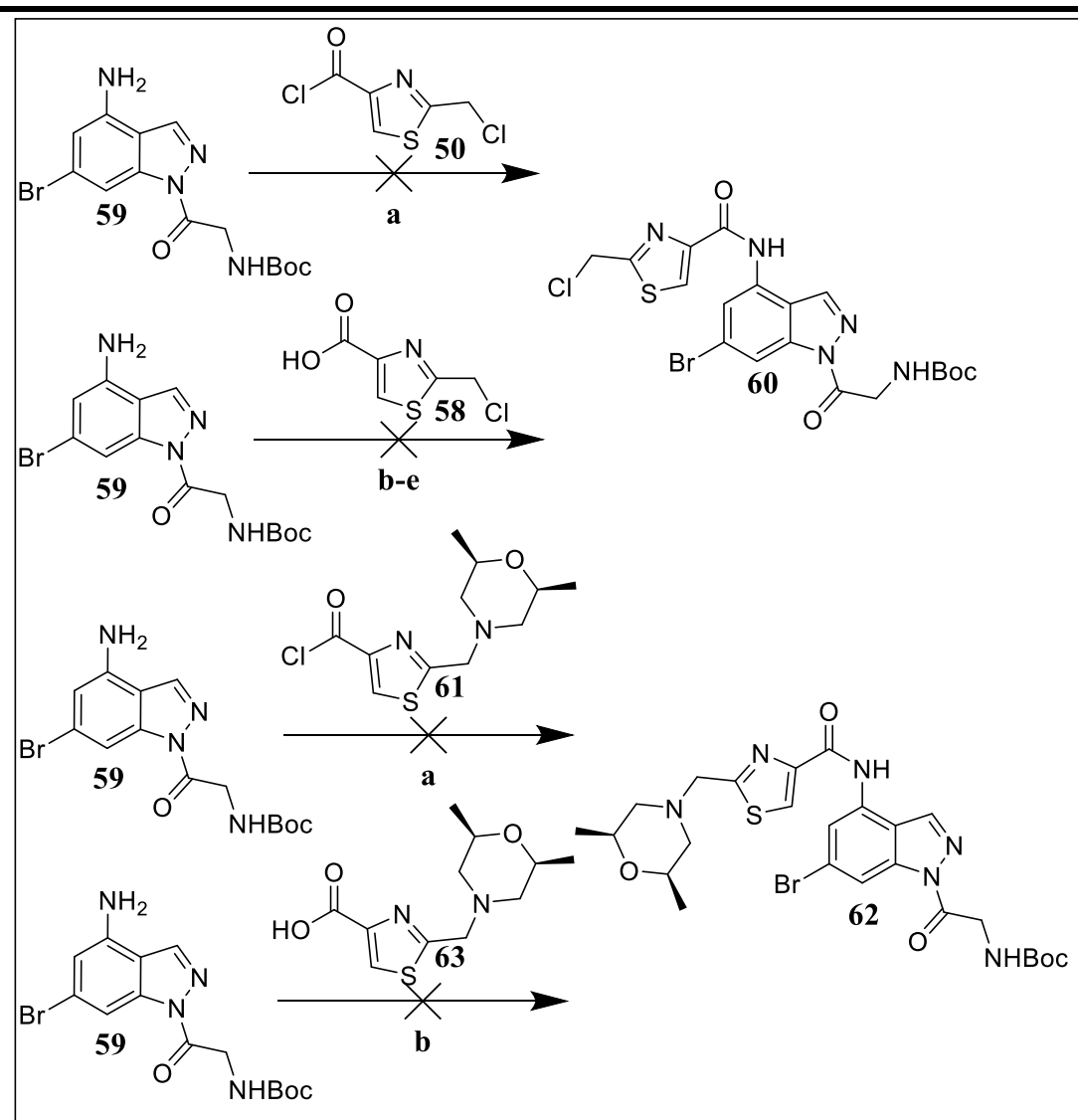
Scheme 34: Unsuccessful Amide Coupling



a) HATU, DMAP, DIPEA, DCM, 40°C

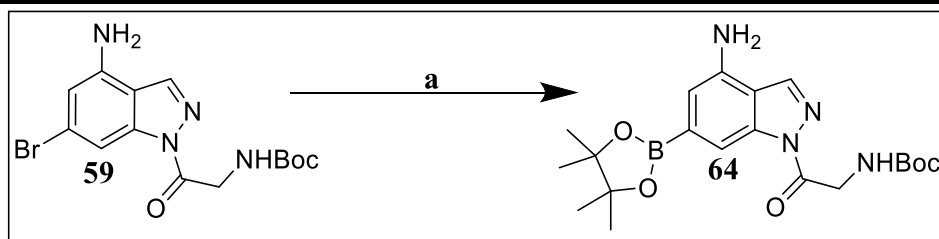
In attempt to reduce the electron withdrawing effect exerted by the tosyl group, it was decided that the first amino acid in the final dipeptide would replace the tosyl group in hope to raise the nucleophilicity of the aniline nitrogen (**Scheme 35**)

Scheme 35: Unsuccessful Amide Coupling



Unfortunately, as the aniline was still unreactive under these conditions, it was hypothesized that if the Suzuki partners were swapped, and the bromine was substituted for the boronic ester then it could further increase the nucleophilicity of the aniline, by removing the deactivating bromine atom (**Scheme 36**).

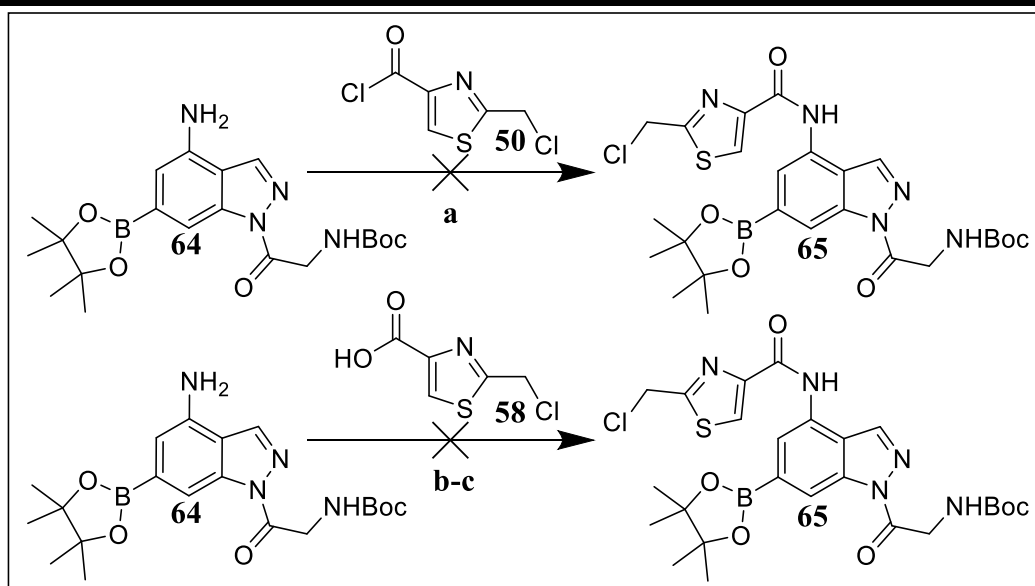
Scheme 36: Boronic Ester Synthesis



a) 4,4,5,5-Tetramethyl-1,3,2-dioxaborolane, KOAc, Pd(dppf).CH₂Cl₂, Dioxane, N₂, 100°C, 7hr, 71%;

Replacement of the bromine with the pinacol boronic ester was easily achieved (**64**), reaching 71% yield in 7 hours. Unfortunately, this substitution did not mitigate the low reactivity of the aniline, and subsequent coupling reactions remained unsuccessful (**Scheme 37**).

Scheme 37: Attempted Amide Bond Formation



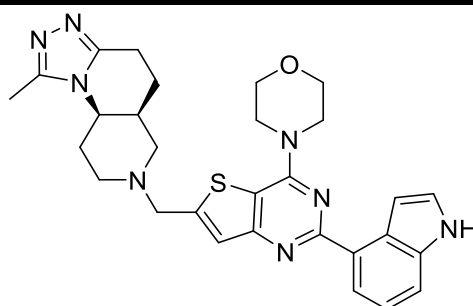
a) Dry DCM, pyridine or DIPEA, -10°C, N₂; b) HATU, DMAP, DIPEA, DCM, 40°C; c) BEP, NMI, DMF

With the purpose of this prodrug series being to simply test the applicability of the developed prodrug system to an intracellular receptor, it was decided that due to the difficult synthesis and over-reaction of the final drug compound, an alternative drug candidate would be identified.

3.3.5 Identification of New Drug Candidates

Although high specific PI3K δ/γ isoform activity is required for a pharmacological response against asthma and COPD symptoms, it is not required to test this drug delivery hypothesis, and thus the search for a drug candidate was expanded to include less selective PI3K inhibitors. By doing so, two suitable candidates were identified which could be incorporated into the prodrug design; PI3K δ -selective Compound **F** (Figure 43) and the pan PI3K inhibitor **Pictilisib** (Figure 45).

Figure 43: Identification of Compound F



Compound F

Physiochemical Property	Compound F
pIC ₅₀	9.1
Selectivity	δ/α : 3981 δ/β : 398 δ/γ : 1995
MWt	540.7

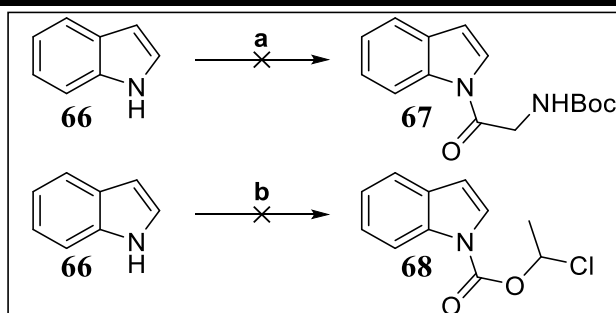
3.3.6. Discovery of Compound F

Schwehm *et al*²³⁰ discovered compound **F** during their search for new molecular scaffolds adaptable to parallel synthesis. Their work underpinned evidence that a substituted heterocycle fused to a nitrogen containing heterocycle was prominent in the scaffold of many successful drug molecules. They wanted to investigate the effect of geometric cis/trans isomerism, dihedral angle and chirality in 1,2,4 substituted triazole rings in effort to discover novel clinical candidates for DPP4 serine protease inhibitors, CCR5 antagonists and PI3 kinases inhibitors. Their SAR investigation

throughout the various domains lead to the discovery of Compound **F** as a highly potent and selective PI3K δ inhibitor, with physiochemical properties suitable for inhaled delivery.

In order to establish whether compound **F** was a suitable candidate, the chemistry of the indole moiety had to be investigated to determine its leaving group ability in the prodrug breakdown mechanism. As per the previous model system, indole was selected as a model for the drug component, and various prodrug syntheses were attempted (**Scheme 38**). Unfortunately, due to the differing reactivities of indole (**66**) compared to indazole, acylation of the basic nitrogen was unachievable.

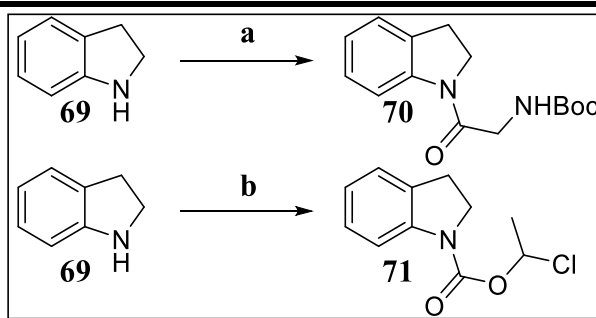
Scheme 38: Attempted Synthesis of Model Indole Prodrugs



a) Boc-Gly-OH, HATU, DMAP, DIPEA, DCM; b) 1-chloroethyl chloroformate, 4-methylmorpholine, DCM, -10°C;

In attempt to overcome the reactivity difference, indoline was used as a replacement, with the hypothesis that this could be reduced back to indole at a later point in the synthesis (**Scheme 39**).

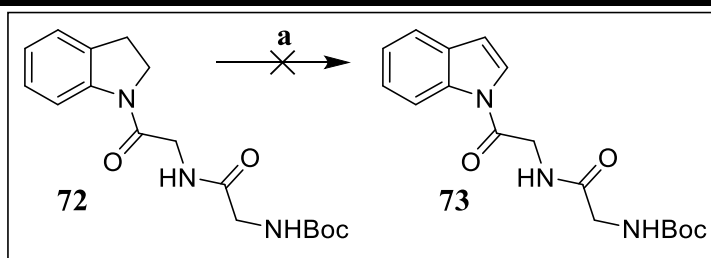
Scheme 39: Attempted Synthesis of Model Indoline Prodrugs



(a) *Boc-Gly-OH*, HATU, DMAP, DIPEA, DCM, 95%; (b) *1-chloroethyl chloroformate*, 4-methylmorpholine, DCM, -10°C, 96%;

Due to the different reactivity of the indoline, and the increased acidity and nucleophilicity of the nitrogen, the synthesis was much more fruitful, yielding both prodrug precursors in high yields. The next steps proceeded as per the previous chapter, with the dibasic moieties being created using simple Silver (I) Oxide and HATU coupling. Unfortunately, reduction of the indoline derivatives back to indole was unsuccessful using manganese (IV) oxide, and due to the high sensitivity of the self-cleaving prodrug, there were few alternatives available (**Scheme 40**).

Scheme 40: Reduction of Indoline Prodrugs



(a) *MnO₂*, DCM, 16 hr.

For this reason, Compound **F** was deemed to be an inappropriate candidate from which to prodrug, and instead, a similar less potent and less selective alternative was found in the form of Compound **G** (**Figure 44**).

Figure 44: Identification of Compound G

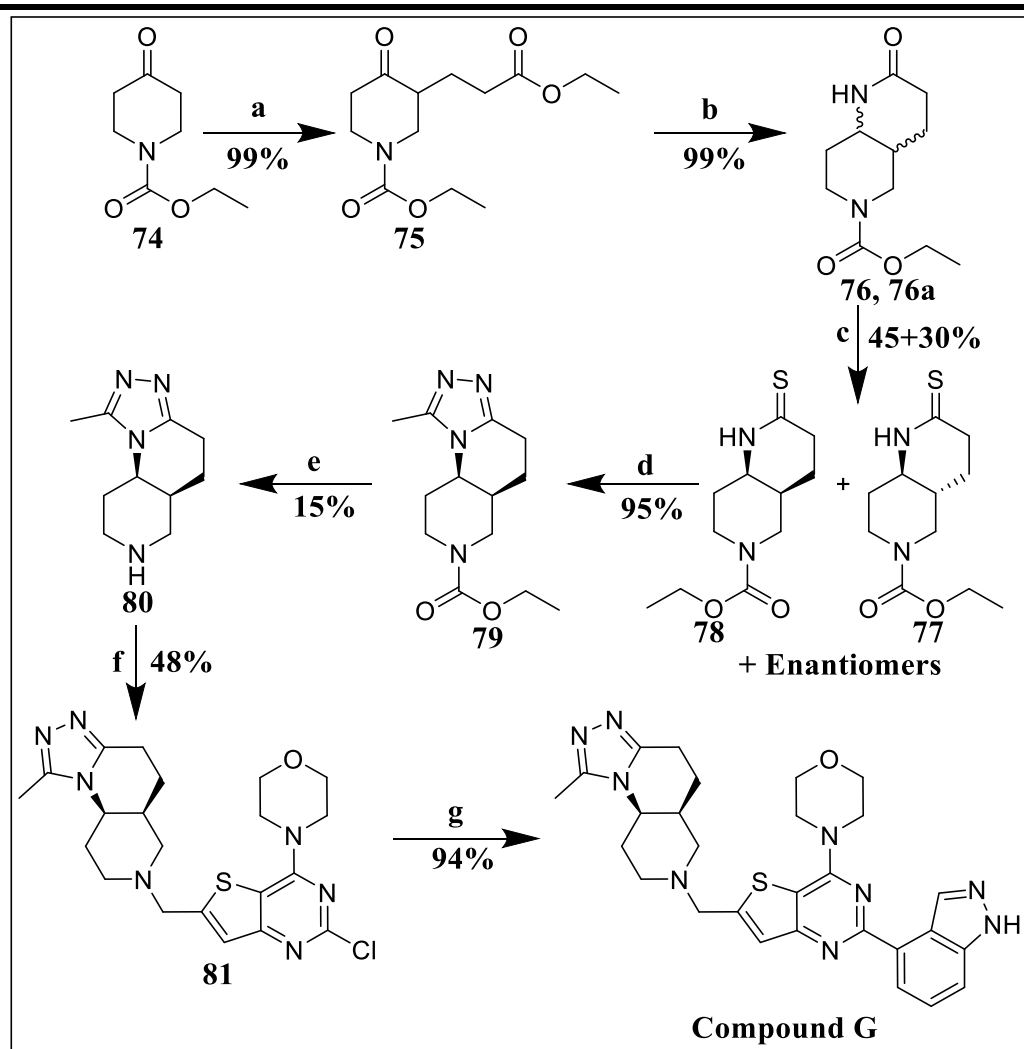
Physiochemical Property	Compound F	Compound G
pIC ₅₀	9.1 ± 0.0	8.5 ± 0.4
Selectivity	δ/α: 3981 δ/β: 398 δ/γ: 1995	δ/α: 501 δ/β: 398 δ/γ: 398
MWt	540.7	541.7

Although less selective than compound **F**, the indazole moiety of compound **G** would provide a suitable handle from which to build prodrugs, similar to that of the original GSK compound, and previous modelling could be used to help design the prodrug with the most suitable stability.

3.3.7. Synthesis of Compound G

The diastereo-synthesis of compound **G**, as described by Schwehm *et al*, follows an adapted procedure originally devised by Catalano *et al* (**Scheme 41**).²³¹ Ethyl 4-oxopiperidine-1-carboxylate (**74**) is first alkylated following azo-enolate conditions using pyrrolidine and ethyl acrylate. Aqueous work up restores the carbonyl, yielding the ester (**75**) in quantitative yield. This is then cyclised through reductive amination using sodium triacetoxyborohydride forming the unsaturated, diastereoisomeric bicyclic structures (**76** and **76a**). Unfortunately, cyclisation through this method creates a roughly 60:40 inseparable cis to trans mixture which sharply reduces the yield. Use

of Lawesson's reagent to create thio-amides (**77** and **78**) gratifyingly creates a pair of partially separable diastereomers from which, various hydrazides such as aceto-hydrazide can be used to generate the triazole ring (**79**). Deprotection of the piperidine ring yields the final amine (**80**) in poor yield, which can then be reductively aminated with the commercially available aldehyde to produce pyrimidine (**81**). Finally, standard Suzuki coupling achieves Compound **G**.

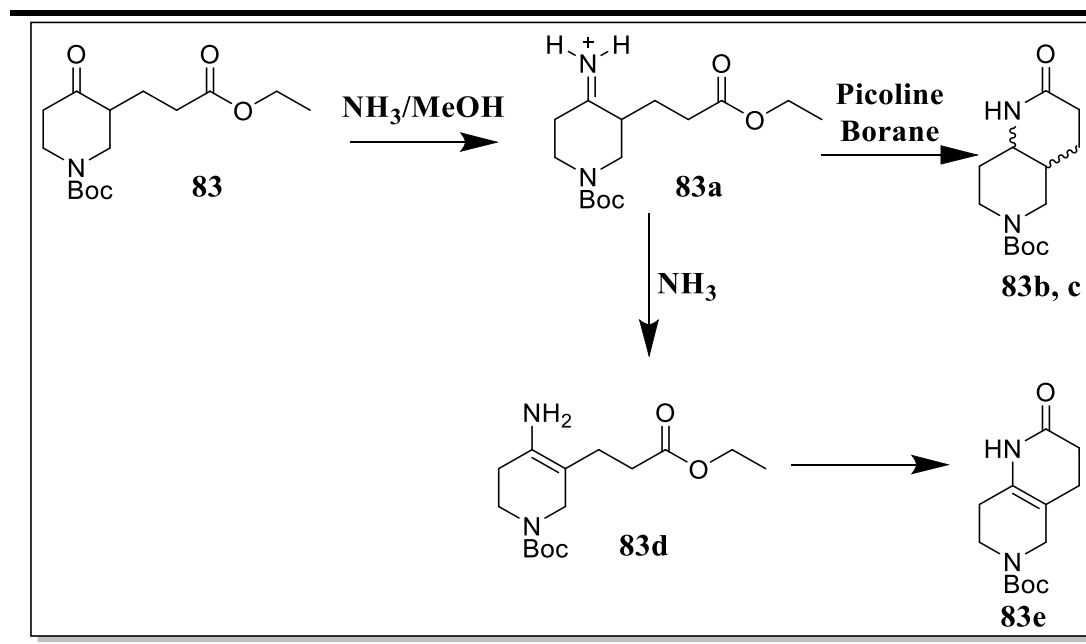
Scheme 41: Literature Synthesis of Compound **G**

a) i) Pyrrolidine, Tol, 170°C, 1 hr; ii) Ethyl acrylate, Tol, 130°C, 16 hr; iii) H₂O, 80°C, 0.5 hr; b) NH₃/MeOH, picoline borane, AcOH, MeOH Na₂SO₄, 40°C 16 hr; c) Lawesson's, DCM, 16 hr; d) Acetohydrazide, Tol, 130°C, 16 hr; e) KOH, water/ethanol, 120 °C, 20 h; f) Aldehyde, picoline borane, AcOH, MeOH Na₂SO₄, 40°C; g) Boronic acid, Na₂CO₃, (PPh₃)₂PdCl₂, EtOH, H₂O.

3.3.7.1 Route Optimisation

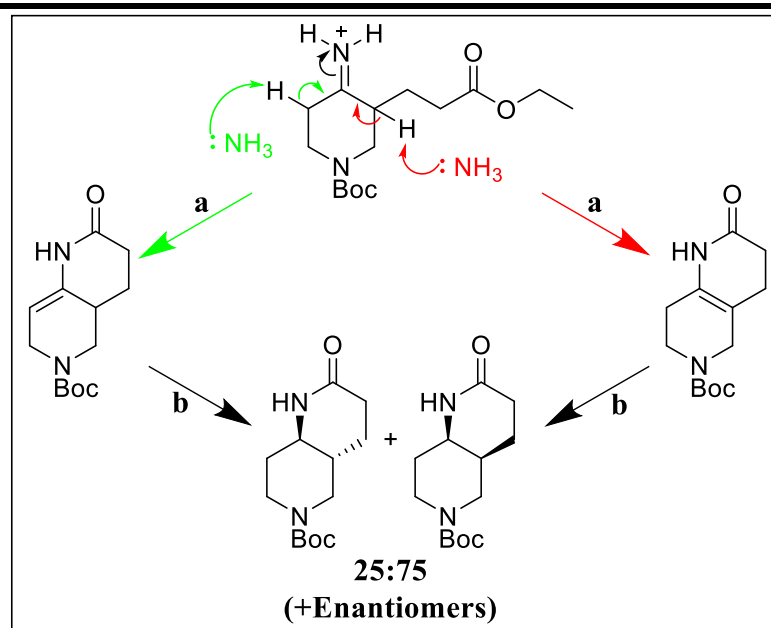
With only the more active cis isomer being required for prodrug synthesis, a revised diastereoselective synthesis was devised and trialled. Immediately, the ethyl carbamate protecting group was replaced for the more accessible Boc group, reducing deprotection time from 20 hours to around 90 mins, and greatly increasing the yield. It was found that the first step did not require 16 hours as stated in the literature, but instead would produce the same outcome under the same conditions in only 4 hours. Unfortunately, the poor yield produced in step 2 during cyclisation, and the difficulty of separating cis/trans isomers, proved to be less easily improved. It was thought that the poor yield could be due to reaction of the iminium cation with excess ammonia, yielding an enamine, similar to the previous step. The enamine would then not react with the picoline borane as intended, but would instead participate in its own cyclisation reaction forming an unsaturated bicyclic structure (**Scheme 42**).

Scheme 42: Cyclisation of 83



When analysing the products of the original reductive amination this hypothesis was confirmed: Over fifty percent of the reaction products were found to be the cyclic alkene, with the remaining products found to be a 60:40 mixture of the cis/trans isomers. To improve the synthesis, the picoline borane was omitted in order to promote alkene synthesis, with the intention that stereoselective catalytic hydrogenation of the alkene would lead to only the cis isomer. Unfortunately, upon hydrogenation, a 75:25 mixture of cis/trans isomers was produced. This meant that the initial conversion of the imine to the enamine was not regioselective and deprotonation by the excess ammonia had occurred on both sides of the carbonyl (Scheme 43).

Scheme 43: Possible Reductive Amination Cyclisation Routes

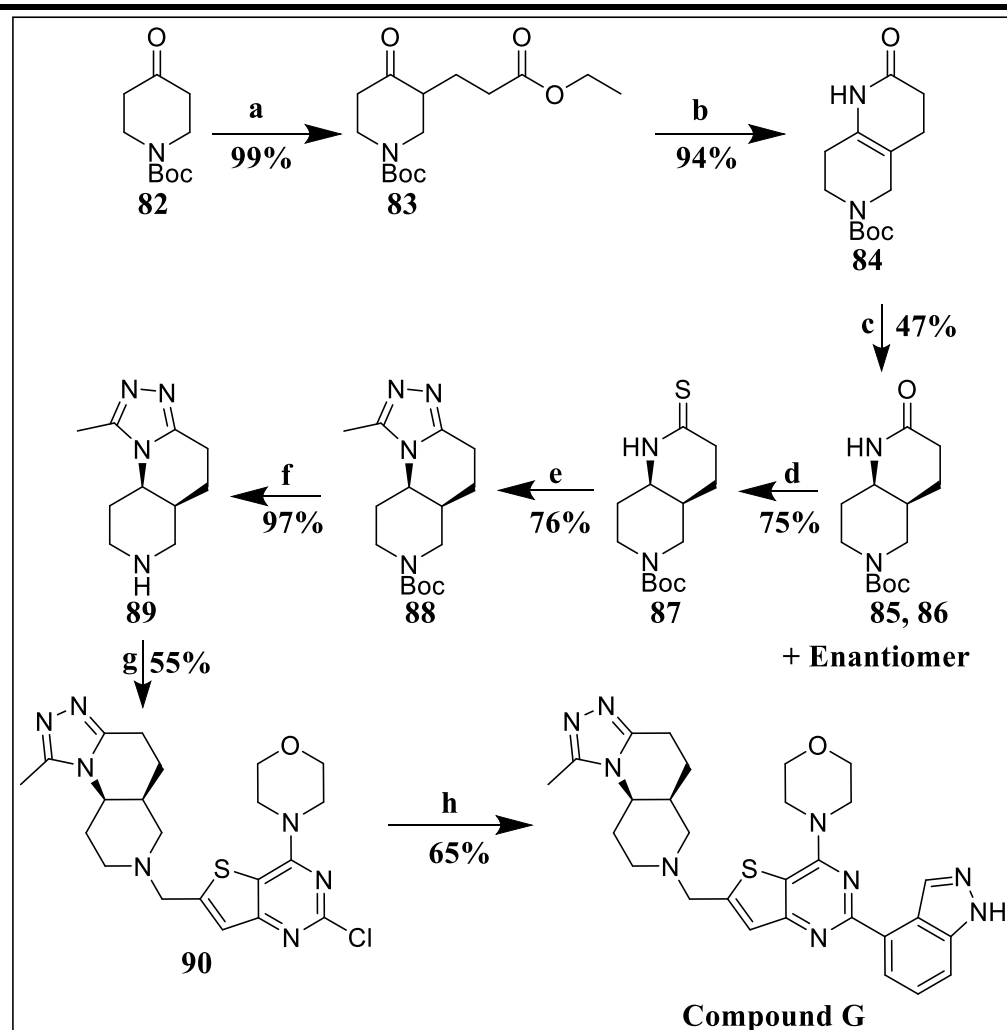


a) NH_3/MeOH , 40°C , AcOH , MeOH Na_2SO_4 , 16 hr; b) H_2 , Pd/C , 2 hr

In order to improve the regioselectivity, higher temperatures up to 120°C were used to push the cis/trans ratio to a maximum of 95:5. This also reduced reaction time to only 3 hours, and meant that separation of the diastereoisomers was much simpler as

there was less of the other diastereoisomers. The final steps remained the same as in the literature, but with HCl used to deprotect the amine instead of KOH. The final diastereoselective synthesis was used to produce compound **G** in an improved total yield of 9% compared to the original 3% (**Scheme 44**).

Scheme 44: Final Synthesis of Compound G



a) i) Pyrrolidine, Tol, 170°C, 1 hr; ii) Ethyl acrylate, Tol, 130°C, 16 hr; iii) H₂O, 80°C, 0.5 hr; b) NH₃/MeOH, AcOH, MeOH Na₂SO₄, 130°C; c) H₂, Pd/C, 4 hr; d) Lawesson's, DCM, 16 hr; e) Acetohydrazide, Tol, 130°C, 16 hr; f) HCl, DCM 1.5 hr; g) Aldehyde, picoline borane, AcOH, MeOH Na₂SO₄, 40°C; h) Boronic acid, Na₂CO₃, (PPh₃)₂PdCl₂, EtOH, H₂O.

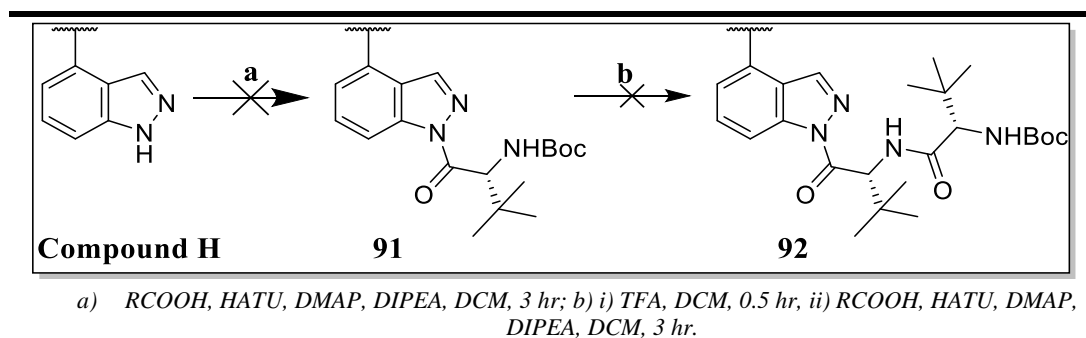
3.3.8. Synthesis of Compound G Prodrugs

With compound **G** synthesised in good yield, dibasic prodrug synthesis could take place. Following the same rationale as with the GSK compound, it was decided that

the use of the Ace Chloride linker should be avoided to circumvent any unnecessary diastereoisomer synthesis and to reduce the amount of cleavage products. As compound **G** already contained a basic component, the dipeptide did not need be itself dibasic, and instead focus could be turned to achieving the best combination of amino acids which had the appropriate steric bulk to achieve the most desirable half-life.

From the results of the initial indazole modelling, it was clear that two amino acids with a high degree of steric bulk would create a dipeptide with the slowest diketopiperazine formation, ultimately leading to the slowest release of drug (**Scheme 45**). By ensuring that the first amino acid was of unnatural chirality, the peptide would also have enzymatic stability as discovered in chapter 1.

Scheme 45: Intended Synthesis of Compound 71 Prodrugs



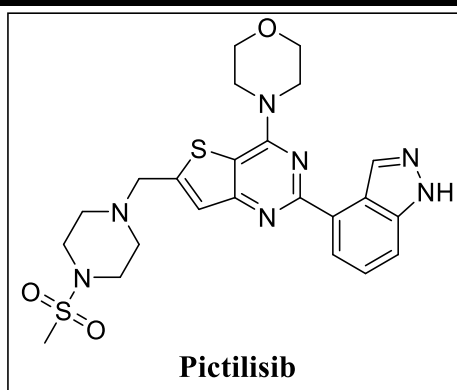
Unfortunately, although crude LCMS analysis showed good conversion of starting material to the mono peptide prodrug, any attempt at purification resulted in isolation of starting material in near quantitative yield. Several attempts were made but each purification attempt lead to the degradation of the mono peptidic product. Even when purification was avoided and the crude product taken further, amine deprotection to insert the second amino acid led to the breakdown of the mono-peptide. In order to

determine whether this instability was a common feature of all conjugated indazole moieties, or whether this was only a feature of this particular compound, the same synthetic strategy was applied to the less selective inhibitor, Pictilisib.

3.3.9. Identification of Pictilisib

In 2008, Genetech published the discovery of a novel pan PI3K α/δ inhibitor (Pictilisib) which displayed potency of 3 nM at both isoforms (**Figure 45**).

Figure 45: Identification of Pictilisib



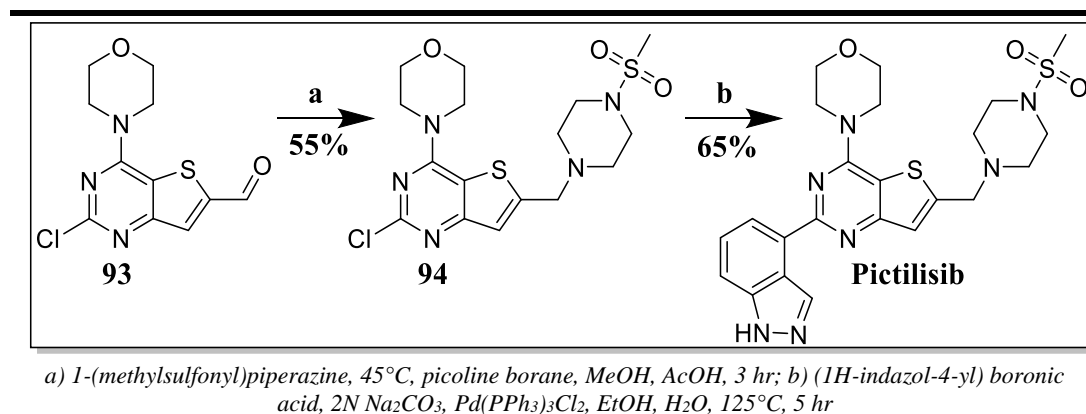
Physiochemical Property	Pictilisib
pIC ₅₀	8.52
Selectivity	α/δ : 1 α/β : 11 α/γ : 25
MWt	513.64

Recently published work within the Stocks' group had utilised the indazole group of Pictilisib as a handle for synthesising a cleavable codrug, and thus demonstrated pleasing stability when linked to other scaffolds.²³² garcgarces

3.3.10 Synthesis of Pictilisib

The synthesis of Pictilisib was achieved through the reductive amination of 1-(methylsulfonyl)piperazine with 2-chloro-4-morpholinothieno[3,2-d] pyrimidine-6-carbaldehyde (**93**) using picoline borane yielding tertiary amine **94**, followed by Suzuki coupling with (1H-indazol-4-yl) boronic acid (**Scheme 46**). All starting materials in this synthesis are commercially available and thus pictilisib was achieved quickly in high yield.

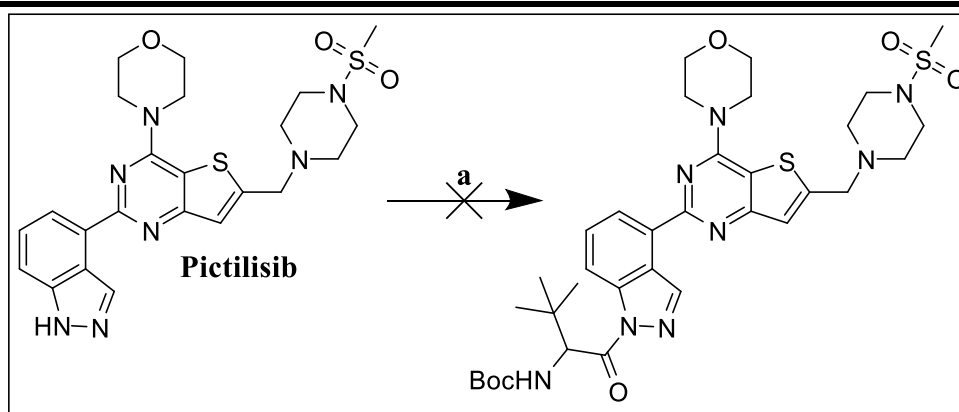
Scheme 46: Synthesis of Pictilisib



3.3.11 Synthesis of Pictilisib Prodrugs

Following pictilisib synthesis, prodrug synthesis was attempted analogous to Compound 71 and the previous GSK compound. Unfortunately, once again, despite reaction monitoring depicting a clean conversion to the mono-peptide, only the original starting material in quantitative yield was isolated (**Scheme 47**). This result has certified that a conjugated indazole moiety is not an appropriate linker for prodrug derivatisation and thus another suitable handle was required.

Scheme 47: Synthesis of Pictilisib Prodrugs

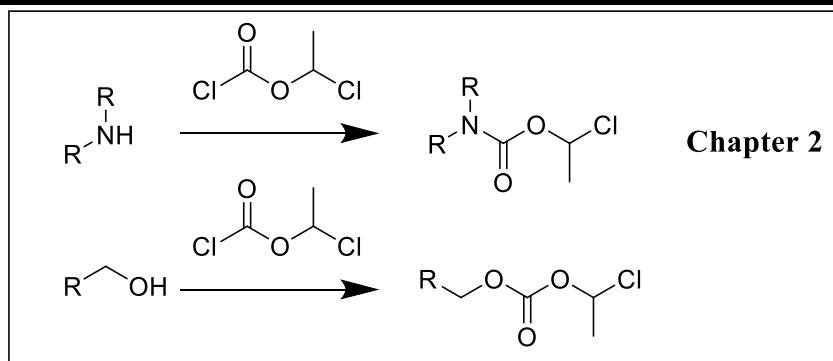


a) RCOOH, HATU, DMAP, DIPEA, DCM, 3 hr;

3.4 Reflections from Failed Prodrug Synthesis

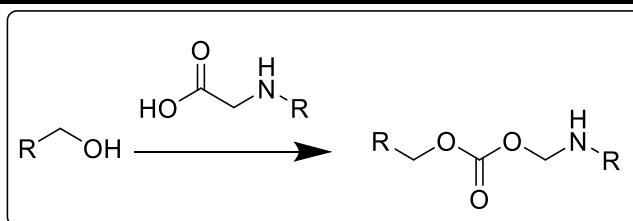
It is clear, that after 2 failed attempts to design a prodrug system based off of an indazole moiety, that this synthetic handle is not suitable. It is therefore necessary to begin searching for drug candidates with different chemical functionalities. It is known from chapter 2 that the current linker system works well with primary or secondary amines, creating a carbamate linker. It is therefore possible that alcohols would react in the same way to create carbonate linkers (**Scheme 48**), which would possess the same breakdown functionality.

Scheme 48: Use of Alcohol Groups to Create Carbonate Linkers



This hypothesis should first be tested in a simple model system, as per the indazole moiety, to prove that the alcohol group provides a good leaving group for activation to occur. It is also worthwhile to test whether direct carbamate synthesis using carboxylic acids is possible, in attempt to eliminate the need for the linker system (Scheme 49).

Scheme 49: Hypothesis to Test the Linker Group Requirement



3.5 Chapter Conclusion

This chapter aimed to complete thesis objective 4 (see **Thesis Aims and Objectives**), by developing the prodrug approach from in chapter 2 to an intracellular receptor inhibitor to determine the effectiveness of the prodrug system to efficaciously deliver an active agent at a sustained rate to an intracellular target. In chapter 2 the high lung homogenate binding value observed highlighted the potential of the prodrug to bind in close proximity to the M₃ receptor. This meant it was possible that a prolonged pharmaceutical activity could be achieved. For PI3K δ , the target receptor is not membrane bound but instead intracellular. This means that binding to the outside of the cell may not be crucial to providing a prolonged pharmacodynamic response. Instead, affinity for transmembrane transport proteins such as OCT's and PEPT2 may be crucial to obtaining high intracellular concentrations of the prodrug, with lysosomal trapping important to maintaining this intracellular concentration, resulting in increased lung retention.

In order to test this hypothesis, it was first necessary to identify a suitable drug candidate. PI3K δ inhibitors were chosen due to their pharmacological potential in the treatment of COPD and asthma, and typical utilisation of the pulmonary delivery route as a method of drug administration.

An initial drug candidate (**E**) was selected due to its high potency (pIC₅₀ 10.0), poor physiochemical properties and potential for characteristic improvement through application of a prodrug system. The indazole moiety present in compound **E** provided an opportunity for structural development to incorporate the prodrug system. A model system consisting of dipeptide indazole prodrugs were created to investigate the requirements of the dipeptide for sustained release due to internal cyclisation. As

witnessed in chapter 2, increased amino acid steric bulk lead to delayed DKP formation, this time with greater effect due to the ability to alter both amino acid side groups in the dipeptide.

Unfortunately, due to synthetic difficulties, and problems with over-acylation, the initial drug candidate (**E**) was deemed to be inappropriate for this prodrug system, and thus alternative candidates were required. Compound **F** from Schwenn *et al* was identified as having a similar potency (pIC_{50} 9.1) and selectivity, but incorporated an indole moiety rather than an indazole moiety. Construction of a model indole dipeptide system, analogous to the indazole model was attempted to test the suitability of the indole as a prodrug construction handle. Unfortunately, due to the differing reactivities of indole and indazole, synthesis was unsuccessful and compound **G** was also deemed inappropriate as the active component of the prodrug system.

Compound **G**, also discovered by Schwenn *et al* was identified as being a structurally similar to compound **F** but with an indazole moiety in place of the indole and with a slightly decreased potency (pIC_{50} 8.5) and selectivity for PI3K δ . Unfortunately, prodrug synthesis was once again unsuccessful, but this time due to the instability of the acylated indazole upon purification. Reaction monitoring displayed good conversion to the final product, but purification only yielded the original indazole in high yield. In order to determine whether this instability was a common feature of all indazole moieties, the same prodrug synthesis was applied to a new drug compound, **Pictilisib**. **Pictilisib** is a pan (α/δ) PI3K inhibitor, again with decreased potency (pIC_{50} 8.52) and selectivity. It was selected due to its easy synthesis, and due to its use in similar work performed within the Stocks group. The short synthesis allowed for a

quick comparison as to stability of acylated indazoles. Unfortunately, isolation of the prodrug was once again unachievable and thus confirmed that an indazole moiety was not an acceptable handle for prodrug synthesis.

Unfortunately, this chapter was not able to satisfy thesis objective 4, in that the prodrug system previously developed in chapter 2 was not adapted to incorporate a drug with an intracellular target. It is clear that both the synthetic handle on a drug molecule from which to develop the prodrug, as well as the linker system itself needs to be re-thought in order to further develop the prodrug system.

3.6 Future Work

Despite being unable to use the indazole nitrogen as an acceptable linker to create a prodrug, this prodrug system still has the potential to increase the lung retention of an inhaled intracellular drug candidate. Therefore, it is necessary to continue searching for an appropriate drug candidate which incorporates a more stable handle from which to link the prodrug. From the results of the SAR approach in chapter 2 alongside the attempted prodrug synthesis in chapter 3, it is clear that an appropriate handle for the prodrug system is one that is not conjugated into an aromatic system, such as an aliphatic secondary amine or alcohol.

Once a successful candidate has been identified, and the prodrug system has been developed, subsequent *in-vitro/in-vivo* analysis alongside a series of cellular assays would be required to determine the membrane penetration and localisation of the

prodrug within the lung epithelial cells. These cellular assays could be designed such that OCT or PEPT transporters are over expressed in the cell line. Incubation of these cells with the prodrug in the presence and absence of transporter inhibitors would then demonstrate the substrate potential of the prodrug, and thus indicate potential membrane permeation. Ultimately this work would conclude with an *in-vivo* PD study to determine if a prolonged pharmacological response is achieved.

4. Quantification of the Lysosomal Trapping Potential of Dibasic Prodrugs

4.1 Introduction

4.1.1 Lysosomal Trapping of Basic Drugs

Lysosomes perform key roles in metabolism due to their highly acidic lumen which contains various metabolic enzymes responsible for the breakdown of biomolecules including peptides, nucleic acids and carbohydrates.^{233,234} As previously mentioned, the high distribution of cationic, amphiphilic drug molecules arises due to a combination of their potential to be substrates for organic cation transporters, facilitating their distribution into cells, and for their potential to be sequestered within acidic organelles.²³⁵ Whilst lysosomal trapping can have a positive influence on the drug's pharmacokinetics, increasing the tissue retention of the administered drug for example, it is also possible for lysosomal trapping to cause a negative pharmacodynamic response, due to interference with the lysosomes natural metabolic processes.²³⁶

Uptake of weakly basic drug molecules into the acidic compartment of the lysosome will raise the internal pH such that it becomes sub-optimal for metabolic proteases, affecting the lysosomes' normal function.^{237,238} Although this process can have wide ranging complications for the cell, the system is in equilibrium thus has the potential to be self-regulating. By increasing the pH of the lysosome's internal environment, the proportion of cationic species will be reduced which will encourage the basic drug molecules to leave the lysosomes, once again lowering the internal pH to optimum levels. This equilibrium is of course driven by various factors including the pKa of the administered drug and thus the sequestering potential, as well as the drug dosage and cellular elimination rate.

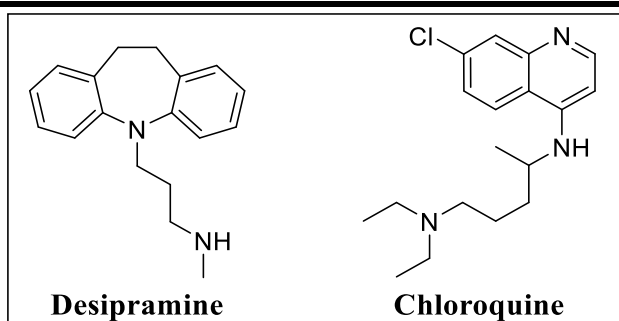
In addition, the presence of high intracellular concentrations of certain cationic amphiphilic drugs is known to induce phospholipidosis, a process in which phospholipids excessively accumulate in tissues such as the lung or liver.²³⁹ It is hypothesised that this process can occur due to changes in the metabolic environment of the lysosome, preventing phospholipid breakdown, or through the binding of drug molecules to the phospholipids, creating a stable drug-phospholipid complex, which enzymes cannot metabolise.²⁴⁰

Although both of these processes can be reversed naturally, their potential to encourage inflammation, histological changes and toxicity, certifies the need to quantify or visualise the uptake of cationic amphiphilic drugs, especially when attempting to exploit lysosomal trapping as a mechanism of sustained delivery.

4.1.2 Predicting/Quantifying Lysosomal Uptake/Trapping

Various methods have been employed to quantify the lysosomal accumulation of basic drugs, and determine the effect that this can have on the natural function of the lysosome.

The use of radio-labelled drugs to determine lysosomotropism in tissue slices of various organs is an established method of monitoring intracellular concentrations of various species. In 1995, Daniel *et al* recorded the contribution of lysosomal trapping to the cellular uptake of basic drug desipramine and dibasic drug chloroquine in the presence and absence of lysosomal inhibitors (**Figure 46**).²⁴¹

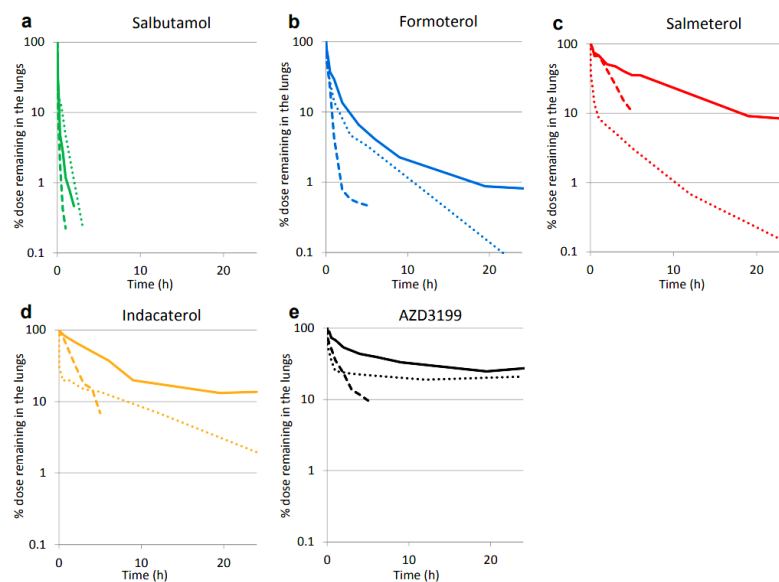
Figure 46: Structures of Desipramine and Chloroquine

Their results demonstrated that drug uptake within lung tissue was much higher than other tissues, corresponding to the tissue with highest concentration of alveolar macrophages, due to their high concentration in lysosomes. In addition, their results showed that uptake of desipramine was less dependent on the size of the lysosomal compartment within the tissue than chloroquine. Uptake of desipramine remained relatively constant among all tissue, but varied widely for chloroquine, with the highest uptake observed in tissues with the biggest lysosomal compartment. The uptake of chloroquine was most affected by the presence of lysosomal inhibitors NH_4Cl , NaF , and Monensin, which prevent a pH difference between the cytosol and internal lysosomal environment by raising the pH of the latter, such that sequestration does not occur.

This *ex-vivo* analysis highlighted the increased propensity for lysosomal trapping of dibasic compounds, to which Daniel *et al* suggested increased cellular transportation due to increased binding to pulmonary surfactant and increased alveolar macrophage presence.

More recently, this methodology was expanded upon by Bäckström *et al*, to determine whether a new methodology of agarose filled lung tissue slices could accurately predict the *in-vivo* PK profile of a range of inhaled β -adrenergic compounds.²⁴² Lung tissue slices preloaded with drug compound were incubated in buffer solution, in the presence and absence of lysosomal trapping inhibitor monensin and the concentration of drug compound at various time points monitored by tandem LC-Mass Spectrometry. They found that their new method supplied *in-vitro* data which closely aligned with that of previous *in-vivo* data, and demonstrated the importance of lysosomal trapping as a mechanism for retention of inhaled β -adrenergic compounds, as retention of all compounds fell in the presence of lysosomal trapping inhibitor, monensin (**Figure 47**).

Figure 47: Kinetic Profiles of Inhaled β -Adrenergic Compounds, Taken from Bäckström *et al*.



Solid lines represent new *in-vitro* data from their new methodology, dashed lines new *in-vitro* data in the presence of monensin, dotted lines represent previous *in-vivo* data after IT delivery.

Whilst variations of the lung slice methodology are able to determine the propensity of a basic drug for lysosomal trapping, the invasive method of homogenising lung tissue in order to sample the concentrations at various time points leads to ambiguity

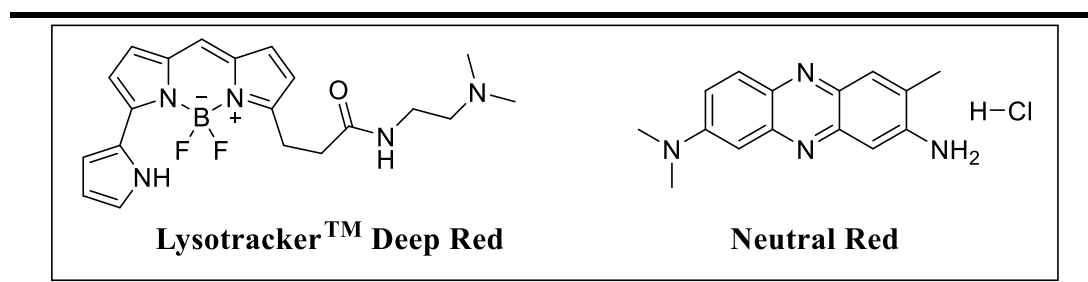
surrounding the location of the compound. The most accessible method of visualising drug compounds inside specific organelles in real time, without the destruction of the tissue/organelle involves the use of fluorescence microscopy.

4.1.3 Lysosome Visualisation using Fluorescence Microscopy

Fluorescence microscopes irradiate fluorophores with a specific wavelength of light, exciting an electron from its ground state energy level into an excited state.²⁴³ This excited electron then rapidly loses energy through collisions or molecular vibrations etc, before relaxing to its ground state level.²⁴⁴ Upon relaxation, the remaining excess energy is released as an emission of a photon of light (fluorescence). This fluorescence is of lower energy and higher wavelength than the emission source, and is detected by the microscope. The difference between the excitation and emission wavelengths is known as the Stokes' shift, and allows the microscope to filter out the excitation wavelengths, and focus solely on emission from the fluorophore.

Through careful design of fluorescent probes various intracellular structures can be detected, with the visualisation of lysosomes depending on the probe's ability to selectively accumulate within the organelle. Unfortunately, the highly digestive nature of these organelles makes it incredibly difficult to create probes which are able to survive in this metabolic environment long enough for fluorescence quantification.

Despite this, there has been varying success in creating lysosomal probes, with the most common lysosome targeting probes including LysoTracker™ (Invitrogen) and Neutral Red (**Figure 48**).^{245,246}

Figure 48: Structure of LysoTracker™ Deep Red and Neutral Red

In both of these examples, the probe is sequestered within lysosomes with varying degrees of specificity. LysoTracker is a boron difluoride species, modified with various scaffold additions in order to fine-tune the conjugated system and thus control the fluorescence excitation and emission wavelengths depending on the desired colour.²⁴⁷ Lysosomal sequestration follows the same principle as with cationic amphiphilic drugs, in that the basicity of the tertiary amine allows for protonation and sequestration within lysosomes.

Neutral red is a phenazine containing heterocycle with excitation and emission wavelengths of roughly 540nm and 621nm respectively (in DMSO).²⁴⁸ Cellular uptake of neutral red is driven through the molecule's high cell permeation through passive diffusion, and sequestration is driven through electrostatic binding to phosphate groups within the lysosomal matrix, although this is non-specific to all acidic organelles.²⁴⁹

In addition to LysoTracker Deep Red™ and Neutral Red, various fluorescent probes have been developed to monitor intracellular ion concentrations, some of which have found applications for visualising lysosomes.

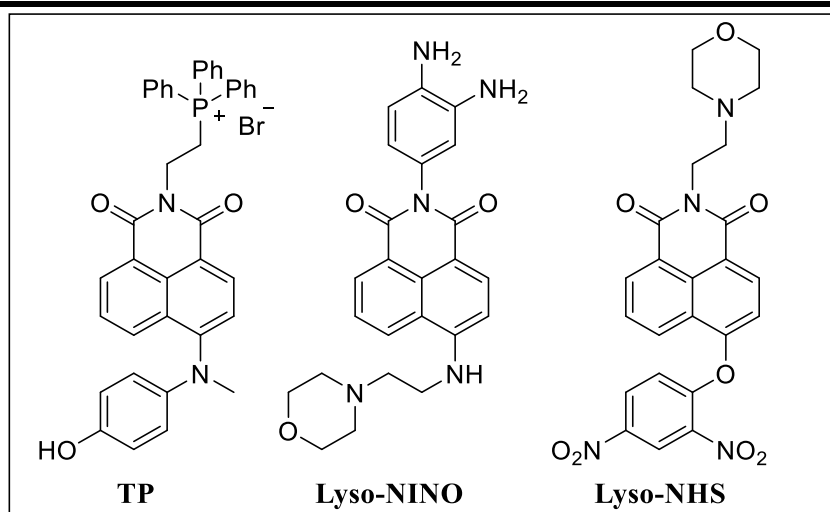
4.1.4 Intracellular Ion Concentration Monitoring

Ion regulation is a fundamental principle behind homeostasis, with the asymmetric maintenance of intracellular and extracellular ion concentrations critical for most biological functions.²⁵⁰ It is therefore highly desirable to be able to easily monitor various ion concentrations across different organelles to help elucidate the biological importance of ion concentration in disease progression.²⁵¹ The use of fluorescent probes and confocal microscopy is an established method for organelle visualization in the surveillance of intracellular ion concentrations as a method of early disease detection.²⁵² Development of organelle specific fluorescent probes is often difficult due to the wide ranging structures and physiochemical properties required of the probe to be able to specifically localize in only one organelle type. The requirement of the probe to also specifically bind only one ion type further complicates this process.

4.1.4.1 Development of 1,8-Naphthalimide Probes

Whilst both LysoTracker Deep RedTM and Neutral Red have lysosomal targeting properties, they have no capacity to help visualise intracellular ion concentrations as they remain permanently fluorescent once incubated into cells. In order to detect intracellular ion concentrations, a range of 1,8- Naphthalimide probes have recently been discovered as novel fluorescent probes with ‘switch functionality’ capable of triggering the fluorescence upon detection of a particular analyte.^{253,254} These include ‘NP’²⁵⁵ which is capable of detecting intracellular peroxy-nitrite, Lyso-NINO²⁵⁶ which is capable of detecting lysosomal nitric oxide, and Lyso-NHS²⁵⁷ which is capable of detecting lysosomal hydrogen sulfide (**Figure 50**).

Figure 49: Structure of TP, Lyso-NINO and Lyso NHS



4.1.4.3 Development of Lyso-NHS

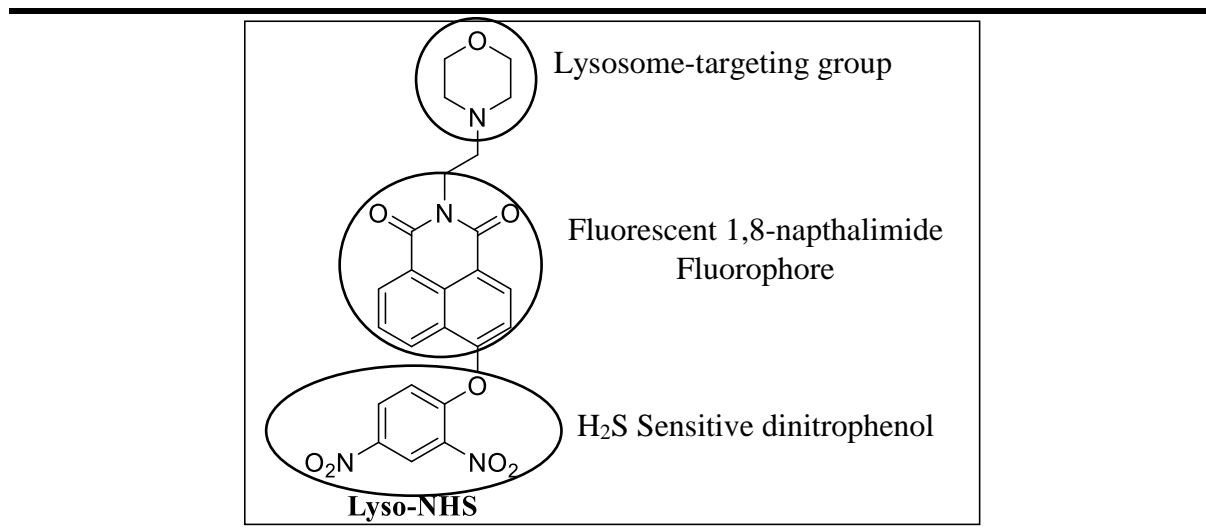
In 2013, Tianyu Liu *et al* published their discovery of the first 1,8-naphthalimide containing compound (Lyso-NHS) which bio-activates in the presence of intracellular H₂S to release a fluorescent probe capable of visualising lysosomal H₂S concentrations.²⁵⁷

H₂S is an important gasotransmitter molecule responsible for regulation of various biological systems including the relaxation of smooth muscle in the cardiovascular system.²⁵⁸ The complete role of H₂S in living systems is not entirely understood and thus being able to visualise various concentrations in different tissue types is an important step for biological H₂S elucidation. The development of Lyso-NHS was unique in that it required only a simple synthesis and a short incubation period, allowing visualisation to take place in just minutes, as opposed to several hours for previously discovered probes (LysoTracker Deep RedTM etc).²⁵⁹ In addition, the design of Lyso NHS meant that it could be used to specifically monitor ion concentrations within lysosomes.

4.1.4.2 1,8-Naphthalimide Probes Design

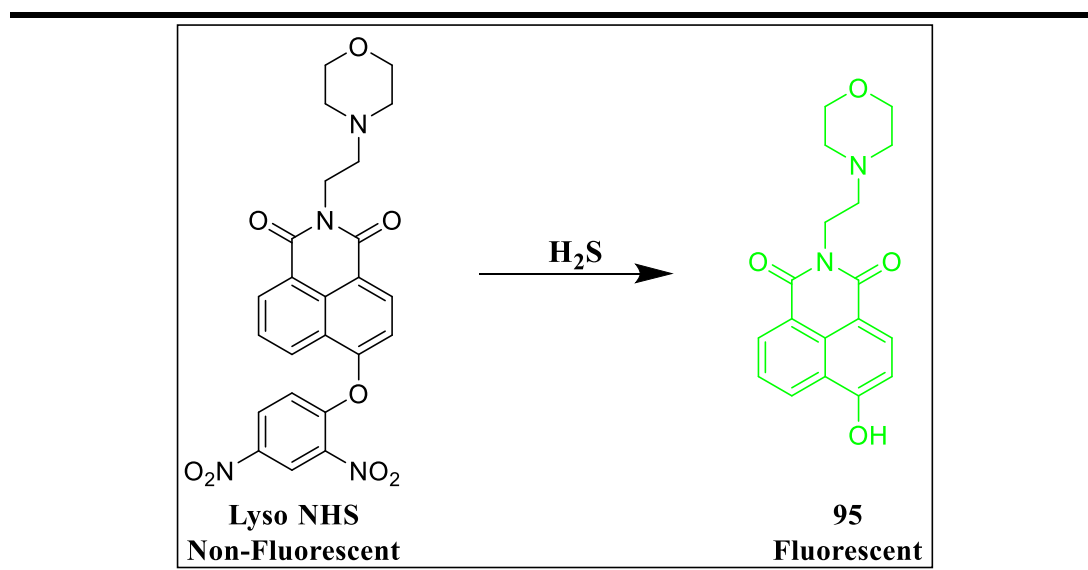
Despite their differing analyte detection capabilities and lysosomal sequestration abilities, TP, Lyso-NINO and Lyso-NHS have very similar structural motifs; a 1,8-naphthalimide heterocyclic core with high fluorescence potential, a fluorescence triggering group sensitive to a particular analyte, and a tissue localising group which determines the localisation of the probe within the cell (**Figure 50**).

Figure 50: Design of Lyso NHS



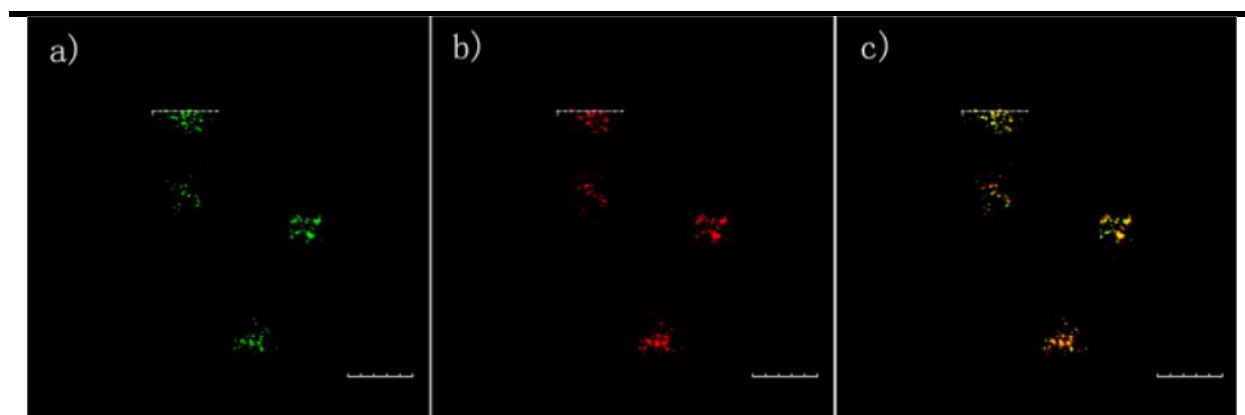
Uniquely, Lyso-NHS was designed such that the compound is non-fluorescent until exposed to H₂S, at which point the ether group connecting the two aromatic components is susceptible to nucleophilic attack from the sulfur, which triggers the release of the fluorescent phenol compound (**Scheme 48**).

Scheme 48: Activation of Lyso-NHS



Both Lyso-NHS and its phenol derivative are readily cell permeable and stable at physiological and lysosomal pH, while the inherent basicity of the morpholine group ensures they are sequestered within lysosomes after only short incubation period, allowing for lysosomal visualisation with confocal microscopy. When incubated alongside known lysosomal probe, neutral red, the fluorescent patterns of neutral red and the phenol derivative of Lyso-NHS aligned, proving the probe's capability to visualise acidic organelles, including lysosomes (**Figure 51**).

Figure 51: Colocalization of 95 and Neutral Red in MCF-7 Cells taken from Tianyu Liu *et al*²⁵⁷



- a) Localisation of 5 μM 95 incubated for 10 mins at 37°C (Channel 1: λ_{ex} = 450 nm, λ_{em} = 520-560 nm)
b) Localisation of 5 μM Neutral Red incubated for 10 mins at 37°C (Channel 2: λ_{ex} = 559 nm, λ_{em} = 565-610 nm)
c) Merged images of A and B, scale bars 20 μm

4.1.5 Application of Lyso-NHS to Lysosome Visualisation

Chapter 2 saw the creation of various dibasic prodrugs with the hypothesis that the inclusion of a dibasic moiety would optimise the prodrug such to increase the molecule's propensity for lysosomal trapping. The short synthesis, simple structure and adaptable design of the phenol derivative of Lyso-NHS makes it an attractive probe to help elucidate the role of the dibasic component in increasing lung retention. Through modification of the chemical scaffold, such to replace the lysosomal targeting morpholine group with variations of the dibasic moiety from chapter 2, it is possible to determine whether the lysosomal targeting nature of the compound, is retained, or even improved. This analysis would then help to conclude whether the prodrug system created in chapter 2 would likely lead to high lysosomal sequestration as expected.

4.2 Aims

This chapter aims to address thesis objective 5 (see **Thesis Aims and Objectives**) and elucidate the increased lung retention witnessed upon pro-drugging of a muscarinic receptor antagonist in chapter 2. As previously mentioned, incorporation of a dibasic component into the prodrug structure can increase the propensity for membrane binding, lysosomal trapping and for OCT transportation. Thus, by synthesising, basic, dibasic and non-basic analogues of a recently discovered, lysosome-targeting, fluorescent probe **95** (**Scheme 48**), it is possible to relate the propensity for lysosomal trapping and membrane binding to the basicity (ion class) of the probe, by comparing the fluorescence distribution patterns. It is hoped that this cellular assay and subsequent confocal microscopy is able to visualise the increase in lung retention when the basicity of a compound is increased.

4.3 Results and Discussion

4.3.1 Experimental Lysosomotropism Determination

It has been established in chapter 1 and 2 that dibasic compounds can exhibit multiple mechanisms by which lung retention can be observed. For this reason, it was decided that fluorescence microscopy was an acceptable experimental technique to be able to differentiate between the two. Through adaptation of the Lyso-NHS probe to include dibasic functionality, subsequent confocal microscopy would be able to visualise the cellular distribution of the probe. If the majority of the compound remained at the cell membrane, it would indicate that membrane/non-specific binding could be responsible for the increased lung retention. If the majority of the compound enters the cell, and accumulates in areas identical to the lysosomal targeting control probe, then it would be clear that lysosomal trapping is the mechanism by which lung retention occurs. In reality, when considering specific cationic and peptidic transporter proteins, the end result is likely to be a mixture of the two mechanisms and kinetics may denote which mechanism is most likely to occur first or which mechanism may predominate. Ultimately, this relationship needs to be discovered.

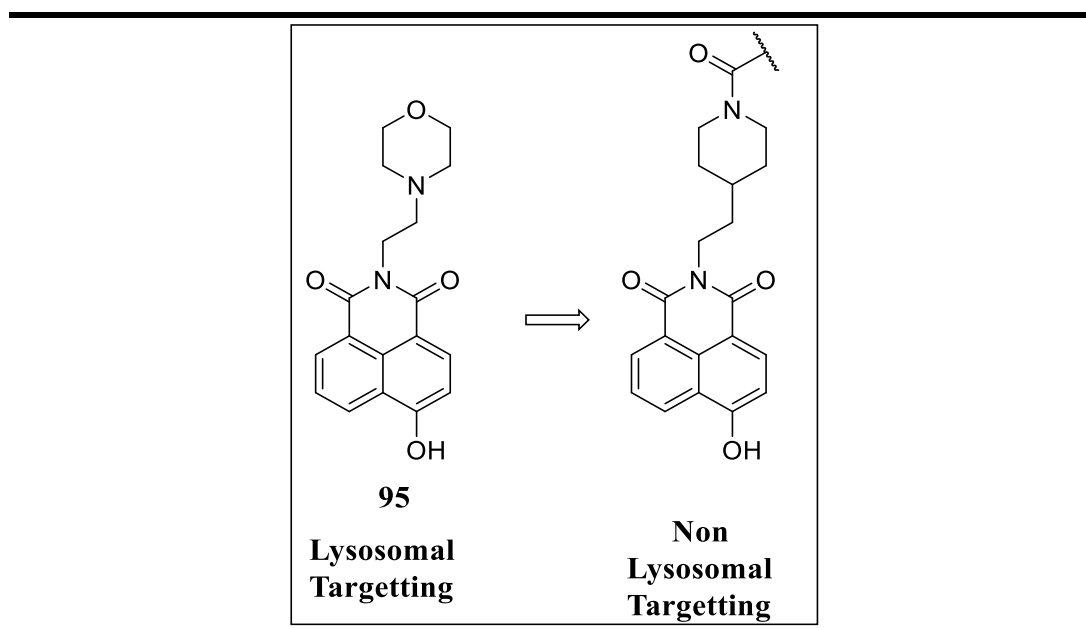
Once a clear relationship between probe basicity and lysosomal trapping has been determined visually using fluorescence microscopy, there are additional lysosomotropism experiments that can be performed on compounds in chapter 2, including compound 24, to be able to measure the extent of lysosomal trapping. By incubation of compound 24 with and without lysosomal trapping inhibitor monensin, it is possible to measure the cellular uptake and retention in the presence and absence of lysosome sequestration. The difference in cellular concentration between these two

experiments will yield a quantitative value for the lysosomal trapping potential. This method is well established in the literature²⁶⁰, however, as previously mentioned, competition between the two mechanisms must first be elucidated using confocal microscopy.

4.3.2 Adaptation of the 1,8-Naphthalimide Probe

As previously mentioned, the original design of the 1,8-naphthalimide fluorescent probe incorporated a cleavable aryl-ether bond which bio-activated in the presence of intracellular concentrations of H₂S (Scheme 1). When the two aryl groups are conjugated, the molecule displayed minute, background levels of fluorescence, but when separated, the naphthalimide containing phenol demonstrated much higher, quantifiable levels of fluorescence. Since there was no significant reason to design or synthesize a non-fluorescent probe, the dinitro-benzene component was omitted, and the lysosome targeting morpholine group of the fluorescent phenol compound (**95**) was replaced with a handle to which dibasic amino acids could be coupled (**Scheme 49**).

Scheme 49: Adaptation of 95

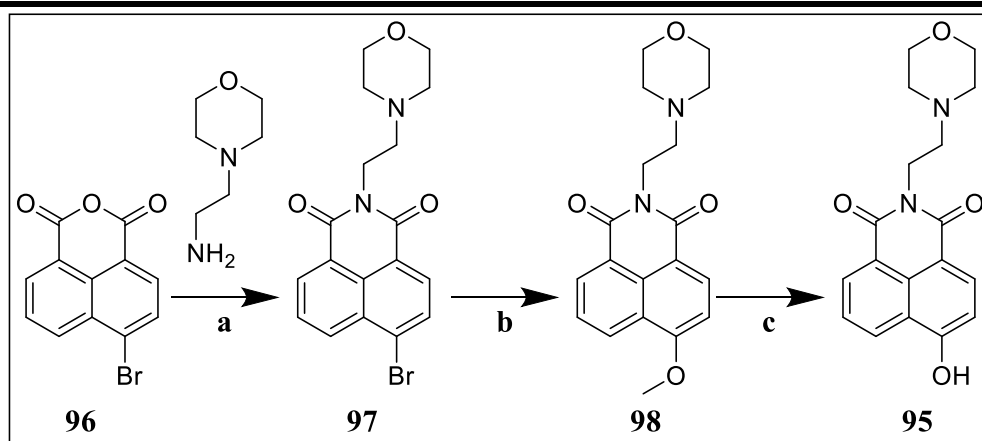


By replacing the morpholine group with an acylated piperidine group, the basic centre is removed and thus any base-driven lysosomal trapping from the scaffold is prevented. The piperidine could then be selectively acylated to incorporate a dibasic or neutral component in order to determine how basicity affects the distribution of the fluorescent component.

4.3.3 Fluorescent Probe Synthesis

To synthesize the fluorescent probe (**95**), 4-bromo-1,8-naphthalic anhydride (**96**) is first coupled with 4-(2-aminoethyl)-morpholine to create the imide species **97**. The bromine was then substituted for a methoxy group **98**, before being hydrolysed to the highly fluorescent phenol **95** (Scheme 50).

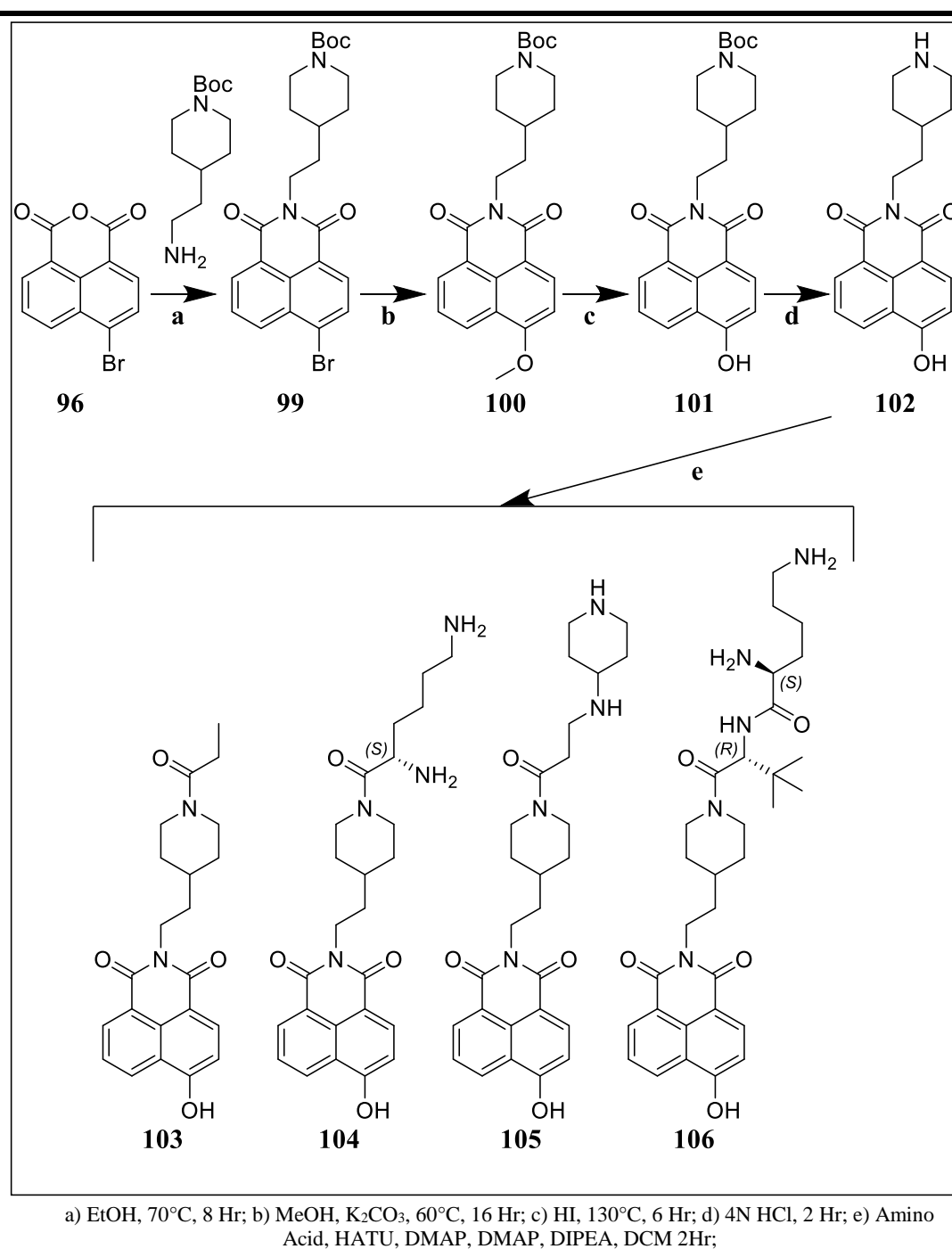
Scheme 50: Synthesis of 95



a) EtOH, 70°C, 8 Hr; b) MeOH, K_2CO_3 , 60°C, 16 Hr; c) HI, 130°C, 6 Hr

Synthesis of the dibasic and neutral analogue probes followed a similar approach, using tert-butyl 4-(2-aminoethyl) piperidine-1-carboxylate (**96**) to create the imide **99** (Scheme 51). As per the previous synthesis, the bromine was then substituted for the methoxy group **100**, before being hydrolysed to the phenol **101**. The amine was then deprotected (**102**) and coupled with various amino acids to create a range of dibasic and neutral fluorescent probes (**103-106**).

Scheme 51: Synthesis of 103-106



A small series of ‘pro-drugged’ probes containing either a neutral or dibasic moiety was synthesised. The original linker group from the muscarinic prodrug series was omitted in order to increase the chemical stability of these compounds in aqueous cell based assays.

4.3.2.1 Fluorescent Probe Prodrug Stability

Due to the omission of the cleavable linker group, and high stability of the amide bond, all of the synthesised probe prodrugs achieved the minimum stability requirement of 24 hours without any observed breakdown in pH 6.5 PBS. This ensured that the probes would be chemically stable throughout any *in-vitro* assays, including cell incubation as a solution in aqueous media.

4.3.4 Fluorescent Probe Prodrug Characterisation

From the original literature, the phenolic naphthalene (**95**) demonstrated an excitation and emission maxima at 450 and 555 nm respectively. Despite containing the same fluorophore, it was important to determine the excitation and emission wavelengths for the prodrugs using a fluorescence spectrophotometer, with samples being prepared as per **Biological Assay Procedure 6**.

Pleasingly all of the synthesised probes possessed excitation and emission wavelengths identical to Lyso NHS (**Table 13**), meaning they could easily be visualised alongside the control probe, LysoTracker Deep Red™ (excitation and emission wavelengths 540 and 627 respectively) using confocal microscopy. LysoTracker Deep Red™ was chosen as a control probe instead of neutral red due to its reported specificity for lysosomal targeting, rather than targeting all acidic organelles as with neutral red.

4.3.3.1 pH Dependent Fluorescence

Due to the highly acidic lysosomal environment, it was important to understand any effect that decreasing pH may have upon the fluorescence emission intensity at 555nm. The emission spectra of all of the synthesized probes was determined at multiple pH levels using a fluorescence spectrophotometer, with samples prepared as per **Biological Assay Procedure 6**.

All of the probes demonstrated a pH dependent fluorescence, with fluorescence intensity at 555nm increasing with increasing pH (**Table 13**). Lyso NHS displayed slightly higher fluorescence levels than the synthesised probes, however all probes were fluorescent at lysosomal pH (4-6) and thus were ideal candidates for lysosomal visualisation. Tianyu Liu *et al* hypothesised that the pH dependence on the fluorescence maxima is due to the acidity of the phenol, where its deprotonation increases the electron donation into the pi-system, resulting in an increased fluorescence.

Table 13: Fluorescence Characterisation Data for Synthesised Probes

Compound	Excitation Wavelength (nm)	Emission Wavelength (nm)	pH Dependent Fluorescence	
			pH	IF ₅₅₅
95	450	555	3	29.43
			4	17.93
			5	32.93
			6	73.16
			7	121.66
103	450	555	3	0.93
			4	2.63
			5	10.85
			6	33.89
			7	58.21
104	450	555	3	0.23
			4	1.48
			5	3.95
			6	12.75
			7	23.25
105	450	555	3	0.17
			4	2.23
			5	7.51
			6	22.41
			7	32.99
106	450	555	3	0.86
			4	4.93
			5	10.36
			6	28.59
			7	39.43

IF₅₅₅ – Fluorescence intensity at 555 nm

4.3.3.2 Cytotoxicity – performed by Paulyna Magaña Gomez

With the knowledge that all the synthesised probes were chemically stable and highly fluorescent across all intracellular pH levels, the next step was to determine the cytotoxicity values associated with the probes to ensure that the cells would be able to tolerate the compounds.

The cytotoxicity of the four novel probes (**103-106**), in addition to the original morpholine containing probe (**95**) was determined using a standard MTT assay as

described in **Biological Assay Procedure 7** and **9**, and the cell viability measured at 0.5 hour and 20.5 hours. The results of this assay demonstrated a high level of tolerability of the cells for the probes at 0.5 hours and modestly reduced tolerability after 20.5 hours. Uniquely, compound **104** maintained a high level of cell metabolic activity at both incubation durations. Considering a desired incubation time of only 30 minutes for the confocal microscopy assay, this MTT assay demonstrated a good level of tolerability of the cells for the probes, meaning that subsequent confocal microscopy could be performed (**Table 14**).

Table 14: Cytotoxicity Data for Compounds (95, 103-106) – Performed by Paulyna Magaña Gomez

Compound	95	103	104	105	106
Cell Metabolic Activity t=0.5 Hour	95 ± 8 %	93 ± 3%	96 ± 8%	105 ± 3%	90 ± 7%
Cell Metabolic Activity t=20.5 Hour	73 ± 15%	70 ± 9%	95 ± 3%	74 ± 10%	78 ± 6%

4.3.3.3 Confocal Microscopy – Performed by Paulyna Magaña Gomez

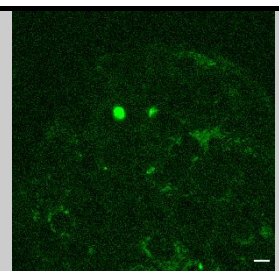
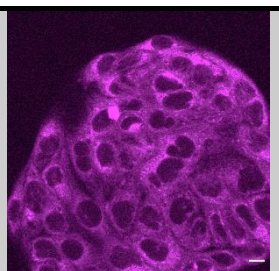
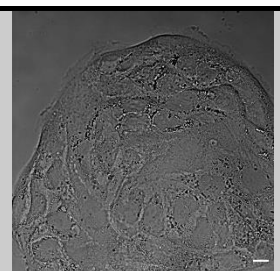
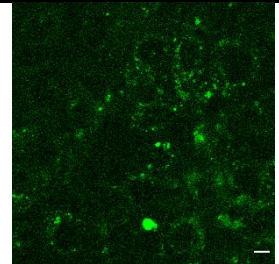
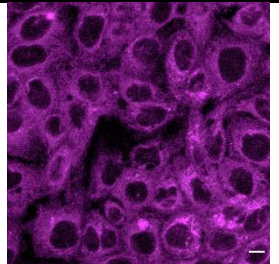
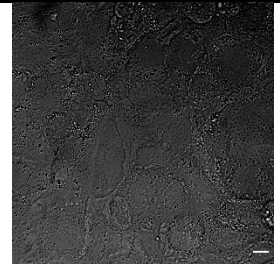
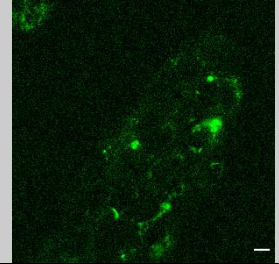
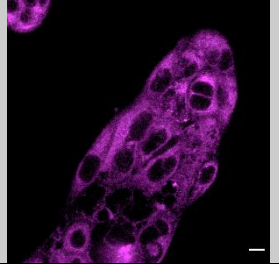
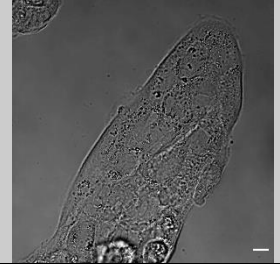
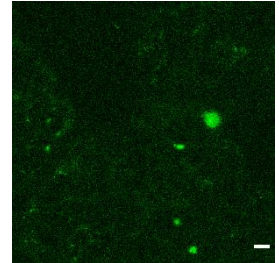
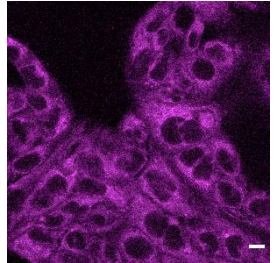
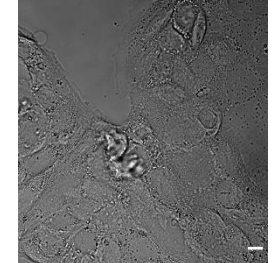
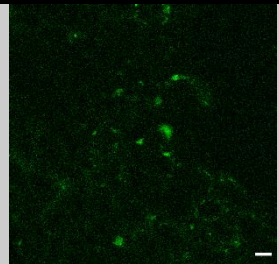
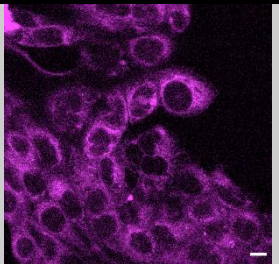
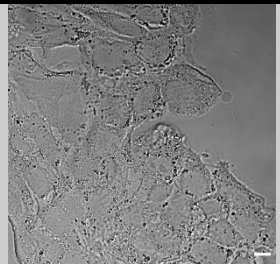
With minimal cytotoxicity confirmed, the synthesised probes were then incubated alongside the control probe, to confirm their cellular distribution. Each probe was incubated into Calu-3 cells for 30 minutes at 5 µM concentrations alongside the control probe, LysoTracker Deep Red™, at a concentration of 50 nm. Subsequent confocal microscopy was then used to visualise the cells as outlined in **Biological Assay Procedures 7** and **9** (**Figure 52**). Each of the 3 (di)basic probes (**104-106**) displayed similar cellular distribution patterns, with localised regions of high fluorescence, but at a much lower intensity and resolution to the control probe. The

neutral probe (**103**) appeared to be more ubiquitously expressed throughout the cell, however due to the poor image quality, this cannot be confirmed.

Unfortunately, when incubated alongside compounds **95** and **103-104**, it was observed that LysoTracker Deep Red™ was unable to specifically accumulate within lysosomes. Instead, LysoTracker Deep Red™ is distributed ubiquitously throughout the cell, with the exception of the nucleus. This means that no clear conclusion as to the location of compounds **103-106** could be drawn as the control probe was ineffective. Initially, it was hypothesised that the short incubation time of 30 mins was insufficient for the LysoTracker Deep Red™ to be sequestered within lysosomes and instead a longer incubation period of 2 hours should be trialled to allow for full sequestration.

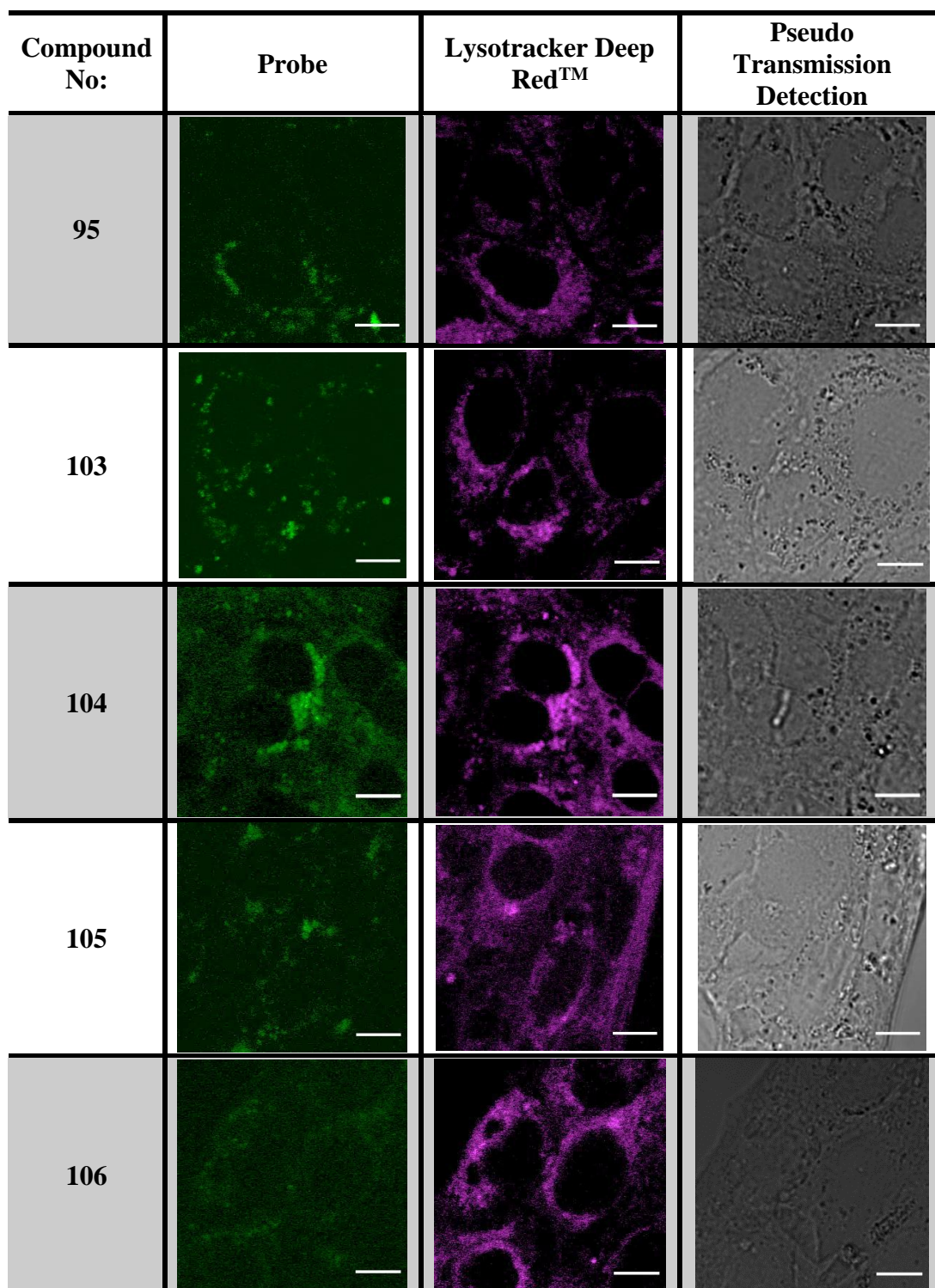
Unfortunately, when the incubation period was increased to 2 hours (data not shown), no significant improvement was made. It was then theorised that sub-optimal cell washing, had resulted in poor quality confocal images. Thus, the confocal imagery was repeated following a 30-minute incubation period which used a more thorough cell washing procedure (**Figure 53**).

Figure 52: Confocal Imagery of the Lysosomal Probes

Compound No:	Probe	Lysotracker Deep Red™	Pseudo Transmission Detection
95			
103			
104			
105			
106			

Confocal laser scanner microscopy images of Calu-3 cells exposed to Compound 1 for 30 min. ^a Synthesised probe, 5 μ M, Ex: 488 nm; ^b Lysotracker Deep Red™, 50 nM, Ex: 633 nm; ^c Pseudo transmission detection. Scale bar: 10 μ m

Figure 53: Confocal Imagery of the Lysosomal Probes



Confocal laser scanner microscopy images of Calu-3 cells exposed to Compound 1 for 30 min. ^a Synthesised probe, 5 μ M, Ex: 488 nm; ^b Lysotracker Deep Red™, 50 nM, Ex: 633 nm; ^c Pseudo transmission detection. Scale bar: 10 μ m

Gratifyingly, the improved cell washing procedure resulted in a clearer depiction of the distribution of the LysoTracker Deep RedTM control, meaning that it was able to display selective lysosomal targeting and thus act as a control probe for compounds **95** and **103-106**.

Compounds **95**, **105** and **106** displayed much lower fluorescence than that of compounds **103** and **104**, which could indicate a reduced cellular uptake. Compound **103** (the neutral analogue) exhibited a larger volume of distribution throughout the cell, with little similarity to the control probe, whilst compound **104** (the lysine containing dibasic analogue) exhibited high fluorescence in small localised regions within the cell which aligned with the control probe, indicating that this compound had selectively accumulated within lysosomes. Compounds **95** and **105** appeared to faintly show similar distribution patterns to the control probe, however, owing to a reduced fluorescence, it is impossible to accurately confirm the cellular distribution of compounds **95**, **105** and **106**, and thus further studies would be required.

As all of the synthesised probes contained the same fluorophore and demonstrated similar fluorescence intensities at the required pH, it is theorized that any difference in the observed fluorescence could be a consequence of reduced cellular uptake, and thus compounds with slower/hindered cellular uptake would have a lower cellular concentration and thus lower fluorescence intensity. Interestingly, the compound which demonstrated the lowest fluorescence (**106**), and thus could be subject to the poorest cellular uptake contains the same dibasic moiety as compound **24** (Chapter 2) which evaded enzymatic degradation. It is possible that the use of the unnatural amino

acid in the dibasic moiety has once again resulted in the evasion of natural cellular processes. If this hypothesis were correct it could have far reaching consequences for use of this prodrug system when targeting intracellular receptors such as PI3K. It is likely that whilst a basicity driven, increased lung retention through membrane binding is possible, an increased pharmacological activity is not possible due to the compounds inability to reach the target receptor.

To test this hypothesis, the natural chirality analogue of **106** should be synthesised alongside a wider range of basic, dibasic and neutral probes. This would help to create a clearer picture as to why the fluorescence was reduced for compounds **105** and **106**. As mentioned in chapter **2**, once a suitable range of compounds has been created and demonstrate higher levels of fluorescence, these cellular assays could be repeated in cell line which is over expressed in OCT or PEPT2 transporters, in the presence and absence of transporter inhibitors. If the fluorescence intensity is reduced inside the cell, it could indicate that transporter proteins were responsible for the uptake of the basic/dibasic probes.

4.4 Chapter Conclusion

This chapter aimed to address thesis objective 5 (see **Thesis Aims and Objectives**) by attempting to elucidate the cellular uptake and distribution of dibasic compounds, when compared to neutral or basic analogues, with fluorescent microscopy chosen as a simple and effective method of quantification. By identifying a recently discovered, lysosome targeting, fluorescent probe, it was possible to amend the structure such that its lysosome targeting nature was removed and replaced by neutral, basic and dibasic scaffolds. The hypothesis was that the lysosome targeting nature should be restored in the (di)basic analogues, if lysosomal trapping is driven by basicity. This series of fluorescent probes were then screened for their fluorescence parameters and cellular toxicity, before being incubated into Calu-3 cells alongside known lysosomal probe LysoTracker Red and visualised using confocal microscopy.

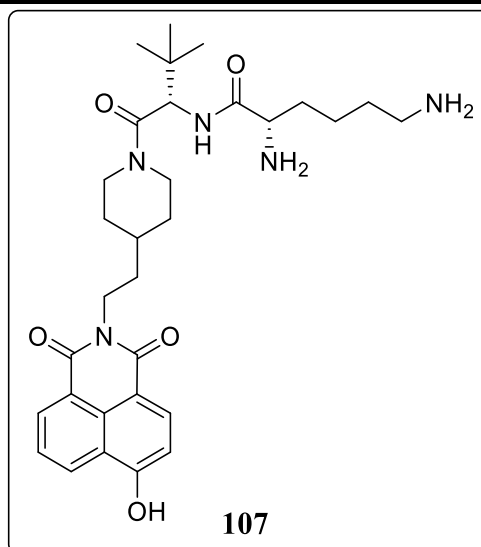
Initially, the images generated were of poor quality due to inadequate cell washing procedures. Fortunately, once a more thorough procedure was implemented, confocal images with interesting results were obtained. Lyso NHS appeared to be much less fluorescent than documented in the literature, whilst the neutral and dibasic probes displayed various results. Unfortunately, the impact of COVID-19 alongside practical difficulties with cell washing meant that no full conclusion as to the distribution of probes could be made. It is clear that a much wider range of analogues are required of which need to be screened at higher excitation intensity. It is also necessary to visualise the cells at various time points to see how the fluorescence changes, as it is not clear if the assay incubation period was long enough for the compound to fully distribute.

4.5 Future Work

Unfortunately, due to the impact of COVID-19, the research within this chapter was adversely affected and thus completion of the intended aims was not achieved. Due to the poor resolution/low fluorescence for compounds **95**, **105** and **106** it is impossible to determine whether the increase in basicity of the compounds **104-106** led to an increase in lysosomal trapping. As previously mentioned, further studies which fully explore the relationship between basicity and lysosomal uptake, alongside the relationship between cellular uptake mechanism and dibasic structure are required to fully understand these results.

In order to confirm whether the unnatural chirality of compound **106** has prevented its cellular uptake, synthesis and subsequent cellular distribution studies should be performed on the natural analogue (**107**) (**Figure 54**).

Figure 54: Compound 107



If the fluorescence intensity of **107** was increased relative to **106** then it could confirm a reduced cell penetration, possibly due to reduced substrate affinity for OCTs.

This hypothesis could then be confirmed, by repeating the microscopy assay but in the presence of OCT inhibitors for the incubation period. This assay would elucidate the role of OCTs in the cellular uptake of dibasic compounds, as any loss of intracellular fluorescence upon co-incubation alongside an OCT inhibitor would indicate a reduced cell penetration for the probe, and suggest the involvement of OCTs in the cellular permeation of dibasic compounds.

As previously mentioned, this results from the confocal microscopy assays could then be used to determine the direct lysosomotropism potential of the dibasic prodrugs synthesised in chapter **2**, including compound **24**.

5. Discussion

Inhalation via the pulmonary drug delivery route is an extensively utilised in method of drug administration in the treatment of asthma and COPD. Owing to the large exchange surface in the lungs, thin epithelial barrier and thus short onset time, avoidance of hepatic first class metabolism and lower drug dosage requirements, pulmonary drug delivery possesses many advantages over other routes of administration. Unfortunately, despite these significant advantages, the mechanical, chemical and immunological barriers present throughout the lung tissue result in significant loss of the administered dose meaning any inhaled therapeutic needs to be incredibly potent to compensate. In addition, the presence of severe side effects as a consequence of uncontrolled drug distribution stalls the development of new long acting bronchodilators and anticholinergics. In order to combat the high levels of drug distribution, several methods designed to stall the drug absorption and thus distribution through the plasma membrane have been trialled, with only a small percentage ever being granted FDA approval.

For the first time, this thesis attempts to combine concept of prodrugging with the reported lung tissue retention of dibasic compounds, to create a novel prodrug system which demonstrates high lung tissue retention, but which is pH triggered such that at physiological pH (6-7), the prodrug bioactivates to gradually liberate a known, potent, muscarinic antagonist, potentially directly at the intended site of action. It is thought that the basicity of the scaffold optimises the prodrug towards high electrostatic membrane binding alongside acidic organelle sequestration. Together, these mechanisms, would be responsible for an increased lung residency of the prodrug compared to the parent drug reducing the fraction of dose that is rapidly eliminated, which both reduces the dosage requirements and occurrence of cardiac side effects.

The controlled release of the active drug would then ensure a slow release of the drug, creating a long acting therapeutic in which the administration requirements align with a once a day dosing frequency.

In order to create such a novel system, a drug candidate had to be first identified. Due to the high expression of M₃ receptors throughout the upper airways and the current requirement of novel long acting anticholinergics, muscarinic antagonists were chosen as the initial drug candidate type. The location of the receptors to the upper airways meant that particle size of the administered dose was less of a problem, alleviating any concerns that a large molecular prodrug molecule would be too big to reach its' target receptor if they were located deeper into the airways, β_2 adrenoceptors for example. In addition, as M₃ receptors are membrane bound, it increased the possibility that high membrane binding would bind the prodrug in close proximity to its target receptor.

In Chapter 2, compound 1 was identified as a drug candidate with high receptor potency and selectivity and which possessed the correct chemical scaffold from which a prodrug structure could be created. In addition, it was important to ensure that any pharmacological activity was lost upon prodrugging so that the prodrug molecule itself did not result in unwanted side effects. Prior chemical development by Stocks et al demonstrated loss of potency in similar models and thus compound 1 was the perfect candidate.

Ultimately the compound **24** was identified as an ideal prodrug which possessed high chemical and enzymatic stability to ensure a controlled release of the prodrug over 24 hours, meaning that a sustained pharmacological response could be achieved. This assumption was further supported by the results of the *in-vivo* PK study in which high concentrations of the drug and prodrug were measured at 24 hours, providing further justification that a prolonged pharmacological activity could be achieved. Unfortunately, the developed prodrug system was in fact too stable that 54% of the prodrug remained after 24 hours, which would not align with a once a day dosing schedule, due to toxicological concerns of drug accumulation. It is therefore clear that this prodrug system needs to be developed further to ensure that the delivery profile and dosing schedule align more closely. However, it should not be understated that this is still a remarkable achievement in that a novel prodrug system which utilises the lung tissue retention of its' dibasic scaffold, alongside its' pH triggered chemical cleavage has increased the lung retention of a M₃ antagonist from less than 30 minutes to over 24 hours. This approach is unseen in the literature and thus it is hoped that this research will prove to be a new frontier in the development of novel long acting treatments to replace the current shortfall of anticholinergics. Further work on this chapter would see the use of bronchial lavaging on the lungs used in the DMPK assay, this flushing technique would help to estimate the percentage of prodrug dose which remains in the bronchial space as a result of membrane or mucus binding. Ultimately, this would help to identify the mechanism by which lung retention of compound **24** has occurred. In addition, mass spectrometry analysis upon the different components of lung homogenate post incubation may help to discover in which tissue the prodrug is likely to reside, and thus which mechanism is responsible for retention.

It is regretful that chapter **3** was unable to produce similar results. After the success of chapter **2**, it was decided that further development of the prodrug scaffold could produce similar lung tissue retention, but this time, optimised for drug candidates with intracellular drug targets. PI3K δ receptors are highly expressed in the nuclear envelopes of the deeper regions of the lung in inflammatory cells such as leukocytes. Inhibition of these receptors provides similar relief to patients suffering with the inflammatory responses of severe and progressive COPD. In order to account for the deeper location of the receptors within the lung, it was hypothesised that by removing the linker system, the molecular weight of the prodrug system could be reduced, and thus the particle size of the inhaled formulation could be reduced to allow for deeper lung penetration upon inhalation. The cleavage of the molecule would still be caused by internal diketopiperazine formation the speed of which could be controlled by the size and chirality of the amino acid R groups. Unfortunately, after multiple failed attempts, a PI3K prodrug could not be developed as the indazole moiety which was first thought to be a suitable chemical handle for prodrugging, was found to be too unstable and as such, all prodrugs immediately broke down. It is thought that with careful consideration of the chemical scaffold design, a PI3K prodrug is possible, and it is hoped that this work will soon be completed.

Finally, chapter **4** attempted to understand why dibasic compounds were lung tissue retentive, in order to better understand how this can be further optimised. Identification of several cellular assays capable of visualising the absorption and distribution of administered compounds was first performed. Ultimately, confocal microscopy of a range of fluorescent probes which had been chemically adapted to include chemical scaffolds of varying acidity and basicity, began to elucidate the

mechanisms by which dibasic compounds are lung tissue retentive. Unfortunately, due to time constraints, the work performed in this chapter requires further development in order to achieve its initial objectives and thus future work has already been considered. Due to the known roles of OCT and PEPT transporter proteins present on cellular membranes, it is thought that incubation of cell lines over expressed with these receptors, alongside known inhibitors of the transporters, could determine their role in the cellular uptake of dibasic and dipeptide compounds. A similar assay but using lysosomal trapping inhibitors could also help to elucidate the role of acidic organelles in the cellular retention of dibasic compounds.

Ultimately, the work performed in this presents a marked step forward in the development of novel long acting asthma and COPD treatments. It has presented a novel prodrug system as method of increasing lung retention, and has laid the foundations for further development and understanding into the mechanism of lung retention. It also presents an alternative to traditional drug discovery approaches, as it aims to use a prodrug system to improve physiochemical properties which would otherwise cause a drug candidate to be disregarded. It is hoped that the work completed helps to improve both the development process for the identification of novel treatments, as well as provide new areas of development for the identification of new long acting asthma and COPD treatments

6. Experimental

Preamble

All Commercially available starting materials including solvents were used as purchased from regular suppliers such as Fischer Scientific or Fluorochem. Flash column chromatography was performed using a Biotage 4 Isolera using puriFlash® pre-packed silica columns and a gradient of Ethyl Acetate in (40-60°C) Petroleum Ether. Purity of all compounds were performed using a Shimadzu UFLCXR system coupled to an Applied Biosystems API2000. pH readings were taken using an eti 8100 pH meter. TLC analysis was performed using Merck Silica gel (60 Å) plates and visualised using UV light. Flash column chromatography was performed using a biotage Isolera one system, using pre-packed (25 micron) silica cartridges of various sizes and makes. All compounds presented purity levels >95%. ¹³Carbon and ¹Hydrogen NMR were performed on a Bruker 400 MHz spectrometer in the indicated solvent at 21°C and analysed using Topspin/MestReNova software. Chemical shifts are recorded in ppm and calibrated against tetramethylsilane and referenced against the residual solvent peaks. Reported yields are not optimised.

LCMS Methods:

Two columns thermostatted at 40°C were used, Phenomenex Gemini-NX 3mm-110A C18, 50x2mm and Phenomenex Luna 3mm (PFP2) 110A, 50x2 mm using a Flow rate 0.5mL/min and UV detection at 220 and 254nm. The solvent compositions used were a gradient of (0.1%) Formic Acid in water (Solvent A) and (0.1%) Formic Acid in MeCN (Solvent B) using one of the two following methods: Pre-equilibration run for one min at 5% B; then method run: 5 to 98% solvent B in 2min, 98% B for 2min, 98 to 5% B in 0.5min then 5% for one min, or Pre-equilibration run for one min at 5% B;

then method run: 5% B for 0.5min, 10 to 98% solvent B in 8min, 98% B for 2min, 98 to 5% B in 0.5min then 5% B for one min.

Fluorescent Spectrophotometry Methods:

Fluorescent spectrophotometry was performed using an Agilent Cary Eclipse Fluorescence Spectrophotometer using a medium (600V) PMT voltage scanning a designated wavelength range at a rate of 600 nm/min with a 5 nm slit length.

Biological Assay Procedures:

-All animal studies were ethically reviewed and carried out in accordance with Animals (Scientific Procedures) Act 1986 and the GSK Policy on the Care, Welfare and Treatment of Animals

Biological Assay Procedure 1: Phosphate Buffer Creation

Dipotassium Hydrogen Phosphate (1.742 g, 0.01 mol) was dissolved in water (or D₂O) (10 mL). Potassium Dihydrogen Phosphate (1.361 g, 0.01 mol) was dissolved in water (or D₂O) (10 mL). To a solution containing Dipotassium Hydrogen Phosphate (2.64 ml, 0.1M) was added Potassium Dihydrogen Phosphate (5.36 ml, 0.1M) to create a PBS solution of pH 6.5. The pH was then adjusted as needed with 0.1 M HCl or 0.1 M NaOH and the pH monitored using a pH meter.

Biological Assay Procedure 2: - Lung Homogenate Creation

Whole lung from Wistar Ham rat was taken, weighed (approximately 1.5g) and placed into a 15 mL Precellys 24 Dual Evolution homogenising vessel containing ceramic beads. The lung was pre-homogenised at 2°C for 5 cycles of 20 seconds at 7400 rpm with 30 second intervals. The homogenate was then diluted 4 times by mass with

HPLC grade water (approximately 6 mL), and then homogenised 1 further time under the same conditions.

Biological Assay Procedure 3: - Crude Buffer Stability Determination

Boc-Deprotected prodrug (12.5 mg/mL) in deuterated DMSO (200 μ L), and water (200 μ L) was heated to 37°C. Pre-warmed phosphate buffer solution (37°C , 700 μ L) was then added and the solution stirred for 24 hours. At predetermined time intervals a mass spec sample was taken (50 μ L), quenching the solution in acetic acid (150 μ L) and using their relative UV peak area ratio to determine the half-life.

Biological Assay Procedure 4: - Accurate Stability Determination

In triplicate, to a 37°C, pre-warmed aliquot of neutral prodrug in DMSO (5 μ L, 200 μ g/mL) in a plastic micronic tube in a 96 well plate was added, pre-warmed stability assay matrix (995 μ L) (phosphate buffer/rat lung homogenate/rat blood). The resultant solution (1 mL, 1000 ng/mL) was maintained at 37°C and shaken continuously throughout the assay. At pre-determined intervals samples of reaction mixture (20 μ L) was diluted in internal standard (300 μ L, 6.25 ng/mL labetalol in MeCN and 17.5 ng/mL Reserpine in MeCN), shaken for 10 minutes and centrifuged for a further 20 minutes. The sample was then submitted for mass-spec analysis, quantifying the relative prodrug/drug mass ion peak against that of the internal standard.

Biological Assay Procedure 5: - Binding Determination

Binding assays were determined in RED plates purchased from Thermofisher. Rat lung homogenate was either created on the day (see **Biological Assay Procedure 2**), or stored at at least -20°C for a maximum of 1 freeze-thaw cycle. Whole rat blood was taken in house and used on day of assay, storing at 4°C if necessary.

RED plates were prepared by placing spiked matrix (100 µL, 1000 ng/mL) [Rat Lung Homogenate] prepared in a t-vial into the first 6 red ring chambers. Unspiked matrix (100 µL) is added to the final 2 red chambers. Dialysis buffer (pH 6.5 Phosphate Buffered Saline, 300 µL) was added to the top 6 buffer chambers, bottom 2 buffer chambers remained empty to calculate recovery. RED plate was sealed with sealant tape and masking tape and incubated at 37°C for 4 hours on an orbital shaker.

Once the RED plate was prepared, spiked matrix from original t-vial (20 µL, 1000 ng/mL) added to a labelled micronic immediately followed by control dialysis buffer (20 µL) and internal standard (300 µL, 6.25 ng/mL labetalol in MeCN and 17.5 ng/mL Reserpine in MeCN), creating the time 0 sample.

After the 4 hours, the RED plate was removed from the incubator, unsealed and spiked matrix from original t-vial (20 µL, 1000 ng/mL) added to a labelled micronic immediately followed by control dialysis buffer (20 µL) and internal standard (300 µL, 6.25 ng/mL labetalol in MeCN and 17.5 ng/mL Reserpine in MeCN), creating the time 240 sample.

The RED plate was then sampled by removing 20 μL from each well into a labelled micronic tube. Incubated control matrix or incubated control PBS (20 μL) was added to matrix match as follows: Incubated control PBS sample (20 μL) was added to sample from red ring (20 μL) in a labelled micronic tube in a 96 well plate, or incubated control matrix (20 μL) was added to buffer sample from buffer wells (20 μL) in a labelled micronic tube in a 96 well plate. All samples consist of matrix:PBS 1:1.

To each micronic tube was added internal standard (300 μL , 6.25 ng/mL labetalol in MeCN and 17.5 ng/mL Reserpine in MeCN), and the plate shaken for 10 minutes and centrifuged for a further 20 minutes. The plate was then submitted for mass-spec analysis, quantifying the relative prodrug/drug mass ion peak against that of the internal standard.

Biological Assay Procedure 6: - Fluorescent Spectrophotometry

To a 200 μL glass cuvette containing PBS (various pH, 180 μL , 0.1M) (see **Biological Assay Procedure 1**) was added (Deprotected) fluorescent probe dissolved in DMSO (20 μL , 100 μM) creating a final probe sample concentration of 10 μM (200 μL). The sample was then analysed using fluorescent spectrophotometry.

Biological Assay Procedure 7: Cell Culture

The human bronchial epithelial Calu-3 cell line (American Type Culture Collection, LGC Standards, UK) were cultured in 75-cm² flasks in Dulbecco's modified Eagle's medium (DMEM)/nutrient mixture F-12 Ham (Sigma Aldrich) supplemented with 10% foetal bovine serum, 100 U/mL penicillin, and 100 $\mu\text{g}/\text{mL}$ streptomycin (Sigma

Aldrich) at 37 °C, 5% CO₂ and 95% humidity. Cells were routinely sub-cultured when reaching 85-90% confluence using trypsin-EDTA.

Biological Assay Procedure 8: Cell Metabolic Activity Assessment

Calu-3 cells were seeded at a density of 1 x 10⁴ cells/well into a 96-well plate (tissue culture grade, flat bottom) in a final volume of 100 µl/well and incubated overnight to allow for cell adherence. Compounds were added at a concentration of 5 µM and incubated for 30 min or 20.5 hours at 37 °C and 5% CO₂. Cells exposed to the culture medium only were used as controls (100% metabolic activity). After incubation, 10 µl of MTT reagent (final concentration 0.5 mg/ml) was added to each well and the plate was then incubated for 4 h in a humidified atmosphere (37 °C and 5% CO₂) to allow for the reduction of the reagent. Medium was carefully removed and insoluble formazan crystals were finally dissolved with 100 µl of DMSO. The cell culture plate was placed on an orbital shaker for 15 min to homogenise the solution before absorbance was measured at 590 nm.

Biological Assay Procedure 9: Confocal Imaging

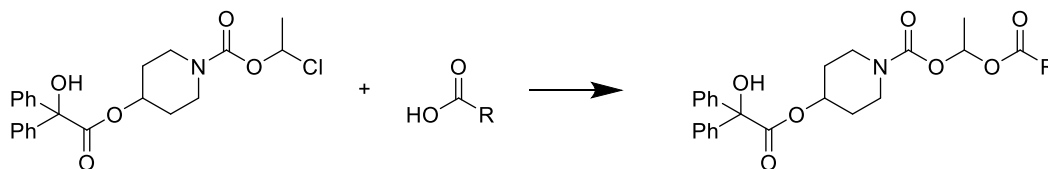
Cells were seeded on ibidi µ-slide 8 well (Ibidi GmbH, Germany) plates at a density of 2.0 x 10⁴ cells/well and incubated overnight to allow for cell adherence. Cells were washed with phosphate buffered saline (PBS), and subsequently treated for 30 min with the compounds and LysoTracker Deep RedTM (ThermoFisher) at 5 µM and 50 nM, respectively, in serum free cell culture medium. After exposure, cells were gently washed twice with PBS and fixed at room temperature with 4% paraformaldehyde

(PFA). PFA was washed twice and the slides were stored covered with PBS until confocal analysis.

The slides were examined with a Zeiss LSM-510 Meta confocal scanning laser microscope (Zeiss, Germany), equipped with a 25 mW argon and a 5 mW helium neon lasers, using a Plan Neofluar 40× objective lens (Zeiss, 1.3, oil immersion), using the built-in camera. Lysotracker Deep RedTM was observed with a long-pass 633 nm line from a helium laser. Compounds were observed with a 488 nm line from an argon laser. Images were acquired with LSM-510 v 2.0. Images were processed with FIJI²⁶¹

General Chemistry Procedures:

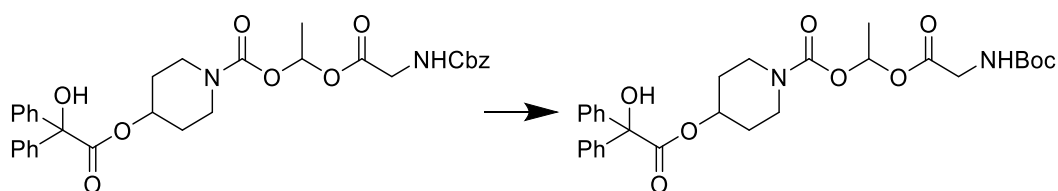
General Chemistry Procedure 1: Silver oxide assisted carboxylic acid coupling



40 (1 eq.) was dissolved in toluene (20 mL). Carboxylic acid (1.2 eq), Silver (I) oxide (1.2 eq) and Tetra-n-butylammonium bromide (0.2 eq) were added and the reaction heated at 65°C for 8 hours, and then left to stir at room temperature overnight.

TLC analysis deemed the reaction to be complete, at which point the reaction mixture was diluted with ethyl acetate (30 mL) and filtered. The solvent was removed under vacuum.

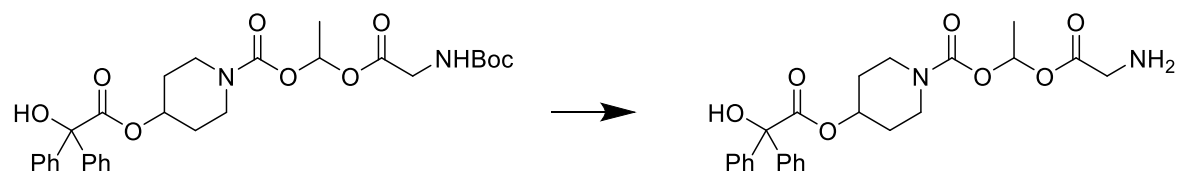
General Chemistry Procedure 2: Conversion of Cbz group to Boc group



A 100 mL round bottom flask was charged with crude Cbz protected prodrug (1 eq) dissolved in MeOH (15 mL). To this was added 20% by weight of 10% Pd/C and the flask placed under an atmosphere of hydrogen. This was left to stir for 2.5 hours, before the palladium was filtered through a celite pad. The filtrate was concentrated and before being redissolved in DCM (15 mL). Boc₂O (1.2 eq) and Net₃ (3 eq) were

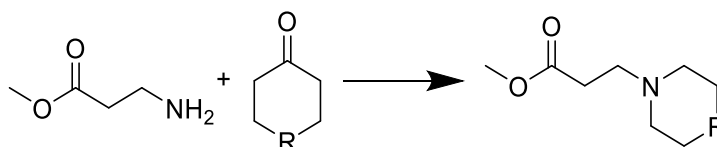
added and the solution left to stir for 2 hours. The solution was then concentrated in vacuo.

General Chemistry Procedure 3: Deprotection of Boc Protected Prodrugs



To a vial containing Boc Protected prodrug (1 eq), 2,2,2-trifluoroacetic acid (1 mL) and DCM (1 mL) were added. Nitrogen was flushed over the vial to remove volatiles. To the residue, 2N HCl in diethyl ether (2 mL) was added. The solution was concentrated under vacuum, without purification to achieve the respective deprotected prodrug.

General Chemistry Procedure 4: Synthesis of Dibasic Ester

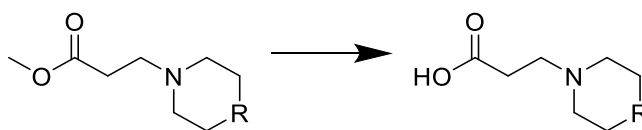


To a solution of monobasic ester (1 eq) in dry methanol (10 mL) was added triethylamine (1 eq) and left to stir for 30 minutes. Piperidinone (1 eq), acetic acid (2.5 mL) and sodium sulfate (0.5 g) were then added and the reaction left to stir overnight. Once TLC analysis (5% MeOH in DCM,) showed disappearance of the starting material, picoline borane (1 eq) was added and the solution stirred overnight at room temperature.

The reaction mixture was then azeotroped with toluene and concentrated under reduced pressure. The mixture was then redissolved in water and extracted with EtOAc (3 x 50 mL). The aqueous layer was then adjusted to pH 14 with aqueous 2N sodium hydroxide and extracted a further three times with EtOAc. The organic layers were then combined, dried over Na₂SO₄ and concentrated under reduced pressure.

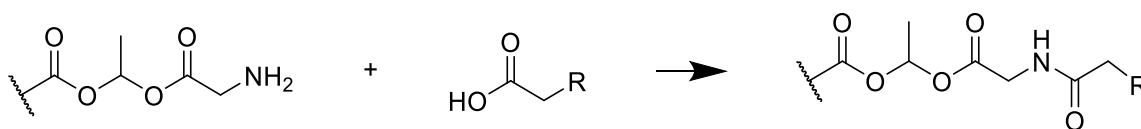
The mixture was then dissolved in DCM and di-*tert*-butyl dicarbonate (1.2 eq) and triethylamine (3 eq) were added and the resultant solution left to stir overnight. The solvent was then removed *in vacuo*.

General Chemistry Procedure 5: Synthesis of Cyclic Dibasic Carboxylic Acid



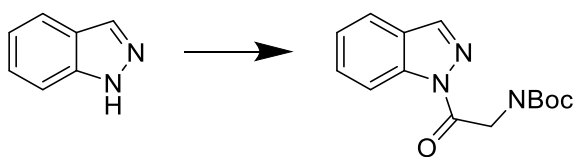
Dibasic Ester (1 eq) in a mixture of THF (4 mL) and MeOH (2 mL) was added LiOH (20 eq) in H₂O (2 mL) and the resultant suspension left to stir overnight.

TLC analysis deemed the reaction to be complete and the solvent was removed under reduced pressure. The residue was then re-dissolved in H₂O (50 mL) and aqueous 2N HCl (50 mL) and stirred for 10 minutes. This solution was then extracted with EtOAc (3 x 25 mL). The organic layers were then combined, dried over Na₂SO₄ and concentrated under reduced pressure to achieve the crude corresponding acid which was used crude.

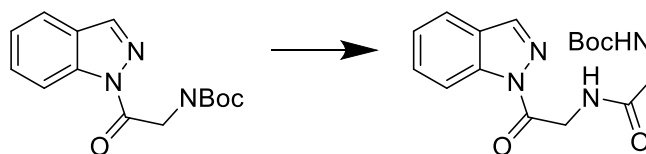
General Chemistry Procedure 6: HATU Coupling

To a 100 mL round bottom flask was added, boc-protected prodrug (1 eq) dissolved in DCM (20 mL), Amino Acid (1.5 eq), HATU (1.5 eq), DMAP (0.5 eq) and DIPEA (6 eq). The resulting yellow solution was left to stir at room temperature for 6 hours. The reaction was monitored by LCSM, and once complete, the solution was poured into a separatory funnel, diluted with DCM (50 mL) and extracted with aqueous sodium hydrogen carbonate (3 x 50 mL). The organic layers were combined, dried over MgSO₄ and concentrated *in vacuo*.

The resulting residue was then re-dissolved in MeOH (15 mL). To this was added 20% by weight (of assumed product) of 10% Pd/C and the flask placed under an atmosphere of hydrogen. This was left to stir for 2.5 hours, before the palladium was filtered through a celite pad. The filtrate was concentrated and before being re-dissolved in DCM (15 mL). Boc₂O (1.2 eq) and NEt₃ (3 eq) were added and the solution left to stir for 2 hours. The solution was then concentrated *in vacuo*.

General Chemistry Procedure 7: Synthesis of Indazole Mono-Peptide

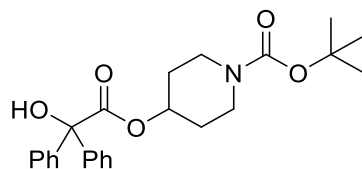
To a stirred solution of Amine (1 eq), in DCM (10 mL) was added Boc Amino Acid 1 (1.5 eq), HATU (1.5 eq), DMAP (0.1 eq) and DIPEA (6 eq) and the resultant solution stirred for 6 hours. TLC analysis deemed the reaction to be complete and the solvent was removed in vacuo. The resultant residue was dissolved in DCM (50 mL) and extracted with NaHCO_3 (3x50 mL). The organic layers were then combined, dried with Na_2SO_4 and concentrated in vacuo.

General Chemistry Procedure 8: Synthesis of Indazole Di-Peptide

To a stirred solution of mono-peptide (1 eq), in DCM (10 mL) was added TFA (5 mL) and the resulting solution stirred for 10 minutes. The solution was concentrated in vacuo and redissolved in DCM (10 mL). To the solution was added Boc Amino Acid 1 (1.5 eq), HATU (1.5 eq), DMAP (0.1 eq) and DIPEA (6 eq) and the resultant solution stirred for 6 hours. TLC analysis deemed the reaction to be complete and the solvent was removed in vacuo. The resultant residue was dissolved in DCM (50 mL) and extracted with NaHCO_3 (3x50 mL). The organic layers were then combined, dried with Na_2SO_4 and concentrated in vacuo.

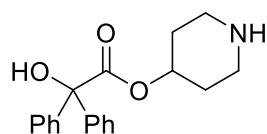
5.1 Chapter 1

tert-Butyl 4-(2-hydroxy-2,2-diphenylacetoxy)piperidine-1-carboxylate **1a**

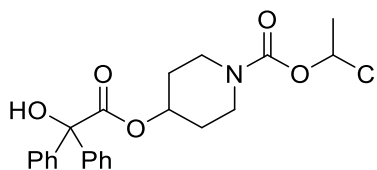


Methyl benzoate (5.0 g, 20 mmol, 1 eq) and *t*-butyl 4-hydroxy piperidine-1-carboxylate (3.02 g, 15 mmol, 0.75 eq) were dissolved in hexane (60 mL) and stirred at room temperature. Sodium (0.034 g, 1.5 mmol, 0.075 eq) and triethylamine (2.8 mL) were added. The reaction was then heated to 60 °C for 16 hours.

TLC analysis showed no change and thus the reaction solvent was evaporated. The crude mixture was then re-dissolved in 1:6 EtOAc:Hexane and separated using silica gel column chromatography using a gradient of 1:6 to 1:4 EtOAc:Hexane to obtain the title compound **39i** (1.467 g, 17%) as a colourless oil which crystallized to a white solid on standing; R_f 0.13 [EtOAc:Hexane (1:10)]; ^1H (400 MHz; CDCl_3) δ 1.46 [9H, s], 1.59-1.68 [2H, m] 1.79- 1.87 [2H, m], 3.31-3.35 [4H, m], 5.28 [1H, bs], 5.15 [1H, h, J 4], 7.31-7.48 [10H, m]; ^{13}C DEPT (101 MHz; CDCl_3) δ 128.09, 127.39, 72.35, 40.30, 31.59, 30.13, 28.38, 22.65, 14.20; m/z (ESI; 99%) Calc. for $\text{C}_{24}\text{H}_{29}\text{NO}_5$ = 411.50 found 412 $[\text{M}+\text{H}]^+$.

Piperidin-4-yl 2-hydroxy-2,2-diphenylacetate **1**

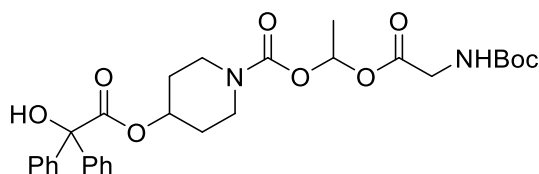
28 (0.801 g, 1.9 mmol, 1 eq) was dissolved in DCM (10 mL) and 4N HCl in dioxane (1 mL) and left to stir for 18 hours. A white precipitate formed. Diethyl ether (50 mL) was added and the white solid filtered and washed with further portions of diethyl ether (2 x 20 mL) to obtain the title compound **1** (0.477 g, 71%) as a white solid; ^1H (400 MHz; CDCl_3) δ 1.91-2.00 [2H, m], 2.17-2.28 [2H, m], 2.71-2.81 [2H, m] 3.07-3.17 [2H, m], 5.22-5.28 [1H, m], 7.36-7.45 [10H, m], 9.50 [1H, bd, J 50]; ^{13}C DEPT (101 MHz; CDCl_3) δ 128.16, 127.37, 71.46, 40.58, 30.06. m/z (ESI; 98%) Calc. for $\text{C}_{19}\text{H}_{21}\text{NO}_3 = 311.38$ found 312.4 $[\text{M}+\text{H}]^+$.

1-Chloroethyl 4-(2-hydroxy-2,2-diphenylacetoxy) piperidine-1-carboxylate **2**

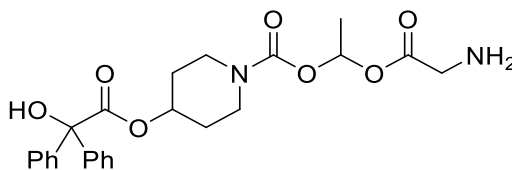
1 (0.1 g, 0.288 mmol, 1 eq) was dissolved in dry DCM (10 mL) and cooled to -10°C . 4-Methylmorpholine (0.105 mL, 0.951 mmol, 3.3 eq) was added followed by 1-chloroethyl chloroformate (0.034 mL, 0.316 mmol, 1.1 eq). This was left to stir for 2 hours.

TLC analysis deemed the reaction to be complete and the reaction solvent was removed under vacuum. The residue was re-dissolved in ethyl acetate (10 mL) and poured onto 2N HCl (10 mL). This was then extracted with water and then the organic layers combined and dried over Na_2SO_4 . This was then filtered, concentrated under vacuum and separated using silica gel column chromatography using a gradient of 1:4 EtOAc:petroleum ether (40:60) to obtain the title compound **2** as a mixture of enantiomers (0.477 g, 71%) as a colourless oil; R_f 0.43 [EtOAc:40-60 Petroleum Ether (1:3)]; ^1H (400 MHz; CDCl_3) δ 1.82 [3H, d, J 5] 3.19-3.73 [8H, m], 4.28 [1H, bs], 5.19 [1H, bs], 6.59 [1H, q, J 5], 7.30-7.48 [10H, m]; ^{13}C DEPT (101 MHz; CDCl_3) δ 128.16, 127.46, 127.38, 71.43, 40.47, 30.12; m/z (ESI; 97%) Calc. for $\text{C}_{22}\text{H}_{23}\text{NO}_5$ = 417.13 found 418.1 $[\text{M}+\text{H}]^+$.

1-(((*tert*-Butoxycarbonyl)glycyl)oxy)ethyl 4-(2-hydroxy-2,2-diphenylacetoxy) piperidine-1-carboxylate **3a**

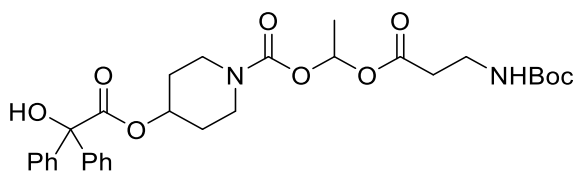


This compound was synthesised according to General Chemistry 1 and purified using silica gel column chromatography using a gradient of 1:5 EtOAc:(40-60) PET to obtain the title compound **3i** (21%) as a colourless oil; R_f 0.5 [EtOAc:(40-60) PET (2:3)]; ^1H (400 MHz; CDCl_3) δ 7.47-7.30 [10H, m], 6.83 [1H, q, J 5], 5.21-5.14 [2H, m], 3.40-3.80 [2H, m], 3.51-3.36 [2H, m], 3.35-3.20 [2H, m], 1.82-1.68 [5H, m], 1.49 [3H, d, J 5], 1.45 [9H, s]; ^{13}C DEPT (101 MHz; CDCl_3) δ 1.77.76, 169.69, 152.40, 128.28, 127.96, 127.53, 90.96, 81.19, 70.39, 65.40, 30.15, 29.91, 20.01, 15.67; m/z (ESI; 99%) Calc. for $\text{C}_{29}\text{H}_{36}\text{N}_2\text{O}_9$ = 556.61 found 557.2 $[\text{M}+\text{H}]^+$ r.t. 2.94.

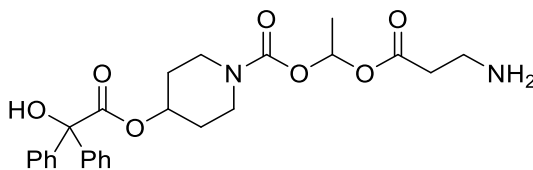
1-(Glycyloxy)ethyl 4-(2-hydroxy-2,2-diphenylacetoxy)piperidine-1-carboxylate **3**

This compound was synthesised according to General Chemistry Procedure 3 to obtain the title compound **3** [Quantitative] as a white solid; ^1H (400 MHz; CDCl_3) δ 8.10 [2H, bs] 7.46-7.30 [10H, m], 6.86 [1H, q, J 4], 6.30 [2H, bs], 5.16, [1H, bs], 3.92 [2H, s], 3.51-3.15 [4H, m], 1.91-1.75 [2H, m], 1.74-1.57 [2H, m], 1.47 [3H, d, J 4]; ^{13}C (101 MHz, DMSO) δ 172.75, 166.63, 152.39, 143.77, 128.27, 127.95, 127.51, 90.94, 81.18, 70.36, 65.39, 40.61, 40.45 29.91, 19.98; m/z (ESI; 90%) Calc. for $\text{C}_{24}\text{H}_{28}\text{N}_2\text{O}_7 = 456.50$ found 457.2 $[\text{M}+\text{H}]^+$ r.t. 2.19.

1-((3-((*tert*-Butoxycarbonyl)amino)propanoyl)oxy)ethyl 4-(2-hydroxy-2,2-diphenyl acetoxy)piperidine-1-carboxylate **4a**

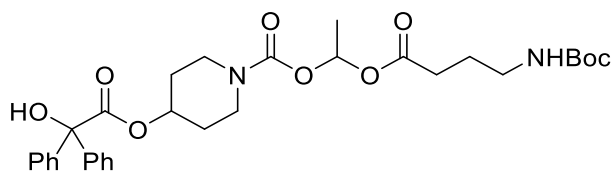


This compound was synthesised according to General Chemistry Procedure **1** and purified using silica gel column chromatography using a gradient of 2:7 EtOAc:(40-60) PET to obtain the title compound **4i** (67%) as a colourless oil; R_f 0.49 [EtOAc:(40-60) PET (2:3)]; ^1H (400 MHz; CDCl_3) δ 7.47-7.30 [10H, m], 6.77 [1H, q, J 5], 5.22-5.09 [1H, m], 3.41- 3.27 [6H, m], 2.51 [2H, t, J 6], 1.93-1.75 [2H, m], 1.74-1.61 [2H, m], 1.48 [3H, d, J 5], 1.44 [9H, s]; ^{13}C (101 MHz, CDCl_3) δ 173.85, 170.67, 152.89, 141.80, 128.19, 128.16, 127.36, 90.10, 81.04, 79.36, 71.68, 40.45, 36.03, 34.73, 30.04, 29.80, 28.40, 19.80; m/z (ESI; 97%) Calc. for $\text{C}_{30}\text{H}_{38}\text{N}_2\text{O}_9$ = 570.64 found 571.3 $[\text{M}+\text{H}]^+$ r.t. 2.99.

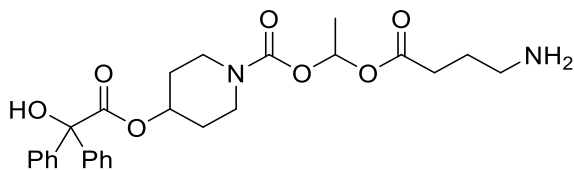
1-((3-Aminopropanoyl)oxy)ethyl 4-(2-hydroxy-2,2-diphenylacetoxy)piperidine-1-carboxylate **4**

This compound was synthesised according to General Chemistry Procedure 3 obtain the title compound **4** [0.012 g, Quantitative] as a white solid; ^1H (400 MHz; DMSO) δ 7.89 [2H, bs], 7.46-7.30 [10H, m] 6.80 [1H, q, J 5], 5.84 [2H, bs], 5.18 [1H, s], 3.52-3.20 [6H, m], 2.94-2.82 [2H, m], 1.96-1.78 [2H, m], 1.75-1.57 [2H, m], 1.48 [3H, d, J 5]; ^{13}C (101 MHz, DMSO) δ 172.75, 169.20, 152.64, 143.77, 132.07, 129.14, 128.31, 128.26, 127.99, 127.94, 127.51, 127.41, 90.35, 81.17, 70.39, 38.55, 35.17, 34.74, 28.83, 15.64; m/z (ESI; 90%) Calc. for $\text{C}_{25}\text{H}_{30}\text{N}_2\text{O}_7$ = 470.52 found 471.2 $[\text{M}+\text{H}]^+$ r.t. 2.20.

1-((4-((*tert*-Butoxycarbonyl)amino)butanoyl)oxy)ethyl 4-(2-hydroxy-2,2-diphenyl
acetoxypiperidine-1-carboxylate **5i**

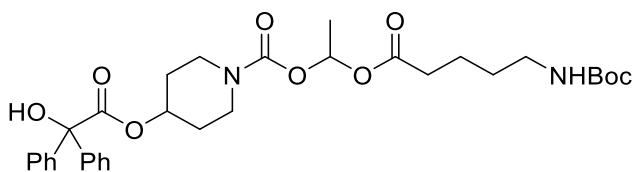


This compound was synthesised according to General Chemistry Procedure **1** and purified using silica gel column chromatography using a gradient of 1:3 EtOAc:hexane to obtain the title compound **5i** (41%) as a colourless oil; R_f 0.34 [EtOAc:hexane (2:3)]; ¹H (400 MHz; CDCl₃) δ 7.40 [10H, m], 6.78 [1H, q, *J* 5], 5.17 [1H, m], 4.70 [1H, bs], 4.27 [1H, bs], 3.41-2.36 [8H, m], 1.81 [4H, m], 1.68 [2H, m], 1.48 [3H, d, *J* 5], 1.45 [9H, s]; ¹³C (101 MHz, CDCl₃) δ 173.86, 171.34, 155.97, 152.86, 128.18, 128.16, 127.37, 90.08, 81.03, 71.75, 40.43, 39.67, 31.36, 30.02, 28.41, 25.00, 19.82.; *m/z* (ESI; 97%) Calc. for C₃₁H₄₀N₂O₉ = 584.67 found 585.2 [M+H]⁺ r.t. 3.01.

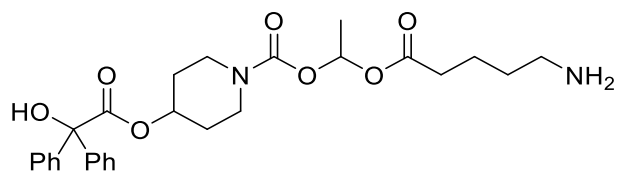
1-((4-Aminobutanoyl)oxy)ethyl 4-(2-hydroxy-2,2-diphenylacetoxy)piperidine-1-carboxylate **5**

This compound was synthesised according to General Chemistry Procedure **3** to obtain the title compound **5** [Quantitative] as a white solid; ^1H (400 MHz; DMSO) δ 7.60 [2H, bs], 7.45-7.31- [10H, m], 6.76 [1H, q, J 5], 5.17 [1H, bs], 3.52-3.36 [2H, m], 3.33-3.23 [2H, m], 3.21-3.08 [2H, m], 2.56-2.46 [2H, m], 2.11-1.99 [2H, m], 1.92-1.75 [2H, m], 1.76-1.61 [2H, m], 1.48 [3H, d, J 5]; ^{13}C (101 MHz, DMSO) δ 174.18, 172.75, 152.70, 143.77, 128.31, 128.27, 128.00, 127.95, 127.51, 127.41, 90.06, 81.17, 67.92, 38.67, 38.41, 30.92, 30.73, 27.06, 22.96, 22.66, 20.07; m/z (ESI; 98%) Calc. for $\text{C}_{26}\text{H}_{32}\text{N}_2\text{O}_7 = 484.55$ found 485.3 $[\text{M}+\text{H}]^+$ r.t. 2.24.

1-((5-((*tert*-Butoxycarbonyl)amino)pentanoyl)oxy)ethyl 4-(2-hydroxy-2,2-diphenylacetoxypiperidine-1-carboxylate **6i**

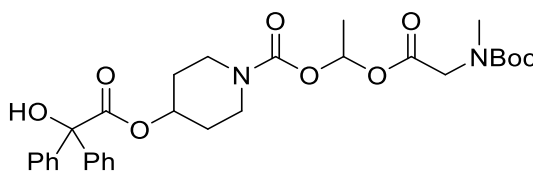


This compound was synthesised according to General Chemistry Procedure **1** and purified using silica gel column chromatography using a gradient of 1:3 EtOAc:hexane to obtain the title compound **6i** (85%) as a colourless oil; R_f 0.19 [EtOAc:hexane (1:3)]; ¹H (400 MHz; CDCl₃) δ 7.50-7.30 [10H, m], 6.78 [1H, q, *J* 5], 5.17 [1H, h, *J* 4], 4.62 [1H, bs], 4.27 [1H, bs], 3.48-3.24 [4H, m], 3.12-3.06 [2H, m], 2.33 [2H, td *J* 7 and 4], 1.90-1.79 [2H, m], 1.72-1.60 [4H, m], 1.56-1.49 [2H, m], 1.48 [3H, d, *J* 5], 1.45 [9H, s]; ¹³C (101 MHz, CDCl₃) δ 173.84, 171.49, 155.99, 152.84, 141.83, 128.15, 127.36, 89.98, 81.03, 79.15, 71.76, 53.44, 40.44, 40.05, 33.67, 30.04, 29.82, 29.70, 29.29, 28.42, 21.78, 19.85; *m/z* (ESI; 97%) Calc. for C₃₂H₄₂N₂O₉ = 598.29 found 599.3 [M+H]⁺ r.t. 3.04.

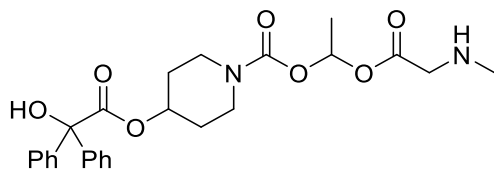
1-((5-Aminopentanoyl)oxy)ethyl 4-(2-hydroxy-2,2-diphenylacetoxy)piperidine-1-carboxylate **6**

This compound was synthesised according to General Chemistry Procedure **3** to obtain the title compound **6** [Quantitative] as a white solid; ^1H (400 MHz; DMSO) δ 7.68 [2H, bs], 7.45-7.30 [10H, m] 6.77 [1H, q, J 5], 5.17 [1H, s] 3.48-3.37 [2H, m], 3.33-3.23 [2H, m], 3.13-3.02 [2H, m], 2.43-2.33 [2H, m] 1.92-1.60 [6H m], 1.48 [3H, d, J 5]; ^{13}C (101 MHz, DMSO) δ 174.63, 172.60, 158.55, 143.72, 129.18, 128.31, 128.26, 127.99, 127.94, 127.60, 127.51, 127.41, 81.17, 67.96, 65.39, 38.92, 38.77, 33.54, 27.03, 26.94, 26.67, 21.89; m/z (ESI; 98%) Calc. for $\text{C}_{27}\text{H}_{34}\text{N}_2\text{O}_7$ = 498.58 found 499.3 $[\text{M}+\text{H}]^+$ r.t. 2.26.

1-((*N*-(*tert*-Butoxycarbonyl)-*N*-methylglycyl)oxy)ethyl 4-(2-hydroxy-2,2-diphenylacetoxypiperidine-1-carboxylate **7i**

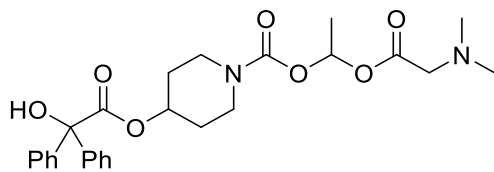


This compound was synthesised according to General Chemistry Procedure **1** and purified using silica gel column chromatography using a gradient of 1:2 EtOAc:(40-60) PET to obtain the title compound **7i** (52%) as a colourless oil; Rf 0.34 [EtOAc:(40-60) PET (2:3)]; ^1H (400 MHz; CDCl_3) δ 7.47-7.30 [10H, m], 6.82 [1H, q, J 5], 5.20-5.12 [1H, m], 4.29 [1H, bs], 3.84 [2H, s], 3.50-3.17 [4H, m], 2.91 [3H, s], 1.82-1.65 [4H, m], 1.46 [12H, s]; ^{13}C (101 MHz, CDCl_3) δ 173.85, 168.08, 141.81, 128.16, 127.36, 90.48, 81.03, 80.22, 71.65, 50.93, 50.08, 40.44, 35.50, 29.82, 28.32, 19.86; m/z (ESI; 97%) Calc. for $\text{C}_{30}\text{H}_{38}\text{N}_2\text{O}_9$ = 570.64 found 571.3 $[\text{M}+\text{H}]^+$ r.t. 3.05.

1-((Methylglycyl)oxy)ethyl 4-(2-hydroxy-2,2-diphenylacetoxy)piperidine-1-carboxylate **7**

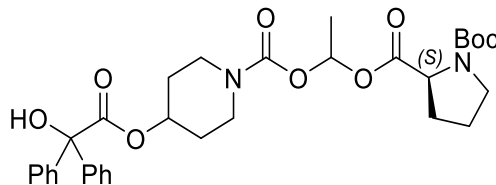
This compound was synthesised according to General Chemistry Procedure **3** obtain the title compound **7** [Quantitative] as a white solid; ^1H (400 MHz; DMSO) δ 7.44-7.32 [10H, m], 6.86 [1H, q, J 5], 5.19 [1H, m], 4.29 [1H, bs], 3.88 [2H, s], 3.48-3.17 [4H, m], 2.84 [3H, s], 1.92-1.78 [2H, m], 1.76-1.62 [2H, m], 1.53 [3H, d, J 5]; ^{13}C (101 MHz, DMSO) δ 172.75, 172.6, 158.99, 143.77, 143.73, 129.79, 129.17, 129.13, 128.30, 128.26, 127.98, 127.94, 127.62, 127.51, 127.41, 90.99, 81.18, 70.35, 67.97, 48.66, 30.14, 19.92 ; m/z (ESI; 94%) Calc. for $\text{C}_{25}\text{H}_{30}\text{N}_2\text{O}_7$ = 470.52 found 471.4 $[\text{M}+\text{H}]^+$ r.t. 2.21.

1-((Dimethylglycyl)oxy)ethyl 4-(2-hydroxy-2,2-diphenylacetoxy)piperidine-1-carboxylate **8**

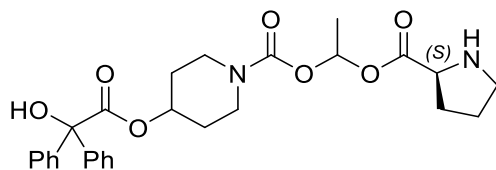


This compound was synthesised according to General Chemistry Procedure **1** and purified using silica gel column chromatography using a gradient of 100% EtOAc to obtain the title compound **8** (43%) as a colourless oil; R_f 0.31 [EtOAc]; ¹H (400 MHz; CDCl₃) δ 7.46-7.30 [10H, m], 6.83 [1H, q, *J* 5], 5.16 [1H, h, *J* 4], 3.46-3.23 [4H, m], 3.20 [2H, s], 2.37 [6H, s], 1.89-1.87 [2H, m], 1.72-1.59 [2H, m], 1.50 [3H, d, *J* 5]; ¹³C DEPT (101 MHz; CDCl₃) δ 128.14, 127.36, 90.23, 71.68, 59.96, 45.00, 40.39, 29.69, 19.83; *m/z* (ESI; 97%) Calc. for C₂₆H₃₂N₂O₇ = 484.22 found 485.3 [M+H]⁺.

1-(*tert*-Butyl) 2-(1-((4-(2-hydroxy-2,2-diphenylacetoxy)piperidine-1-carbonyloxy)ethyl) pyrrolidine-1,2-dicarboxylate **9i**

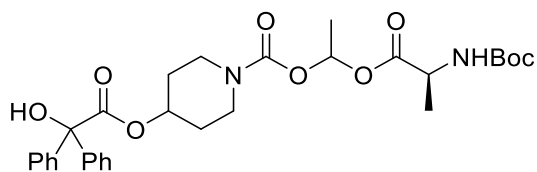


This compound was synthesised according to General Chemistry Procedure **1** and purified using silica gel column chromatography using a gradient of 1:2 EtOAc:(40-60) PET to obtain the title compound **9i** (67%) as a colourless oil; R_f 0.49 [EtOAc:(40-60) PET (2:5)]; ¹H (400 MHz; CDCl₃) δ 7.40-7.29 [10H, m], 6.77 [1H, q, *J* 5], 5.21-5.10 [1H, m], 4.29 [1H, bs], 3.59-3.27 [6H, m], 2.17-2.10 [1H, m], 2.01-1.82 [6H, m], 1.70-1.58 [2H, m], 1.51-1.47 [3H, m], 1.44 [9H, s]; ¹³C DEPT (101 MHz; CDCl₃) δ 128.12, 127.36, 90.53, 71.76, 71.62, 60.38, 46.29, 30.85, 28.31, 23.45, 19.76; m/z (ESI; 99%) Calc. for C₂₇H₃₂N₂O₉ = 596.22 found 597.2 [M+H]⁺ r.t. 3.07.

1-(Propyloxy)ethyl 4-(2-hydroxy-2,2-diphenylacetoxy)piperidine-1-carboxylate **9**

This compound was synthesised according to General Chemistry Procedure **3** to obtain the title compound **9** [Quantitative] as a white solid; ^1H (400 MHz; DMSO) δ 9.05 [1H, bs], 7.40-7.29 [10H, m], 6.72 [1H, q, J 5], 5.06 [1H, s], 4.39 [1H, bs], 4.29 [1H, bs], 3.97 [1H, s], 3.44-3.30- [3H, m], 2.33-2.16 [1H, m], 2.08-1.69 [6H, m], 1.58-1.47 [5H, m]; ^{13}C (101 MHz, DMSO) δ 172.75, 170.87, 152.58, 143.77, 128.31, 128.27, 127.95, 127.51, 91.37, 81.18, 70.32, 59.10, 45.84, 45.75, 28.39, 28.32, 28.28, 23.58, 23.35, 19.82; m/z (ESI; 99%) Calc. for $\text{C}_{27}\text{H}_{32}\text{N}_2\text{O}_7$ = 496.56 found 497.3 $[\text{M}+\text{H}]^+$ r.t. 2.25.

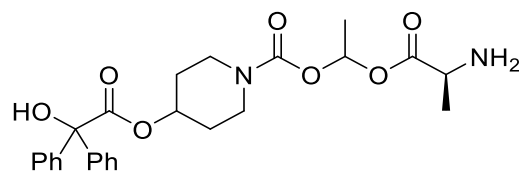
1-(((*tert*-Butoxycarbonyl)-L-alanyl)oxy)ethyl 4-(2-hydroxy-2,2-diphenylacetoxy) piperidine-1-carboxylate **10i**



This compound was synthesised according to General Chemistry Procedure **1** and purified using flash column chromatography using a gradient of 20-80% EtOAc:(40-60) PET to obtain the title compound **10i** (49%) as a colourless oil; R_f 0.21 [EtOAc:(40-60) PET (1:5)]; ¹H (400 MHz; CDCl₃) δ 7.48-7.29 [10H, m], 6.77 [1H, q, *J* 5], 5.21-5.04 [2H, m], 4.30 [2H, m], 3.66 [1H, bs], 3.51-3.16 [4H, m], 1.91-1.77 [2H, m], 1.72-1.61 [2H, m], 1.51-1.47 [3H, m], 1.36 [3H, dd, *J* 7 and 11] 1.44 [9H, s]; ¹³C (101 MHz; CDCl₃) δ 173.84, 171.71, 155.05, 152.72, 141.85, 128.15, 127.38, 90.68, 81.06, 79.92, 71.65, 49.14, 40.91, 40.44, 29.80, 29.78, 28.32, 18.37, 17.29; m/z (ESI; 99%) Calc. for C₃₀H₃₈N₂O₉ = 570.64 found 571.3 [M+H]⁺ r.t. 3.01.

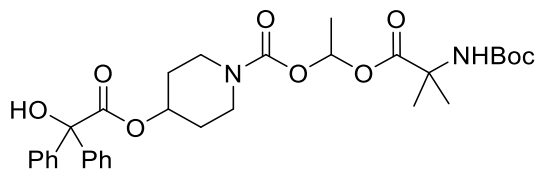
1-((*L*-Alanyl)oxy)ethyl 4-(2-hydroxy-2,2-diphenylacetoxy)piperidine-1-carboxylate

10



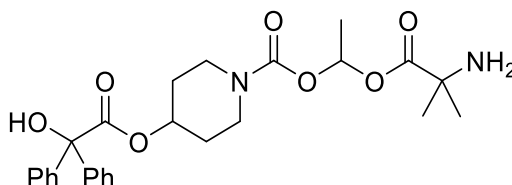
This compound was synthesised according to General Chemistry Procedure **3** to obtain the title compound **10** [Quantitative] as a white solid; ^1H (400 MHz; DMSO) δ 8.25 [2H, bs], 7.48-7.29- [10H, m], 6.71 [1H, q, J 5], 5.06 [1H, bs], 4.14-3.69 [4H, m], 3.45-3.14 [2H, m], 1.84-1.70 [2H, m], 1.60-1.44 [5H, m], 1.35 [3H, dd, J 7 and 11]; ^{13}C (101 MHz; DMSO) δ 172.75, 168.86, 152.50, 143.77, 129.14, 128.31, 128.27, 127.99, 127.95, 127.62, 127.51, 127.41, 91.14, 81.18, 70.32, 48.28, 48.17, 19.85, 16.22; m/z (ESI; 99%) Calc. for $\text{C}_{25}\text{H}_{30}\text{N}_2\text{O}_7 = 470.52$ found 471.2 $[\text{M}+\text{H}]^+$ r.t. 2.22.

1-((2-((*tert*-Butoxycarbonyl)amino)-2-methylpropanoyl)oxy)ethyl 4-(2-hydroxy-2,2-diphenylacetoxypiperidine-1-carboxylate **11i**



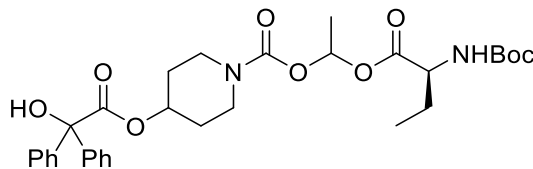
This compound was synthesised according to General Chemistry Procedure **1** and purified using flash column chromatography using a gradient of 20-80% EtOAc:(40-60) PET to obtain the title compound **11i** (49%) as a colourless oil; Rf 0.27 [EtOAc:(40-60) PET (1:5)]; ^1H (400 MHz; CDCl_3) δ 7.46-7.29 [10H, m], 6.68 [1H, q, J 5], 5.16 [1H, m], 5.04 [1H, bs], 3.66 [1H, bs], 3.51-3.20 [4H, m], 1.92-1.77 [2H, m], 1.72-1.61 [2H, m], 1.50-1.45 [9H, m], 1.43 [9H, s]; ^{13}C (101 MHz, CDCl_3) δ 173.86, 172.84, 154.47, 152.87, 141.85, 128.15, 127.38, 90.88, 81.05, 79.86, 71.81, 55.96, 40.91, 40.49, 33.84, 30.05, 28.32, 25.03, 19.72; m/z (ESI; 99%) Calc. for $\text{C}_{31}\text{H}_{40}\text{N}_2\text{O}_9 = 584.67$ found 585.3 $[\text{M}+\text{H}]^+$.

1-((2-Amino-2-methylpropanoyl)oxy)ethyl 4-(2-hydroxy-2,2-diphenylacetoxy) piperidine-1-carboxylate **11**



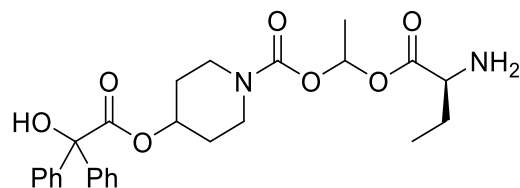
This compound was synthesised according to General Chemistry Procedure **3** to obtain the title compound **11** [Quantitative] as a white solid; ^1H (400 MHz; CDCl_3) δ 8.73 [2H, bs], 7.46-7.29 [10H, m], 6.69 [1H, q, J 5], 5.16 [1H, m], 5.05 [1H, bs], 3.53-3.18 [4H, m], 1.57-1.39 [15H, m], 1.92-1.77 [2H, m], 1.85-1.72 [2H, m]; ^{13}C (101 MHz, DMSO) δ 173.83, 172.74, 152.50, 143.77, 129.14, 128.26, 127.94, 127.61, 127.51, 91.38, 81.17, 70.36, 56.21, 30.19, 29.90, 19.73; m/z (ESI; 99%) Calc. for $\text{C}_{26}\text{H}_{32}\text{N}_2\text{O}_7 = 484.55$ found 485.6 $[\text{M}+\text{H}]^+$ r.t. 2.25.

1-(((S)-2-((tert-Butoxycarbonyl)amino)butanoyloxy)ethyl 4-(2-hydroxy-2,2-diphenylacetoxy)piperidine-1-carboxylate **12i**



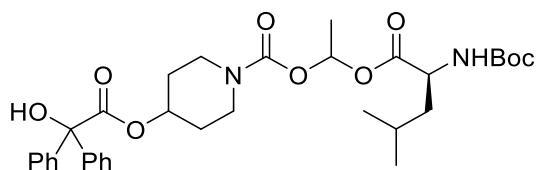
This compound was synthesised according to General Chemistry Procedure **1** and purified using flash column chromatography using a gradient of 20-80% EtOAc:(40-60) PET to obtain the title compound **12i** (54%) as a colourless oil; R_f 0.57 [EtOAc:(40-60) PET (2:5)]; ¹H (400 MHz; CDCl₃) δ 7.47-7.30 [10H, m], 6.82 [1H, q, *J* 5], 5.16 [1H, bs], 5.07 [1H, bs], 4.32-4.20 [2H, m], 3.52-3.32 [4H, m], 1.90-1.77 [2H, m], 1.74-1.60 [4H, m], 1.52-1.47 [3H, m], 1.45 [9H, s], 0.96-0.90 [2H, m]; ¹³C (101 MHz; CDCl₃) δ 173.85, 171.11, 155.39, 152.67, 141.84, 128.16, 127.38, 90.59, 81.05, 77.40, 54.39, 43.63, 30.04, 28.32, 23.87, 19.77, 9.38; m/z (ESI; 97%) Calc. for C₃₁H₄₀N₂O₉ = 584.67 found 585.3 [M+H]⁺ r.t. 3.06

1-(((*S*)-2-Aminobutanoyl)oxy)ethyl 4-(2-hydroxy-2,2-diphenylacetoxy)piperidine-1-carboxylate **12**



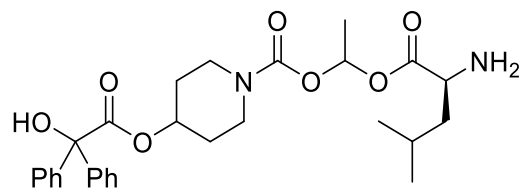
This compound was synthesised according to General Chemistry Procedure **3** to obtain the title compound **12** [Quantitative] as a white solid; ^1H (400 MHz; CDCl_3) δ 8.61 [2H, bs], 7.47-7.30 [10H, m], 6.76 [1H, q, J 5], 5.06 [1H, bs], 4.00 [1H, bs], 3.44-3.20 [4H, m], 1.89-1.69 [4H, m], 1.57-1.44 [5H, m], 0.96-0.82 [3H, m]; ^{13}C (101 MHz; CDCl_3) δ 172.73, 171.35, 152.44, 143.77, 128.26, 127.94, 127.51, 127.41, 91.13, 81.17, 65.39, 53.43, 53.19, 23.74, 23.70, 19.88, 19.86, 9.10.; m/z (ESI; 99%) Calc. for $\text{C}_{26}\text{H}_{32}\text{N}_2\text{O}_7 = 484.55$ found 485.3 $[\text{M}+\text{H}]^+$ r.t. 2.24.

1-(((*tert*-Butoxycarbonyl)-L-leucyl)oxy)ethyl 4-(2-hydroxy-2,2-diphenylacetoxy) piperidine-1-carboxylate **13i**



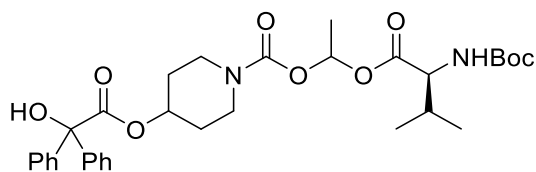
This compound was synthesised according to General Chemistry Procedure **1** and purified using flash column chromatography using a gradient of 20-80% EtOAc:(40-60) PET to obtain the title compound **13i** (46%) as a colourless oil; R_f 0.55 [EtOAc:(40-60) PET (3:10)]; ¹H (400 MHz; CDCl₃) δ 7.47-7.30 [10H, m], 6.82 [1H, q, *J* 5], 5.17 [1H, bs], 4.93 [1H, bs], 4.35-4.23 [2H, m], 3.52-3.16 [4H, m], 1.89-1.78 [2H, m], 1.75-1.61 [4H, m], 1.60-1.56 [1H, m], 1.52-1.47 [3H, m], 1.44 [9H, s], 0.98-0.91 [6H, m]; ¹³C (101 MHz; DMSO) δ 171.48, 168.72, 144.67, 130.19, 129.40, 129.33, 129.05, 128.50, 128.42, 82.22, 62.40, 41.38, 41.17, 40.96, 40.75, 40.55, 40.34, 40.13, 34.66, 34.15, 27.75, 27.46, 20.82; m/z (ESI; 99%) Calc. for C₃₃H₄₄N₂O₉ = 612.72 found 613.3 [M+H]⁺ r.t. 3.15.

1-((*L*-Leucyl)oxy)ethyl 4-(2-hydroxy-2,2-diphenylacetoxy)piperidine-1-carboxylate

13

This compound was synthesised according to General Chemistry Procedure **3** to obtain the title compound **13** [Quantitative] as a white solid; ^1H (400 MHz; DMSO) δ 8.59 [2H, bs] 7.47-7.30 [10H, m], 6.74 [1H, q, J 5], 5.05 [1H, bs], 3.99-3.86 [1H, m], 3.43-3.15 [5H, m], 1.85-1.37 [10H, m], 1.08-0.97 [6H, m]; ^{13}C (101 MHz; DMSO) δ 172.75, 168.98, 158.90, 143.76, 129.13, 128.30, 128.26, 127.94, 127.52, 127.41, 117.53, 114.64, 91.15, 81.17, 70.36, 50.91, 50.81, 29.88, 24.20, 24.15, 22.56, 19.80; m/z (ESI; 99%) Calc. for $\text{C}_{28}\text{H}_{36}\text{N}_2\text{O}_7 = 512.60$ found 513.4 $[\text{M}+\text{H}]^+$ r.t. 2.31.

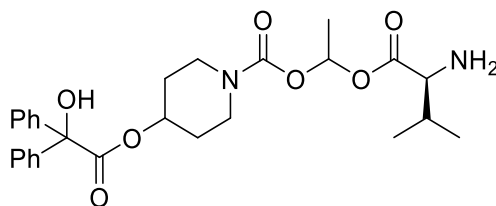
1-(((*tert*-Butoxycarbonyl)-L-valyl)oxy)ethyl 4-(2-hydroxy-2,2-diphenylacetoxy) piperidine-1-carboxylate **14i**



This compound was synthesised according to General Chemistry Procedure **1** and purified using flash column chromatography using a gradient of 20-80% EtOAc:(40-60) PET to obtain the title compound **14i** (41%) as a colourless oil; R_f 0.50 [EtOAc:(40-60) PET (1:5)]; ¹H (400 MHz; CDCl₃) δ 7.47-7.26 [10H, m], 6.62 [1H, q, *J* 5], 5.15 [1H, bs], 5.07 [1H, bs], 4.20 [1H, m], 3.49-3.12 [4H, m], 2.11 [1H, m], 1.87-1.72 [2H, m], 1.70-1.57 [2H, m], 1.50-1.40 [12H, m], 1.45 [9H, s], 0.98-0.82 [6H, m]; ¹³C (101 MHz; CDCl₃) δ 173.76, 171.15, 157.58, 155.68, 141.89, 128.10, 127.36, 120.21, 90.49, 82.35, 81.04, 71.59, 60.38, 29.78, 28.48, 28.30, 20.88; m/z (ESI; 96%) Calc. for C₃₂H₄₂N₂O₉ = 598.69 found 599.0 [M+H]⁺ r.t. 3.13.

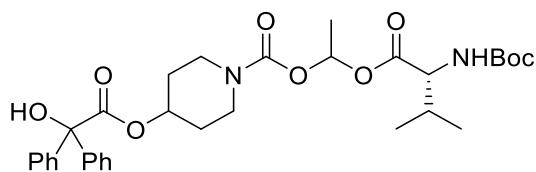
1-((*L*-Valyl)oxy)ethyl 4-(2-hydroxy-2,2-diphenylacetoxy)piperidine-1-carboxylate

14



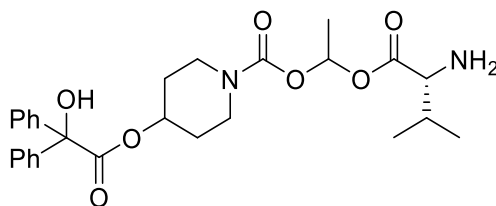
This compound was synthesised according to General Chemistry Procedure **3** to obtain the title compound **14** [Quantitative] as a white solid; ^1H (400 MHz; CDCl_3) δ 8.22 [2H, bs], 7.47-7.31 [10H, m], 6.67 [1H, q, J 5], 5.14 [1H, bs], 3.92-3.71 [2H, m], 3.48-3.16 [4H, m], 3.09-2.89 [1H, m], 1.22-1.92 [2H, m], 1.85-1.66 [2H, m], 1.59-1.44 [3H, m], 1.00-0.84 [6H, m]; ^{13}C (101 MHz; CDCl_3) δ 170.76, 170.43, 166.22, 143.65, 126.35, 128.29, 128.06, 126.00, 127.47, 127.38, 81.19, 73.60, 65.39, 30.80, 29.50, 19.80, 19.46; m/z (ESI; 99%) Calc. for $\text{C}_{27}\text{H}_{34}\text{N}_2\text{O}_7$ = 498.58 found 499.3 $[\text{M}+\text{H}]^+$ r.t. 2.29.

1-(((tert-butoxycarbonyl)-D-valyl)oxy)ethyl 4-(2-hydroxy-2,2-diphenylacetoxy) piperidine-1-carboxylate **14ii**



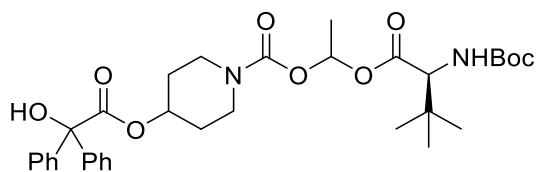
This compound was synthesised according to General Chemistry Procedure **1** and purified using flash column chromatography using a gradient of 20-80% EtOAc:(40-60) PET to obtain the title compound **14ii** (41%) as a colourless oil; Rf 0.50 [EtOAc:(40-60) PET (1:5)]; ^1H (400 MHz; CDCl_3) δ 7.47-7.30 [10H, m], 6.85 [1H, q, J 5], 5.17 [1H, bs], 5.06 [1H, bs], 4.22 [2H, d, J 3], 3.52-3.17- [4H, m], 2.13 [1H, m], 1.91-1.77 [2H, m], 1.71-1.59 [2H, m], 1.52-1.47 [3H, m], 1.45 [9H, s], 1.00-0.50 [6H, ddd, J 3, 7 and 30]; ^{13}C (101 MHz; CDCl_3) δ 173.85, 170.75, 155.71, 152.63, 141.85, 128.15, 127.38, 90.53, 81.06, 79.87, 71.67, 58.26, 40.91, 40.44, 30.07, 29.75, 28.31, 18.87, 17.30; m/z (ESI; 96%) Calc. for $\text{C}_{32}\text{H}_{42}\text{N}_2\text{O}_9$ = 598.69 found 599.0 $[\text{M}+\text{H}]^+$ r.t. 3.12.

1-((D-valyl)oxy)ethyl 4-(2-hydroxy-2,2-diphenylacetoxy)piperidine-1-carboxylate

14iii

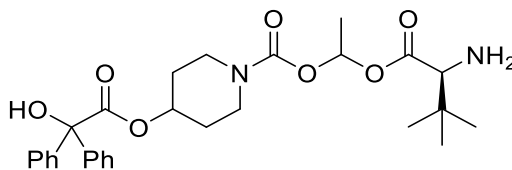
This compound was synthesised according to General Chemistry Procedure **3** to obtain the title compound **14iii** [Quantitative] as a white solid; ^1H (400 MHz; DMSO) δ 8.24 [2H, bs], 7.47-7.30 [10H, m], 6.77 [1H, q, J 5], 5.04 [1H, bs], 3.92-3.72 [2H, m], 3.48-3.16 [4H, m], 3.09-2.89 [1H, m], 1.22-1.93 [2H, m], 1.85-1.66 [2H, m], 1.59-1.43 [3H, m], 1.00-0.86 [6H, m]; ^{13}C (101 MHz; CDCl_3) δ 170.76, 169.43, 166.22, 143.65, 128.35, 128.29, 128.06, 128.00, 127.47, 127.38, 81.19, 74.60, 65.39, 29.80, 29.50, 19.80, 18.46; m/z (ESI; 99%) Calc. for $\text{C}_{27}\text{H}_{34}\text{N}_2\text{O}_7$ = 498.58 found 499.3 $[\text{M}+\text{H}]^+$ r.t. 2.27.

1-(((S)-2-((*tert*-Butoxycarbonyl)amino)-3,3-dimethylbutanoyl)oxy)ethyl 4-(2-hydroxy-2,2-diphenylacetoxy)piperidine-1-carboxylate **15i**



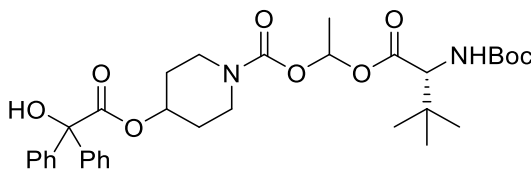
This compound was synthesised according to General Chemistry Procedure **1** and purified using flash column chromatography using a gradient of 20-80% EtOAc:(40-60) PET to obtain the title compound **15i** (75%) as a colourless oil; R_f 0.54 [EtOAc:(40-60) PET (3:10)]; ¹H (400 MHz; CDCl₃) δ 7.47-7.30 [10H, m], 6.83 [1H, q, *J* 5], 5.14 [1H, bs], 4.22 [1H, d, *J* 3], 4.15-4.02 [1H, bs], 3.51-3.23 [2H, m], 3.22-3.07 [1H, m], 1.88-1.72 [2H, m], 1.70-1.52 [2H, m], 1.51-1.40 [14H, m], 0.96 [9H, s]; ¹³C (101 MHz; CDCl₃) 173.77, 171.17, 157.58, 155.67, 141.87, 137.98, 128.10, 127.36, 121.11, 90.39, 84.98, 82.42, 62.28, 40.97, 38.60, , 29.67, 29.33, 28.47, 28.38, 19.88; m/z (ESI; 98%) Calc. for C₃₃H₄₄N₂O₉ = 612.72 found 613.3 [M+H]⁺ r.t. 3.13.

1-(((S)-2-Amino-3,3-dimethylbutanoyl)oxy)ethyl 4-(2-hydroxy-2,2-diphenylacetoxypiperidine-1-carboxylate **15**



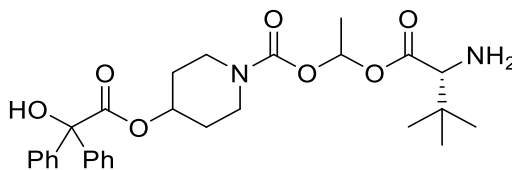
This compound was synthesised according to General Chemistry Procedure **3** obtain the title compound **15** [Quantitative] as a white solid; ^1H (400 MHz; DMSO) δ 8.19 [2H, bs], 7.47-7.29 [10H, m], 6.82 [1H, q, J 5], 5.14 [1H, bs], 3.42-3.10 [4H, m], 3.09-2.84 [1H, m], 1.85-1.74 [2H, m], 1.85-1.61 [2H, m], 1.57-1.42 [3H, m], 0.97 [9H, s]; ^{13}C (101 MHz; DMSO) δ 173.76, 170.58, 155.54, 152.81, 141.82, 128.11, 127.31, 90.36, 81.02, 79.69, 71.76, 66.38, 44.52, 43.46, 30.01, 28.35, 26.40, 17.02; m/z (ESI; 99%) Calc. for $\text{C}_{28}\text{H}_{36}\text{N}_2\text{O}_7 = 512.60$ found 513.3 $[\text{M}+\text{H}]^+$ r.t. 2.31.

1-(((R)-2-((*tert*-Butoxycarbonyl)amino)-3,3-dimethylbutanoyl)oxy)ethyl 4-(2-hydroxy-2,2-diphenylacetoxy)piperidine-1-carboxylate **15ii**



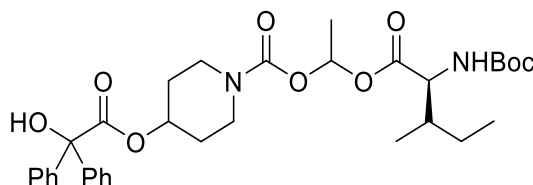
This compound was synthesised according to General Chemistry Procedure **1** and purified using flash column chromatography using a gradient of 20-80% EtOAc:(40-60) PET to obtain the title compound **15ii** (75%) as a colourless oil; R_f 0.54 [EtOAc:(40-60) PET (3:10)]; ¹H (400 MHz; DMSO) δ 7.47-7.29 [10H, m], 6.85 [1H, q, *J* 5], 5.11 [1H, bs], 4.22 [1H, m], 4.05 [1H, bs], 3.68-3.58 [2H, m], 3.52-3.28 [2H, m], 3.17 [1H, m], 1.85-1.74 [2H, m], 1.69-1.56 [2H, m], 1.52-1.45 [3H, m], 1.43 [9H, s], 0.97 [9H, s]; ¹³C (101 MHz; DMSO) δ 171.48, 168.72, 152.25, 144.67, 130.19, 129.40, 129.33, 129.05, 128.50, 128.42, 94.88, 82.22, 62.40, 41.38, 27.75, 27.46, 20.82.; m/z (ESI; 98%) Calc. for C₃₃H₄₄N₂O₉ = 612.72 found 613.3 [M+H]⁺ r.t. 3.14.

1-(((R)-2-Amino-3,3-dimethylbutanoyl)oxy)ethyl 4-(2-hydroxy-2,2-diphenylacetoxy) piperidine-1-carboxylate **15iii**



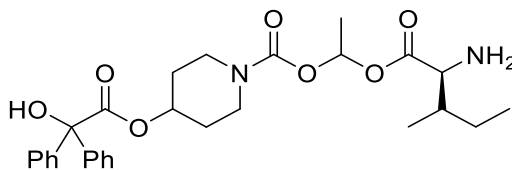
This compound was synthesised according to General Chemistry Procedure **3** obtain the title compound **15iii** [Quantitative] as a white solid; ^1H (400 MHz; DMSO) δ 8.19 [2H, bs], 7.47-7.30 [10H, m], 6.77 [1H, q, J 5], 5.04 [1H, bs], 3.44-3.10 [4H, m], 3.02-2.86 [1H, m], 1.85-1.74 [2H, m], 1.85-1.61 [2H, m], 1.57-1.42 [3H, m], 1.04-0.91 [9H, s]; ^{13}C (101 MHz; DMSO) δ 173.76, 170.42, 155.55, 152.81, 141.89, 128.11, 127.36, 90.37, 81.03, 79.77, 71.72, 66.37, 44.42, 43.86, 30.03, 28.29, 26.42, 17.50; m/z (ESI; 99%) Calc. for $\text{C}_{28}\text{H}_{36}\text{N}_2\text{O}_7 = 512.60$ found 513.3 $[\text{M}+\text{H}]^+$ r.t. 2.30.

1-(((*tert*-Butoxycarbonyl)-*L*-isoleucyl)oxy)ethyl 4-(2-hydroxy-2,2-diphenylacetoxy) piperidine-1-carboxylate **16i**



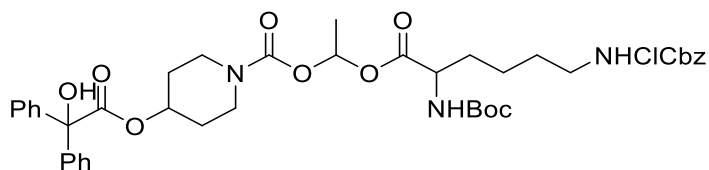
This compound was synthesised according to General Chemistry Procedure **1** and purified using flash column chromatography using a gradient of 20-80% EtOAc:(40-60) PET to obtain the title compound **16i** (35%) as a colourless oil; R_f 0.38 [EtOAc:(40-60) PET (2:10)]; ^1H (400 MHz; CDCl_3) δ 7.46-7.31 [10H, m], 6.84 [1H, q, J 5], 5.17 [1H, bs], 5.07 [1H, bs], 4.37-4.21 [2H, m], 3.70-3.61 [1H, bs], 3.52-3.13 [4H, m], 1.78-1.58 [2H, m], 1.57-1.52 [2H, m], 1.51-1.47 [3H, m], 1.43 [9H, s], 0.95-0.85 [8H, s]; ^{13}C (101 MHz; CDCl_3) δ 173.83, 170.66, 155.61, 152.57, 141.86, 128.14, 127.38, 90.36, 81.05, 79.83, 71.72, 57.75, 40.93, 40.43, 37.92, 29.69, 28.32, 24.97, 19.86, 15.43, 11.70; m/z (ESI; 97%) Calc. for $\text{C}_{33}\text{H}_{44}\text{N}_2\text{O}_9$ = 612.72 found 613.7 $[\text{M}+\text{H}]^+$ r.t. 3.17.

1-((*L*-Isoleucyl)oxy)ethyl 4-(2-hydroxy-2,2-diphenylacetoxy)piperidine-1-carboxylate **16**



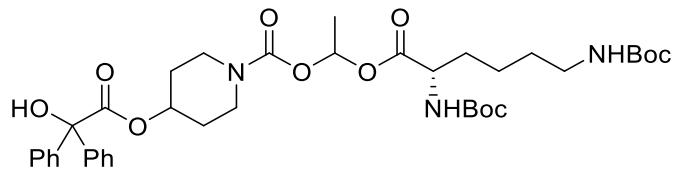
This compound was synthesised according to General Chemistry Procedure **3** to obtain the title compound **16** [Quantitative] as a white solid; ^1H (400 MHz; DMSO) δ 8.57 [2H, bs], 7.46-7.31 [10H, m], 6.74 [1H, q, J 5], 5.17 [1H, bs], 5.05 [1H, bs], 3.94 [1H, bs], 3.42-3.21 [4H, m], 1.95-1.85 [2H, m], 1.84-1.72 [2H, m], 1.60-1.34- [7H, m], 0.96-0.75 [6H, s]; ^{13}C (101 MHz; DMSO) δ 172.75, 167.18, 159.05, 143.77, 129.13, 128.26, 127.94, 127.52, 127.41, 91.10, 81.17, 70.36, 56.35, 36.43, 25.69, 19.94, 19.82, 14.55, 12.02, 11.98; m/z (ESI; 98%) Calc. for $\text{C}_{28}\text{H}_{36}\text{N}_2\text{O}_7$ = 512.60 found 513.2 $[\text{M}+\text{H}]^+$ r.t 2.32.

1-((5-(((benzyloxy)carbonyl)amino)-2-((tert-butoxycarbonyl)amino)pentanoyl)oxy)ethyl 4-(2-hydroxy-2,2-diphenylacetoxy)piperidine-1-carboxylate **17ii**



This compound was synthesised according to General Chemistry Procedure **1** to obtain the title compound **17ii** (83%) as a colourless oil; R_f 0.38 [EtOAc:(40-60) Pet Ether (1:5)]; ¹H (400 MHz; CDCl₃) δ 1.34-1.41 [2H, m], 1.44 [9H, s] 1.47 [3H, d, *J* 5], 1.50-1.57 [2H, m], 1.60-1.71 [3H, m], 1.74-1.81 [3H, m], 3.09-2.50 [6H, m], 4.28 [1H, s], 4.98 [1H, bs], 5.04-5.20 [4H, m], 6.82 [1H, q, *J* 5], 7.30-7.48 [10H, m]; ¹³C DEPT (101 MHz; CDCl₃) δ 128.52, 128.49, 128.15, 128.11, 128.07, 127.37, 90.93, 71.69, 66.54, 53.22, 53.10, 40.53, 40.47, 33.84, 31.95, 29.73, 28.32, 23.88, 19.75; m/z (ESI; 99%) Calc. for C₄₁H₅₀N₃O₁₁Cl = 795.31 found 796 (M+H),

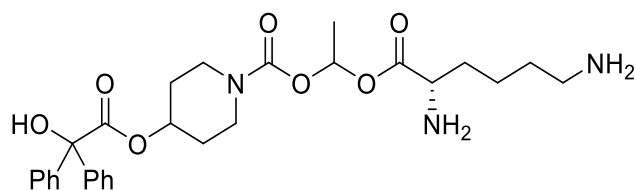
1-((*L*-Lysyl)oxy)ethyl 4-(2-hydroxy-2,2-diphenylacetoxy)piperidine-1-carboxylate

17i

This compound was synthesised according to General Chemistry Procedure **1** to obtain the title compound **17i** (75%) as a colourless oil; R_f 0.57 [EtOAc:(40-60) PET (2:10)]; ¹H (400 MHz; CDCl₃) δ 1.31-1.54 [24H, m], 1.58-1.72 [2H, m], 1.77-1.88 [2H, m], 3.10-3.47 [5H, m], 4.28 [1H, bs], 5.04-5.20 [4H, m], 5.07 [1H, bs], 6.82 [1H, q, *J* 5], 7.31-7.46 [10H, m]; ¹³C (101 MHz, DMSO) δ 172.75, 152.29, 143.77, 143.74, 129.13, 128.26, 127.94, 127.52, 127.41, 91.10, 81.17, 70.36, 56.35, 40.61, 40.45, 40.40, 40.25, 40.20, 39.99, 39.78, 39.57, 39.36, 36.43, 25.69, 19.94, 19.82, 14.55, 12.02, 11.98; m/z (ESI; 99%) Calc. for C₃₈H₅₃N₃O₁₁ = 727.85 found 728.4 [M+H]⁺ r.t. 3.11.

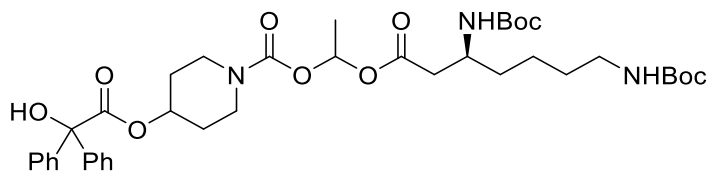
1-((*L*-Lysyl)oxy)ethyl 4-(2-hydroxy-2,2-diphenylacetoxy)piperidine-1-carboxylate

17



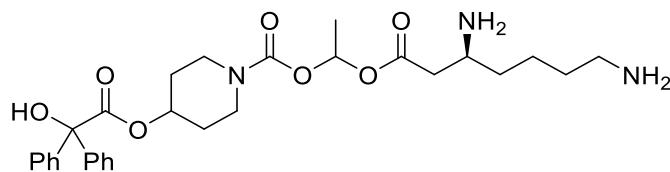
This compound was synthesised according to General Chemistry Procedure **3** to obtain the title compound **17** [Quantitative] as a white solid; ^1H (400 MHz; DMSO) δ 8.65 [2H, bs], 8.03 [2H, bs], 7.46-7.31 [10H, m], 6.74 [1H, q, J 5], 5.05 [1H, bs], 4.06-3.96 [1H, bs], 3.42-3.15 [4H, m], 2.75-2.65 [2H, m], 1.85-1.71 [4H, m], 1.82-1.28 [10H, m]; ^{13}C (101 MHz, DMSO) δ 172.76, 168.49, 158.91, 143.77, 129.15, 128.27, 127.95, 127.51, 91.22, 81.18, 70.31, 51.94, 38.63, 29.65, 29.57, 26.69, 26.63, 21.45, 19.84; m/z (ESI; 99%) Calc. for $\text{C}_{28}\text{H}_{37}\text{N}_3\text{O}_7 = 527.62$ found 528.2 $[\text{M}+\text{H}]^+$ r.t. 1.96.

1-(((S)-3,7-bis((tert-butoxycarbonyl)amino)heptanoyl)oxy)ethyl 4-(2-hydroxy-2,2-diphenylacetoxypiperidine-1-carboxylate **18i**

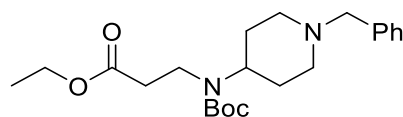


This compound was synthesised according to General Chemistry Procedure **1** to obtain the title compound **18i** (75%) as a colourless oil; R_f 0.52 [EtOAc:(40-60) PET (2:10)]; ^1H (400 MHz; CDCl_3) δ 7.46-7.31 [10H, m], 6.77 [1H, q, J 5], 5.17 [1H, bs], 5.18 [1H, bs], 4.25 [1H, bs], 3.95-3.82 [1H, m], 3.47-3.37 [2H, m], 3.36-3.25 [2H, m], 3.15-3.04 [2H, m], 2.56-2.48 [2H, m], 1.90-1.79 [2H, m], 1.72-1.62 [3H, m], 1.57-1.30 [30H, m]; ^{13}C (101 MHz; CDCl_3) δ 173.84, 156.06, 155.82, 141.82, 128.16, 127.36, 90.09, 81.03, 78.98, 48.45, 47.35, 40.43, 40.16, 28.45, 28.42, 28.40, 23.22, 19.82; m/z (ESI; 99%) Calc. for $\text{C}_{39}\text{H}_{55}\text{N}_3\text{O}_{11}$ = 741.88 found 742.4 $[\text{M}+\text{H}]^+$ r.t. 3.12.

1-(((S)-3,7-Diaminoheptanoyl)oxy)ethyl 4-(2-hydroxy-2,2-diphenylacetoxy)piperidine-1-carboxylate **18**

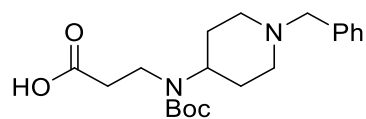


This compound was synthesised according to General Chemistry Procedure **3** to obtain the title compound **18** as a mixture of diastereoisomers [Quantitative] as a white solid; ^1H (400 MHz; DMSO) δ 1.34-1.46 [5H, m], 1.47-1.68 [7H, m], 1.70-1.82 [2H, m], 2.70-2.80 [1H, m], 3.17-3.44 [4H, m], 3.25-3.36 [2H, m], 5.05 [1H, bs], 6.67 [1H, q, J 5], 7.31-7.46 [10H, m] 7.98 [2H, bs], 8.21 [2H, bs]; ^{13}C (101 MHz; DMSO) δ 173.84, 156.06, 155.82, 141.82, 128.16, 127.36, 90.09, 81.03, 78.98, 48.45, 47.35, 40.43, 40.16, 28.45, 28.42, 28.40, 23.22, 19.82; m/z (ESI; 99%) Calc. for $\text{C}_{29}\text{H}_{39}\text{N}_3\text{O}_7$ = 541.65 found 542.4 $[\text{M}+\text{H}]^+$, r.t. 1.98

Ethyl 3-((1-benzylpiperidin-4-yl)(*tert*-butoxycarbonyl)amino)propanoate **34ii**

This compound was synthesised according to General Chemistry Procedure **4** and purified using silica gel column chromatography using a gradient of 5-10% EtOAc in (40-60) PET [1% NH₃] to obtain the title compound **34ii** (71%) as a pale yellow oil; R_f 0.52 [EtOAc:(40-60) PET (1:5)]; ¹H (400 MHz; CDCl₃) δ 7.36-7.16 [5H, m], 4.12-4.04 [2H, q, *J* 7], 3.46-3.41 [2H, s], 3.37 [1H, m], 2.93-2.84 [2H, m], 2.73-2.66 [1H, m], 2.54-2.45 [2H, m], 2.44-2.38 [1H, m], 2.04-1.93, [2H, m], 1.79-1.64 [2H, m], 1.61-1.53 [2H, m], 1.43 [9H, s], 1.21 [3H, t, *J* 7]; ¹³C (101 MHz; CDCl₃) δ 171.54, 155.18, 138.14, 129.10, 128.90, 128.34, 128.16, 127.02, 79.69, 62.89, 61.93, 60.31, 52.86, 41.17, 35.57, 29.97, 28.41, 14.16; m/z (ESI; 99%) Calc. for C₂₂H₃₄N₂O₄ = 390.52 found 391.6 [M+H]⁺, 413.7 [M+Na]⁺.

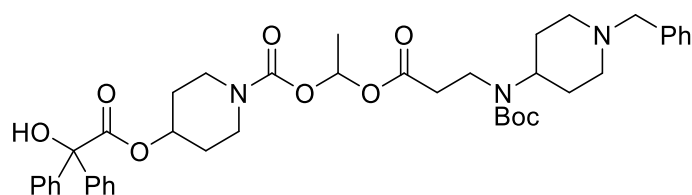
3-((1-Benzylpiperidin-4-yl)(*tert*-butoxycarbonyl)amino)propanoic acid **34**



This compound was synthesised according to General Chemistry Procedure **5** to obtain the title compound **43** which was used without purification; *m/z* (ESI; 99%)

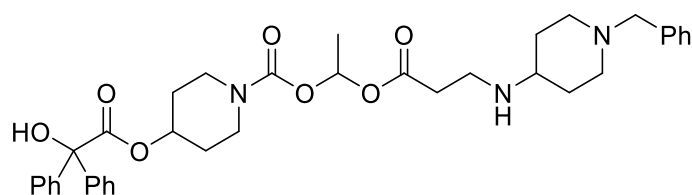
Calc. for $C_{20}H_{30}N_2O_4 = 362.47$ found 363.5 $[M+H]^+$.

1-((3-((1-Benzylpiperidin-4-yl)(*tert*-butoxycarbonyl)amino)propanoyl)oxy)ethyl 4-(2-hydroxy-2,2-diphenylacetoxy)piperidine-1-carboxylate **19i**



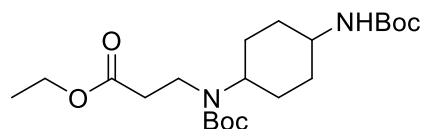
This compound was synthesised according to General Chemistry Procedure **1** and purified using silica gel column chromatography using a gradient of 33% EtOAc in (40-60) PET [1% NH₃] to obtain the title compound **19i** [65%] as a pale yellow oil; R_f 0.37 {35% EtOAc in (30-60) PET [1% NH₃]}; ¹H (400 MHz; CDCl₃) δ 7.46-7.30 [15H, m], 6.80 [1H, q, *J* 5], 5.17 [1H, bs], 4.26 [1H, s], 3.51 [2H, s], 3.36-2.47 [4H, m], 3.25-2.35 [2H, m], 2.99-2.92 [2H, m], 2.60-2.51 [2H, m], 2.10-2.04 [2H, m], 1.89-1.78 [3H, m], 1.59-1.78 [6H, m], 1.47 [12H, s]; ¹³C (101 MHz; CDCl₃) δ 173.85, 169.69, 155.20, 152.74, 141.83, 129.17, 128.27, 128.15, 127.37, 127.14, 89.99, 81.03, 79.89, 71.77, 62.89, 60.41, 53.13, 40.40, 38.29, 35.41, 30.02, 29.80, 28.46, 19.88; m/z (ESI; 96%) Calc. for C₄₂H₅₃N₃O₉ = 743.90 found 745.2 [M+H]⁺, r.t. 2.51.

1-((3-((1-Benzylpiperidin-4-yl)amino)propanoyl)oxy)ethyl 4-(2-hydroxy-2,2-diphenyl acetoxy)piperidine-1-carboxylate **19**



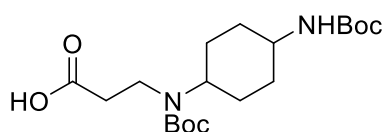
This compound was synthesised according to General Chemistry Procedure **3** to obtain the title compound **19** [Quantitative] as a white solid; ^1H (400 MHz; DMSO) δ 9.42 [1H, bs] 7.46-7.30 [15H, m] 6.67 [1H, q, J 5], 5.04 [1H, bs], 4.28 [1H,bs], 3.47-3.34 [4H, m], 3.19-3.10 [2H, m], 3.01-2.90 [1H, m], 2.80 [2H, t, J 7], 2.25 [2H, d, J 13], 2.03-2.90 [2H, m], 1.82-1.71 [2H, m], 1.56-1.46 [2H, m], 1.42 [3H, d, J 5]; ^{13}C (101 MHz; DMSO) δ 172.75, 159.46, 152.61, 143.77, 133.62, 131.98, 131.35, 130.01, 129.94, 129.24, 129.12, 128.25, 127.93, 127.83, 127.51, 120.47, 117.57, 114.68, 111.78, 90.40, 81.18, 70.31, 65.38, 59.23, 52.19, 49.89, 46.45, 30.59, 25.72, 20.01; m/z (ESI; 99%) Calc. for $\text{C}_{37}\text{H}_{45}\text{N}_3\text{O}_7 = 643.78$ found 645.5 $[\text{M}+\text{H}]^+$ r.t. 2.09.

Ethyl 3-((*tert*-butoxycarbonyl)(4-((*tert*-butoxycarbonyl) amino)cyclohexyl)amino)propanoate **35ii**



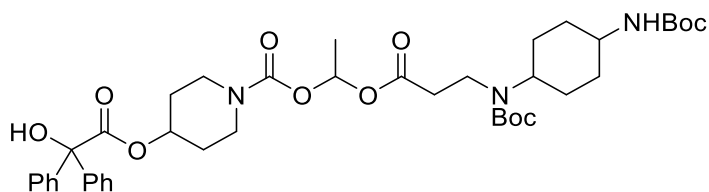
This compound was synthesised according to General Chemistry Procedure **4** and purified using silica gel column chromatography using a gradient of 10% EtOAc in (40-60) PET to obtain the title compound **35ii** (93%) as a colourless oil; R_f 0.42 [EtOAc:(40-60) PET (1:4)]; ¹H (400 MHz; CDCl₃) δ 4.16-4.05 [2H, m], 3.81-3.78 [2H, m], 3.42-3.36 [2H, m], 2.55-2.45 [2H, m], 2.05-1.97 [2H, m], 1.89-1.80, [2H, m], 1.72-1.63 [2H, m], 1.61-1.46 [2H, m], 1.44-1.38 [18H, s], 1.26-1.20 [3H, m]; ¹³C (101 MHz; CDCl₃) δ 171.14, 155.19, 155.08, 79.82, 60.44, 60.35, 53.85, 48.92, 33.82, 29.30, 28.40, 25.26, 14.15.

3-((*tert*-Butoxycarbonyl)4-((*tert*-
butoxycarbonyl)amino)cyclohexyl)amino)propanoic acid **35**



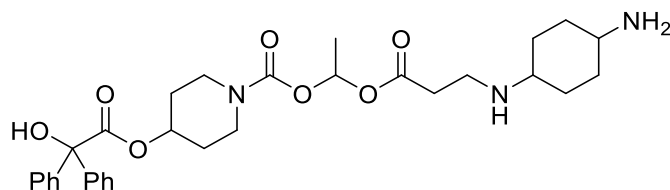
This compound was synthesised according to General Chemistry Procedure **5** and purified using silica gel column chromatography using a gradient of 20-100% EtOAc in (40-60) PET(1% AcOH) obtain the title compound **35** (53%) as a colourless oil; R_f 0.42 [EtOAc:(40-60) PET (1:3) (1% AcOH)]; ¹H (400 MHz; CDCl₃) δ 11.52-10.36 [1H, m], 3.83-3.63 [2H, m], 3.53-3.00 [2H, m], 2.50 [2H, s], 2.06-2.04 [2H, m], 1.87-1.74, [2H, m], 1.73-1.61 [2H, m], 1.57-1.47 [2H, m], 1.43 [18H, s]; ¹³C (101 MHz; CDCl₃) δ 176.57, 157.75, 155.42, 80.28, 67.59, 53.72, 45.16, 35.07, 29.95, 28.31, 27.60.

1-((3-((*tert*-Butoxycarbonyl) (4-((*tert*-butoxycarbonyl)amino)cyclohexyl) amino) propanoyl)oxy)ethyl 4-(2-hydroxy-2,2-diphenylacetoxy)piperidine-1-carboxylate
20i



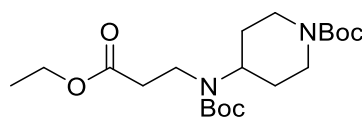
This compound was synthesised according to General Chemistry Procedure **1** and purified using silica gel column chromatography using a gradient of 33% EtOAc in (40-60) PET to obtain the title compound **20i** (66%) as a colourless oil; R_f 0.47 [30% EtOAc in (40-60) PET]; ¹H (400 MHz; CDCl₃) δ 7.46-7.29 [10H, m], 6.77 [1H, q, *J* 5], 5.19-5.12 [1H, bs], 3.51-3.20 [8H, m], 2.63-2.48 [2H, m], 1.82-1.48 [15H, m], 1.44 [18H, s]; ¹³C (101 MHz; CDCl₃) δ 171.37, 155.38, 155.23, 152.80, 141.81, 128.11, 127.34, 90.06, 82.74, 81.06, 71.67, 60.47, 58.60, 45.20, 44.18, 33.83, 30.02, 29.86, 28.41, 25.32, 19.81; m/z (ESI; 99%) Calc. for C₄₁H₅₇N₃O₁₁ = 767.92 found 768.4 [M+H]⁺ r.t. 3.23.

1-((3-((4-Aminocyclohexyl)amino)propanoyl)oxy)ethyl 4-(2-hydroxy-2,2-diphenyl acetoxy)piperidine-1-carboxylate **20**



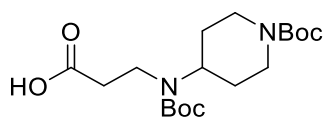
This compound was synthesised according to General Chemistry Procedure **3** obtain the title compound **20** [Quantitative] as a white solid; ^1H (400 MHz; CDCl_3) δ 8.09 [3H, bs], 7.46-7.29 [10H, m], 6.67 [1H, q, J 5], 5.04 [1H, bs], 3.49-3.09 [8H, m], 3.06-2.91 [1H, m], 2.88-2.76 [2H, m], 2.15-1.96 [2H, m], 1.90-1.69 [4H, m], 1.57-1.33 [8H, m]; ^{13}C (101 MHz; DMSO) δ 172.75, 159.43, 143.77, 129.12, 128.25, 127.93, 127.51, 120.60, 117.70, 114.79, 111.89, 90.40, 81.17, 70.40, 54.96, 48.50, 46.24, 31.75, 30.72, 30.67, 28.52, 26.74, 20.02,.; m/z (ESI; 99%) Calc. for $\text{C}_{31}\text{H}_{41}\text{N}_3\text{O}_7 = 567.68$ found 568.2[M+H] $^+$ r.t. 2.00.

tert-Butyl 4-((*tert*-butoxycarbonyl)(3-ethoxy-3-oxopropyl)amino)piperidine-1-carboxylate **33ii**



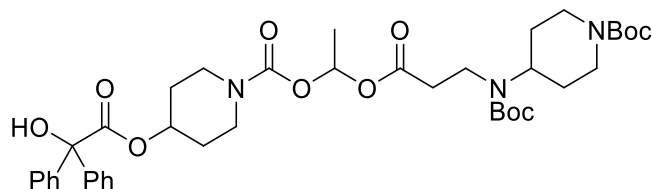
This compound was synthesised according to General Chemistry Procedure **4** and purified using silica gel column chromatography using a gradient of 5-10% EtOAc in (40-60) PET [1% NH₃] to obtain the title compound **33ii** (71%) as a pale yellow oil; R_f 0.46 [EtOAc:(40-60) PEPET (1:5)]; ¹H (400 MHz; DMSO) δ 4.24-4.17 [1H, m], 4.12-4.01 [2H, q, *J* 7], 3.43-3.33 [2H, m], 2.78-2.69 [2H, m], 2.58-2.51 [2H, m], 1.79-1.64 [2H, m], 1.68-1.61 [2H, m], 1.45 [18H, s], 1.28 [3H, t, *J* 7]; ¹³C (101 MHz; DMSO) δ 171.54, 155.18, 138.14, 129.10, 128.90, 128.34, 128.16, 127.02, 79.69, 62.89, 61.93, 60.31, 52.86, 41.17, 35.57, 29.97, 28.41, 14.16; m/z (ESI; 99%) Calc. for C₂₀H₃₆N₂O₆ = 400.52 found 401.5 [M+H]⁺, 423.6 [M+Na]⁺.

3-((*tert*-Butoxycarbonyl)(1-(*tert*-butoxycarbonyl)piperidin-4-yl)amino)propanoic acid **33**



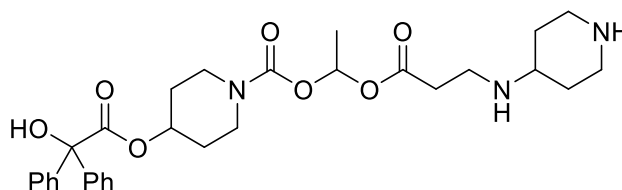
This compound was synthesised according to General Chemistry Procedure **5** to obtain the title compound **33** which was used without purification; m/z (ESI; 97%)
Calc. for C₁₈H₃₂N₂O₆ = 372.46 found 373.5 [M+H]⁺.

1-((3-((*tert*-Butoxycarbonyl)(1-(*tert*-butoxycarbonyl)piperidin-4-yl)amino)propanoyl oxy)ethyl 4-(2-hydroxy-2,2-diphenylacetoxy)piperidine-1-carboxylate **21i**



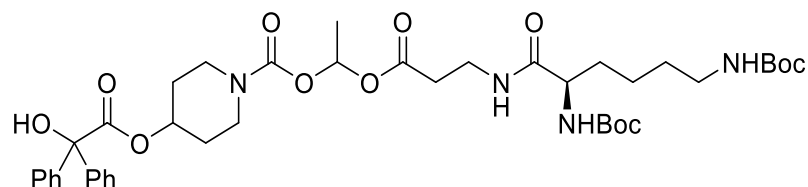
This compound was synthesised according to General Chemistry Procedure **1** and purified using silica gel column chromatography using a gradient of 1:3 EtOAc:(40-60) PET to obtain the title compound **21i** (88%) as a colourless oil; R_f 0.1 [EtOAc]; ¹H (400 MHz; CDCl₃) δ 7.28-7.41 [10H, m], 6.78 [1H, q, *J* 5], 5.13 [1H, h, *J* 4], 4.15 [2H, s], 3.22-3.44 [6H, m], 2.62-1.74 [2H, m], 2.48-2.56 [2H, m], 1.75-1.86 [2H, m], 1.57-1.69 [6H, m], 1.40-1.48 [21H, s]; ¹³C (101 MHz; CDCl₃) δ ¹³C (101 MHz, CDCl₃) δ 174.79, 173.85, 155.11, 154.67, 154.61, 152.73, 141.82, 128.15, 127.36, 90.01, 81.04, 80.18, 79.80, 79.76, 71.72, 40.42, 35.10, 30.08, 28.44, 23.85, 19.87.; *m/z* (ESI; 94%) Calc. for C₄₀H₅₅N₃O₁₁ = 753.38 found 754.4 [M+H]⁺ r.t.3.25.

1-((3-(Piperidin-4-ylamino)propanoyl)oxy)ethyl 4-(2-hydroxy-2,2-diphenylacetoxy) piperidine-1-carboxylate **21**



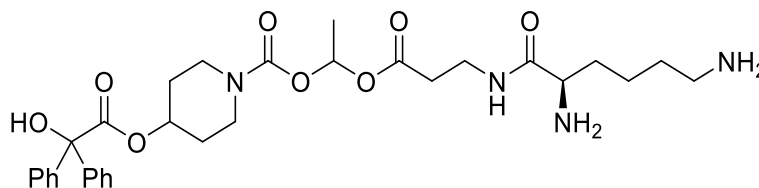
This compound was synthesised according to General Chemistry Procedure **3** to obtain the title compound **26** [Quantitative] as a white solid; ^1H (400 MHz; DMSO) δ 9.08 [1H, bs], 8.87 [1H, bs], 7.41-7.28 [10H, m], 6.67 [1H, q, J 5], 5.13 [1H, bs], 3.43-3.10 [6H, m], 2.92 [3H, q, J 12], 2.80 [2H, t, J 7], 2.70 [1H, t, J 7], 2.56-2.48 [2H, m], 2.24-2.13 [3H, m], 1.85-1.70 [4H, m], 1.57-1.39 [4H, s]; ^{13}C (101 MHz; DMSO) δ 172.75, 143.77, 129.11, 128.25, 127.93, 127.51, 127.41, 120.74, 117.84, 114.93, 112.02, 90.41, 81.17, 70.33, 52.24, 52.16, 41.97, 40.57, 38.55, 31.74, 30.26, 28.82, 20.00; m/z (ESI; 94%) Calc. for $\text{C}_{30}\text{H}_{39}\text{N}_3\text{O}_7$ = 553.66 found 554.3 $[\text{M}+\text{H}]^+$ r.t. 2.01.

(10*R*)-10-((*tert*-Butoxycarbonyl)amino)-2,2-dimethyl-4,11,15-trioxo-3,16-dioxo-5,12-diazaoctadecan-17-yl 4-(2-hydroxy-2,2-diphenylacetoxy)piperidine-1-carboxylate **22i**



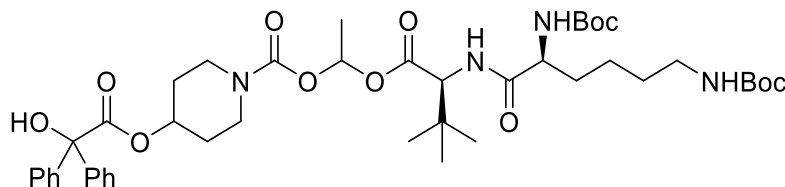
This compound was synthesised according to General Chemistry Procedure **6** and purified using flash column chromatography using a gradient of 20-80% EtOAc:(40-60) PET to obtain the title compound **22i** as a mixture of diastereoisomers (37%) as a colourless oil; R_f 0.44 [50% EtOAc in (40-60) PET]; ^1H (400 MHz; CDCl_3) δ 7.47-7.30 [10H, m], 6.74 [1H, q, J 5], 5.22-5.09 [2H, m], 4.55 [1H, m], 4.05 [1H, bs], 3.51-3.06 [6H, m], 2.58-2.48 [2H, m], 1.92-1.75 [3H, m], 1.74-1.63 [3H, m], 1.62-1.532 [2H, m], 1.49 [3H, d, J 5], 1.44 [18H, s], 1.40-1.29 [2H, m]; ^{13}C (101 MHz; CDCl_3) δ 173.83, 171.18, 169.89, 156.18, 152.56, 141.81, 128.14, 127.35, 127.10, 90.46, 82.78, 81.04, 71.69, 60.41, 40.88, 40.45, 29.69, 28.44, 28.30, 23.86, 22.62, 14.20, 11.58; m/z (ESI; 99%) Calc. for $\text{C}_{41}\text{H}_{58}\text{N}_4\text{O}_{12}$ = 798.93 found 799.4 $[\text{M}+\text{H}]^+$ r.t. 3.03.

1-((3-((*R*)-2,6-Diaminohexanamido)propanoyl)oxy)ethyl 4-(2-hydroxy-2,2-diphenylacetoxy)piperidine-1-carboxylate **22**



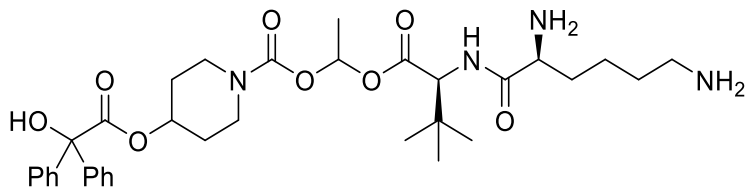
This compound was synthesised according to General Chemistry Procedure **3** to obtain the title compound **22** [Quantitative] as a white solid; ^1H (400 MHz; DMSO) δ 7.90 [4H, bs], 7.47-7.30 [10H, m], 6.62 [1H, q, J 5], 5.05 [1H, bs], 4.23-4.12 [1H, m], 3.40-3.16 [2H, m], 3.01-2.90 [2H, m], 2.80-2.66 [2H, m], 2.59-2.52 [2H, m], 1.83-1.70 [2H, m], 1.69-1.45 [6H, m], 1.45-1.30 [6H, m]; ^{13}C (101 MHz, DMSO) δ 173.83, 171.18, 156.68, 140.81, 128.24, 126.35, 127.10, 90.56, 82.75, 71.54, 60.42, 40.72, 40.10, 29.41, 28.25, 28.34, 23.86, 22.62, 14.20, 11.58. m/z (ESI; 99%) Calc. for $\text{C}_{31}\text{H}_{42}\text{N}_4\text{O}_8 = 598.70$ found 599.2 $[\text{M}+\text{H}]^+$ r.t. 2.04.

(10*S*,13*S*)-10-((*tert*-Butoxycarbonyl)amino)-13-(*tert*-butyl)-2,2-dimethyl-4,11,14-trioxo-3,15-dioxo-5,12-diazaheptadecan-16-yl 4-(2-hydroxy-2,2-diphenylacetoxy) piperidine-1-carboxylate **23i**



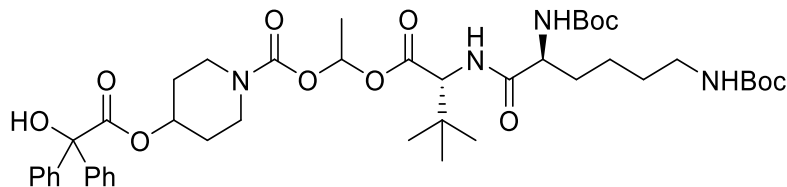
This compound was synthesised according to General Chemistry Procedure **6** and purified using flash column chromatography using a gradient of 20-80% EtOAc:(40-60) PET to obtain the title compound **23i** as a mixture of diastereoisomers (94%) as a colourless oil; R_f 0.44 [50% EtOAc in (40-60) PET]; ^1H (400 MHz; CDCl_3) δ 7.47-7.30 [10H, m], 6.81 [1H, q, J 5], 5.32 [4H, m], 5.18 [1H, bs], 4.83-4.64 [1H, m], 4.06 [1H, bs], 3.66 [1H, bs], 3.72-3.29 [4H, m], 3.15-3.05 [2H, m], 1.88-1.75 [3H, m], 1.70-1.59 [3H, m], 1.58-1.50 [2H, m], 1.50-1.46 [3H, m], 1.45 [18H, s], 1.37-1.30 [2H, m], 1.02-0.94 [9H, m]; ^{13}C (101 MHz, CDCl_3) δ 173.74, 172.33, 171.15, 156.18, 155.81, 152.55, 141.91, 128.08, 127.34, 90.51, 82.41, 81.05, 71.54, 60.36, 40.94, 40.42, 39.86, 33.81, 30.95, 30.04, 29.58, 28.40, 27.62, 23.90, 22.57, 18.68; m/z (ESI; 99%) Calc. for $\text{C}_{44}\text{H}_{64}\text{N}_4\text{O}_{12}$ = 841.01 found 841.4 $[\text{M}+\text{H}]^+$ r.t. 3.17.

1-(((S)-2-((S)-2,6-Diaminohexanamido)-3,3-dimethylbutanoyloxy)ethyl 4-(2-hydroxy-2,2-diphenylacetoxy)piperidine-1-carboxylate **23**



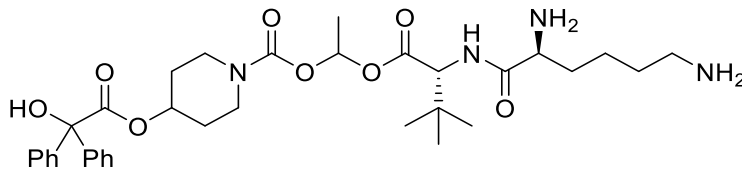
This compound was synthesised according to General Chemistry Procedure **3** to obtain the title compound **23** [Quantitative] as a white solid; ^1H (400 MHz; DMSO) δ 8.34 [2H, bs], 8.06 [2H, bs], 7.47-7.30 [10H, m], 6.69 [1H, q, J 5], 5.04 [1H, bs], 4.12-4.00 [2H, m], 3.42-3.29 [4H, m], 3.15-3.05 [2H, m], 3.41-3.15 [2H, m], 2.79-2.70 [2H, m], 1.77-1.67 [2H, m], 1.63-1.43 [4H, m], 1.44-1.34 [6H, m], 0.97 [9H, s]; ^{13}C (101 MHz, DMSO) δ 172.74, 172.72, 169.67, 159.38, 143.76, 129.11, 128.24, 127.92, 127.51, 120.28 90.20, 81.17, 70.39, 65.37, 51.83, 38.69, 33.93, 33.91, 30.98, 30.90, 30.26, 28.82, 19.92; m/z (ESI; 99%) Calc. for $\text{C}_{34}\text{H}_{48}\text{N}_4\text{O}_8$ = 640.78 found 642.2 $[\text{M}+\text{H}]^+$ r.t. 2.11.

(10*S*,13*R*)-10-((*tert*-Butoxycarbonyl)amino)-13-(*tert*-butyl)-2,2-dimethyl-4,11,14-trioxo-3,15-dioxo-5,12-diazaheptadecan-16-yl 4-(2-hydroxy-2,2-diphenylacetoxy) piperidine-1-carboxylate **24i**



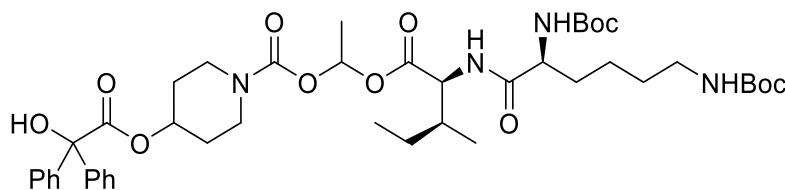
This compound was synthesised according to General Chemistry Procedure **6** and purified using flash column chromatography using a gradient of 20-80% EtOAc:(40-60) PET to obtain the title compound **24i** as a mixture of diastereoisomers (86%) as a colourless oil; R_f 0.44 [50% EtOAc in (40-60) PET]; ^1H (400 MHz; CDCl_3) δ 7.47-7.30 [10H, m], 6.81 [1H, q, J 5], 5.32 [4H, m], 5.18 [1H, bs], 4.83-4.64 [1H, m], 4.06 [1H, bs], 3.66 [1H, bs], 3.72-3.29 [6H, m], 3.15-3.05 [2H, m], 1.88-1.75 [3H, m], 1.70-1.59 [3H, m], 1.58-1.50 [2H, m], 1.50-1.46 [3H, m], 1.45 [18H, s], 1.37-1.30 [2H, m], 1.02-0.94 [9H, m]; ^{13}C (101 MHz, CDCl_3) δ 173.74, 172.33, 171.15, 156.18, 155.81, 152.55, 141.91, 128.08, 127.34, 90.51, 82.41, 81.05, 71.54, 60.36, 40.94, 40.42, 39.86, 33.81, 30.95, 30.04, 29.58, 28.40, 27.62, 23.90, 22.57, 18.68; m/z (ESI; 99%) Calc. for $\text{C}_{44}\text{H}_{61}\text{N}_4\text{O}_{12}$ = 841.01 found 841.5 $[\text{M}+\text{H}]^+$ r.t. 3.17.

1-(((*R*)-2-((*S*)-2,6-Diaminohexanamido)-3,3-dimethylbutanoyl)oxy)ethyl 4-(2-hydroxy-2,2-diphenylacetoxy)piperidine-1-carboxylate **24**



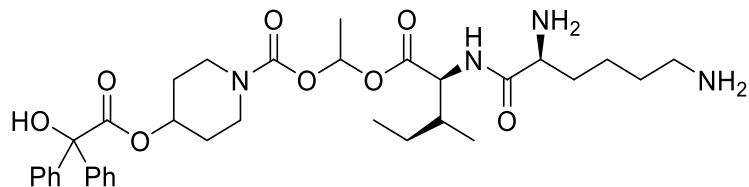
This compound was synthesised according to General Chemistry Procedure **3** to obtain the title compound **29** [Quantitative] as a white solid; ^1H NMR (400 MHz, D^6 -DMSO) δ 8.76 (1H, dd, $J = 8.7, 2.7$ Hz), 8.17 (3H, s), 7.80 (3H, s), 7.43 – 7.22 (10H, m), 6.81 – 6.68 (1H, m), 6.63 (1H, s), 5.10-5.05 (1H, m), 4.21 (1H, 2d, $J = 8.6$ Hz), 3.95-3.90 (1H, m), 3.35-3.25 (4H, m), 2.76-2.74 (2H, m), 1.75-1.72 (4H, m), 1.65 – 1.31 (4H, m), 1.43 (3H, 2d, $J = 8.6$ Hz), 1.40-1.35 (2H, m), 0.93 (9H, 2s) ppm; ^{13}C (101 MHz, CDCl_3) δ 172.76, 172.53, 169.61, 158.63, 143.81, 128.29, 127.95, 127.57, 90.59, 81.18, 70.54, 52.28, 38.97, 38.77, 34.60, 34.42, 31.32, 26.95, 26.81, 26.75, 21.45, 19.96; m/z (ESI; 99%) Calc. for $\text{C}_{34}\text{H}_{48}\text{N}_4\text{O}_8 = 640.78$ found 641.4 $[\text{M}+\text{H}]^+$ r.t. 2.12.

(10*S*,13*S*)-10-((*tert*-Butoxycarbonyl)amino)-13-((*S*)-*sec*-butyl)-2,2-dimethyl-4,11,14-trioxo-3,15-dioxo-5,12-diazaheptadecan-16-yl 4-(2-hydroxy-2,2-diphenylacetoxypiperidine-1-carboxylate **25i**



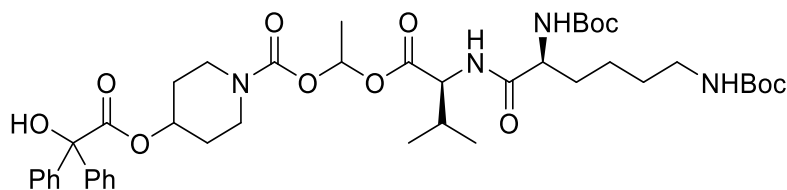
This compound was synthesised according to General Chemistry Procedure **6** and purified using flash column chromatography using a gradient of 20-80% EtOAc:(40-60) PET to obtain the title compound **25i** as a mixture of diastereoisomers (94%) as a colourless oil; R_f 0.46 [50% EtOAc in (40-60) PET]; ^1H (400 MHz; CDCl_3) δ 7.47-7.30 [10H, m], 6.75 [1H, q, J 5], 5.32 [4H, m], 5.20-5.10 [2H, m], 4.70 [1H, bs], 4.60-4.50 [1H, m], 4.83-4.64 [1H, m], 4.06 [1H, bs], 3.50-3.05 [6H, m], 1.95-1.75 [2H, m], 1.74-1.58 [3H, m], 1.56-1.52 [2H, m], 1.51-1.47 [3H, m], 1.46 [18H, s], 1.43-1.34 [2H, m], 0.95-0.84 [9H, m]; ^{13}C (101 MHz, CDCl_3) δ 173.85, 171.20, 169.91, 156.19, 152.58, 141.88, 128.16, 127.37, 127.12, 90.48, 81.05, 79.14, 71.70, 56.31, 51.58, 41.35, 37.69, 29.69, 28.30, 27.67, 23.87, 22.62, 21.05, 19.72, 14.20, 11.58; m/z (ESI; 99%) Calc. for $\text{C}_{44}\text{H}_{64}\text{N}_4\text{O}_{12}$ = 841.01 found 842.5 $[\text{M}+\text{H}]^+$ r.t. 3.16.

1-((*L*-Lysyl-*L*-alloisoleucyl)oxy)ethyl 4-(2-hydroxy-2,2-diphenylacetoxy) piperidine-1-carboxylate **25**

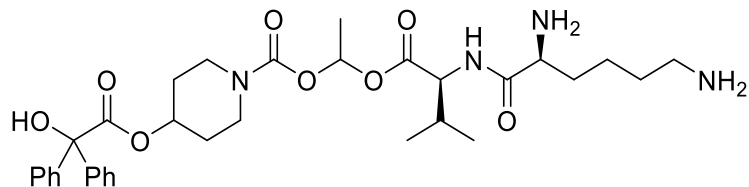


This compound was synthesised according to General Chemistry Procedure **3** to obtain the title compound **25** [Quantitative] as a white solid; ^1H (400 MHz; CDCl_3) δ 8.35 [2H, bs], 8.07 [2H, bs], 7.47-7.30 [10H, m], 6.68 [1H, q, J 5], 5.32 [4H, m], 5.20-5.10 [2H, m], 5.05 [1H, bs], 4.25-4.18 [2H, m], 3.94 [1H, bs], 3.35-3.20 [4H, m], 2.76-2.70 [2H, m], 1.86-1.69 [4H, m], 1.64-1.46 [4H, m], 1.46-1.36 [7H, m], 1.30-1.18 [3H, m], 0.92-0.76 [6H, m]; ^{13}C (101 MHz, DMSO) δ 172.74, 169.58, 169.53, 158.98, 143.76, 132.19, 132.05, 129.12, 128.24, 127.93, 127.51, 90.39, 81.17, 67.87, 57.25, 51.92, 38.71, 38.67, 36.60, 30.85, 30.26, 26.69, 25.13, 25.05, 19.96, 15.57, 11.68; m/z (ESI; 99%) Calc. for $\text{C}_{34}\text{H}_{48}\text{N}_4\text{O}_8$ = 640.78 found 641.5 $[\text{M}+\text{H}]^+$ r.t. 2.08.

(10*S*,13*S*)-10-((*tert*-Butoxycarbonyl)amino)-13-isopropyl-2,2-dimethyl-4,11,14-trioxo-3,15-dioxo-5,12-diazaheptadecan-16-yl 4-(2-hydroxy-2,2-diphenylacetoxypiperidine-1-carboxylate **26i**

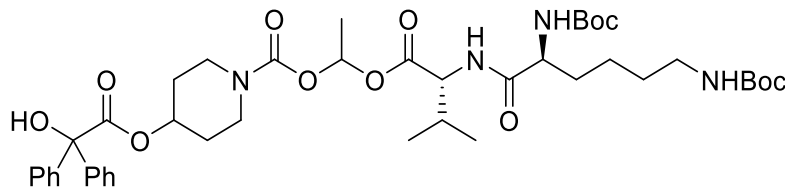


This compound was synthesised according to General Chemistry Procedure **6** and purified using flash column chromatography using a gradient of 20-80% EtOAc:(40-60) obtain the title compound **26i** as a mixture of diastereoisomers (95%) as a colourless oil; R_f 0.65 [EtOAc]; ^1H (400 MHz; CDCl_3) δ 7.45-7.30 [10H, m], 6.76 [1H, q, J 5], 5.32 [4H, m], 5.27 [1H, bs], 4.86-4.74 [1H, bs], 4.53-4.37 [1H, m], 3.57-3.00 [6H, m], 2.19-2.08 [1H, m], 1.84-1.72 [3H, m], 1.67-1.55 [3H, m], 1.53-1.48 [2H, m], 1.47-1.43 [3H, d, J 5], 1.41 [18H, s], 1.37-1.30 [2H, m], 0.93-0.84 [6H, m]; ^{13}C (101 MHz; CDCl_3) δ 173.74, 172.23, 171.15, 156.18, 152.55, 141.91, 128.08, 127.34, 90.51, 81.05, 79.94, 71.54, 60.36, 56.83, 41.31, 40.94, 40.42, 33.81, 31.55, 31.09, 29.58, 28.27, 27.62, 23.90, 18.86, 18.68; m/z (ESI; 97%) Calc. for $\text{C}_{43}\text{H}_{62}\text{N}_4\text{O}_{12}$ = 826.99 found 827.5 $[\text{M}+\text{H}]^+$ r.t. 3.12.

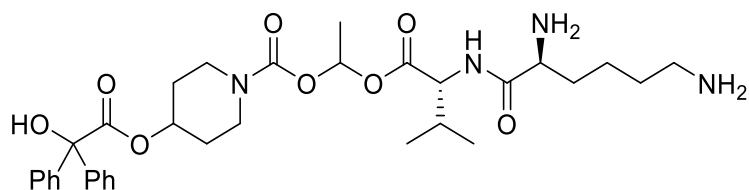
1-((*L*-Lysyl-*L*-valyl)oxy)ethyl 4-(2-hydroxy-2,2-diphenylacetoxy)piperidine-1-carboxylate **26**

This compound was synthesised according to General Chemistry Procedure **3** to obtain the title compound **26** [Quantitative] as a white solid; ^1H (400 MHz; DMSO) δ 8.35 [2H, bs], 8.06 [2H, bs], 7.45-7.30 [10H, m], 6.68 [1H, q, J 5], 5.04 [1H, bs], 4.48-4.10 [2H, m], 3.39-3.17 [2H, m], 2.80-2.70 [2H, m], 2.13-2.03 [1H, m], 1.84-1.72 [2H, m], 1.80-1.68 [2H, m], 1.67-1.55 [2H, m], 1.65-1.54 [2H, m], 1.53-1.46 [2H, m], 1.45-1.34 [4H, m], 0.96-0.85 [6H, m]; ^{13}C (101 MHz; DMSO) δ 172.75, 171.34, 169.76, 158.59, 152.54, 143.76, 128.26, 127.94, 127.51, 117.77, 114.87, 90.33, 81.17, 70.39, 51.93, 38.71, 30.84, 30.03, 26.73, 26.69, 21.39, 19.99, 19.19; m/z (ESI; 97%) Calc. for $\text{C}_{33}\text{H}_{46}\text{N}_4\text{O}_8 = 626.75$ found 627.4 $[\text{M}+\text{H}]^+$ r.t. 2.07.

(10*S*,13*R*)-10-((*tert*-Butoxycarbonyl)amino)-13-isopropyl-2,2-dimethyl-4,11,14-trioxo-3,15-dioxo-5,12-diazaheptadecan-16-yl 4-(2-hydroxy-2,2-diphenylacetoxypiperidine-1-carboxylate) **27i**

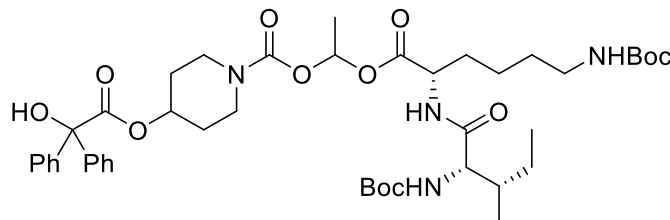


This compound was synthesised according to General Chemistry Procedure **6** and purified using flash column chromatography using a gradient of 20-80% EtOAc:(40-60) PET to obtain the title compound **27i** as a mixture of diastereoisomers (92%) as a colourless oil; R_f 0.48 [40% EtOAc in (40-60) PET]; ^1H (400 MHz; CDCl_3) δ 7.30-7.45 [10H, m], 6.76 [1H, q, J 5], 5.32 [4H, m], 5.27 [1H, bs], 4.74-4.86 [1H, bs], 4.37-4.53 [1H, m], 3.00-3.57 [6H, m], 2.08-2.19 [1H, m], 1.72-1.84 [3H, m], 1.55-1.67 [3H, m], 1.48-1.53 [2H, m], 1.43-1.47 [3H, d, J 5], 1.41 [18H, s], 1.30-1.37 [2H, m], 0.84-0.93 [6H, m]; ^{13}C (101 MHz, CDCl_3) δ 173.74, 172.23, 171.15, 156.18, 152.55, 141.91, 128.08, 127.34, 90.51, 81.05, 79.94, 71.54, 60.36, 56.83, 41.31, 40.94, 40.42, 33.81, 31.55, 31.09, 29.58, 28.27, 27.62, 23.90, 18.86, 18.68; m/z (ESI; 99%) Calc. for $\text{C}_{43}\text{H}_{62}\text{N}_4\text{O}_{12}$ = 826.99 found 827.5 $[\text{M}+\text{H}]^+$ r.t. 3.15.

1-((*L*-Lysyl-*D*-valyl)oxy)ethyl 4-(2-hydroxy-2,2-diphenylacetoxy)piperidine-1-carboxylate **27**

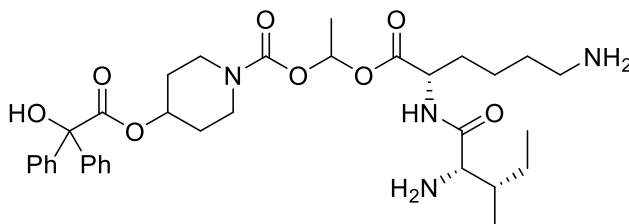
This compound was synthesised according to General Chemistry Procedure **3** to obtain the title compound **27** [Quantitative] as a white solid; ^1H (400 MHz; DMSO) δ 8.35 [2H, bs], 8.06 [2H, bs], 7.45-7.30 [10H, m], 6.68 [1H, q, J 5], 5.04 [1H, bs], 4.48-4.10 [2H, m], 3.39-3.17 [2H, m], 2.80-2.70 [2H, m], 2.13-2.03 [1H, m], 1.84-1.72 [2H, m], 1.67-1.56 [2H, m], 1.81-1.67 [2H, m], 1.64-1.55 [2H, m], 1.52-1.44 [2H, m], 1.46-1.35 [4H, m], 0.95-0.85 [6H, m]; ^{13}C (101 MHz, DMSO) δ 172.73, 169.94, 169.63, 152.55, 143.77, 132.07, 129.13, 128.26, 127.94, 127.51, 90.54, 81.17, 67.88, 57.83, 52.16, 31.09, 30.43, 30.26, 28.83, 26.63, 23.72, 22.86, 21.54, 20.00, 19.96; m/z (ESI; 97%) Calc. for $\text{C}_{33}\text{H}_{46}\text{N}_4\text{O}_8 = 626.75$ found 627.4 $[\text{M}+\text{H}]^+$ r.t. 2.10.

(6*S*,9*S*)-9-(4-((*tert*-Butoxycarbonyl)amino)butyl)-6-((*S*)-*sec*-butyl)-2,2-dimethyl-4,7,10-trioxo-3,11-dioxo-5,8-diazatridecan-12-yl-4-(2-hydroxy-2,2-diphenyl acetoxyl) piperidine-1-carboxylate **28i**



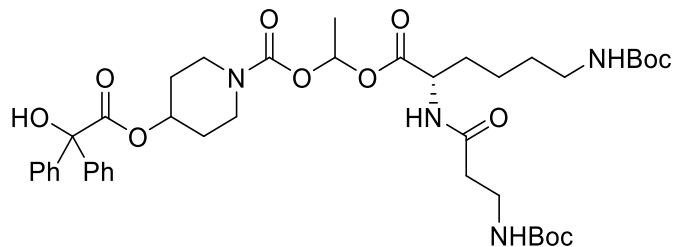
This compound was synthesised according to General Chemistry Procedure **6** and purified using flash column chromatography using a gradient of 20-80% EtOAc:(40-60) PET to obtain the title compound **28i** as a mixture of diastereoisomers (49%) as a colourless oil; R_f 0.42 [40% EtOAc in (40-60) PET]; ^1H (400 MHz; CDCl_3) δ 7.48-7.30 [10H, m], 6.69 [1H, q, J 5], 5.21-5.10 [2H, m], 5.62-5.11 [1H, m], 4.38-4.34 [1H, m], 3.94 [1H, bs], 3.48-2.97 [6H, m], 1.90-1.78 [3H, m], 1.73-1.62 [3H, m], 1.57-1.51 [2H, m], 1.51-1.46 [3H, d, J 5], 1.44 [9H, s], 1.40-1.30 [2H, m], 0.96-0.87 [8H, m]; ^{13}C (101 MHz; CDCl_3) δ 173.81, 171.68, 170.29, 156.08, 152.65, 141.84, 128.14, 127.35, 90.75, 82.71, 81.05, 71.64, 59.23, 51.84, 40.91, 40.46, 36.99, 36.96, 31.57, 29.79, 29.21, 28.46, 28.31, 24.76, 23.90, 19.73, 17.30, 14.66; m/z (ESI; 99%) Calc. for $\text{C}_{44}\text{H}_{64}\text{N}_4\text{O}_{12}$ = 841.01 found 841.5 $[\text{M}+\text{H}]^+$ r.t. 3.16.

1-((*L*-Isoleucyl-*L*-lysyl) oxy)ethyl 4-(2-hydroxy-2,2-diphenylacetoxy) piperidine-1-carboxylate **28**



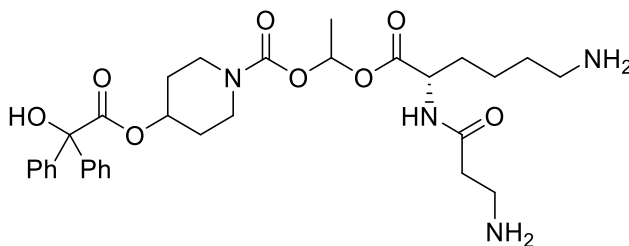
This compound was synthesised according to General Chemistry Procedure **3** to obtain the title compound **28** [Quantitative] as a white solid; ^1H (400 MHz; CDCl_3) δ 8.26 [2H, bs], 7.95 [2H, bs], 7.48-7.30 [10H, m], 6.63 [1H, q, J 5], 5.05 [1H, m], 4.27 [1H, bs], 3.48-3.11 [6H, m], 2.69-2.80 [2H, m], 1.90-1.78 [3H, m], 1.87-1.62 [6H, m], 1.57-1.51 [2H, m], 1.60-1.47 [5H, m], 1.46-1.36 [6H, m], 0.96-0.80 [6H, m]; ^{13}C (101 MHz; DMSO) δ 174.59 172.75, 168.51, 161.04, 143.77, 128.27, 127.95, 127.51, 81.18, 65.39, 56.64, 52.37, 40.68, 40.47, 38.73, 36.68, 30.18, 26.79, 19.96, 15.64, 11.64; m/z (ESI; 97%) Calc. for $\text{C}_{34}\text{H}_{48}\text{N}_4\text{O}_8$ = 640.78 found 641.8 $[\text{M}+\text{H}]^+$ r.t. 2.08.

(10*S*)-10-(4-((*tert*-butoxycarbonyl)amino)butyl)-2,2-dimethyl-4,8,11-trioxo-3,12-dioxo-5,9-diazatetradecan-13-yl 4-(2-hydroxy-2,2-diphenylacetoxy)piperidine-1-carboxylate **29i**



This compound was synthesised according to General Chemistry Procedure **6** and purified using flash column chromatography using a gradient of 20-80%EtOAc:(40-60) PET to obtain the title compound **29i** as a mixture of diastereoisomers (34%) as a colourless oil; R_f 0.41 [40% EtOAc in (40-60) PET]; ^1H (400 MHz; CDCl_3) δ 7.47-7.30 [10H, m], 6.73 [1H, q, J 5], 5.30-5.09 [2H, m], 4.01 [1H, bs], 3.47-3.05 [6H, m], 2.48-2.33 [2H, m], 1.85-1.73 [3H, m], 1.71-1.58 [3H, m], 1.57-1.50 [2H, m], 1.50-1.44 [3H, d, J 5], 1.41 [18H, s], 1.37-1.31 [2H, m]; ^{13}C (101 MHz; CDCl_3) δ 173.73, 171.73, 170.68, 156.49, 152.73, 141.89, 134.40, 133.40, 129.64, 129.61, 129.46, 129.44, 129.34, 129.31, 128.12, 127.35, 126.88, 126.86, 90.92, 81.07, 79.28, 71.55, 63.83, 63.76, 52.01, 40.58, 38.60, 36.65, 35.98, 31.21, 29.75, 28.39, 23.93, 19.63; m/z (ESI; 99%) Calc. for $\text{C}_{41}\text{H}_{58}\text{N}_4\text{O}_{12}$ = 798.93 found 800.0 $[\text{M}+\text{H}]^+$ r.t. 3.09.

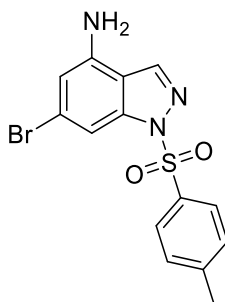
1-(((3-Aminopropanoyl)-L-lysyl)oxy)ethyl 4-(2-hydroxy-2,2-diphenylacetoxy) piperidine-1-carboxylate **29**



This compound was synthesised according to General Chemistry Procedure **3** obtain the title compound **29** [Quantitative] as a white solid; ^1H (400 MHz; CDCl_3) δ 7.90 [4H, bs], 7.47-7.30 [10H, m], 6.62 [1H, q, J 5], 5.05 [1H, bs], 4.14-4.13 [1H, m], 3.41-3.15 [6H, m], 3.01-2.91 [2H, m], 2.76-2.66 [2H, m], 2.59-2.54 [2H, m], 1.83-1.70 [2H, m], 1.68-1.46 [6H, m], 1.45-1.31 [6H, m]; ^{13}C (101 MHz, DMSO) δ 172.75, 170.23, 152.64, 143.77, 128.28, 127.96, 127.51, 90.55, 81.18, 75.02, 61.63, 52.29, 38.82, 35.58, 32.20, 30.31, 26.90, 22.49, 20.00; m/z (ESI; 99%) Calc. for $\text{C}_{41}\text{H}_{48}\text{N}_4\text{O}_8$ = 598.70 found 599.8 $[\text{M}+\text{H}]^+$ r.t. 1.99.

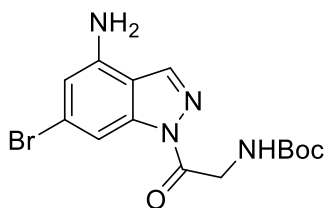
5.2 Chapter 2

6-Bromo-1-tosyl-1H-indazol-4-amine **52a**



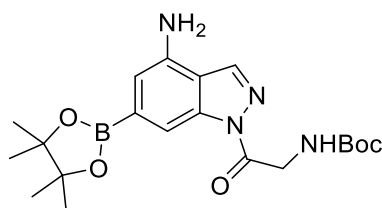
To a stirred, 0°C solution of 6-bromo-1H-indazol-4-amine (0.1 g, 0.47 mmol, 1 eq) in DMF (2 ml) was added 60% NaH in mineral oil (0.019 g, 0.756 mmol, 1.6 eq) and the solution stirred at 0°C for 1 hour. Tosyl Chloride (0.090 g, 0.474 mmol, 1.0 eq) was added and the resulting solution stirred for a further hour. TLC analysis deemed the reaction to be complete, and the solution was poured onto ice water (100 ml), and extracted with EtOAc (3x100 mL). The organic layers were combined, dried over MgSO₄, filtered and concentrated in vacuo. The crude mixture was dissolved in DCM (1 ml) then purified via silica gel chromatography using a gradient of 5-25% EtOAc in PET to obtain the title compound **52a** (0.13 g, 51%) as a colourless oil; R_f 0.41 (40% EtOAc in PET), ¹H (400 MHz; CDCl₃) δ 2.40 [3H, s], 4.30 [2H, bs], 6.66 [1H, d, *J* 2], 7.29 [2H, t, *J* 2], 7.75 [1H, t, *J* 1] 7.86-7.90 [2H, m] 8.07 [1H, d, *J* 1]; ¹³C (101 MHz; CDCl₃) δ 145.63, 142.10, 140.90, 137.88, 134.41, 129.91, 127.68, 125.12, 114.24, 111.10, 105.75, 21.77; *m/z* (ESI; 99%) Calc. for C₁₄H₁₂BrN₃O₂S = 366.23 found 365.4/367.6 [M+H]⁺

tert-Butyl (2-(4-amino-6-bromo-1H-indazol-1-yl)-2-oxoethyl)carbamate **59**

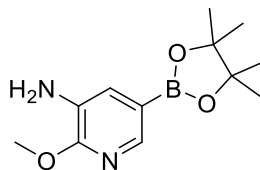


This compound was synthesised according to General Procedure **6**. The crude material was redissolved in DCM (1 mL) and separated by silica gel chromatography using a gradient of 0-40% EtOAc in PET to obtain the title compound **59** (42 %) as a colourless oil; R_f 0.30 (40% EtOAc in PET), ¹H (400 MHz; CDCl₃) δ 1.51 [9H, s], 4.45 [2H, bs], 5.96 [2H, d, *J* 6], 6.66 [1H, s], 7.82 [1H, s], 7.99 [1H, s]; ¹³C (101 MHz; CDCl₃) δ 169.47, 156.17, 140.90, 140.69, 137.53, 125.51, 114.08, 111.94, 107.72, 80.31, 40.93, 28.48; *m/z* (ESI; 99%) Calc. for C₁₄H₁₇BrN₄O₃ = 369.22 found 368.2/370 [M+H]⁺

tert-Butyl (2-(4-amino-6-(4,4,5,5-tetramethyl-1,3,2-dioxaborolan-2-yl)-1H-indazol-1-yl)-2-oxoethyl) carbamate **64**

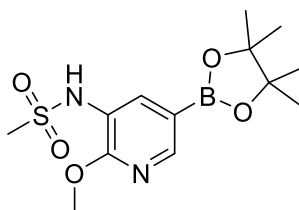


To a stirred solution of *tert*-Butyl (2-(4-amino-6-bromo-1H-indazol-1-yl)-2-oxoethyl)carbamate (0.10 g, 0.27 mmol, 1 eq) in 1,4, dioxane (20 mL) under a nitrogen atmosphere was added 4,4,5,5-Tetramethyl-1,3,2-dioxaborolane (0.138 g, 0.542 mmol, 2 eq), potassium acetate (0.08 g, 0.813 mmol, 3 eq) and [1,1'-Bis(diphenylphosphino) ferrocene] dichloropalladium (II), complex with dichloromethane (0.02 g, 0.03 mmol, 0.1 eq) and the resulting solution refluxed overnight at 80°C. TLC analysis deemed the reaction to be complete and the solution was filtered through celite and concentrated in vacuo. The crude mixture was then dissolved in DCM (1 ml) and purified by silica gel chromatography using a gradient of 20-40% EtOAc in PET to obtain the title compound **64** (0.80 g, 71%) as colourless oil; R_f 0.45 (40% EtOAc in PET), ¹H (400 MHz; DMSO) δ 1.30 [12H, s], 1.51 [9H, s], 4.50 [2H, d, *J* 6], 6.18 [2H, bs], 6.85 [1H, s], 7.74 [1H, s], 8.53 [1H, s]; ¹³C (101 MHz; DMSO) δ 170.01, 156.48, 143.04, 140.19, 139.82, 116.35, 113.22, 107.51, 84.13, 78.70, 43.81, 28.81, 25.31; *m/z* (ESI; 99%) Calc. for C₂₀H₂₉BN₄O₅ = 416.29 found 417.3 [M+H]⁺

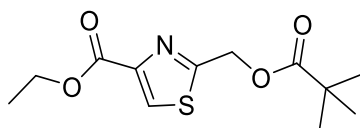
2-Methoxy-5-(4,4,5,5-tetramethyl-1,3,2-dioxaborolan-2-yl) pyridin-3-amine **54**

To a stirred solution of 5-bromo-2-methoxypyridin-3-amine (1.00 g, 4.95 mmol, 1 eq) in 1,4-dioxane (20 mL) under a nitrogen atmosphere was added 4,4,5,5-Tetramethyl-1,3,2-dioxaborolane (2.51 g, 9.90 mmol, 2 eq), potassium acetate (1.46 g, 14.90 mmol, 3 eq) and [1,1'-Bis(diphenylphosphino) ferrocene] dichloropalladium (II), complex with dichloromethane (0.40 g, 0.50 mmol, 0.1 eq) and the resulting solution refluxed overnight at 80°C. TLC analysis deemed the reaction to be complete and the solution was filtered through celite and concentrated in vacuo. The crude mixture was then dissolved in DCM (1 ml) and purified by silica gel chromatography using a gradient of 20-40% EtOAc in PET to obtain the title compound **54** (1.20 g, 97%) as colourless oil; R_f 0.30 (20% EtOAc in PET), ¹H (400 MHz; CDCl₃) δ 1.34 [12H, s], 4.01 [3H, s], 7.24 [1H, d, *J* 1], 8.00 [1H, d, *J* 1]; ¹³C (101 MHz; CDCl₃) δ 155.20, 142.8, 130.2, 125.6, 83.74, 83.12, 75.05, 53.48, 24.83, 24.54, *m/z* (ESI; 99%) Calc. for C₁₂H₁₉BN₂O₃ = 250.15 found 251.2 [M+H]⁺

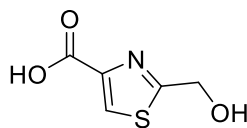
N- (2-methoxy-5- (4,4,5,5-tetramethyl-1,3,2-dioxaborolan-2-yl) pyridin-3-yl) methane sulphonamide **55**



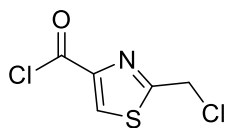
To a stirred solution of 2-methoxy-5-(4,4,5,5-tetramethyl-1,3,2-dioxaborolan-2-yl)pyridin-3-amine (0.50 g, 2.00 mmol, 1 eq) in pyridine (5 ml) was added Methanesulfonyl chloride (0.31 mL, 4.00 mmol, 2 eq) and the resulting solution stirred for 18 hours at room temperature. TLC analysis deemed the reaction to be complete and the solution concentrated under high vacuo. The crude mixture was then redissolved in DCM (1 mL) and purified by silica gel chromatography using a gradient of 20-40% EtOAc in PET to obtain the title compound **55** (0.41 g, 63%) as a yellow oil; R_f 0.21 (30% EtOAc in PET), ¹H (400 MHz; CDCl₃) δ 1.35 [12H, s], 4.01 [3H, s], 4.25 [3H, s], 7.22 [1H, d, *J* 1], 8.10 [1H, d, *J* 1]; ¹³C (101 MHz; CDCl₃) δ 155.20, 142.8, 130.2, 125.6, 120.24, 83.74, 83.12, 53.48, 39.98, 24.83, 24.54, *m/z* (ESI; 99%)
Calc. for C₁₂H₁₉BN₂O₃ = 328.19 found 329.9 [M+H]⁺

Ethyl 2-((pivaloyloxy)methyl)thiazole-4-carboxylate **49**

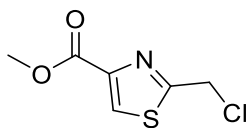
To a stirred solution of bromopyruvic acid (0.10 g, 0.57 mmol, 1 eq) in ethanol (10 mL) was added 2-amino-2-thioxoethyl pivalate (0.11 g, 0.69 mmol, 1.2 eq) and the resulting solution stirred at 80°C overnight. TLC analysis deemed the reaction to be complete and the solution was concentrated in vacuo before being redissolved in DCM (1 ml) and purified by silica gel chromatography using a gradient of 20-80 % EtOAc in PET to obtain the title compound **49** (0.11 g, 68 %) as a yellow oil; Rf 0.41 (20% EtOAc in PET), ¹H (400 MHz; CDCl₃) δ 1.24 [9H, s], 1.39 [3H, t, *J* 7], 4.42 [2H, q, *J* 7], 5.14 [2H, s], 8.18 [1H, s]; ¹³C (101 MHz; CDCl₃) δ 177.63, 166.64, 161.18, 147.15, 128.35, 62.70, 61.64, 38.82, 27.07, 14.33; *m/z* (ESI; 96%) Calc. for C₁₂H₁₇NO₄ = 271.33 found 272.3 [M+H]⁺

2-(Hydroxymethyl)thiazole-4-carboxylic acid **49a**

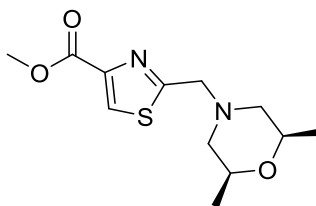
To a stirred, refluxed solution of Ethyl 2-((pivaloyloxy)methyl) thiazole-4-carboxylate (0.14 g, 0.64 mmol, 1 eq) in MeOH (10 mL) and water (3 mL) was added potassium carbonate (0.29 g, 2.06 mmol, 4 eq) and the resulting solution stirred under reflux conditions for 4 hours. TLC analysis deemed the reaction to be complete and aqueous 2N HCl (40 mL) was added. The biphasic solution was then concentrated under high vacuo. The crude mixture was then suspended in 2:1 mixture of hot ethanol: EtOAc and the solid KCl filtered through filter paper. The resulting solution was then concentrated in vacuo to achieve the title compound **49a** (0.076 g, 92%) as a yellow oil which crystallized on standing; Rf 0.01 (20% MeOH in DCM 1% AcOH), ^1H (400 MHz; DMSO) δ 5.00 [2H, s], 8.50 [1H, s]; ^{13}C (101 MHz; DMSO) δ 178.6, 160.4, 143.6, 128.2, 60.0; m/z (ESI; 96%) Calc. for $\text{C}_{12}\text{H}_{17}\text{NO}_4 = 271.33$ found 272.3 [M+H] $^+$

2-(Chloromethyl) thiazole-4-carbonyl chloride **50**

To a stirred solution of 2-(hydroxymethyl) thiazole-4-carboxylic acid (0.14 g, 0.09 mmol, 1 eq) in CHCl_3 (5 mL) and DMF (0.1 mL) was added thionyl chloride (0.38 mL, 0.53 mmol, 6 eq) and the resulting solution stirred at reflux for 1 hour. The solution was the concentrated under high vacuo to achieve the title compound **50** (Quantitative) as a black oil, which was used immediately without purification; m/z (ESI; 96%) Calc. for $\text{C}_5\text{H}_3\text{Cl}_2\text{NOS}$ = 159.16 found 191.6 (Methyl Ester) $[\text{M}+\text{H}]^+$

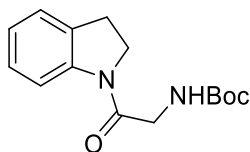
Methyl 2-(chloromethyl)thiazole-4-carboxylate **58a**

To a stirred solution of 2-(hydroxymethyl) thiazole-4-carboxylic acid (0.3 g, 0.19 mmol, 1 eq) in CHCl_3 (5 mL) and DMF (1 mL) was added thionyl chloride (0.82 mL, 1.13 mmol, 6 eq) and the resulting solution stirred at reflux for 1 hour. Dry methanol (10 mL) was added and the solution stirred for 30 mins. LCMS determined the crude mixture to be 60:40 Ester:Acid and the solution was concentrated under high vacuo. The crude mixture was then dissolved in DCM (1 mL) and purified by silica gel chromatography using a EtOAc to obtain the title compound **58a** (0.96 g, 60%) as a yellow oil, which was used immediately without purification; m/z (ESI; 96%) Calc. for $\text{C}_6\text{H}_6\text{ClNO}_2\text{S}$ = 191.63 found 192.7 $[\text{M}+\text{H}]^+$.

Methyl 2-(((2S,6R)-2,6-dimethylmorpholino) methyl)thiazole-4-carboxylate **61a**

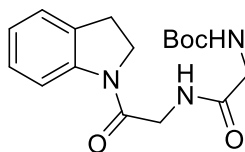
To a dry 100 mL round bottom flask under a nitrogen atmosphere was charged Methyl 2-(chloromethyl)thiazole-4-carboxylate (0.06 g, 0.31 mmol, 1 eq) as a solution in dry 1,4, dioxane (10 mL). To the solution was added (2S,6R)-2,6-dimethylmorpholine (0.116 mL, 0.939 eq, 3 eq) and the resulting solution stirred at room temperature overnight. TLC analysis deemed the reaction to be complete and the solution was concentrated in vacuo. The crude mixture was then redissolved in DCM (1 mL) and purified by silica gel chromatography using a gradient of 20-60% EtOAc in PET to obtain the title compound **61a** (0.08g, 95%) as a yellow oil; R_f 0.43 (40% EtOAc in PET), ¹H (400 MHz; DMSO) δ 1.21[6H, s], 1.96 [2H, t, *J* 11], 2.75 [2H, d, *J* 11], 3.69 [2H, M], 3.83 [2H, s], 3.92 [3H, s] 5.00 [2H, s], 8.15 [1H, s]; ¹³C (101 MHz; DMSO) δ 172.3, 162.1, 146.6, 128.8, 71.7 59.5, 52.4, 41.1, 19.1; *m/z* (ESI; 96%) Calc. for C₁₂H₁₈N₂O₃S = 270.35 found 271.4 [M+H]⁺

tert-butyl (2-(indolin-1-yl)-2-oxoethyl)carbamate **70**

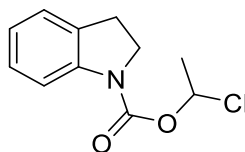


This compound was synthesised via General Chemistry Procedure 7 and purified by silica gel chromatography to using a gradient of 0-40% EtOAc in Cy to obtain the title compound **70** (95%) as a colourless oil; Rf 0.13 (20% EtOAc in Cy); ^1H (400 MHz; CDCl_3) δ 1.49 [9H, s], 3.25 [2H, t, J 8], 3.99-4.09 [4H, m], 5.58 [1H, bs], 7.07 [1H, t, J 8], 7.19-7.26 [2H, m], 8.20 [1H, d, J 8]; ^{13}C (101 MHz; CDCl_3) δ 166.51, 155.84, 142.46, 130.94, 127.73, 124.71, 124.22, 116.88, 79.86, 46.57, 44.05, 28.47, 28.19; m/z (ESI; 98%) Calc. for $\text{C}_{15}\text{H}_{20}\text{N}_2\text{O}_3 = 276.34$ found 277.3 $[\text{M}+\text{H}]^+$

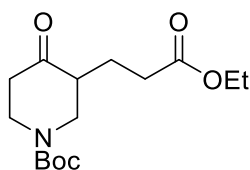
tert-butyl (2-((2-(indolin-1-yl)-2-oxoethyl)amino)-2-oxoethyl)carbamate **72a**



This compound was synthesised via General Chemistry Procedure 8 and purified by silica gel chromatography to using a gradient of 20-60% EtOAc in Cy to obtain the title compound **72a** (54%) as a colourless oil; R_f 0.09 (40% EtOAc in Cy); ^1H (400 MHz; CDCl_3) δ 1.48 [9H, s], 3.26 [2H, t, J 8], 3.93 [2H, d, J 6], 4.04 [2H, t, J 8], 4.18 [2H, d, J 6], 5.21 [1H, bs], 7.09 [1H, t, J 8], 7.18-7.28 [2H, m], 8.18 [1H, d, J 8]; ^{13}C (101 MHz; CDCl_3) δ 169.54, 165.75, 142.29, 131.10, 127.76, 124.79, 124.43, 116.85, 80.48, 46.72, 42.75, 38.64, 28.34, 28.10; m/z (ESI; 98%) Calc. for $\text{C}_{17}\text{H}_{23}\text{N}_3\text{O}_4$ = 333.39 found 334.5 $[\text{M}+\text{H}]^+$

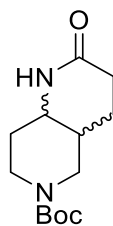
1-chloroethyl indoline-1-carboxylate **71**

To a stirred solution of indoline (0.1 g, 0.84 mmol, 1 eq) in dry DCM (10 mL) at -10°C was added, 4-Methylmorpholine (0.30 mL, 2.77 mmol, 3.3 eq) and 1-chloroethyl chloroformate (0.099 mL, 0.923 mmol, 1.1 eq), and the resulting solution left to stir for 2 hours. TLC analysis deemed the reaction to be complete and the reaction solvent was removed under vacuum. The residue was re-dissolved in ethyl acetate (10 mL) and poured onto 2N HCl (10 mL). This was then extracted with water and then the organic layers combined and dried over Na₂SO₄. This was then filtered, concentrated under vacuum and purified by silica gel column chromatography using a gradient of 0-40% EtOAc in Cy obtain the title compound **71** (0.141 g, 74%) as a mixture of enantiomers, as a colourless oil; *R_f* 0.74 (20% EtOAc in Cy); ¹H (400 MHz; CDCl₃) δ 1.51 [3H, d, *J* 5], 3.32 [2H, t, *J* 8], 3.94 [2H, t, *J* 8], 6.76-6.95 [1H, m], 7.10 [1H, t, *J* 8], 7.17-7.28 [2H, m], 8.25 [1H, d, *J* 8]; ¹³C DEPT (101 MHz; CDCl₃) δ 154.75, 136.21, 134.77, 129.37, 128.44, 125.83, 119.67, 88.24, 53.40, 27.56, 22.21; *m/z* (ESI; 95%) Calc. for C₁₁H₁₂ClNO₂ = 225.67 found 226.7 [M+H]⁺.

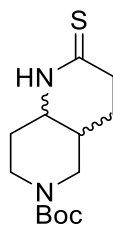
tert-Butyl 3-(3-ethoxy-3-oxopropyl)-4-oxopiperidine-1-carboxylate **83**

To a stirred solution of tert-butyl 4-oxopiperidine-1-carboxylate (20.00 g, 100.37 mmol, 1 eq) in toluene (240 mL) under dean stark conditions was added, pyrrolidine (11.08 mL, 135.51 mmol, 1.35 eq) and the resulting solution refluxed at 160°C for 4 hours, collecting 2.3 mL of water. After 4 hours the solution was concentrated under high vacuo and the resulting oil redissolved in toluene (240 mL) and Ethyl Acrylate (21.16 mL, 200.75 mmol, 2 eq) was added. The resulting solution was refluxed at 160°C for 16 hours. TLC analysis deemed the reaction to be complete and the solution was allowed to cool to 60°C before water (100 mL) was added. The biphasic solution was then stirred at 60°C for 1 hour before being concentrated in vacuo to remove the toluene. The aqueous solution was then acidified with 2N HCl (100 mL) and extracted with EtOAc (3X 100 mL). The organic layers were then combined, dried over MgSO₄, filtered and concentrated in vacuo. The crude mixture was then absorbed onto silica and purified using silica gel chromatography to achieve the title compound **83** (30.06 g, 99%) as an orange oil; R_f 0.56 (40% EtOAc in Cy); ¹H (400 MHz; CDCl₃) δ 1.26 [3H, t, *J* 7], 1.49 [9H, s], 1.54-1.66 [1H, m], 2.00-2.19 [1H, m], 2.35-2.52 [5H, m], 3.00-3.18 [1H, m], 3.36-3.48 [1H, m], 4.02-4.16 [4H, m]; ¹³C (101 MHz; CDCl₃) δ 209.05, 173.00, 154.50, 128.38, 80.57, 60.45, 49.43, 48.33, 43.73, 40.81, 31.72, 28.48, 22.52, 14.21;

tert-Butyl 2-oxooctahydro-1,6-naphthyridine-6(2H)-carboxylate **83 b, c**

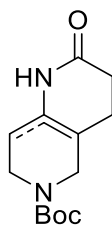


To a stirred solution of tert-Butyl 3-(3-ethoxy-3-oxopropyl)-4-oxopiperidine-1-carboxylate (5.00 g, 16.70 mmol, 1 eq) in MeOH (40 mL) and Acetic Acid (11.4 mL) was added 7N NH₃ in MeOH (14 mL, 5 eq) and MgSO₄ (5 g) and the suspension stirred at 40°C for 1 hour. After 1 hour, to the suspension was added 2-picoline borane (2.60 g, 25.10 mmol, 1.5 eq) and the suspension stirred at 40°C for 5 hours. TLC analysis deemed the reaction to be complete and the MgSO₄ was filtered, and the solution concentrated in vacuo. The crude mixture was then absorbed onto silica and purified by silica gel chromatography using a gradient of 10% MeOH in EtOAc to obtain the title compounds **83 b, c** (1.36 g, 32%) as an orange oil, an inseparable 6:4 Cis:Trans isomeric mixture; R_f 0.18 (10% MeOH in EtOAc); ¹H (400 MHz; CDCl₃) δ 1.48 [9H, s], 1.62-1.92 [4H, m], 2.00-2.11 [1H, m], 2.33-2.40 [1H, m], 3.12-3.24 [2H, m], 3.39-3.52 [1H, m], 3.63-3.78 [1H, m] 3.84-4.21 [1H, m]; ¹³C (101 MHz; CDCl₃) δ 172.5, 154.7, 80.1, 56.33, 53.48, 50.63, 38.77, 30.88, 28.36, 24.45; *m/z* (ESI; 96%) Calc. for C₁₃H₂₂N₂O₃ = 254.16 found 255.2 [M+H]⁺

tert-Butyl 2-thioxooctahydro-1,6-naphthyridine-6(2H)-carboxylate **84**

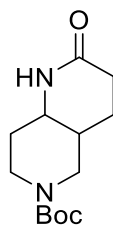
To a stirred solution of tert-Butyl 2-oxooctahydro-1,6-naphthyridine-6(2H)-carboxylate (0.60 g, 2.36 mmol, 1 eq) in DCM (40 mL) was added Lawesson's Reagent (1.43 g, 3.54 mmol, 1.5 eq) and the resulting suspension stirred at 50 °C overnight. TLC analysis deemed the reaction to be complete and water (100 mL) was added and the emulsion stirred for 15 mins before being filtered through celite. The aqueous layer was separated, and the organic layer re-extracted with water (2x 50 mL). The organic layers were combined, dried over MgSO₄, filtered and concentrated in vacuo. The crude mixture was then absorbed onto silica, wetted with PET and left to age overnight. The following day the crude mixture was purified by silica gel chromatography using a gradient of 0-40% EtOAc in PET to obtain the title compound **84** (0.06 g, 10%) as a yellow oil; R_f 0.15 (40% EtOAc in Cy); ¹H (400 MHz; CDCl₃) δ 1.50 [9H, s], 1.70-1.89 [4H, m], 2.80-3.06 [2H, m], 3.12-3.45 [2H, m], 3.47-3.74 [2H, m], 9.01 [1H, bs]; ¹³C (101 MHz; CDCl₃) δ 202.68, 154.78, 80.10, 53.48, 40.72, 39.05, 37.67, 31.67, 29.64, 28.37, 21.44; *m/z* (ESI; 96%) Calc. for C₁₃H₂₂N₂O₂S = 270.39 found 271.4 [M+H]⁺

tert-Butyl 2-oxo-1,3,4,5,7,8-hexahydro-1,6-naphthyridine-6(2H)-carboxylate **84**, **84a**



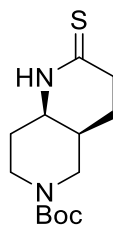
To a stirred solution of tert-Butyl 3-(3-ethoxy-3-oxopropyl)-4-oxopiperidine-1-carboxylate (3.30 g, 11.0 mmol, 1 eq) in MeOH (40 mL) and Acetic Acid (11.4 mL) was added 7N NH₃ in MeOH (7 mL, 5 eq) and MgSO₄ (5 g) and the suspension stirred at 40°C for overnight. TLC analysis deemed the reaction to be complete and the MgSO₄ was filtered, and the solution concentrated in vacuo. The crude mixture was then dissolved in EtOAc (50 mL) and extracted with H₂O (3x50 mL). The organic layers were combined, dried over MgSO₄, filtered and concentrated in vacuo. The crude mixture was then absorbed onto silica and purified by silica gel chromatography using a gradient of 0-100% EtOAc in PET to obtain the title compound (1.32 g, 94%) as an orange oil, a 50:50 mixture of regio-isomers **84**, **84a**; R_f 0.10 (50% EtOAc in Cy); ¹H (400 MHz; CDCl₃) δ 1.45 [9H, s], 2.11-2.17 [2H, m], 2.21 [2H, t, *J* 8], 2.49 [2H, t, *J* 8], 3.54 [2H, t, *J* 6], 3.78-3.84 [2H, m], 8.47 [1H, bs]; ¹³C (101 MHz; CDCl₃) δ 171.5, 154.76, 127.51, 80.03, 53.32, 44.57, 30.32, 28.42, 25.80 23.01; *m/z* (ESI; 96%) Calc. for C₁₃H₂₀N₂O₃ = 252.31 found 253.3 [M+H]⁺

tert-Butyl 2-oxooctahydro-1,6-naphthyridine-6(2H)-carboxylate **85, 86**



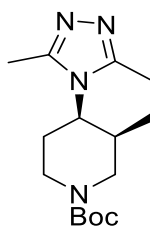
To a stirred solution of tert-Butyl 2-oxo-1,3,4,5,7,8-hexahydro-1,6-naphthyridine-6(2H)-carboxylate (1.5 g, 5.30 mmol, 1 eq) as a 50:50 mixture of regio-isomers in MeOH (20 mL) was added 10% Pd/C (0.30g, 20% w/w) and the resulting suspension placed under a hydrogen atmosphere. The suspension was stirred for 2 hours, until TLC analysis deemed the reaction to be complete, and the palladium was filtered through celite. The solution was concentrated in vacuo to obtain the title product **85, 86** (0.72 g, 47%) as a yellow oil, an inseparable 75:25 mixture of enantiomers; Rf 0.18 (10% MeOH in EtOAc); ^1H (400 MHz; CDCl_3) δ 1.47 [9H, s], 1.64-1.89 [4H, m], 2.02-2.11 [1H, m], 2.36-2.41 [1H, m], 3.14-3.23 [2H, m], 3.34-3.51 [1H, m], 3.64-3.71 [1H, m] 3.82-4.23 [1H, m]; ^{13}C (101 MHz; CDCl_3) δ 172.41, 154.72, 80.14, 56.33, 53.48, 50.63, 38.77, 30.88, 28.36, 24.45; m/z (ESI; 96%) Calc. for $\text{C}_{13}\text{H}_{22}\text{N}_2\text{O}_3$ = 254.16 found 255.2 $[\text{M}+\text{H}]^+$

tert-Butyl (4S,8R)-2-thioxooctahydro-1,6-naphthyridine-6(2H)-carboxylate **87**



To a stirred solution of tert-Butyl 2-oxooctahydro-1,6-naphthyridine-6(2H)-carboxylate (1.50 g, 5.90 mmol, 1 eq) in DCM (40 mL) was added Lawesson's Reagent (3.58 g, 8.80 mmol, 1.5 eq) and the resulting suspension stirred at 50 °C overnight. TLC analysis deemed the reaction to be complete and water (100 mL) was added and the emulsion stirred for 15 mins before being filtered through celite. The aqueous layer was separated, and the organic layer re-extracted with water (2x 50 mL). The organic layers were combined, dried over MgSO₄, filtered and concentrated in vacuo. The crude mixture was then absorbed onto silica, wetted with PET and left to age overnight. The following day the crude mixture was purified by silica gel chromatography using a gradient of 0-40% EtOAc in PET to obtain the title compound **87** (0.77 g, 75%) as a yellow oil; R_f 0.35 (50% EtOAc in Cy); ¹H (400 MHz; CDCl₃) δ 1.46 [9H, s], 1.70-1.92 [4H, m], 2.02-2.13 [1H, m], 2.82-2.93 [1H, m], 2.94-3.05 [1H, m], 3.09-3.29 [1H, m], 3.30-3.45 [1H, m], 3.48-3.66, [2H, m], 9.25s [1H, bs]; ¹³C (101 MHz; CDCl₃) δ 202.69, 154.72, 80.53, 32, 45.91, 44.41, 40.63, 37.69, 31.62, 29.58, 28.43, 24.46; *m/z* (ESI; 98%) Calc. for C₁₃H₂₂N₂O₂S = 270.39 found 271.4 [M+H]⁺

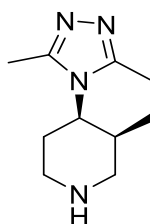
tert-butyl (5a*S*,9a*R*)-1-methyl-4,5,5a,8,9,9a-hexahydro-[1,2,4]triazolo[4,3-*a*][1,6]naphthyridine-7(6*H*)-carboxylate **88**



To a stirred solution of tert-Butyl (4*S*,8*R*)-2-thioxooctahydro-1,6-naphthyridine-6(2*H*)-carboxylate (0.50 g, 1.8 mmol, 1 eq) in toluene (5 mL) was added acetyl hydrazide (0.27 g, 3.7 mmol, 2 eq) and the resulting solution stirred for 2 days at 130°C. TLC analysis deemed the reaction to be complete and the solution was concentrated in vacuo. The crude mixture was absorbed onto silica and purified using silica gel chromatography using a gradient of 0-10% MeOH in EtOAc to obtain the title compound **88** (0.43 g, 76 %) as a colourless oil; R_f 0.33 (10 % MeOH in DCM); ^1H (400 MHz; CDCl_3) δ 1.49 [9H, s], 1.70-1.81 [1H, m], 1.92-2.07 [3H, m], 2.25-2.34 [1H, m], 2.54 [3H, bs], 2.77-2.31 [5H, m]; ^{13}C (101 MHz; CDCl_3) δ 156.20, 155.10, 154.72, 80.32, 45.91, 44.41, 40.60, 37.69, 31.62, 29.58, 28.43, 24.46, 11.27; m/z (ESI; 94%) Calc. for $\text{C}_{15}\text{H}_{24}\text{N}_4\text{O}_2 = 292.38$ found 293.4 $[\text{M}+\text{H}]^+$

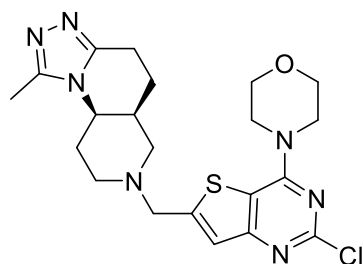
(5S,9R)-1-methyl-4,5,5a,6,7,8,9,9a-octahydro-[1,2,4]

triazolo[4,3-a][1,6]

naphthyridine **89**

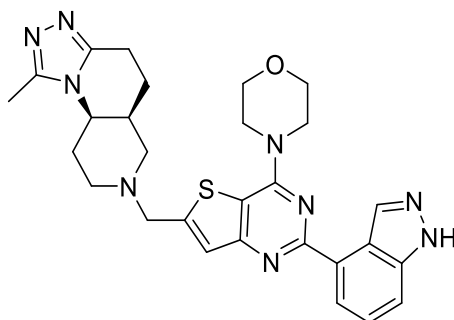
To a stirred solution of tert-butyl (5aS,9aR)-1-methyl-4,5,5a,8,9,9a-hexahydro-[1,2,4] triazolo[4,3-a][1,6] naphthyridine-7(6H)-carboxylate (0.50 g, 1.7 mmol, 1 eq) in DCM (10 mL) was added 4N HCl (5 mL) and the resulting solution stirred for 2 hours at room temperature. TLC analysis deemed the reaction to be complete and the solution concentrated in vacuo to obtain the title compound (0.38 g, 97%) as a white gum; Rf 0.1 (10 % MeOH in DCM); ^1H (400 MHz; DMSO) δ 1.72-1.80 [1H, m], 1.95-2.03 [3H, m], 2.24-2.29 [1H, m], 2.51 [3H, bs], 2.76-2.31 [5H, m]; ^{13}C (101 MHz; DMSO) δ , 156.20, 155.10, 45.91, 44.41, 40.63, 37.69, 31.62, 29.58, 24.46, 11.25; m/z (ESI; 99%) Calc. for $\text{C}_{10}\text{H}_{16}\text{N}_4 = 192.27$ found 192.3 $[\text{M}+\text{H}]^+$

4-(5-chloro-2-(((5a*S*,9a*R*)-1-methyl-4,5,5a,8,9,9a-hexahydro-[1,2,4]triazolo[4,3-*a*][1,6] naphthyridine-7(6*H*)-yl)methyl)benzo[*b*]thiophen-7-yl)morpholine **90**



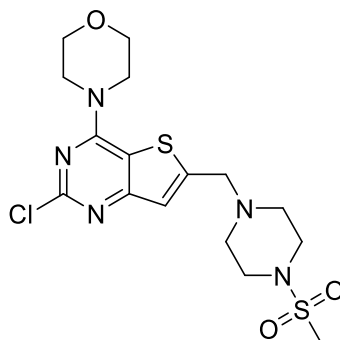
To a stirred solution of (5*S*,9*R*)-1-methyl-4,5,5a,6,7,8,9,9a-octahydro- [1,2,4] triazolo[4,3-*a*] [1,6] naphthyridine (0.27 g, 0.96 mmol, 1.1 eq) in MeOH (9 mL) was added sodium acetate (0.29 g, 3.50 mmol, 4 eq) and the resulting solution stirred at 40°C for 1 hour. After 1 hour, acetic acid (1 mL) and 5-chloro-7-morpholinobenzo[*b*]thiophene-2-carbaldehyde (0.20g, 0.874 mmol, 1 eq) was added and the suspension stirred for 1 further hour at 40°C. After 1 hour, the solution was cooled to room temperature and 2-picoline borane complex was added and the suspension stirred for 16 hours at room temperature. TLC analysis deemed the reaction to be complete and the suspension was filtered through filter paper and the solution concentrated in vacuo. The crude mixture was then absorbed onto silica before being purified by silica gel chromatography using a gradient of 0-20% MeOH in DCM to obtain the title compound **90** (0.22 g, 55%) as yellow solid; *R*_f 0.5 (20 % MeOH in DCM 1% NH₃); ¹H (400 MHz; CDCl₃) δ 1.92 [2H, dt, *J* 4 and 12], 1.97-2.06 [1H, m], 2.24-2.32 [2H, m], 2.51 [3H, s], 2.52-2.57 [2H, m], 2.85-2.95 [1H, m], 3.07 [2H, t, *J* 12], 3.30 [1H, dd, *J* 6 and 17 Hz], 3.87 [4H, t, *J* 4], 3.99-4.04 [4H, m], 4.15 [1H, qu, *J* 6], 7.20 [1H, s]; ¹³C (101 MHz; CDCl₃) δ, 160.21, 156.04, 149.72, 142.26, 124.56, 121.59, 66.45, 57.75, 56.84, 56.47, 52.16, 46.55, 35.01, 28.62, 22.53, 20.84, 11.86; *m/z* (ESI; 98%) Calc. for C₃₀H₃₃N₇OS = 460.00 found 461.1 [M+H]⁺

4-(5-(1H-indazol-4-yl)-2-(((5a*S*,9a*R*)-1-methyl-4,5,5a,8,9,9a-hexahydro-[1,2,4]triazolo[4,3-*a*][1,6]naphthyridin-7(6*H*)-yl)methyl)benzo[*b*]thiophen-7-yl)morpholine

Q

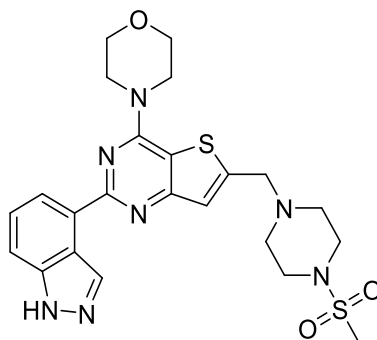
To a stirred solution of 4-(5-chloro-2-(((5a*S*,9a*R*)-1-methyl-4,5,5a,8,9,9a-hexahydro-[1,2,4]triazolo[4,3-*a*][1,6] naphthyridine-7(6*H*)-yl) methyl)benzo[*b*]thiophen-7-yl)morpholine (1.00 g, 2.174 mmol, 1 eq) in EtOH (3 mL) and H₂O (1 mL) was added (1H-indazol-4-yl)boronic acid (0.53 g, 3.26 mmol, 1.5 eq), 2*N* Na₂CO₃ (3.26 mL, 6.52 mmol, 3 eq) and Bis(triphenylphosphine)palladium(II) dichloride (0.153 g, 0.217 mmol, 0.1 eq) and the resulting suspension stirred for 2 hours at 100°C. TLC analysis deemed the reaction to be complete and the suspension was filtered through celite and the resulting solution concentrated in vacuo. The crude mixture was dissolved in DCM (2 mL) and purified by silica gel chromatography using a gradient of 0-20 % MeOH in DCM to obtain the title compound **Q** (0.77g, 65%) as a yellow solid; R_f 0.5 (10% MeOH in DCM); ¹H (400 MHz; CDCl₃) δ 1.65-1.78 [2H, m], 1.90-2.00 [1H, m], 2.07-2.16 [1H, m], 2.32 [3H, s], 2.38-2.44 [2H, m], 2.64-2.82 [2H, m], 2.90-3.04 [3H, m], 3.79-3.87 [4H, m], 3.96-4.04 [4H, m], 4.16-2.42 [2H, s], 4.67-7.50 [3H, m], 7.68 [1H, d, *J* 8], 8.23 [1H, d, *J* 8], 8.90 [1H, s], 13.23 [1H, s]; ¹³C (101 MHz; CDCl₃) δ 162.72, 160.12, 158.02, 151.92, 151.20, 150.57, 150.12, 149.88, 149.31, 141.28, 135.58, 131.64, 126.14, 123.59, 121.72, 121.48, 112.76, 112.56, 66.48, 58.65, 56.92, 56.47, 52.17, 51.98, 51.46, 46.65, 34.07, 28.82, 21.43, 20.85, 13.86; *m/z* (ESI; 98%) Calc. for C₂₈H₃₁N₉OS = 541.68 found 542.7 [M+H]⁺

4-(2-chloro-6-((4-(methylsulfonyl)piperazin-1-yl)methyl)thieno[3,2-d]pyrimidin-4-yl)morpholine **94**



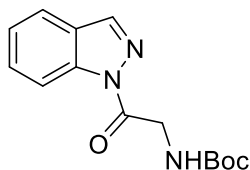
To a stirred solution of 2-chloro-4-morpholinothiemo[3,2-d] pyrimidine-6-carbaldehyde (0.5 g, 1.765 mmol, 1 eq) in MeOH:AcOH (10:1) (5 mL) was added 1-(methylsulfonyl)piperazine (0.40 g, 2.1 mmol, 1.5 eq) and Na₂SO₄ (0.5 g) and the resulting suspension stirred for 1 hour at 40°C. After 1 hour, picoline borane (0.20 g, 1.92 mmol, 2 eq) was added and the suspension stirred for a further hour. After 1 hour, TLC analysis deemed the reaction to be complete and the suspension was filtered through celite and the resulting solution concentrated in vacuo. The crude mixture was dissolved in DCM (2 mL) and purified by silica gel chromatography using a gradient of 0-20 % MeOH in DCM to obtain the title compound **94** (0.60 g, 79%) as a yellow solid; R_f 0.5 (10% MeOH in DCM); ¹H (400 MHz; CDCl₃) δ 2.58 [4H, t, *J* 5], 2.90 [3H, m], 3.15 [4H, t, *J* 5], 3.72-3.77 [4H, m], 3.85-3.92 [6H, m], 7.30 [1H, s]; ¹³C (101 MHz; CDCl₃) δ 163.1, 158.4, 156.3, 152.8, 122.6, 112.8, 66.2, 56.5, 52.5, 46.31, 45.84, 34.1; *m/z* (ESI; 98%) Calc. for C₂₈H₃₁N₉OS = 432.91 found 434.0[M+H]⁺

4-(2-(1H-indazol-4-yl)-6-((4-(methylsulfonyl)piperazin-1-yl)methyl)thieno[3,2-d]pyrimidin-4-yl)morpholine **Pictilisib**



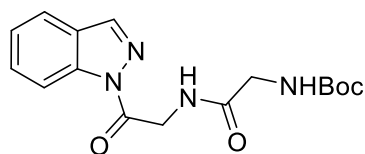
To a stirred solution of 4-(2-chloro-6-((4-(methylsulfonyl)piperazin-1-yl)methyl)thieno[3,2-d]pyrimidin-4-yl)morpholine (1.59 g, 3.70 mmol, 1eq) in EtOH (3 mL) and H₂O (1 mL) was added (1H-indazol-4-yl)boronic acid (0.89 g, 5.50 mmol, 1.5 eq), 2N Na₂CO₃ (3.26 mL, 6.52 mmol, 3 eq) and Bis(triphenylphosphine)palladium(II) dichloride (0.258 g, 0.401 mmol, 0.1 eq) and the resulting suspension stirred for 2 hours at 100°C. TLC analysis deemed the reaction to be complete and the suspension was filtered through celite and the resulting solution concentrated in vacuo. The crude mixture was dissolved in DCM (2 mL) and purified by silica gel chromatography using a gradient of 0-20 % MeOH in DCM to obtain **Pictilisib** (0.77g, 65%) as a yellow solid; R_f 0.7 (10% EtOAc in Cy); ¹H (400 MHz; CDCl₃) δ 2.58-2.65 [4H, m], 2.91 [3H, s], 3.12-3.21 [4H, m], 3.81-3.87 [4H, m], 3.94 [2H, s], 3.98-4.02 [4H, m], 7.45-7.52 [2H, m], 7.67 [1H, d, *J* 8], 8.24 [1H, d, *J* 8], 8.90 [1H, s]; ¹³C (101 MHz; CDCl₃) δ 170.82, 162.74, 160.21, 158.11, 150.77, 141.28, 135.60, 131.60, 126.11, 124.07, 121.70, 121.47, 112.81, 112.54, 66.47, 60.26, 56.69, 52.36, 46.57, 45.87, *m/z* (ESI; 98%) Calc. for C₂₃H₂₇N₇O₃ = 513.64 found 514.7 [M+H]⁺

tert-butyl (2-(1H-indazol-1-yl)-2-oxoethyl)carbamate **36a**



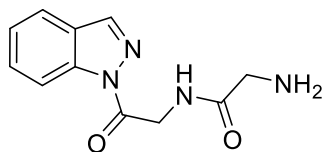
This compound was synthesised according to General Chemistry Procedure **6**. The crude reaction mixture was separated using silica gel chromatography using a gradient of 20-80% EtOAc in (40-60) PET to obtain the title compound **36a** (83%) as a white solid; R_f 0.62 (30 % EtOAc in PET); ¹H (400 MHz; CDCl₃) δ 1.52 [9H, s], 4.86 [2H, d, J 5 Hz], 7.38 [1H, t, *J* 7 Hz], 7.52 [1H, t, *J* 7 Hz], 7.75 [1H, d, *J* 7 Hz], 8.15 [1H, s], 8.41 [1H, d, *J* 7 Hz]; ¹³C (101 MHz; CDCl₃) δ 169.8, 155.9 140.9, 139.2, 129.9, 126.3124.9, 121.4, 115.280.1, 44.3, 28.5; *m/z* (ESI; 99%) Calc. for C₁₄H₁₇N₃O₃ = 275.31 found 276.3 [M+H]⁺.

tert-Butyl (2-((2-(1H-indazol-1-yl)-2-oxoethyl)amino)-2-oxoethyl) carbamate **36b**



This compound was synthesised according to General Chemistry Procedure **6**. The crude reaction mixture was separated using silica gel chromatography using a gradient of 20-80% EtOAc in (40-60) PET to obtain the title compound **36** (83%) as a white solid; Rf 0.63 (80 % EtOAc in PET); ^1H (400 MHz; CDCl_3) δ 1.44 [9H, s], 3.91-4.00 [2H, m] 4.92 [2H, d, J 5 Hz], 5.69 [1H, bs], 7.28-7.5 [2H, m], 7.49 [1H, t, J 8 Hz], 7.67 [1H, d, J 8 Hz], 8.07 [1H, s], 8.27 [1H, d, J 8 Hz]; ^{13}C (101 MHz; CDCl_3) δ 170.40, 168.77, 156.24, 140.77, 138.94, 129.67, 126.09, 124.86, 121.09, 114.99, 80.10, 44.23, 42.85, 28.29; m/z (ESI; 99%) Calc. for $\text{C}_{16}\text{H}_{20}\text{N}_4\text{O}_4$ = 332.36 found 333.4 $[\text{M}+\text{H}]^+$.

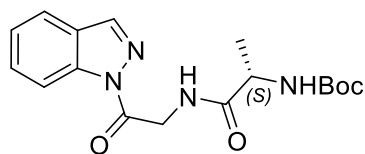
N-(2-(1H-indazol-1-yl)-2-oxoethyl)-2-aminoacetamide **36**



This compound was synthesised according to General Chemistry Procedure **3** to obtain the title compound **36** [100% (theoretical)] as a white solid; m/z (ESI; 99%)

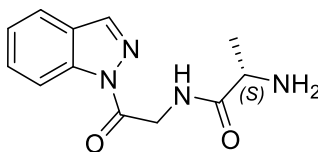
Calc. for $C_{11}H_{12}N_4O_2 = 232.34$ found 233.4 $[M+H]^+$.

tert-butyl (S)-1-((2-(1H-indazol-1-yl)-2-oxoethyl)amino)-1-oxopropan-2-yl)carbamate **37a**



This compound was synthesised according to General Chemistry Procedure **6**. The crude reaction mixture was separated using silica gel chromatography using a gradient of 20-80% EtOAc in (40-60) PET to obtain the title compound **37a** (98%) as a colourless oil; Rf 0.47 (60 % EtOAc in PET); ^1H (400 MHz; CDCl_3) δ 1.39-1.44 [12H, m], 4.31-4.42 [1H, bs], 4.89 [2H, d, J 5 Hz], 5.48-5.57 [1H, m], 7.28 [1H, t, J 8 Hz], 7.34-7.42 [1H, bs] 7.46 [1H, t, J 8 Hz], 7.65 [1H, d, J 8 Hz], 8.04 [1H, s], 8.26 [1H, d, J 8 Hz]; ^{13}C (101 MHz; CDCl_3) δ 171.12, 168.76, 155.59, 140.64, 138.92, 129.58, 126.05, 124.77, 121.04, 114.98, 79.88, 60.33, 40.96, 28.29, 18.60; m/z (ESI; 98%) Calc. for $\text{C}_{17}\text{H}_{22}\text{N}_4\text{O}_4 = 346.39$ found 347.4 $[\text{M}+\text{H}]^+$.

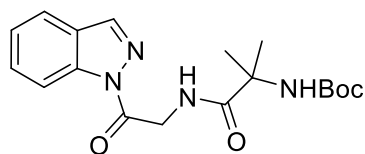
(S)-N-(2-(1H-indazol-1-yl)-2-oxoethyl)-2-aminopropanamide **37**



This compound was synthesised according to General Chemistry Procedure **3** to obtain the title compound **37** [100% (theoretical)] as a white solid; m/z (ESI; 99%)

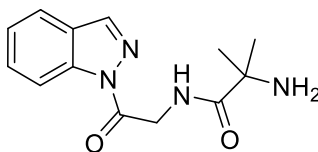
Calc. for C₁₂H₁₄N₄O₂ = 246.27 found 247.4 [M+H]⁺.

tert-butyl (1-((2-(1H-indazol-1-yl)-2-oxoethyl)amino)-2-methyl-1-oxopropan-2-yl) carbamate **38a**



This compound was synthesised according to General Chemistry Procedure **6**. The crude reaction mixture was separated using silica gel chromatography using a gradient of 20-80% EtOAc in (40-60) PET to achieve to obtain the title compound **38a** (82%) as a colourless oil; R_f 0.67 (33 % EtOAc in PET); ¹H (400 MHz; CDCl₃) δ 1.32 [9H, s], 1.47 [6H,s], 4.80 [2H, d, J 5Hz], 7.21 [1H, t, J 8Hz], 7.39 [1H, t, J 8 Hz], 7.59 [1H, d, J 8 Hz], 7.99 [1H, s], 8.19 [1H, d, J 8 Hz]; ¹³C (101 MHz; CDCl₃) δ 175.54, 168.89, 154.76, 140.49, 138.85, 129.44, 124.66, 121.02, 114.86, 79.74, 56.69, 43.03, 28.22, 25.90; *m/z* (ESI; 96%) Calc. for C₁₈H₂₄N₄O₄ = 360.41 found 361.5 [M+H]⁺.

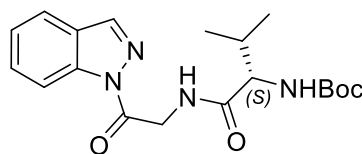
N-(2-(1H-indazol-1-yl)-2-oxoethyl)-2-amino-2-methylpropanamide **38**



This compound was synthesised according to General Chemistry Procedure **3** to obtain the title compound **38** [100% (theoretical)] as a white solid; m/z (ESI; 99%)

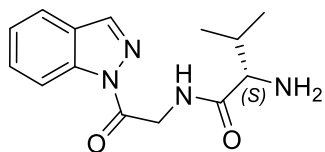
Calc. for C₁₃H₁₆N₄O₂ = 260.30 found 261.4 [M+H]⁺.

tert-butyl (S)-1-((2-(1H-indazol-1-yl)-2-oxoethyl)amino)-3-methyl-1-oxobutan-2-yl)carbamate **39a**



This compound was synthesised according to General Chemistry Procedure **6**. The crude reaction mixture was separated using silica gel chromatography using a gradient of 20-80% EtOAc in (40-60) PET to obtain the title compound **39a** (84%) as a colourless oil; Rf 0.67 (80 % EtOAc in PET); ^1H (400 MHz; CDCl_3) δ 0.97-1.07 [6H, dd, J 7 and 18 Hz], 1.48 [9H, s], 2.25 [1H, m], 4.14 [1H, m], 4.97 [2H, m], 5.26 [1H, bs], 7.00 [1H, bs], 7.37 [1H, t, J 8 Hz], 7.56 [1H, t, J 8 Hz], 7.74 [1H, d, J 8 Hz], 8.13 [1H, s], 8.34 [1H, d, J 8 Hz]; ^{13}C (101 MHz; CDCl_3) δ 172.17, 168.74, 155.98, 140.80, 139.03, 129.72, 124.90, 121.11, 115.11, 79.94, 59.93, 42.90, 30.97, 28.34, 19.32; m/z (ESI; 99%) Calc. for $\text{C}_{19}\text{H}_{26}\text{N}_4\text{O}_4$ = 374.44 found 375.4 $[\text{M}+\text{H}]^+$.

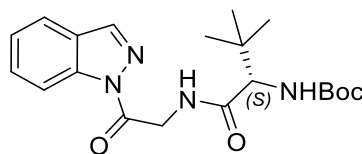
(S)-N-(2-(1H-indazol-1-yl)-2-oxoethyl)-2-amino-3-methylbutanamide **39**



This compound was synthesised according to General Chemistry Procedure **3** to obtain the title compound **39** [100% (theoretical)] as a white solid; m/z (ESI; 99%)

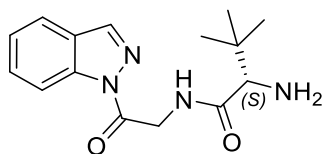
Calc. for $C_{14}H_{18}N_4O_2 = 274.32$ found 275.4 $[M+H]^+$.

tert-butyl (S)-1-((2-(1H-indazol-1-yl)-2-oxoethyl)amino)-3,3-dimethyl-1-oxobutan-2-yl)carbamate **40a**



This compound was synthesised according to General Chemistry Procedure 6. The crude reaction mixture was separated using silica gel chromatography using a gradient of 20-80% EtOAc in (40-60) PET to obtain the title compound **40a** (95%) as a colourless oil; R_f 0.80 [40% EtOAc in PET] ^1H (400 MHz; CDCl_3) δ 0.97-1.07 [9H, s], 1.41 [9H, s], 4.76-5.08 [1H, m], 5.52 [2H, s], 7.29 [1H, t, J 8 Hz], 7.46 [1H, t, J 8 Hz], 7.64 [1H, d, J 8 Hz], 8.05 [1H, s], 8.27 [1H, d, J 8 Hz]; ^{13}C (101 MHz; CDCl_3) δ 171.76, , 168.65, 156.06, 140.54, 138.98, 129.51, 126.04, 124.72, 121.00, 115.13, 79.59, 62.19, 42.78, 34.59, 28.29 26.06, 23.96; m/z (ESI; 998) Calc. for $\text{C}_{20}\text{H}_{28}\text{N}_4\text{O}_4$ = 388.47 found 389.5 $[\text{M}+\text{H}]^+$.

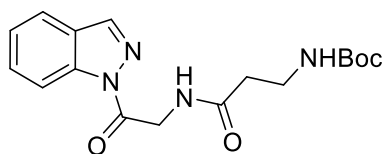
(S)-N-(2-(1H-indazol-1-yl)-2-oxoethyl)-2-amino-3,3-dimethylbutanamide **40**



This compound was synthesised according to General Chemistry Procedure **3** to obtain the title compound **40** [100% (theoretical)] as a white solid; m/z (ESI; 99%)

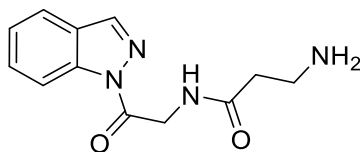
Calc. for C₁₅H₂₀N₄O₂ = 288.35 found 289.4 [M+H]⁺.

tert-butyl (3-((2-(1H-indazol-1-yl)-2-oxoethyl)amino)-3-oxopropyl) carbamate **41a**



This compound was synthesised according to General Chemistry Procedure **6**. The crude reaction mixture was separated using silica gel chromatography using a gradient of 20-80% EtOAc in (40-60) PET to obtain the title compound **41a** (94%) as a colourless oil; R_f 0.61 (80 % EtOAc in PET); ¹H (400 MHz; CDCl₃) δ 1.38 [9H, s], 2.54 [2H, t, J 6 Hz], 3.43 [2H, q, J 6 Hz], 4.86 [2H, d, J 5 Hz], 5.44-5.54 [1H, bs], 7.11 [1H, m], 7.29 [1H, t, J 8Hz], 7.48 [1H, t, J 8 Hz], 7.66 [1H, d, J 8 Hz], 8.06 [1H, s], 8.27 [1H, d, J 8 Hz]; ¹³C (101 MHz; CDCl₃) δ 168.94, 165.71, 156.21, 140.74, 138.95, 129.65, 126.06, 124.84, 121.09, 115.00, 79.17, 40.97, 36.73, 36.08, 28.36; *m/z* (ESI; 95%) Calc. for C₁₇H₂₂N₄O₅ = 346.39 found 347.4 [M+H]⁺.

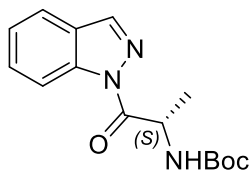
N-(2-(1H-indazol-1-yl)-2-oxoethyl)-3-aminopropanamide **41**



This compound was synthesised according to General Chemistry Procedure **3** to obtain the title compound **41** [100% (theoretical)] as a white solid; m/z (ESI; 99%)

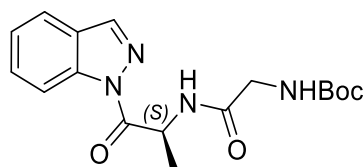
Calc. for C₁₂H₁₄N₄O₂ = 246.27 found 247.4 [M+H]⁺.

tert-butyl (S)-(1-(1H-indazol-1-yl)-1-oxopropan-2-yl)carbamate **42i**



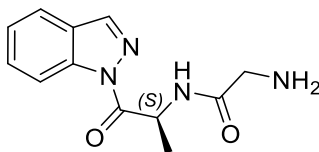
This compound was synthesised according to General Chemistry Procedure 7. The crude reaction mixture was separated using silica gel chromatography using a gradient of 20-80% EtOAc in (40-60) PET to obtain the title compound **42i** (83%) as a white solid; R_f 0.35 (20 % EtOAc in PET); ¹H (400 MHz; DMSO) δ 1.24-1.31 [12H, m], 3.82-3.93 [1H, m], 7.10 [1H, t, *J* 7 Hz], 7.33 [1H, t, *J* 7 Hz], 7.55 [1H, d, *J* 7 Hz], 7.76 [1H, d, *J* 7 Hz] 8.06 [1H, s]; ¹³C (101 MHz; DMSO₃) δ 169.7, 140.4, 133.9, 126.4, 123.4, 120.95, 120.67, 110.73, 53.49, 45.83, 19.54, 12.73; *m/z* (ESI; 99%) Calc. for C₁₅H₁₉N₃O₃ = 289.34 found 290.3 [M+H]⁺.

tert-butyl (S)-2-((1-(1H-indazol-1-yl)-1-oxopropan-2-yl)amino)-2-oxoethyl)carbamate **42ii**



This compound was synthesised according to General Chemistry Procedure 6. The crude reaction mixture was separated using silica gel chromatography using a gradient of 20-80% EtOAc in (40-60) PET to obtain the title compound **42ii** (98%) as a colourless oil; R_f 0.67 (60 % EtOAc in PET); ¹H (400 MHz; CDCl₃) δ 1.48 [9H, s], 1.61 [3H, d, J 7 Hz], 3.83-3.99 [2H, m], 5.39 [1H, bs], 5.83-5.93 [1H, m], 7.13 [1H, bs], 7.38 [1H, t, J 8 Hz], 7.57 [1H, t, J 8 Hz], 7.75 [1H, d, J 8 Hz], 8.18 [1H, s], 8.38 [1H, d, J 8 Hz]; ¹³C (101 MHz; CDCl₃) δ 172.65, 169.07, 156.08, 140.87, 139.24, 129.74, 126.33, 124.99, 121.12, 115.41, 80.22, 48.29, 44.29, 28.31, 19.10; *m/z* (ESI; 99%) Calc. for C₁₇H₂₂N₄O₄ = 346.39 found 347.5 [M+H]⁺.

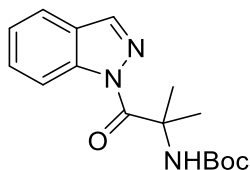
(S)-N-(1-(1H-indazol-1-yl)-1-oxopropan-2-yl)-2-aminoacetamide **42**



This compound was synthesised according to General Chemistry Procedure **6** to obtain the title compound **42** [100% (theoretical)] as a white solid; m/z (ESI; 99%)

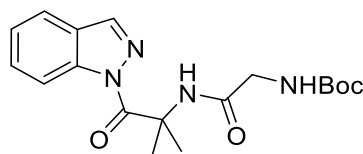
Calc. for C₁₂H₁₄N₄O₂ = 246.27 found 247.4 [M+H]⁺.

tert-butyl (1-(1H-indazol-1-yl)-2-methyl-1-oxopropan-2-yl)carbamate **43a**



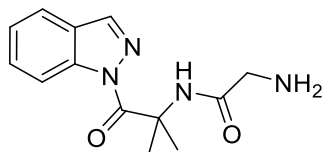
This compound was synthesised according to General Chemistry Procedure **6**. The crude reaction mixture was separated using silica gel chromatography using a gradient of 20-80% EtOAc in (40-60) PET to obtain the title compound **43a** (83%) as a white solid; R_f 0.52 (30 % EtOAc in PET); ¹H (400 MHz; CDCl₃) δ 1.46 [9H, m], 1.92 [6H, s], 7.52 [1H, t, *J* 7 Hz], 7.28 [1H, t, *J* 7 Hz], 7.98 [1H, d, *J* 7 Hz], 8.35 [1H, d, *J* 7 Hz] 8.66 [1H, s]; ¹³C (101 MHz; CDCl₃) δ 173.83 142.53, 139.85, 131.00, 126.14, 126.00, 122.72, 115.57, 79.52, 56.11, 24.10, 23.80; *m/z* (ESI; 98%) Calc. for C₁₆H₂₁N₃O₃ = 303.36 found 304.4 [M+H]⁺.

tert-butyl (2-((1-(1H-indazol-1-yl)-2-methyl-1-oxopropan-2-yl)amino)-2-oxoethyl) carbamate **43b**



This compound was synthesised according to General Chemistry Procedure **6**. The crude reaction mixture was separated using silica gel chromatography using a gradient of 20-80% EtOAc in (40-60) PET to obtain the title compound **43b** (75%) as a colourless oil R_f 0.6 (60 % EtOAc in PET); ^1H (400 MHz; CDCl_3) δ 1.45 [9H, s], 1.83 [6H,s], 3.67 [2H, s], 5.29 [1H, bs], 7.25 [1, bs], 7.33 [1H, t, J 8Hz], 7.57[1H, t, J 8 Hz], 7.69 [1H, d, J 8 Hz], 8.05 [1H, s], 8.46 [1H, d, J 8 Hz]; ^{13}C (101 MHz; CDCl_3) δ 172.98, 169.04, 156.11, 140.05, 139.34, 129.60, 125.25, 124.56, 120.9, 116.09, 79.96, 58.43, 38.60, 28.32, 25.61; m/z (ESI; 99%) Calc. for $\text{C}_{18}\text{H}_{24}\text{N}_4\text{O}_4$ = 360.41 found 361.4 $[\text{M}+\text{H}]^+$.

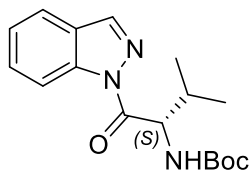
N-(1-(1H-indazol-1-yl)-2-methyl-1-oxopropan-2-yl)-2-aminoacetamide **43**



This compound was synthesised according to General Chemistry Procedure **3** to obtain the title compound **43** [100% (theoretical)] as a white solid; m/z (ESI; 99%)

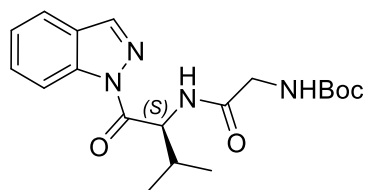
Calc. for C₁₃H₁₄N₄O₂ = 260.30 found 261.4 [M+H]⁺.

tert-butyl (S)-(1-(1H-indazol-1-yl)-3-methyl-1-oxobutan-2-yl)carbamate **44a**



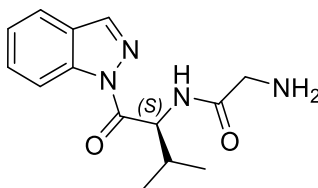
This compound was synthesised according to General Chemistry Procedure **6**. The crude reaction mixture was separated using silica gel chromatography using a gradient of 20-80% EtOAc in (40-60) PET to obtain the title compound **44a** (83%) as a white solid; Rf 0.52 (30 % EtOAc in PET); ^1H (400 MHz; CDCl_3) δ 0.99 [6H, d, J 6 Hz], 1.30 [9H, m], 3.93-4.13 [1H, m], 7.10 [1H, t, J 7 Hz], 7.33 [1H, t, J 7 Hz], 7.98 [1H, d, J 7 Hz], 8.33 [1H, d, J 7 Hz] 8.64 [1H, s]; ^{13}C (101 MHz; DMSO) δ 172.91, 155.50, 138.76, 129.32, 124.81, 120.98, 114.62, 79.67, 57.82, 31.05, 28.33, 26.48; m/z (ESI; 98%) Calc. for $\text{C}_{17}\text{H}_{23}\text{N}_3\text{O}_3 = 317.17$ found 318.2 $[\text{M}+\text{H}]^+$.

tert-butyl (S)-2-((1-(1H-indazol-1-yl)-3-methyl-1-oxobutan-2-yl)amino)-2-oxoethyl)carbamate **44b**



This compound was synthesised according to General Chemistry Procedure **6**. The crude reaction mixture was separated using silica gel chromatography using a gradient of 20-80% EtOAc in (40-60) PET to obtain the title compound **44b** (59%) as a colourless oil; R_f 0.51 (60 % EtOAc in PET); ¹H (400 MHz; CDCl₃) δ 0.88 [3H, d, J 7Hz], 0.99 [3H, d, J 7Hz] 1.41 [9H,s], 2.39 [1H, o, J 4Hz], 3.78-3.96 [2H, m], 5.73 [1H, bs], 5.84 [1H, dd, J 5 and 9Hz], 7.30 [1H, t, J 8Hz], 7.48 [1H, t, J 8 Hz], 7.67 [1H, d, J 8 Hz], 8.12 [1H, s], 8.33 [1H, d, J 8 Hz]; ¹³C (101 MHz; CDCl₃) δ 171.87, 170.02, 156.26, 140.64, 139.02, 129.58, 126.32, 124.89, 121.11, 115.33, 79.92, 56.41, 44.37, 31.54, 28.26, 19.65; *m/z* (ESI; 95%) Calc. for C₁₉H₂₆N₄O₄ = 374.44 found 375.5 [M+H]⁺.

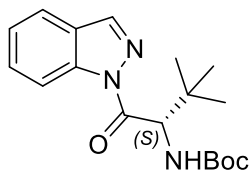
(S)-N-(1-(1H-indazol-1-yl)-3-methyl-1-oxobutan-2-yl)-2-aminoacetamide **44**



This compound was synthesised according to General Chemistry Procedure **3** to obtain the title compound **44** [100% (theoretical)] as a white solid; m/z (ESI; 99%)

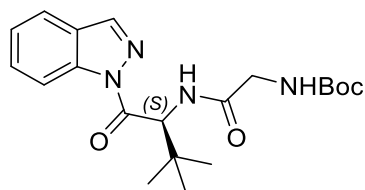
Calc. for $C_{14}H_{18}N_4O_2 = 274.32$ found 275.4 $[M+H]^+$.

tert-butyl (S)-(1-(1H-indazol-1-yl)-3,3-dimethyl-1-oxobutan-2-yl)carbamate **45a**



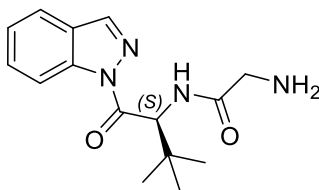
This compound was synthesised according to General Chemistry Procedure **6**. The crude reaction mixture was separated using silica gel chromatography using a gradient of 20-80% EtOAc in (40-60) PET to obtain the title compound **45a** (83%) as a white solid; Rf 0.69 (30 % EtOAc in PET); ^1H (400 MHz; DMSO) δ 1.03 [9H, m], 1.42 [9H, s], 3.93 [2H, s], 5.35-5.46 [1H, m], 7.35 [1H, t, J 7 Hz], 7.53 [1H, t, J 7 Hz], 7.71 [1H, d J 7 Hz], 8.15 [1H, s], 8.44 [1H, d, J 7 Hz]; ^{13}C (101 MHz; DMSO) δ 172.97, 155.46, 138.89, 129.38, 124.78, 120.99, 115.60, 79.66, 58.56, 35.74, 28.35, 26.49; m/z (ESI; 98%) Calc. for $\text{C}_{18}\text{H}_{25}\text{N}_3\text{O}_3 = 331.41$ found 332.4 $[\text{M}+\text{H}]^+$.

tert-butyl (S)-2-((1-(1H-indazol-1-yl)-3-methyl-1-oxobutan-2-yl)amino)-2-oxoethyl)carbamate **45b**



This compound was synthesised according to General Chemistry Procedure **6**. The crude reaction mixture was separated using silica gel chromatography using a gradient of 20-80% EtOAc in (40-60) PET to obtain the title compound **45b** (35 %) as a colourless oil; Rf 0.37 [40% EtOAc in PET ¹H (400 MHz; CDCl₃) δ 1.07 [9H, s], 1.49 [9H, s], 3.76-3.97 [2H, m], 5.29 [1H, s], 7.06 [1H, d, *J* 8], 7.40 [1H, t, *J* 8 Hz], 7.56 [1H, t, *J* 8 Hz], 7.76 [1H, d, *J* 8 Hz], 8.20 [1H, s], 8.45 [1H, d, *J* 8 Hz]; ¹³C (101 MHz; CDCl₃) δ 171.76, , 168.65, 156.06, 140.54, 138.98, 129.51, 126.04, 124.72, 121.00, 115.13, 79.59, 62.19, 42.78, 34.59, 28.29 26.06, 23.96; *m/z* (ESI; 99%) Calc. for C₂₀H₂₈N₈O₄ = 388.47 found 389.5 [M+H]⁺.

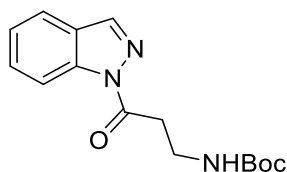
(S)-N-(1-(1H-indazol-1-yl)-3,3-dimethyl-1-oxobutan-2-yl)-2-aminoacetamide **45**



This compound was synthesised according to General Chemistry Procedure **3** to obtain the title compound **45** [100% (theoretical)] as a white solid; m/z (ESI; 99%)

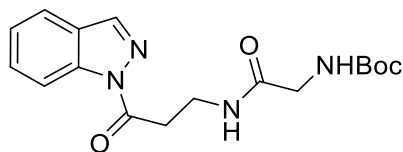
Calc. for C₁₅H₂₀N₄O₂ = 288.35 found 289.6 [M+H]⁺.

tert-butyl (3-(1H-indazol-1-yl)-3-oxopropyl)carbamate **46a**



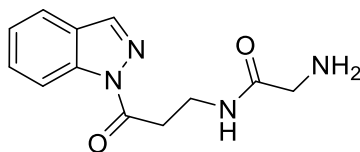
This compound was synthesised according to General Chemistry Procedure **6**. The crude reaction mixture was separated using silica gel chromatography using a gradient of 20-80% EtOAc in (40-60) PET to obtain the title compound **46a** (83%) as a white solid; Rf 0.40 (20 % EtOAc in PET); ¹H (400 MHz; DMSO) δ 1.26 [9H, m], 3.24 [2H, t, J 6 Hz], 3.61 [2H, t, J 6 Hz], 7.45 [1H, t, J 7 Hz], 7.67 [1H, t, J 7 Hz], 7.94 [1H, d, J 7 Hz], 8.33 [1H, d, J 7 Hz] 8.54 [1H, s]; ¹³C (101 MHz; DMSO) δ 171.09, 141.44, 138.80, 130.26, 126.58, 125.29, 122.36, 115.01, 53.01, 45.80, 34.68, 33.14, 18.18; *m/z* (ESI; 98%) Calc. for C₁₅H₁₉N₃O₃ = 289.34 found 290.3 [M+H]⁺.

tert-butyl (2-((3-(1H-indazol-1-yl)-3-oxopropyl)amino)-2-oxoethyl) carbamate **46b**



This compound was synthesised according to General Chemistry Procedure **6**. The crude reaction mixture was separated using silica gel chromatography using a gradient of 20-80% EtOAc in (40-60) PET to obtain the title compound **46b** (39%) as a colourless oil; R_f 0.58 (60 % EtOAc in PET); ¹H (400 MHz; CDCl₃) δ 1.42 [9H, s], 3.45 [2H, t, J 6Hz], 3.73-3.83 [4H, m], 5.39 [1H, bs], 7.00 [1H, bs], 7.35 [1H, t, J 8 Hz], 7.54 [1H, t, J 8 Hz] 7.71 [1H, d, J 8 Hz], 8.10 [1H, s], 8.37 [1H, d, J 8 Hz]; ¹³C (101 MHz; CDCl₃) δ 172.39, 169.64, 156.02, 140.26, 138.93, 129.56, 126.24, 124.69, 121.04, 115.30, 80.09, 44.29, 38.59, 34.62, 28.27; *m/z* (ESI; 97%) Calc. for C₁₇H₂₂N₄O₄ = 346.39 found 347.4 [M+H]⁺.

N-(3-(1H-indazol-1-yl)-3-oxopropyl)-2-aminoacetamide **46**

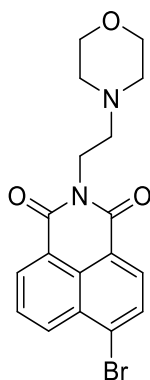


This compound was synthesised according to General Chemistry Procedure **3** to obtain the title compound **46** [100% (theoretical)] as a white solid; m/z (ESI; 99%)

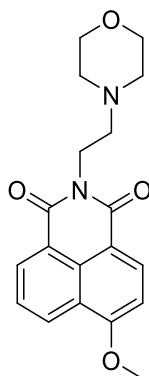
Calc. for C₁₂H₁₄N₄O₂ = 246.27 found 247.4 [M+H]⁺.

5.3 Chapter 3

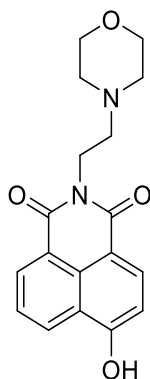
6-bromo-2-(2-morpholinoethyl)-1H-benzo[de]isoquinoline-1,3(2H)-dione **97**



To a stirred solution of 6-bromo-1H,3H-benzo[de]isochromene-1,3-dione (0.10 g, 0.44 mmol, 1 eq) in EtOH (20 mL) was added 2-morpholinoethan-1-amine (0.12 mL, 0.88 mmol, 2 eq) and the resulting solution stirred for 3 hours at 80°C. TLC analysis deemed the reaction to be complete and the solution was cooled to room temperature and the yellow solid filtered and washed with cold EtOH (3x 10 mL) to obtain the title compound **97** (0.12 g, 74%) as a yellow solid; R_f 0.46 (100 % EtOAc); ¹H (400 MHz; CDCl₃) δ 2.60 [4H, t, *J* 5], 2.71 [2H, t, *J* 5], 3.70 [4H, t, *J* 5], 4.34 [2H, t, *J* 6], 7.84, [1H, t, *J* 8.5], 8.04 [1H, d, *J* 8.5], 8.40 [1H, d, *J* 8.5], 8.55 [1H, d, *J* 9], 8.64 [1H, d, *J* 8.5]; ¹³C (101 MHz; CDCl₃) δ 160.87, 159.99, 133.51, 131.59, 128.74, 126.02, 123.48, 67.03, 56.26, 53.85, 37.14; *m/z* (ESI; 99%) Calc. for C₁₈H₁₇BrN₂O₃ = 389.25 found 388.3/340.3 [M+H]⁺

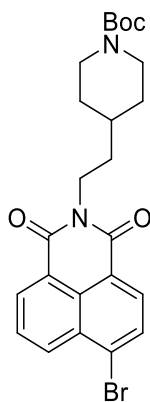
6-methoxy-2-(2-morpholinoethyl)-1H-benzo[de]isoquinoline-1,3(2H)-dione **98**

To a stirred solution of 6-bromo-2-(2-morpholinoethyl)-1H-benzo[de]isoquinoline-1,3(2H)-dione (0.10 g, 0.26 mmol, 1 eq) in MeOH (10 mL) was added potassium carbonate (0.14 g, 1.03 mmol, 4 eq) and the resulting solution stirred at room temperature overnight. TLC analysis deemed the reaction to be complete and the solution was concentrated in vacuo. The crude mixture was redissolved in DCM (20 mL) and extracted with H₂O (3 x 40 mL). The organic layers were combined, dried over MgSO₄, filtered and concentrated in vacuo to obtain the title compound **98** (0.08 g, 86%) as yellow solid; R_f 0.83 (5% MeOH in DCM 1% NH₃); ¹H (400 MHz; CDCl₃) δ 2.63 [4H, t, *J* 5], 2.73 [2H, t, *J* 5], 3.71 [4H, t, *J* 5], 4.14 [3H, s], 4.35 [2H, t, *J* 6], 7.06, [1H, d, *J* 8.5], 7.72 [1H, t, *J* 8.5], 8.56 [1H, d, *J* 8.5], 8.58 [1H, d, *J* 9], 8.60 [1H, d, *J* 8.5]; ¹³C (101 MHz; CDCl₃) δ 164.52, 163.96, 160.87, 133.51, 131.59, 128.74, 126.02, 123.48, 115.13, 105.29, 67.03, 56.26, 53.85, 37.14; *m/z* (ESI; 99%) Calc. for C₁₈H₁₈N₂O₄ = 340.38 found 341.4 [M+H]⁺

6-hydroxy-2-(2-morpholinoethyl)-1H-benzo[de]isoquinoline-1,3(2H)-dione **95**

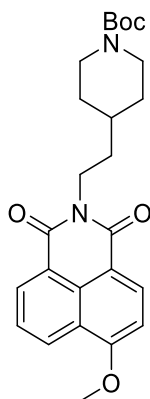
To a stirred solution of 6-methoxy-2-(2-morpholinoethyl)-1H-benzo[de]isoquinoline-1,3(2H)-dione (0.45 g, 1.3 mmol, 1 eq) in DCM (5 mL) was added Hydroiodic Acid 57% Aqueous solution (20 mL) and the resulting solution refluxed at 110°C for 3 hours. LCMS deemed the reaction to be complete and the solution was cooled to room temperature, neutralised with 2N NaOH (10 mL) and the solution concentrated under high vacuo. The crude mixture was then absorbed onto silica and purified by silica gel chromatography using a gradient of 0-100% EtOAc in Cy to obtain the title compound **95** (0.40 g, 93%) as an orange solid; R_f 0.7 (10% MeOH in DCM 1% NH₃); ¹H (400 MHz; DMSO) δ 2.84 [4H, t, *J* 5], 2.92 [2H, t, *J* 5], 3.64 [4H, t, *J* 5], 4.24 [2H, t, *J* 6], 7.11, [1H, d, *J* 8.5], 7.32 [1H, t, *J* 8.5], 8.31 [1H, d, *J* 8.5], 8.42 [1H, d, *J* 9], 8.50 [1H, d, *J* 8.5]; ¹³C (101 MHz; DMSO) δ 164.7, 163.9, 161.2, 134.2, 131.7, 129.8, 126.1, 123.0, 122.2, 112.80, 110.50, 65.55, 55.60, 35.12, 36.1; *m/z* (ESI; 99%) Calc. for C₁₈H₁₈N₂O₄ = 326.35 found 327.5 [M+H]⁺

tert-Butyl 4-(2-(6-bromo-1,3-dioxo-1H-benzo[de]isoquinolin-2(3H)-yl)ethyl)piperidine-1-carboxylate **99**



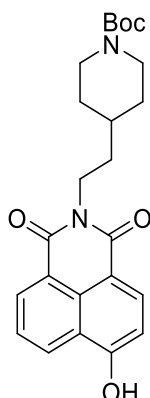
To a stirred solution of 6-bromo-1H,3H-benzo[de]isochromene-1,3-dione (0.50 g, 1.80 mmol, 1 eq) in EtOH (20 mL) was added *tert*-butyl 4-(2-aminoethyl) piperidine-1-carboxylate (0.82 mL, 3.6 mmol, 2 eq) and the resulting solution stirred for 3 hours at 80°C. TLC analysis deemed the reaction to be complete and the solution concentrated in vacuo. The crude mixture was absorbed onto silica and purified by silica gel chromatography using a gradient of 0-20% EtOAc in Cy to obtain the title compound **99** (0.53 g, 53%) as a yellow solid; *R*_f 0.7 (100% EtOAc); ¹H (400 MHz; CDCl₃) δ 1.15-1.29 [2H, m], 1.47 [9H, s], 1.51-1.60 [1H, m], 1.69 [2H, q, *J* 11], 1.81 [2H, d, *J* 11], 2.73 [2H, t, *J* 11], 4.20 [3H, s], 4.22 [2H, t, *J* 6], 7.83 [1H, t, *J* 8.5], 8.02 [1H, d, *J* 8.5], 8.37 [1H, d, *J* 9], 8.53 [1H, d, *J* 9] 8.62 [1H, d, *J* 9]; ¹³C (101 MHz; CDCl₃) δ 164.49, 154.90, 133.27, 131.98, 131.19, 131.10, 130.57, 130.29, 128.90, 128.11, 123.02, 122.17, 79.25, 38.30, 34.56, 34.19, 32.06, 28.54, 26.97; *m/z* (ESI; 98%) Calc. for C₂₄H₂₇BrN₂O₄ = 487.39 found 487.5/489.5 [M+H]⁺

tert-butyl 4-(2-(6-methoxy-1,3-dioxo-1H-benzo[de]isoquinolin-2(3H)-yl)ethyl)piperidine-1-carboxylate **100**

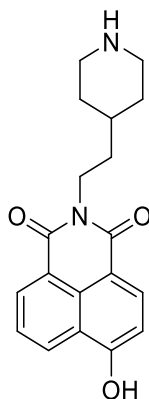


To a stirred solution of *tert*-Butyl 4-(2-(6-bromo-1,3-dioxo-1H-benzo[de]isoquinolin-2(3H)-yl) ethyl) piperidine-1-carboxylate (0.53 g, 1.1 mmol, 1 eq) in MeOH (10 mL) was added potassium carbonate (0.30 g, 2.20 mmol, 2 eq) and the resulting solution stirred at room temperature overnight. TLC analysis deemed the reaction to be complete and the solution was concentrated in vacuo. The crude mixture was absorbed onto silica and purified by silica gel chromatography using a gradient of 10-30% EtOAc in Cy to obtain the title compound **100** (0.42 g, 79%) as yellow solid; R_f 0.7 (100% EtOAc); ^1H (400 MHz; CDCl_3) δ 1.17-1.29 [2H, m], 1.48 [9H, s], 1.52-1.61 [1H, m], 1.69 [2H, q, J 11], 1.83 [2H, d, J 11], 2.74 [2H, t, J 11], 4.15 [3H, s], 4.22 [2H, t, J 6], 7.06, [1H, d, J 8.5], 7.72 [1H, t, J 8.5], 8.56 [1H, d, J 9], 8.60 [1H, d, J 9] 8.64 [1H, d, J 9]; ^{13}C (101 MHz; CDCl_3) δ 164.255, 163.97, 160.88, 154.96, 133.48, 131.56, 128.73, 126.06, 123.53, 122.47, 115.09, 105.21, 79.19, 56.30, 38.11, 34.74, 34.24, 32.11, 28.52, 26.94; m/z (ESI; 99%) Calc. for $\text{C}_{25}\text{H}_{30}\text{N}_2\text{O}_5$ = 438.52 found 439.6 $[\text{M}+\text{H}]^+$

tert-butyl 4-(2-(6-hydroxy-1,3-dioxo-1H-benzo[de]isoquinolin-2(3H)-yl) ethyl) piperidine-1-carboxylate **101**

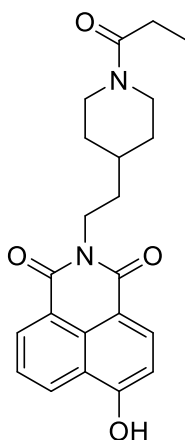


To a stirred solution of tert-butyl 4-(2-(6-methoxy-1,3-dioxo-1H-benzo[de]isoquinolin-2(3H)-yl) ethyl)piperidine-1-carboxylate (0.40 g, 0.90 mmol, 1 eq) in DCM (5 mL) was added Hydroiodic Acid 57% Aqueous solution (20 mL) and the resulting solution refluxed at 110°C for 3 hours. LCMS deemed the reaction to be complete and the solution was cooled to room temperature, neutralised with 2N NaOH (10 mL) and the solution concentrated under high vacuo. The crude mixture was then redissolved in DCM (10 mL), and Di-tert-butyl decarbonate (0.24 g, 1.10 mmol, 1.2 eq) and NEt₃ (0.38 mL, 2.70 mmol, 3 eq) was added and the resulting solution stirred for 30 minutes at room temperature. TLC analysis deemed the reaction to be complete and the solution was concentrated in vacuo. The crude mixture was then absorbed on to silica and purified by silica gel chromatography to obtain the title compound **101** (0.35 g, 90%) as an orange solid; R_f 0.7 (100% EtOAc); ¹H (400 MHz; CDCl₃) δ 1.17-1.30 [2H, m], 1.49 [9H, s], 1.53-1.63 [1H, m], 1.70 [2H, q, *J* 11], 1.84 [2H, d, *J* 11], 2.76 [2H, d, *J* 11], 4.23 [2H, t, *J* 6], 7.17, [1H, d, *J* 8.5], 7.67 [1H, t, *J* 8.5], 8.46 [1H, d, *J* 9], 8.60 [1H, d, *J* 9] 8.64 [1H, d, *J* 9]; ¹³C (101 MHz; CDCl₃) δ 164.87, 164.25, 161.54, 155.20, 134.10, 131.71, 130.08, 129.57, 125.18, 122.16, 112.93, 110.61, 79.99, 38.06, 34.67, 34.11, 31.97, 28.58, 18.15; *m/z* (ESI; 99%) Calc. for C₂₄H₂₈N₂O₅ = 590.49 found 591.6 [M+H]⁺

6-hydroxy-2-(2-(piperidin-4-yl)ethyl)-1H-benzo[de]isoquinoline-1,3(2H)-dione **102**

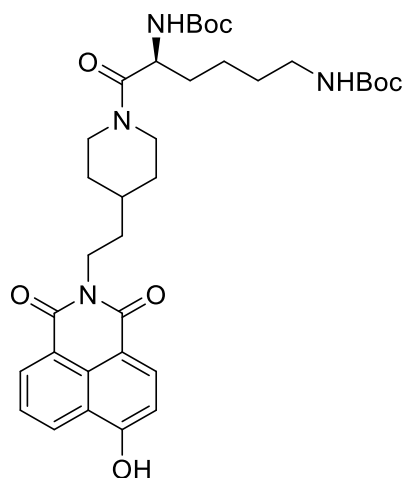
To a stirred solution of tert-butyl 4-(2-(6-hydroxy-1,3-dioxo-1H-benzo[de]isoquinolin-2(3H)-yl)ethyl)piperidine-1-carboxylate (1.5 g, 2.5 mmol, 1 eq) in DCM (5 mL) was added 4N HCl in 1,4, dioxane and the resulting solution stirred at room temperature for 20 minutes. TLC analysis deemed the reaction to be complete and the solution was concentrated in vacuo. The crude mixture was absorbed on to silica and purified by silica gel chromatography using a gradient of 0-20% MeOH in DCM to obtain the title compound **102** as a yellow solid (0.35 g, 96%) as a yellow solid; Rf 0.1 [MeOH: DCM (1:4) 1% NH₃]; ¹H (400 MHz; DMSO) δ 1.25-1.34 [2H, m], 1.35-1.49 [2H, m], 1.51-1.65 [3H, m], 1.9 [1H, bs], 2.74-2.88 [2H, m], 3.18-3.26 [2H, m], 4.04 [2H, t, *J* 7], 7.29 [1H, d, *J* 8.5], 7.76 [1H, t, *J* 8.5], 8.34 [1H, d, *J* 8.5], 8.46 [1H, dd, *J* 1 and 7.4], 8.54 [1H, dd, *J* 1 and 7.4], 9.03 [1H, bs]; ¹³C (101 MHz; DMSO) δ 164.19, 163.54, 161.07, 134.09, 131.67, 129.73, 129.52, 126.05, 122.95, 122.27, 112.87, 110.56, 43.45, 37.37, 34.37, 31.37, 28.76, 17.15; *m/z* (ESI; 99%) Calc. for C₁₉H₂₀N₂O₃ = 324.48 found 325 [M+H]⁺.

6-hydroxy-2-(2-(1-propionylpiperidin-4-yl)ethyl)-1H-benzo[de]isoquinoline-1,3(2H)-dione **103**

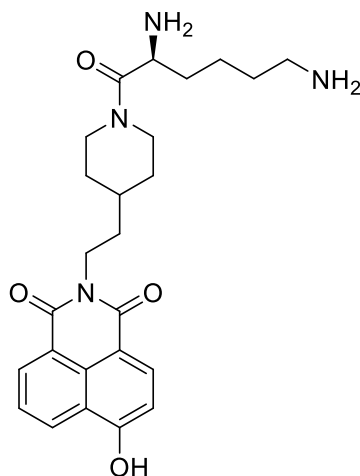


This compound was then synthesised according to General Chemistry Procedure **6**. The crude material was then dissolved in DCM (1 mL) and purified by silica gel chromatography using a gradient of 0-100% EtOAc in Cy to obtain the title compound (64%) as a yellow solid; R_f 0.22 (100% EtOAc); ¹H (400 MHz; CDCl₃) δ 1.12-1.18 [3H, t, *J* 7.3], 1.20-1.27 [2H, m], 1.33-1.51 [2H, m], 1.60-1.75 [3H, m], 1.91 [1H, bs], 2.38 [2H, q, *J* 7.3], 3.16 [2H, q, *J* 7.4], 3.69 [2H, q, *J* 7.4], 4.21 [2H, t, *J* 6.8], 7.46 [1H, d, *J* 8.5], 7.65 [1H, t, *J* 8.5], 8.43 [1H, d, *J* 8.5], 8.56 [1H, dd, *J* 1 and 7.4], 8.60 [1H, dd, *J* 1 and 7.4]; ¹³C (101 MHz; CDCl₃) δ 172.60, 164.77, 164.22, 160.82, 133.96, 131.53, 129.87, 129.60, 125.14, 122.99, 122.14, 113.24, 110.57, 45.83, 42.67, 42.06, 34.14, 32.57, 31.94, 26.64, 17.26, 9.70; *m/z* (ESI; 97%) Calc. for C₂₂H₂₄N₂O₄ = 380.44 found 381.4 [M+H]⁺.

di-tert-butyl (6-(4-(2-(6-hydroxy-1,3-dioxo-1H-benzo[de]isoquinolin-2(3H)-yl)ethyl) piperidin-1-yl)-6-oxohexane-1,5-diyl)dicarbamate **104a**

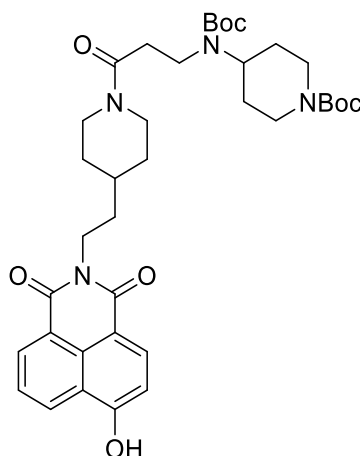


This compound was then synthesised according to General Chemistry Procedure **6**. The crude material was then dissolved in DCM (1 mL) and purified by silica gel chromatography using a gradient of 0-100% EtOAc in Cy to obtain the title compound **104a** (65%) as a yellow oil; R_f 0.43 (100% EtOAc; ^1H (400 MHz; CDCl_3) δ 1.08-1.25 [2H, m], 1.44 [18H, s], 1.45-1.48 [2H, m], 1.57-1.74 [7H, m], 1.78-1.92 [2H, m], 3.00-3.08 [2H, m], 3.17 [1H, q, J 7.3], 3.71 [2H, q, J 7.4], 4.17-4.22 [2H, m], 4.60 [1H, q, J 7.4], 7.05 [1H, d, J 8.5], 7.65 [1H, t, J 8.5], 8.42 [1H, d, J 8.5], 8.56 [1H, dd, J 1 and 7.4], 8.61 [1H, dd, J 1 and 7.4]; ^{13}C (101 MHz; CDCl_3) δ 170.60, 164.90, 164.20, 155.82, 139.90, 131.19, 130.51, 129.40, 125.2, 122.5, 113.54, 110.4, 110.22, 79.80, 55.82, 43.64, 42.68, 34.2, 32.70, 32.57, 31.85, 28.53, 26.68, 22.51, 18.21; m/z (ESI; 98%) Calc. for $\text{C}_{35}\text{H}_{48}\text{N}_4\text{O}_8$ = 652.79 found 653.9 $[\text{M}+\text{H}]^+$

6-hydroxy-2-(2-(1-lysylpiperidin-4-yl)ethyl)-1H-benzo[de]isoquinoline-1,3(2H)-dione **104**

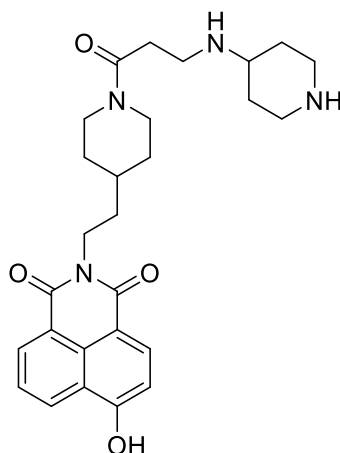
This compound was synthesised according to General Chemistry Procedure **3** to obtain the title compound **104** [100% (theoretical)] as a white solid; ^1H (400 MHz; DMSO) δ 1.07-1.24 [2H, m], 1.31-1.44 [4H, m], 1.49-1.73 [3H, m], 1.79-1.94 [2H, m], 2.62-3.81 [2H, m], 3.13 [2H, q, J 7.4], 3.61 [2H, q, J 7.4], 3.80-3.90 [1H, m], 4.07 [2H, t, J 6], 4.37 [2H, q, J 7.4], 7.20 [1H, d, J 8.5], 7.76 [1H, t, J 8.5], 7.86 [2H, bs], 8.15 [2H, bs], 8.35 [1H, d, J 8.5], 8.47 [1H, dd, J 1 and 7.4], 8.54 [1H, dd, J 1 and 7.4]; ^{13}C (101 MHz; CDCl_3) δ 167.31, 164.21, 163.52, 160.99, 134.97, 131.64, 129.68, 126.01, 122.98, 122.26, 120.31, 117.43, 114.60, 112.96, 111.65, 110.47, 53.97, 49.80, 45.63, 42.18, 38.87, 37.57, 34.68, 34.34, 30.33, 27.05, 21.30, 18.42, 170.60, 164.90, 164.20, 155.82, 139.9, 131.19, 130.51, 129.40, 125.2, 122.5, 113.54, 110.4, 110.22, 79.80, 55.82, 43.64, 42.68, 34.2, 32.70, 32.57, 31.85, 28.53, 26.68, 22.51, 18.21; m/z (ESI; 98%) Calc. for $\text{C}_{25}\text{H}_{32}\text{N}_4\text{O}_4 = 452.56$ found 453.7 $[\text{M}+\text{H}]^+$

tert-butyl 4-((tert-butoxycarbonyl)(3-(4-(2-(6-hydroxy-1,3-dioxo-1H-benzo[de]isoquinolin-2(3H)-yl)ethyl)piperidin-1-yl)-3-oxopropyl)amino)piperidine-1-carboxylate **105a**



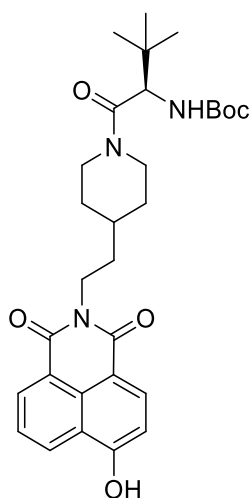
This compound was then synthesised according to General Chemistry Procedure **6**. The crude material was then dissolved in DCM (1 mL) and purified by silica gel chromatography using a gradient of 0-100% EtOAc in Cy to obtain the title compound **105a** (34%) as a yellow oil; R_f 0.71 (100% EtOAc; ¹H (400 MHz; CDCl₃) δ 1.11-1.28 [2H, m], 1.44 [18H, s], 1.53-1.75 [7H, m], 1.81-2.00 [2H, m], 2.54-2.65 [2H, m], 3.03 [1H, t, *J* 7.3], 3.43-3.48 [2H, m], 3.83-3.94 [2H, m], 4.12-4.40 [4H, m], 4.60 [1H, q, *J* 7.4], 7.10 [1H, d, *J* 8.5], 7.66 [1H, t, *J* 8.5], 8.44 [1H, d, *J* 8.5], 8.57 [1H, dd, *J* 1 and 7.4], 8.61 [1H, dd, *J* 1 and 7.4]; ¹³C (101 MHz; CDCl₃) δ 171.60, 164.71, 164.12, 158.69, 155.48, 154.75, 133.94, 131.68, 130.01, 129.47, 125.26, 123.18, 122.23, 113.32, 110.33, 80.34, 80.37, 63.20, 53.70, 50.89, 46.01, 42.12, 37.86, 34.47, 34.15, 32.62, 28.54, 28.50, 18.32; *m/z* (ESI; 99%) Calc. for C₃₇H₅₀N₄O₈ = 678.83 found 679.9 [M+H]⁺

6-hydroxy-2-(2-(1-(3-(piperidin-4-ylamino)propanoyl)piperidin-4-yl)ethyl)-1H-benzo[de]isoquinoline-1,3(2H)-dione **105**



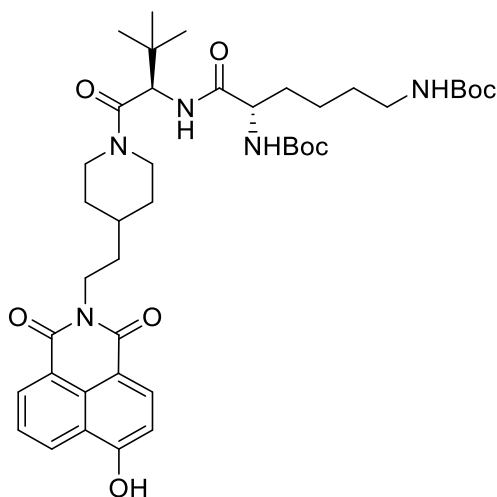
This compound was synthesised according to General Chemistry Procedure **3** to obtain the title compound **105** [100% (theoretical)] as a white solid; ^1H (400 MHz; DMSO) δ 1.54-1.62 [3H, m], 1.70-1.89 [4H, m], 1.81-2.00 [2H, m], 2.19 [2H, d, J 12] 2.60 [1H, t, J 12] 2.72-2.79 [2H, m], 2.87-3.02 [3H, m], 3.11-3.22 [2H, m], 3.33-3.44 [3H, m], 3.78 [1H, d J 12.0], 4.06 [2H, t, J 7.1] 4.33-4.32 [1H, d, J 12], 7.18 [1H, d, J 8.5], 7.45 [1H, t, J 8.4], 8.44 [1H, d, J 8.5], 8.84 [1H, dd, J 1 and 8.4], 8.53 [1H, dd, J 1 and 8.4] 8.83 [2H, bd]; ^{13}C (101 MHz; DMSO) δ 167.87, 164.17, 163.49, 160.91, 134.05, 131.56, 129.64, 129.40, 125.98, 122.91, 122.28, 120.44, 117.49, 114.60, 112.99, 111.71, 110.46, 53.98, 52.41, 45.29, 42.13, 41.73, 36.67, 34.62, 33.87, 32.46, 31.96, 29.34, 25.58; m/z (ESI; 99%) Calc. for $\text{C}_{27}\text{H}_{34}\text{N}_4\text{O}_4$ = 478.59 found 479.7 $[\text{M}+\text{H}]^+$

tert-Butyl (R)-(1-(4-(2-(6-hydroxy-1,3-dioxo-1H-benzo[de]isoquinolin-2(3H)-yl)ethyl)piperidin-1-yl)-3,3-dimethyl-1-oxobutan-2-yl)carbamate **106b**



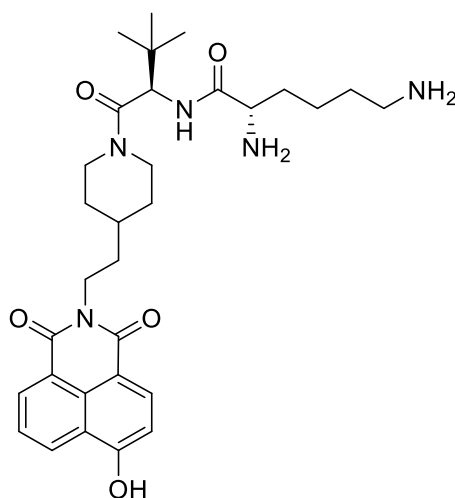
This compound was then synthesised according to General Chemistry Procedure **6**. The crude material was then dissolved in DCM (1 mL) and purified by silica gel chromatography using a gradient of 0-100% EtOAc in Cy to obtain the title compound **106b** (51%) as a yellow oil; *R*_f 0.15 [EtOAc: Cy (7:3)]; ¹H (400 MHz; CDCl₃) δ 0.98 [9H, s], 1.42 [9H, s], 1.56-1.74 [2H, m], 1.79-1.95 [2H, m], 2.57 [1H, q, *J* 7.3], 3.161 [2H, q, *J* 7.4], 3.65 [2H, q, *J* 7.4], 4.14-4.4 [2H, m], 4.57 [1H, q, *J* 7.4], 6.95 [1H, d, *J* 8.5], 7.72 [1H, t, *J* 8.5], 8.42 [1H, d, *J* 8.5], 8.56 [1H, dd, *J* 1 and 7.4], 8.60 [1H, dd, *J* 1 and 7.4], 9.30 [1H, bs]; ¹³C (101 MHz; CDCl₃) δ 173.47, 164.99, 164.27, 160.82, 134.51, 131.65, 129.71, 129.60, 124.71, 123.28, 122.24, 113.24, 110.24, 79.63, 65.73, 47.48, 46.45, 42.68, 35.55, 32.57, 31.88, 28.54, 26.68, 18.21; *m/z* (ESI; 98%) Calc. for C₃₀H₃₉N₃O₆ = 537.66 found 538.7 [M+H]⁺

Di-*tert*-butyl ((*S*)-6-(((*R*)-1-(4-(2-(6-hydroxy-1,3-dioxo-1H-benzo[de]isoquinolin-2(3H)-yl)ethyl)piperidin-1-yl)-3,3-dimethyl-1-oxobutan-2-yl)amino)-6-oxohexane-1,5-diyl)dicarbamate **106b**



To a stirred solution of *tert*-butyl (*R*)-(1-(4-(2-(6-hydroxy-1,3-dioxo-1H-benzo[de]isoquinolin-2(3H)-yl)ethyl)piperidin-1-yl)-3,3-dimethyl-1-oxobutan-2-yl) carbamate (0.50 g, 0.1 mmol, 1 eq) in DCM (5 mL) was added TFA (2 mL) and the solution stirred for 20 mins. This compound was then synthesised according to General Chemistry Procedure 6. The crude material was then dissolved in DCM (1 mL) and purified by silica gel chromatography using a gradient of 0-100% EtOAc in Cy to obtain the title compound **106b** (46%) as a yellow oil; R_f 0.5 (100% EtOAc); δ 0.98 [9H, s], 1.42 [9H, s], 1.56-1.74 [2H, m], 1.79-1.95 [2H, m], 2.57 [1H, q, J 7.3], 3.161 [2H, q, J 7.4], 3.65 [2H, q, J 7.4], 4.14-4.4 [2H, m], 4.57 [1H, q, J 7.4], 6.95 [1H, d, J 8.5], 7.72 [1H, t, J 8.5], 8.42 [1H, d, J 8.5], 8.56 [1H, dd, J 1 and 7.4], 8.60 [1H, dd, J 1 and 7.4], 9.30 [1H, bs]; ^{13}C (101 MHz; CDCl_3) δ 173.47, 164.99, 164.27, 160.82, 134.51, 131.65, 129.71, 129.60, 124.71, 123.28, 122.24, 113.24, 110.24, 79.63, 65.73 47.48, 46.45, 42.68, 35.55, 32.57, 31.88, 28.54, 26.68, 18.21; m/z (ESI; 98%) Calc. for $\text{C}_{30}\text{H}_{39}\text{N}_3\text{O}_6 = 537.66$ found 538.7 $[\text{M}+\text{H}]^+$

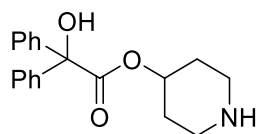
(S)-2,6-diamino-N-((R)-1-(4-(2-(6-hydroxy-1,3-dioxo-1H-benzo[de]isoquinolin-2(3H)-yl)ethyl)piperidin-1-yl)-3,3-dimethyl-1-oxobutan-2-yl)hexanamide **106**



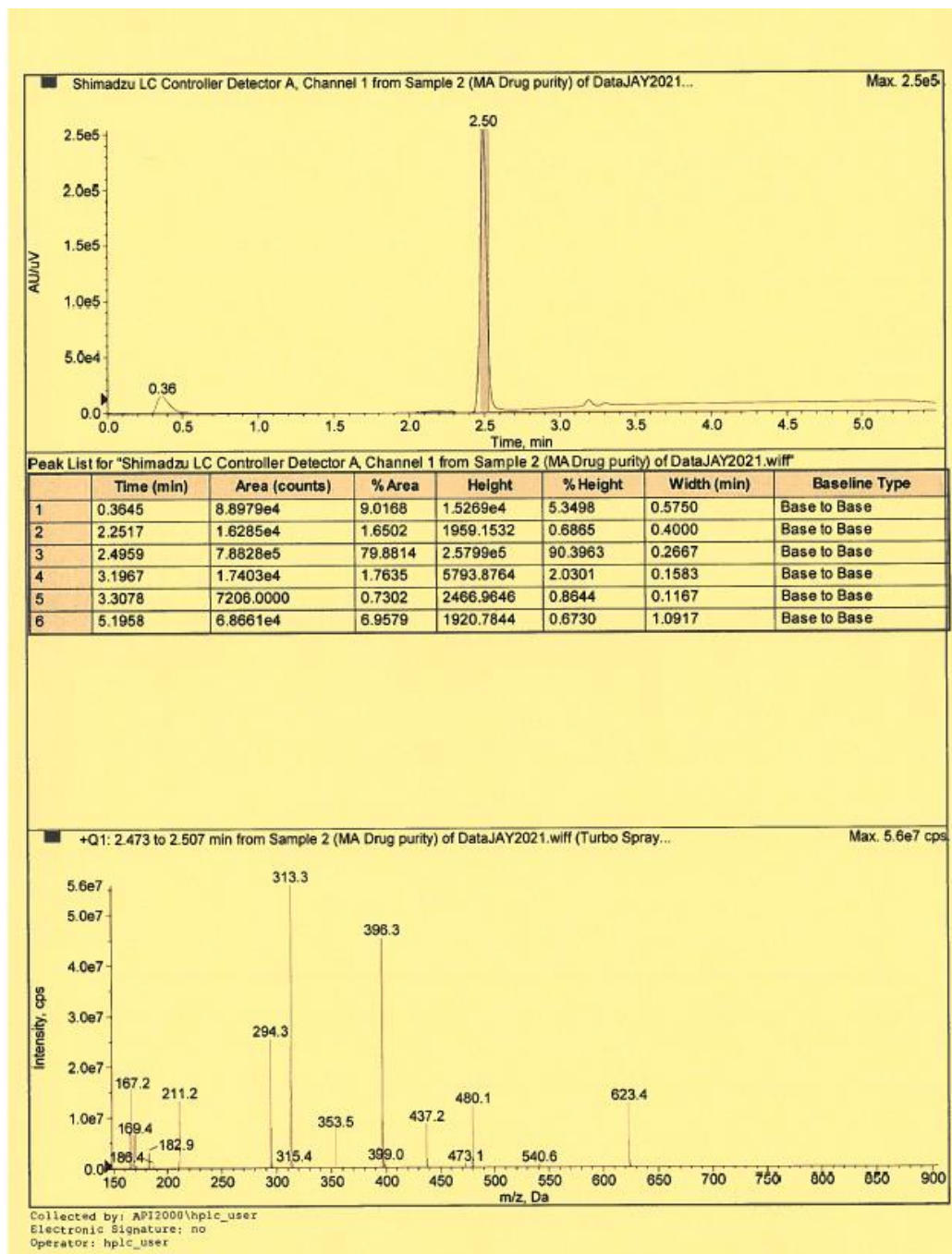
This compound was synthesised according to General Chemistry Procedure **3** to obtain the title compound **106** [100% (theoretical)] as a white solid; ^1H (400 MHz; DMSO) δ 0.98 [9H, s], 1.34-1.36 [2H, m], 1.50-1.67 [6H, m], 1.68-1.91 [4H, m], 2.74 [1H, q, J 7.3], 3.00-3.08 [1H, m], 3.56-3.65 [2H, m], 4.03-4.20 [4H, m], 4.42 [1H, q, J 7.4], 4.75-4.85 [2H, m], 6.27 [1H, d, J 8.5], 7.79 [1H, t, J 8.5], 7.96 [2H, bs] 8.19 [2H, bs], 8.36 [1H, d, J 8.5], 8.49 [1H, dd, J 1 and 7.4], 8.56 [1H, dd, J 1 and 7.4]; ^{13}C (101 MHz; DMSO) δ 169.2, 164.5, 163.4, 160.8, 134.23, 131.75, 129.86, 129.56, 126.13, 122.92, 122.34, 112.99, 110.55, 53.92, 52.20, 46.27, 44.06, 42.16, 38.82, 35.55, 35.34, 31.46, 27.06, 21.65, 18.52, 17.17 173.47, 164.99, 164.27, 160.82, 134.51, 131.65, 129.71, 129.60, 124.71, 123.28, 122.24, 113.24, 110.24, 79.63, 65.73 47.48, 46.45, 42.68, 35.55, 32.57, 31.88, 28.54, 26.68, 18.21; m/z (ESI; 98%) Calc. for $\text{C}_{31}\text{H}_{43}\text{N}_5\text{O}_5 = 565.72$ found 566.8 $[\text{M}+\text{H}]^+$

7. Appendix

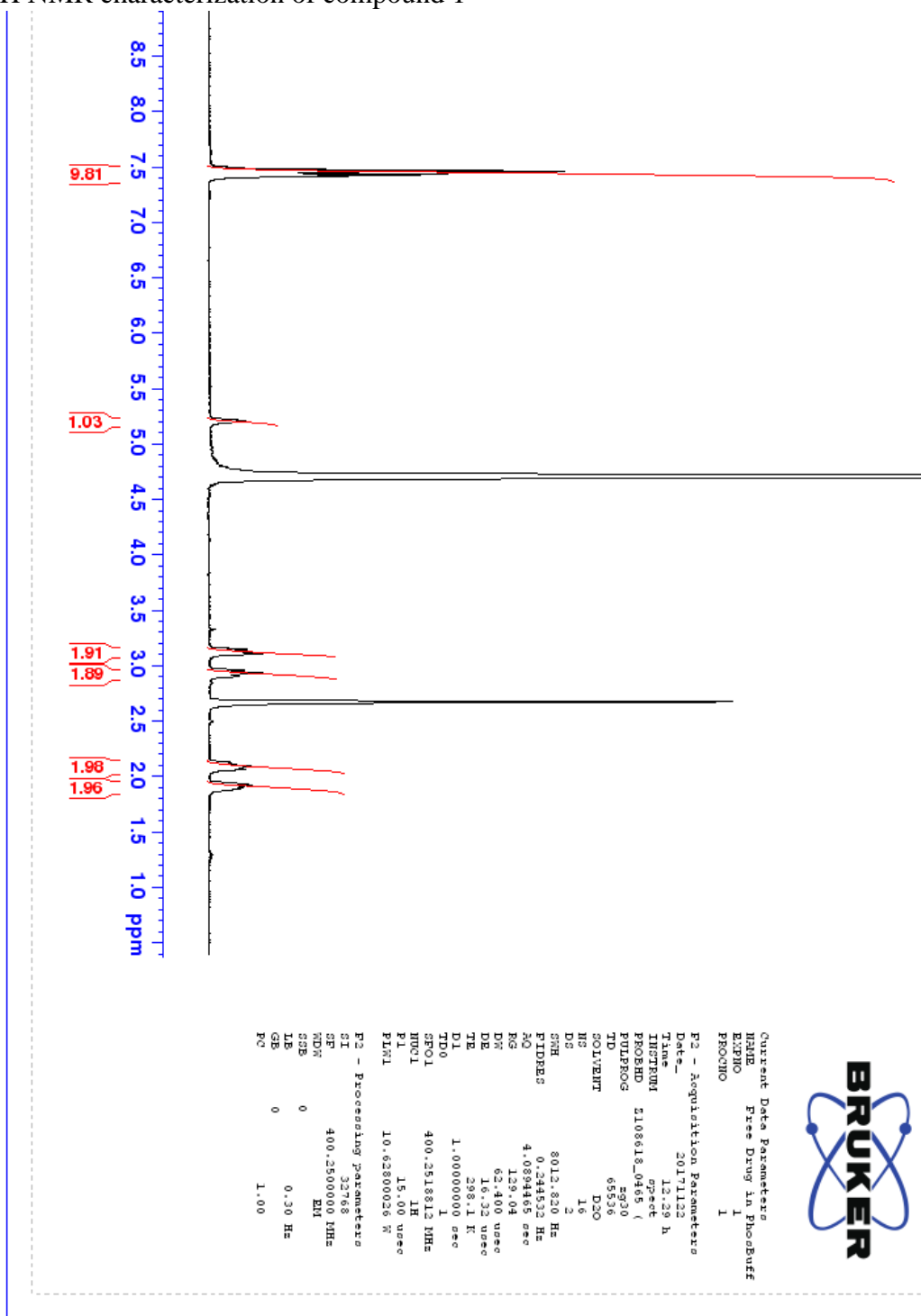
7.1 Structural characterization of compound 1



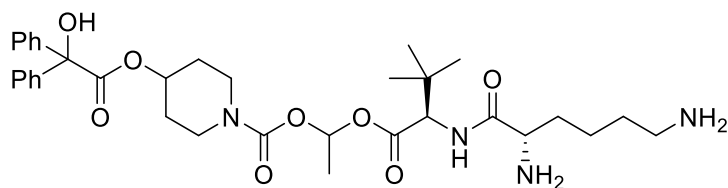
LCMS purity and molecular weight trace:



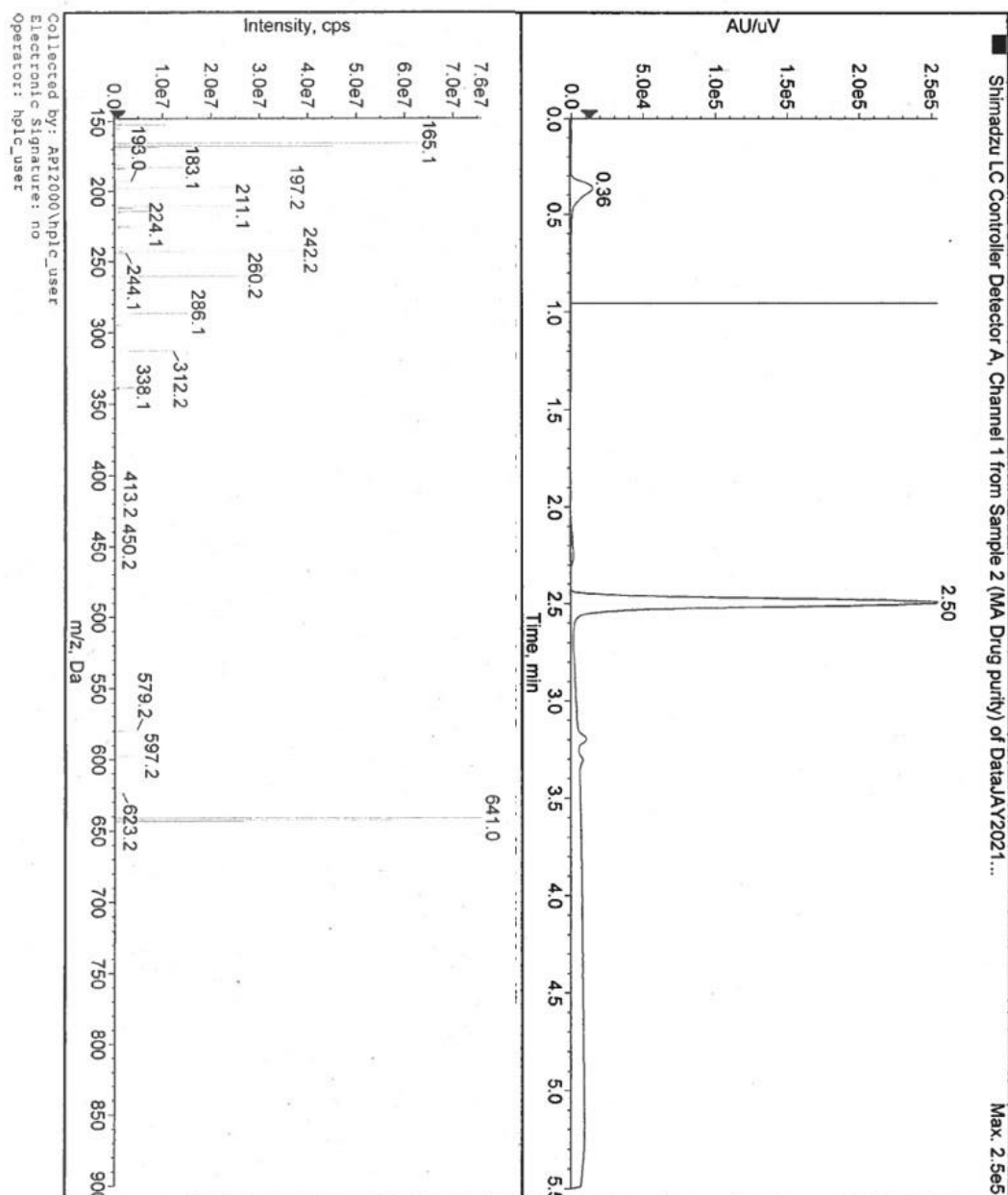
¹H NMR characterization of compound 1



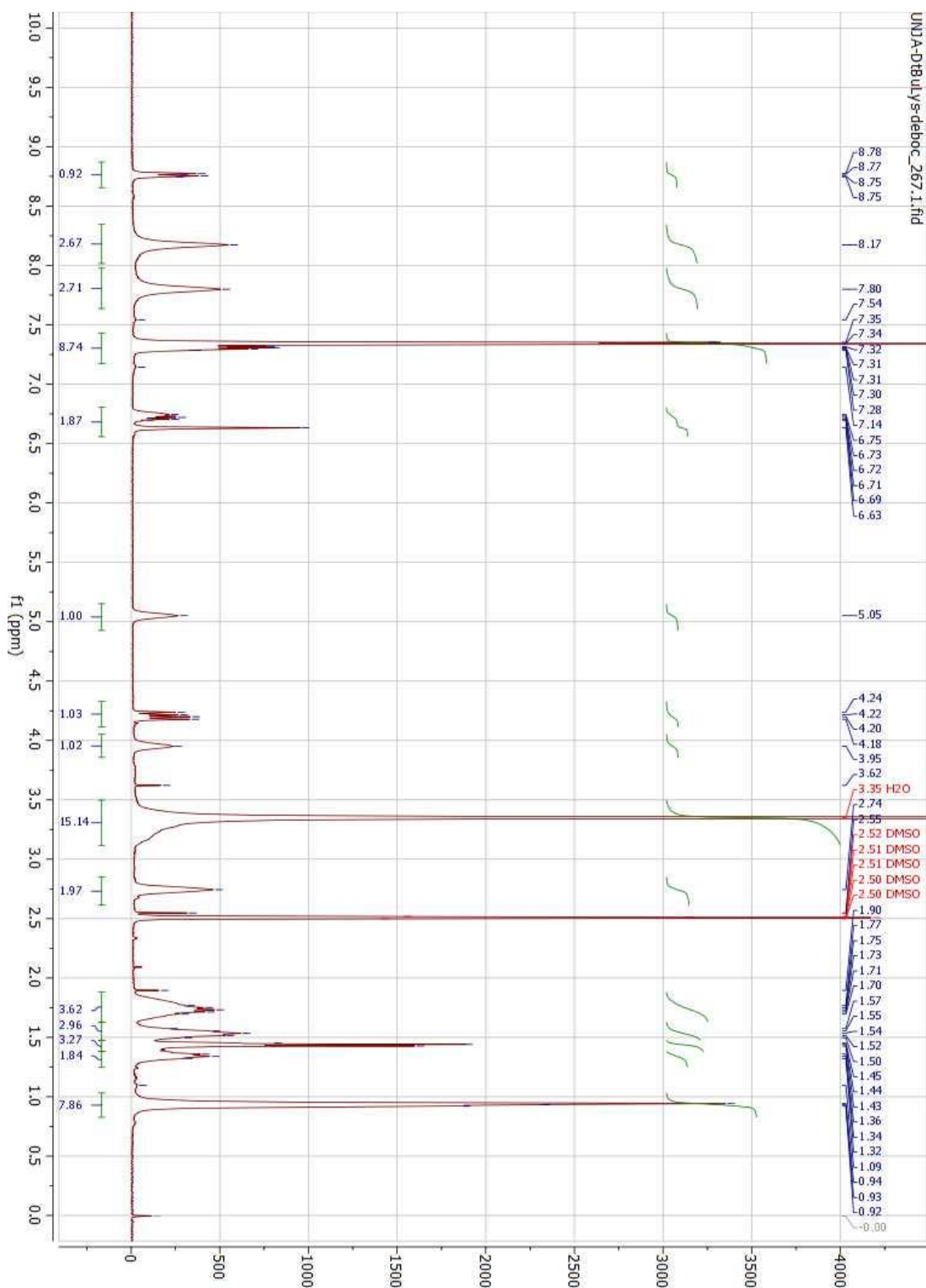
7.2 Structural characterization of compound 24



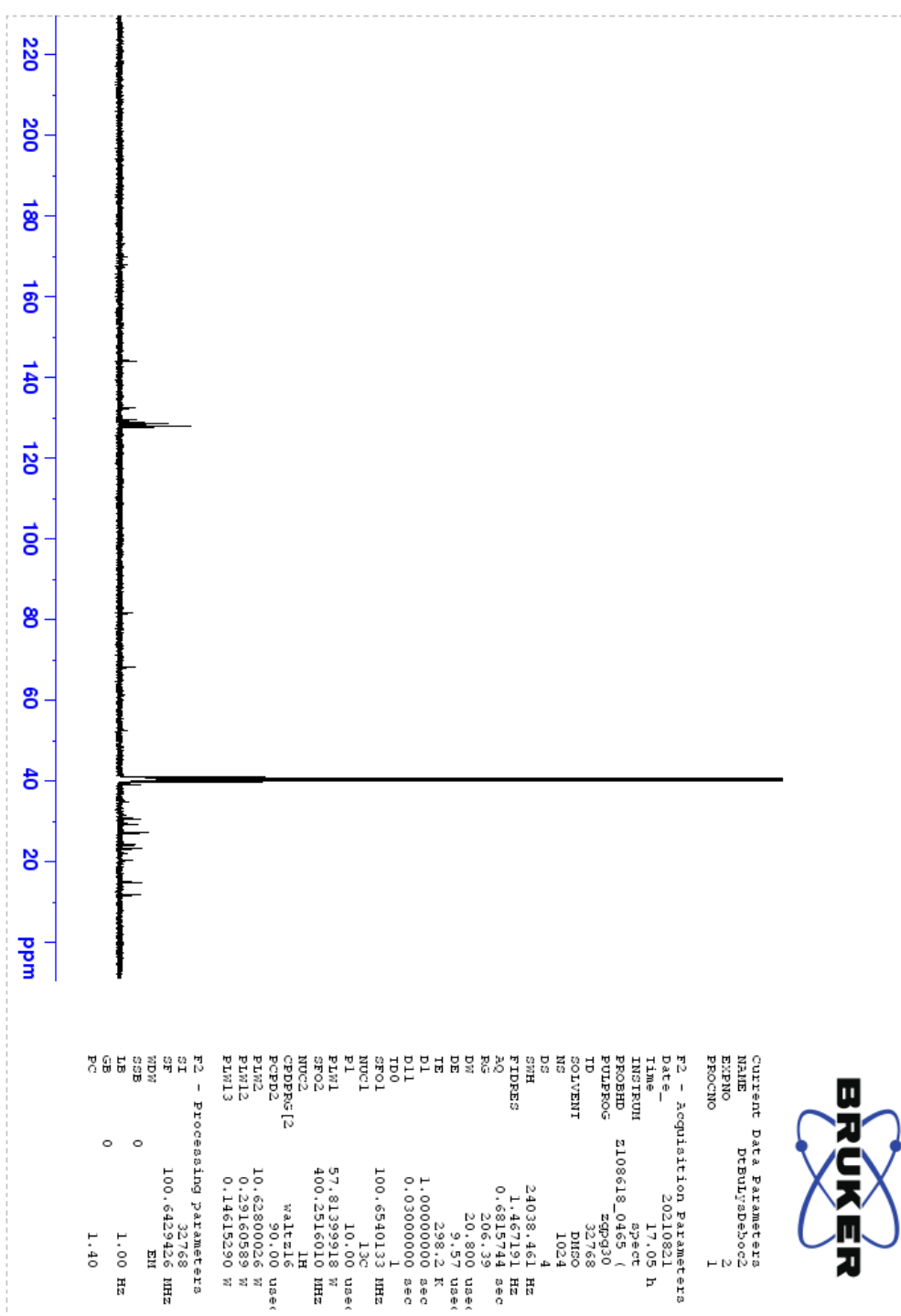
LCMS purity and molecular weight trace:



¹H NMR characterization of compound 24



¹³C NMR characterization of compound 24

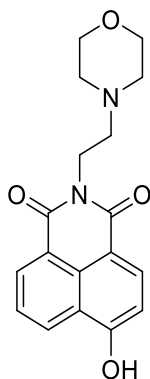


Current Data Parameters
 NAME: Drcbujspdboc2
 EXPNO: 2
 PROCNO: 1

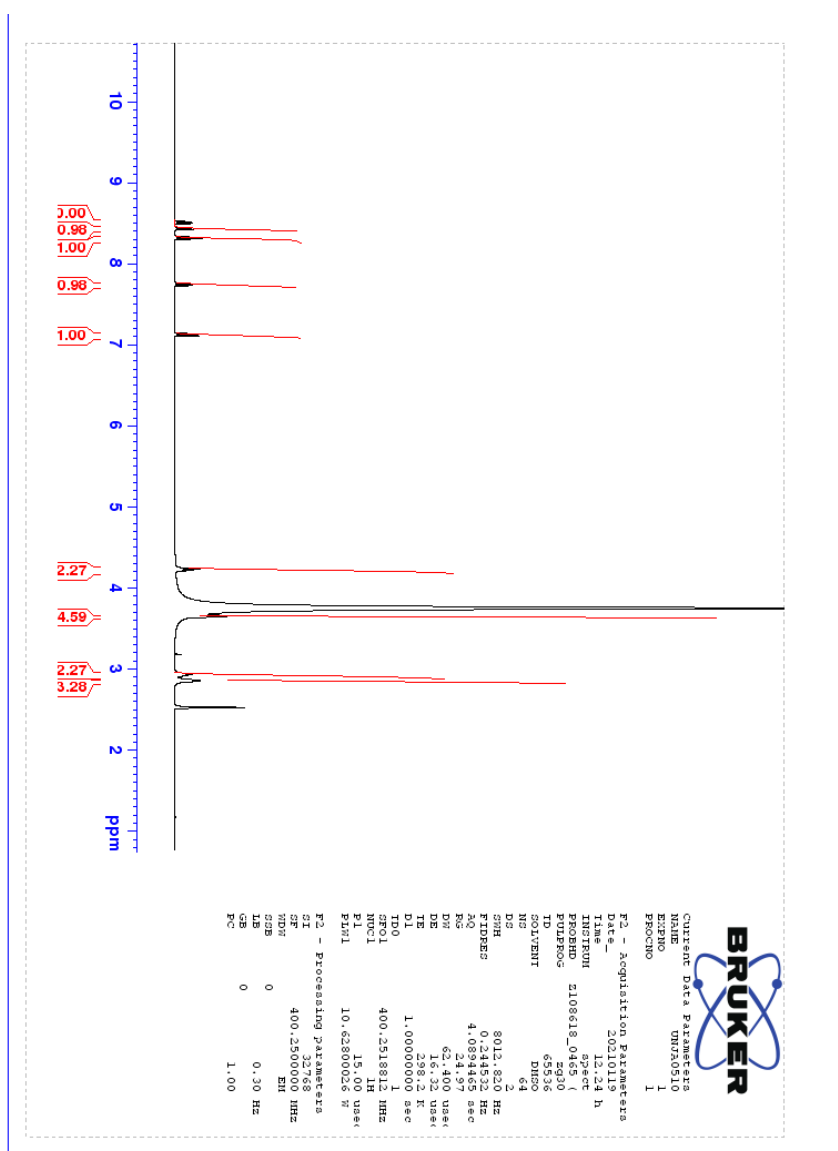
F2 - Acquisition Parameters
 Date_: 20210821
 Time: 17.05 h
 INSTRUM: spect
 PROBHD: zgpg30
 PULPROG: zgpg30
 TD: 32768
 SOLVENT: DMSO
 NS: 1024
 DS: 4
 SWH: 24038.461 Hz
 FIDRES: 1.487191 Hz
 AQ: 0.6815744 sec
 RG: 206.39
 DW: 20.800 usec
 DE: 9.57 usec
 TE: 298.2 K
 D1: 1.00000000 sec
 D11: 0.03000000 sec
 TDO: 1
 SFO1: 100.6540133 MHz
 NUC1: ¹³C
 F1: 10.00 usec
 PLM1: 57.8139918 W
 SFO2: 400.2516010 MHz
 NUC2: ¹H
 CPDPRG2: waltz16
 PCPD2: 90.00 usec
 PLM2: 10.62800026 W
 PLM12: 0.29180589 W
 PLM13: 0.14615290 W

F2 - Processing parameters
 SI: 32768
 SF: 100.6429426 MHz
 MDW: EH
 SSB: 0
 IB: 1.00 Hz
 GB: 0
 PC: 1.40

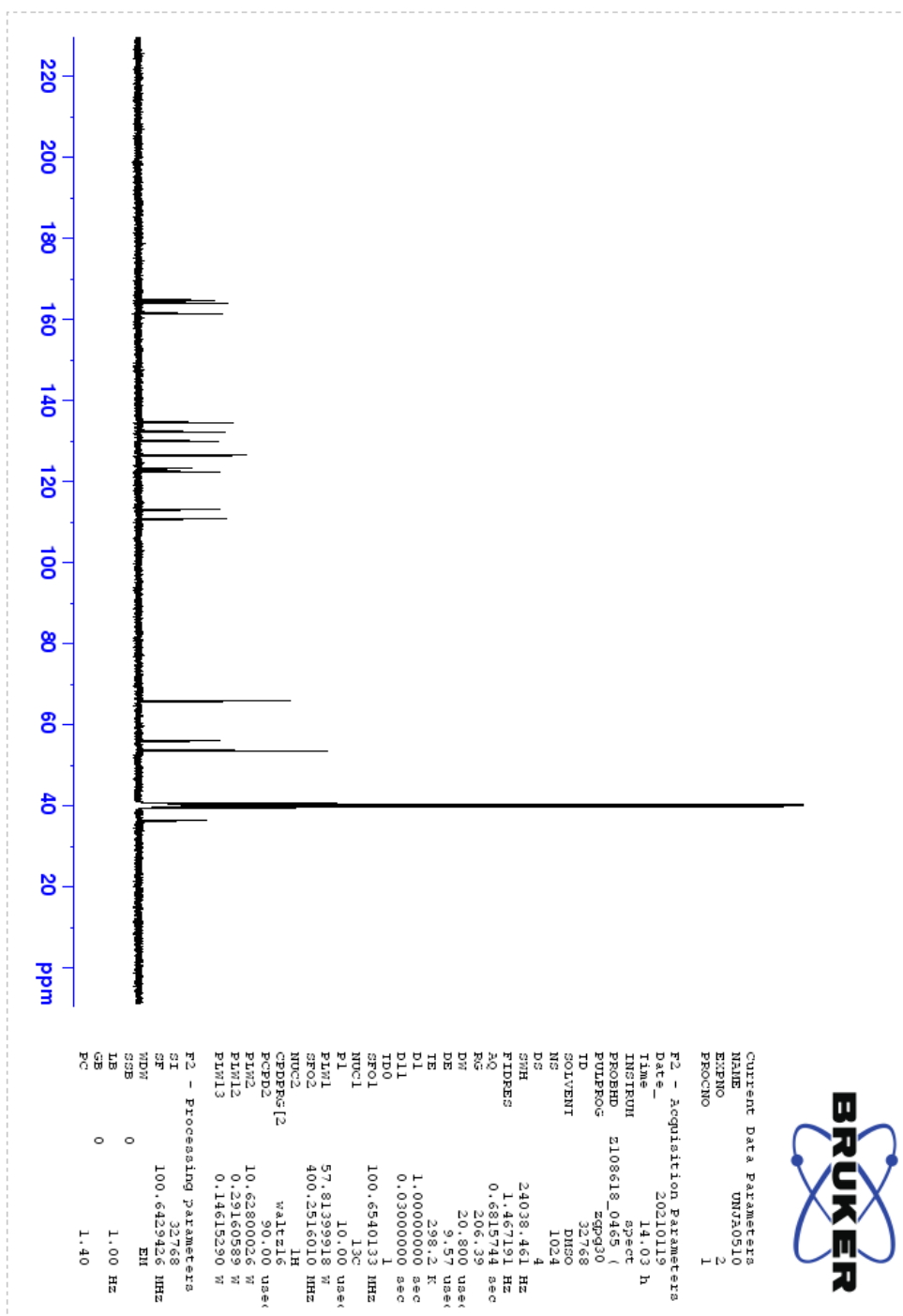
7.3 Structural characterization of compound 95



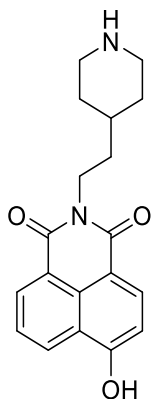
¹H NMR characterization of compound 95



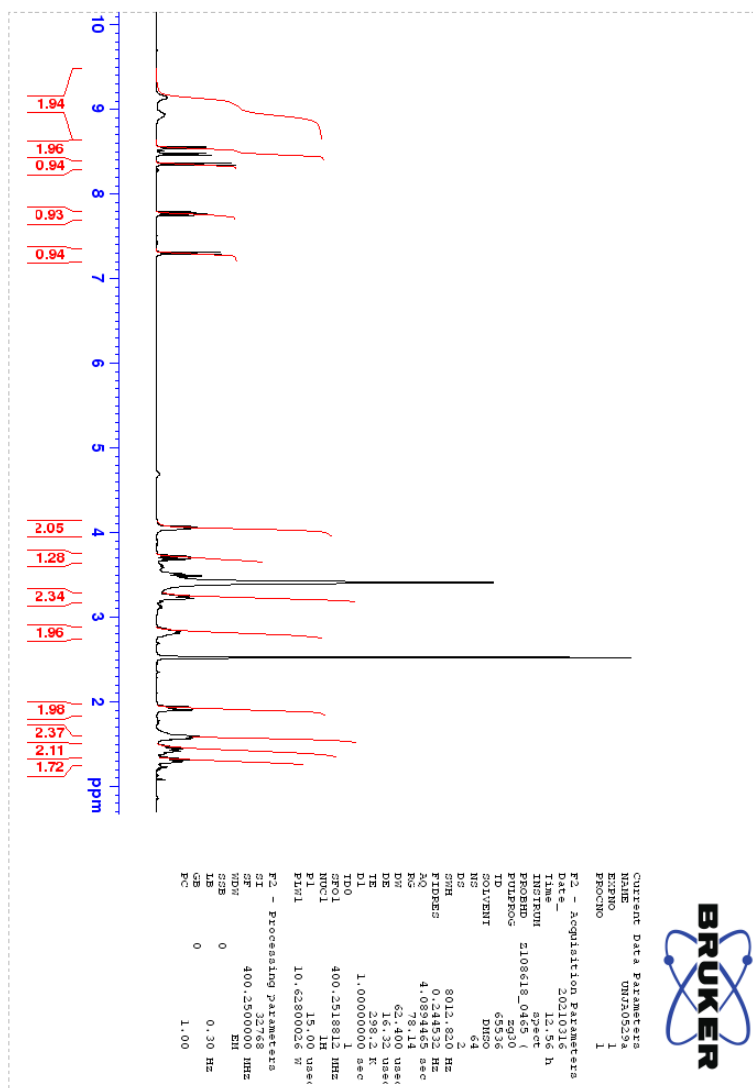
¹³C NMR characterization of compound 95



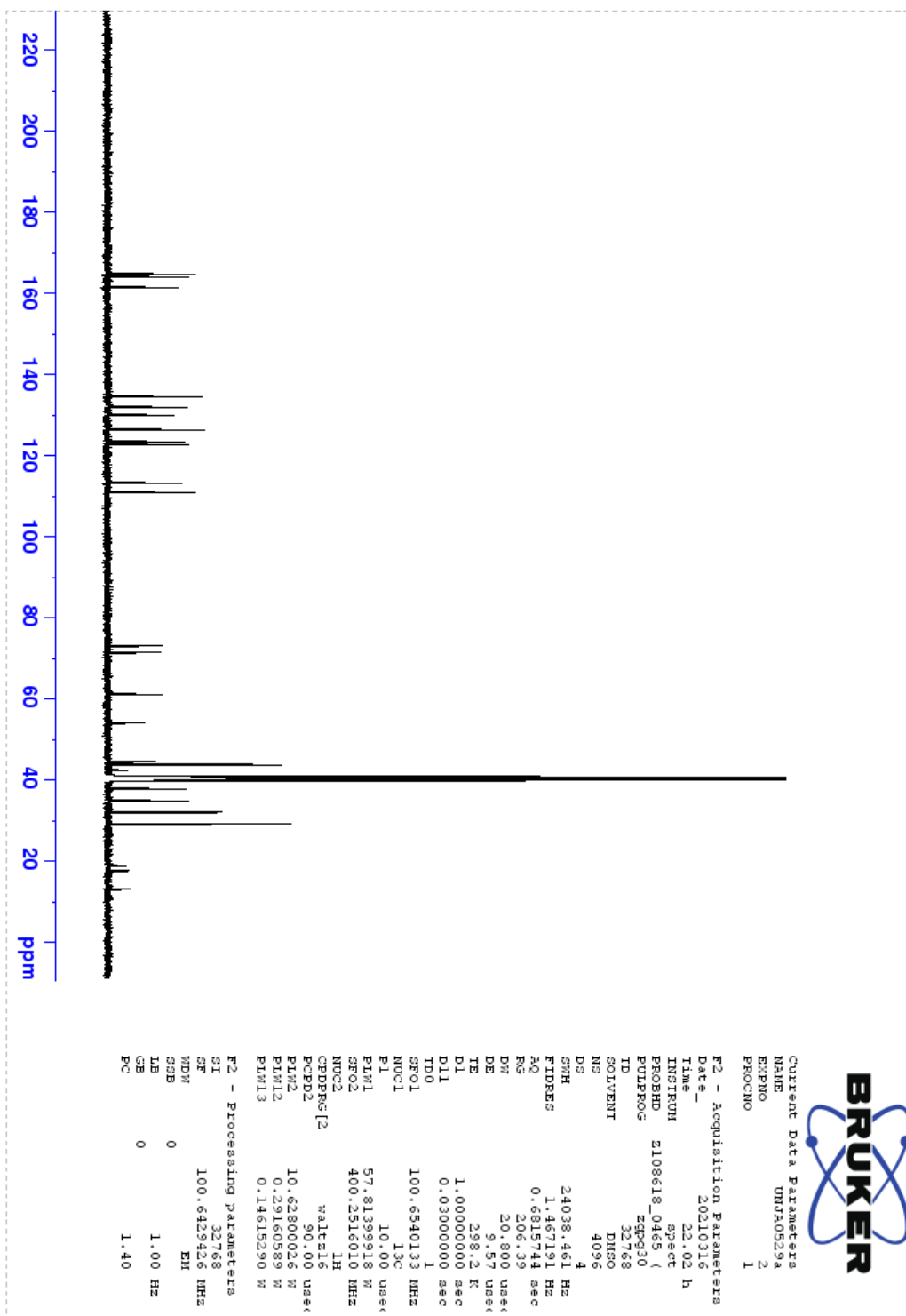
7.4 Structural characterization of compound 102



¹H NMR characterization of compound 102



¹³C NMR characterization of compound 102



8. References

- (1) Stein, S. W.; Thiel, C. G. The History of Therapeutic Aerosols: A Chronological Review. *J. Aerosol Med. Pulm. Drug Deliv.* **2017**, *30* (1), 20–41.
- (2) Stein, S. W.; Sheth, P.; Hodson, P. D.; Myrdal, P. B. Advances in Metered Dose Inhaler Technology: Hardware Development. *AAPS PharmSciTech* **2014**, *15* (2), 326–338.
- (3) White, S.; Bennett, D. B.; Cheu, S.; Conley, P. W.; Guzek, D. B.; Gray, S.; Howard, J.; Malcolmson, R.; Parker, J. M.; Roberts, P.; et al. EXUBERA®: Pharmaceutical Development of a Novel Product for Pulmonary Delivery of Insulin. *Diabetes Technol. Ther.* **2005**, *7* (6), 896–906.
- (4) Patton, J. S. Mechanisms of Macromolecule Absorption by the Lungs. *Adv. Drug Deliv. Rev.* **1996**, *19* (1), 3–36.
- (5) Feng, Y.; Xu, Z.; Haghnegahdar, A. Computational Fluid-Particle Dynamics Modeling for Unconventional Inhaled Aerosols in Human Respiratory Systems. In *Aerosols - Science and Case Studies*; InTech, 2016.
- (6) Camelo, A.; Dunmore, R.; Sleeman, M. A.; Clarke, D. L. The Epithelium in Idiopathic Pulmonary Fibrosis: Breaking the Barrier. *Front. Pharmacol.* **2014**, *4*.
- (7) Kia'i, N.; Bajaj, T. *Histology, Respiratory Epithelium*; 2021.
- (8) Dao, D.-P. D.; Le, P. H. *Histology, Goblet Cells*; 2021.
- (9) Weibel, E. R. *Morphometry of the Human Lung*; Elsevier, 1963.
- (10) Rokicki, W.; Rokicki, M.; Wojtacha, J.; Dzeljijli, A. The Role and Importance of Club Cells (Clara Cells) in the Pathogenesis of Some Respiratory Diseases. *Polish J. Cardio-Thoracic Surg.* **2016**, *1*, 26–30.
- (11) Brandt, J. P.; Mandiga, P. *Histology, Alveolar Cells*; 2021.
- (12) Ng, A. W.; Bidani, A.; Heming, T. A. Innate Host Defense of the Lung: Effects of Lung-Lining Fluid PH. *Lung* **2004**, *182* (5), 297–317.
- (13) Bernhard, W. Lung Surfactant: Function and Composition in the Context of Development and Respiratory Physiology. *Ann. Anat. - Anat. Anzeiger* **2016**, *208*, 146–150.
- (14) Wiedmann, T. .; Bhatia, R.; Wattenberg, L. . Drug Solubilization in Lung Surfactant. *J. Control. Release* **2000**, *65* (1–2), 43–47.
- (15) Mirastschijski, U.; Dembinski, R.; Maedler, K. Lung Surfactant for Pulmonary Barrier Restoration in Patients With COVID-19 Pneumonia. *Front. Med.* **2020**, *7*.
- (16) Veldhuizen, E. J. .; Haagsman, H. P. Role of Pulmonary Surfactant Components in Surface Film Formation and Dynamics. *Biochim. Biophys. Acta - Biomembr.* **2000**, *1467* (2), 255–270.
- (17) Rubin, B. K.; Williams, R. W. Emerging Aerosol Drug Delivery Strategies: From Bench to Clinic. *Adv. Drug Deliv. Rev.* **2014**, *75*, 141–148.
- (18) Sanchis, J.; Corrigan, C.; Levy, M. L.; Viejo, J. L. Inhaler Devices – From Theory to Practice. *Respir. Med.* **2013**, *107* (4), 495–502.
- (19) Garcia-Contreras, L.; Ibrahim, M.; Verma, R. Inhalation Drug Delivery Devices: Technology Update. *Med. Devices Evid. Res.* **2015**, 131.
- (20) Rau, J. L. The Inhalation of Drugs: Advantages and Problems. *Respir. Care* **2005**, *50* (3), 367–382.
- (21) Godara, N.; Khullar, M.; Godara, R. Impact of Inhalation Therapy on Oral Health. *Lung India* **2011**, *28* (4), 272.

-
- (22) Ibrahim, M.; Garcia-Contreras, L. Mechanisms of Absorption and Elimination of Drugs Administered by Inhalation. *Ther. Deliv.* **2013**, *4* (8), 1027–1045.
- (23) Labiris, N. R.; Dolovich, M. B. Pulmonary Drug Delivery. Part I: Physiological Factors Affecting Therapeutic Effectiveness of Aerosolized Medications. *Br. J. Clin. Pharmacol.* **2003**, *56* (6), 588–599.
- (24) Bustamante-Marin, X. M.; Ostrowski, L. E. Cilia and Mucociliary Clearance. *Cold Spring Harb. Perspect. Biol.* **2017**, *9* (4), a028241.
- (25) Patton, J. S. The Lungs as a Portal of Entry for Systemic Drug Delivery. *Proc. Am. Thorac. Soc.* **2004**, *1* (4), 338–344.
- (26) Ritchie, T. J.; Luscombe, C. N.; Macdonald, S. J. F. Analysis of the Calculated Physicochemical Properties of Respiratory Drugs: Can We Design for Inhaled Drugs Yet? *J. Chem. Inf. Model.* **2009**, *49* (4), 1025–1032.
- (27) Stocks, M. The Small Molecule Drug Discovery Process – from Target Selection to Candidate Selection. In *Introduction to Biological and Small Molecule Drug Research and Development*; Elsevier, 2013; pp 81–126.
- (28) Le Vée, M.; Jouan, E.; Fardel, O. Carrier-Mediated Uptake of Clonidine in Cultured Human Lung Cells. *Naunyn. Schmiedeberg's Arch. Pharmacol.* **2018**, *391* (4), 361–369.
- (29) Ingoglia, F.; Visigalli, R.; Rotoli, B. M.; Barilli, A.; Riccardi, B.; Puccini, P.; Dall'Asta, V. Functional Characterization of the Organic Cation Transporters (OCTs) in Human Airway Pulmonary Epithelial Cells. *Biochim. Biophys. Acta - Biomembr.* **2015**, *1848* (7), 1563–1572.
- (30) Groneberg, D. A.; Nickolaus, M.; Springer, J.; Döring, F.; Daniel, H.; Fischer, A. Localization of the Peptide Transporter PEPT2 in the Lung. *Am. J. Pathol.* **2001**, *158* (2), 707–714.
- (31) Hayer-Zillgen, M.; Brüss, M.; Bönisch, H. Expression and Pharmacological Profile of the Human Organic Cation Transporters HOCT1, HOCT2 and HOCT3. *Br. J. Pharmacol.* **2002**, *136* (6), 829–836.
- (32) Wang, J. The Plasma Membrane Monoamine Transporter (PMAT): Structure, Function, and Role in Organic Cation Disposition. *Clin. Pharmacol. Ther.* **2016**, *100* (5), 489–499.
- (33) Koepsell, H.; Lips, K.; Volk, C. Polyspecific Organic Cation Transporters: Structure, Function, Physiological Roles, and Biopharmaceutical Implications. *Pharm. Res.* **2007**, *24* (7), 1227–1251.
- (34) Mukherjee, M.; Cingolani, E.; Pritchard, D. I.; Bosquillon, C. Enhanced Expression of Organic Cation Transporters in Bronchial Epithelial Cell Layers Following Insults Associated with Asthma – Impact on Salbutamol Transport. *Eur. J. Pharm. Sci.* **2017**, *106*, 62–70.
- (35) Moreau, A.; Le Vee, M.; Jouan, E.; Parmentier, Y.; Fardel, O. Drug Transporter Expression in Human Macrophages. *Fundam. Clin. Pharmacol.* **2011**, *25* (6), 743–752.
- (36) Bosquillon, C. Drug Transporters in the Lung—Do They Play a Role in the Biopharmaceutics of Inhaled Drugs? *J. Pharm. Sci.* **2010**, *99* (5), 2240–2255.
- (37) Gumbleton, M.; Al-Jayyousi, G.; Crandon-Lewis, A.; Francombe, D.; Kreitmeyr, K.; Morris, C. J.; Smith, M. W. Spatial Expression and Functionality of Drug Transporters in the Intact Lung: Objectives for Further Research. *Adv. Drug Deliv. Rev.* **2011**, *63* (1–2), 110–118.
- (38) Gupta, D.; Varghese Gupta, S.; Dahan, A.; Tsume, Y.; Hilfinger, J.; Lee, K.-D.; Amidon, G. L. Increasing Oral Absorption of Polar Neuraminidase Inhibitors: A Prodrug Transporter Approach Applied to Oseltamivir Analogue. *Mol. Pharm.* **2013**, *10* (2), 512–522.
- (39) Groneberg, D. A. Distribution and Function of the Peptide Transporter PEPT2 in Normal and Cystic Fibrosis Human Lung. *Thorax* **2002**, *57* (1), 55–60.
- (40) Biegel, A.; Gebauer, S.; Brandsch, M.; Neubert, K.; Thondorf, I. Structural Requirements for

- the Substrates of the H⁺/Peptide Cotransporter PEPT2 Determined by Three-Dimensional Quantitative Structure–Activity Relationship Analysis. *J. Med. Chem.* **2006**, *49* (14), 4286–4296.
- (41) Biegel, A.; Gebauer, S.; Hartrodt, B.; Brandsch, M.; Neubert, K.; Thondorf, I. Three-Dimensional Quantitative Structure–Activity Relationship Analyses of β -Lactam Antibiotics and Tripeptides as Substrates of the Mammalian H⁺/Peptide Cotransporter PEPT1. *J. Med. Chem.* **2005**, *48* (13), 4410–4419.
- (42) Terada, T.; Sawada, K.; Irie, M.; Saito, H.; Hashimoto, Y.; Inui, K. Structural Requirements for Determining the Substrate Affinity of Peptide Transporters PEPT1 and PEPT2. *Pflügers Arch. - Eur. J. Physiol.* **2000**, *440* (5), 679–684.
- (43) Terada, T.; Saito, H.; Inui, K. Interaction of β -Lactam Antibiotics with Histidine Residue of Rat H⁺/Peptide Cotransporters, PEPT1 and PEPT2. *J. Biol. Chem.* **1998**, *273* (10), 5582–5585.
- (44) Döring, F.; Walter, J.; Will, J.; Föcking, M.; Boll, M.; Amasheh, S.; Clauss, W.; Daniel, H. Delta-Aminolevulinic Acid Transport by Intestinal and Renal Peptide Transporters and Its Physiological and Clinical Implications. *J. Clin. Invest.* **1998**, *101* (12), 2761–2767.
- (45) Rubio-Aliaga, I.; Daniel, H. Mammalian Peptide Transporters as Targets for Drug Delivery. *Trends Pharmacol. Sci.* **2002**, *23* (9), 434–440.
- (46) Biegel, A.; Knütter, I.; Hartrodt, B.; Gebauer, S.; Theis, S.; Luckner, P.; Kottra, G.; Rastetter, M.; Zebisch, K.; Thondorf, I.; et al. The Renal Type H⁺/Peptide Symporter PEPT2: Structure-Affinity Relationships. *Amino Acids* **2006**, *31* (2), 137–156.
- (47) Daniel, H.; Spanier, B.; Kottra, G.; Weitz, D. From Bacteria to Man: Archaic Proton-Dependent Peptide Transporters at Work. *Physiology* **2006**, *21* (2), 93–102.
- (48) Ganapathy, M. E.; Huang, W.; Wang, H.; Ganapathy, V.; Leibach, F. H. Valacyclovir: A Substrate for the Intestinal and Renal Peptide Transporters PEPT1 and PEPT2. *Biochem. Biophys. Res. Commun.* **1998**, *246* (2), 470–475.
- (49) Sawada, K.; Terada, T.; Saito, H.; Hashimoto, Y.; Inui, K. I. Recognition of L-Amino Acid Ester Compounds by Rat Peptide Transporters PEPT1 and PEPT2. *J. Pharmacol. Exp. Ther.* **1999**, *291* (2), 705–709.
- (50) Hendrickx, R.; Lamm Bergström, E.; Janzén, D. L. I.; Fridén, M.; Eriksson, U.; Grime, K.; Ferguson, D. Translational Model to Predict Pulmonary Pharmacokinetics and Efficacy in Man for Inhaled Bronchodilators. *CPT Pharmacometrics Syst. Pharmacol.* **2018**, *7* (3), 147–157.
- (51) Bäckström, E.; Hamm, G.; Nilsson, A.; Fihn, B.-M.; Strittmatter, N.; Andrén, P.; Goodwin, R. J. A.; Fridén, M. Uncovering the Regional Localization of Inhaled Salmeterol Retention in the Lung. *Drug Deliv.* **2018**, *25* (1), 838–845.
- (52) Hamm, G. R.; Bäckström, E.; Brülls, M.; Nilsson, A.; Strittmatter, N.; Andrén, P. E.; Grime, K.; Fridén, M.; Goodwin, R. J. A. Revealing the Regional Localization and Differential Lung Retention of Inhaled Compounds by Mass Spectrometry Imaging. *J. Aerosol Med. Pulm. Drug Deliv.* **2020**, *33* (1), 43–53.
- (53) Ascenzi, P.; Fanali, G.; Fasano, M.; Pallottini, V.; Trezza, V. Clinical Relevance of Drug Binding to Plasma Proteins. *J. Mol. Struct.* **2014**, *1077*, 4–13.
- (54) Salahudeen, M. S.; Nishtala, P. S. An Overview of Pharmacodynamic Modelling, Ligand-Binding Approach and Its Application in Clinical Practice. *Saudi Pharm. J.* **2017**, *25* (2), 165–175.
- (55) Davis, J. L. Pharmacologic Principles. In *Equine Internal Medicine*; Elsevier, 2018; pp 79–137.
- (56) Deb, P. K.; Al-Attraqchi, O.; Prasad, M. R.; Tekade, R. K. Protein and Tissue Binding. In *Dosage Form Design Considerations*; Elsevier, 2018; pp 371–399.

- (57) Valotis, A.; Högger, P. Human Receptor Kinetics and Lung Tissue Retention of the Enhanced-Affinity Glucocorticoid Fluticasone Furoate. *Respir. Res.* **2007**, *8* (1), 54.
- (58) Salter, M.; Biggadike, K.; Matthews, J. L.; West, M. R.; Haase, M. V.; Farrow, S. N.; Uings, I. J.; Gray, D. W. Pharmacological Properties of the Enhanced-Affinity Glucocorticoid Fluticasone Furoate in Vitro and in an in Vivo Model of Respiratory Inflammatory Disease. *Am. J. Physiol. Cell. Mol. Physiol.* **2007**, *293* (3), L660–L667.
- (59) E. Cooper, A.; Ferguson, D.; Grime, K. Optimisation of DMPK by the Inhaled Route: Challenges and Approaches. *Curr. Drug Metab.* **2012**, *13* (4), 457–473.
- (60) Bäckström, E.; Lundqvist, A.; Boger, E.; Svanberg, P.; Ewing, P.; Hammarlund-Udenaes, M.; Fridén, M. Development of a Novel Lung Slice Methodology for Profiling of Inhaled Compounds. *J. Pharm. Sci.* **2016**, *105* (2), 838–845.
- (61) Forgac, M. Structure and Function of Vacuolar Class of ATP-Driven Proton Pumps. *Physiol. Rev.* **1989**, *69* (3), 765–796.
- (62) Macintyre, A. C.; Cutler, D. J. The Potential Role of Lysosomes in Tissue Distribution of Weak Bases. *Biopharm. Drug Dispos.* **1988**, *9* (6), 513–526.
- (63) Goldman, S. D.; Funk, R. S.; Rajewski, R. A.; Krise, J. P. Mechanisms of Amine Accumulation in, and Egress from, Lysosomes. *Bioanalysis* **2009**, *1* (8), 1445–1459.
- (64) Ohkuma, S.; Poole, B. Cytoplasmic Vacuolation of Mouse Peritoneal Macrophages and the Uptake into Lysosomes of Weakly Basic Substances. *J. Cell Biol.* **1981**, *90* (3), 656–664.
- (65) Duvvuri, M.; Konkar, S.; Funk, R. S.; Krise, J. M.; Krise, J. P. A Chemical Strategy To Manipulate the Intracellular Localization of Drugs in Resistant Cancer Cells †. *Biochemistry* **2005**, *44* (48), 15743–15749.
- (66) Logan, R.; Funk, R. S.; Axcell, E.; Krise, J. P. Drug-Drug Interactions Involving Lysosomes: Mechanisms and Potential Clinical Implications. *Expert Opin. Drug Metab. Toxicol.* **2012**, *8* (8), 943–958.
- (67) Daniel, W. A.; Wójcikowski, J. Lysosomal Trapping as an Important Mechanism Involved in the Cellular Distribution of Perazine and in Pharmacokinetic Interaction with Antidepressants. *Eur. Neuropsychopharmacol.* **1999**, *9* (6), 483–491.
- (68) Bäckström, E.; Boger, E.; Lundqvist, A.; Hammarlund-Udenaes, M.; Fridén, M. Lung Retention by Lysosomal Trapping of Inhaled Drugs Can Be Predicted In Vitro With Lung Slices. *J. Pharm. Sci.* **2016**, *105* (11), 3432–3439.
- (69) Himstedt, A.; Braun, C.; Wicha, S. G.; Borghardt, J. M. Towards a Quantitative Mechanistic Understanding of Localized Pulmonary Tissue Retention—A Combined In Vivo/In Silico Approach Based on Four Model Drugs. *Pharmaceutics* **2020**, *12* (5), 408.
- (70) Stocks, M. J.; Alcaraz, L.; Bailey, A.; Bonnert, R.; Cadogan, E.; Christie, J.; Dixon, J.; Connolly, S.; Cook, A.; Fisher, A.; et al. Discovery of AZD3199, An Inhaled Ultralong Acting β 2 Receptor Agonist with Rapid Onset of Action. *ACS Med. Chem. Lett.* **2014**, *5* (4), 416–421.
- (71) Alcaraz, L.; Bailey, A.; Cadogan, E.; Connolly, S.; Jewell, R.; Jordan, S.; Kindon, N.; Lister, A.; Lawson, M.; Mullen, A.; et al. From Libraries to Candidate: The Discovery of New Ultra Long-Acting Dibasic β 2-Adrenoceptor Agonists. *Bioorganic Med. Chem. Lett.* **2012**, *22* (1), 689–695.
- (72) Austin, R. P.; Barton, P.; Bonnert, R. V.; Brown, R. C.; Cage, P. A.; Cheshire, D. R.; Davis, A. M.; Dougall, I. G.; Ince, F.; Pairaudeau, G.; et al. QSAR and the Rational Design of Long-Acting Dual D 2 -Receptor/ β 2 -Adrenoceptor Agonists. *J. Med. Chem.* **2003**, *46* (15), 3210–3220.
- (73) Perry, M. W. D.; Björhall, K.; Bonn, B.; Carlsson, J.; Chen, Y.; Eriksson, A.; Fredlund, L.; Hao, H.; Holden, N. S.; Karabelas, K.; et al. Design and Synthesis of Soluble and Cell-Permeable PI3K α Inhibitors for Long-Acting Inhaled Administration. *J. Med. Chem.* **2017**, *60*

- (12), 5057–5071.
- (74) Alven, S.; Nqoro, X.; Buyana, B.; Aderibigbe, B. A. Polymer-Drug Conjugate, a Potential Therapeutic to Combat Breast and Lung Cancer. *Pharmaceutics* **2020**, *12* (5), 406.
- (75) Guo, Y.; Bera, H.; Shi, C.; Zhang, L.; Cun, D.; Yang, M. Pharmaceutical Strategies to Extend Pulmonary Exposure of Inhaled Medicines. *Acta Pharm. Sin. B* **2021**.
- (76) Gursahani, H.; Riggs-Sauthier, J.; Pfeiffer, J.; Lechuga-Ballesteros, D.; Fishburn, C. S. Absorption of Polyethylene Glycol (PEG) Polymers: The Effect of PEG Size on Permeability. *J. Pharm. Sci.* **2009**, *98* (8), 2847–2856.
- (77) Bayard, F. J. C.; Thielemans, W.; Pritchard, D. I.; Paine, S. W.; Young, S. S.; Bäckman, P.; Ewing, P.; Bosquillon, C. Polyethylene Glycol-Drug Ester Conjugates for Prolonged Retention of Small Inhaled Drugs in the Lung. *J. Control. Release* **2013**, *171* (2), 234–240.
- (78) Wu, K.; Ma, J.; Bai, W.; Cui, X.; Han, T.; Wang, S.; Xie, Y.; Xie, Y. Short-Term Intratracheal Use of PEG-Modified IL-2 and Glucocorticoid Persistently Alleviates Asthma in a Mouse Model. *Sci. Rep.* **2016**, *6* (1), 31562.
- (79) Koussoroplis, S. J.; Paulissen, G.; Tyteca, D.; Goldansaz, H.; Todoroff, J.; Barilly, C.; Uyttenhove, C.; Van Snick, J.; Cataldo, D.; Vanbever, R. PEGylation of Antibody Fragments Greatly Increases Their Local Residence Time Following Delivery to the Respiratory Tract. *J. Control. Release* **2014**, *187*, 91–100.
- (80) Megwa, S. A.; Cross, S. E.; Benson, H. A. E.; Roberts, M. S. Ion-Pair Formation as a Strategy to Enhance Topical Delivery of Salicylic Acid. *J. Pharm. Pharmacol.* **2010**, *52* (8), 919–928.
- (81) Li, Y.; Zhang, Y.; Li, P.; Mi, G.; Tu, J.; Sun, L.; Webster, T. J.; Shen, Y. Ion-Paired Pirenzepine-Loaded Micelles as an Ophthalmic Delivery System for the Treatment of Myopia. *Nanomedicine Nanotechnology, Biol. Med.* **2017**, *13* (6), 2079–2089.
- (82) Samiei, N.; Mangas-Sanjuan, V.; González-Álvarez, I.; Foroutan, M.; Shafaati, A.; Zarghi, A.; Bermejo, M. Ion-Pair Strategy for Enabling Amifostine Oral Absorption: Rat in Situ and in Vivo Experiments. *Eur. J. Pharm. Sci.* **2013**, *49* (4), 499–504.
- (83) Samiei, N.; Shafaati, A.; Zarghi, A.; Moghimi, H. R.; Foroutan, S. M. Enhancement and in Vitro Evaluation of Amifostine Permeation through Artificial Membrane (PAMPA) via Ion Pairing Approach and Mechanistic Selection of Its Optimal Counter Ion. *Eur. J. Pharm. Sci.* **2014**, *51*, 218–223.
- (84) Dutton, B.; Woods, A.; Sadler, R.; Prime, D.; Barlow, D. J.; Forbes, B.; Jones, S. A. Using Polar Ion-Pairs to Control Drug Delivery to the Airways of the Lungs. *Mol. Pharm.* **2020**, *17* (5), 1482–1490.
- (85) Haggi, M.; Traini, D.; Bebawy, M.; Young, P. M. Deposition, Diffusion and Transport Mechanism of Dry Powder Microparticulate Salbutamol, at the Respiratory Epithelia. *Mol. Pharm.* **2012**, *9* (6), 1717–1726.
- (86) Lamy, B.; Tewes, F.; Serrano, D. R.; Lamarche, I.; Gobin, P.; Couet, W.; Healy, A. M.; Marchand, S. New Aerosol Formulation to Control Ciprofloxacin Pulmonary Concentration. *J. Control. Release* **2018**, *271*, 118–126.
- (87) Brillault, J.; Tewes, F.; Couet, W.; Olivier, J. In Vitro Biopharmaceutical Evaluation of Ciprofloxacin/Metal Cation Complexes for Pulmonary Administration. *Eur. J. Pharm. Sci.* **2017**, *97*, 92–98.
- (88) Tewes, F.; Bahamondez-Canas, T. F.; Smyth, H. D. C. Efficacy of Ciprofloxacin and Its Copper Complex against *Pseudomonas Aeruginosa* Biofilms. *AAPS PharmSciTech* **2019**, *20* (5), 205.
- (89) Huang, W.-H.; Yang, Z.-J.; Wu, H.; Wong, Y.-F.; Zhao, Z.-Z.; Liu, L. Development of Liposomal Salbutamol Sulfate Dry Powder Inhaler Formulation. *Biol. Pharm. Bull.* **2010**, *33* (3), 512–517.

-
- (90) Waldrep, J. .; Arppe, J.; Jansa, K. .; Vidgren, M. Experimental Pulmonary Delivery of Cyclosporin A by Liposome Aerosol. *Int. J. Pharm.* **1998**, *160* (2), 239–249.
- (91) Finlay, W. .; Wong, J. . Regional Lung Deposition of Nebulized Liposome-Encapsulated Ciprofloxacin. *Int. J. Pharm.* **1998**, *167* (1–2), 121–127.
- (92) WANG, J.; BEN-JEBRIA, A.; EDWARDS, D. A. Inhalation of Estradiol for Sustained Systemic Delivery. *J. Aerosol Med.* **1999**, *12* (1), 27–36.
- (93) Tolman, J. A.; Williams, R. O. Advances in the Pulmonary Delivery of Poorly Water-Soluble Drugs: Influence of Solubilization on Pharmacokinetic Properties. *Drug Dev. Ind. Pharm.* **2010**, *36* (1), 1–30.
- (94) Voelkel, N. F.; Mizuno, S.; Cool, C. D. The Spectrum of Pulmonary Disease in COPD. In *COPD*; Springer Berlin Heidelberg: Berlin, Heidelberg, 2017; pp 195–207.
- (95) Reddy, K. S. Global Burden of Disease Study 2015 Provides GPS for Global Health 2030. *Lancet* **2016**, *388* (10053), 1448–1449.
- (96) Vestbo, J.; Hurd, S. S.; Agustí, A. G.; Jones, P. W.; Vogelmeier, C.; Anzueto, A.; Barnes, P. J.; Fabbri, L. M.; Martinez, F. J.; Nishimura, M.; et al. Global Strategy for the Diagnosis, Management, and Prevention of Chronic Obstructive Pulmonary Disease. *Am. J. Respir. Crit. Care Med.* **2013**, *187* (4), 347–365.
- (97) Stone, K. C.; Mercer, R. R.; Gehr, P.; Stockstill, B.; Crapo, J. D. Allometric Relationships of Cell Numbers and Size in the Mammalian Lung. *Am. J. Respir. Cell Mol. Biol.* **1992**, *6* (2), 235–243.
- (98) Masoli, M.; Fabian, D.; Holt, S.; Beasley, R. The Global Burden of Asthma: Executive Summary of the GINA Dissemination Committee Report. *Allergy* **2004**, *59* (5), 469–478.
- (99) *Global Strategy For Asthma Management and Prevention.*
- (100) Cukic, V.; Lovre, V.; Dragisic, D.; Ustamujic, A. Asthma and Chronic Obstructive Pulmonary Disease (COPD) and #8211; Differences and Similarities. *Mater. Socio Medica* **2012**, *24* (2), 100.
- (101) Decramer, M.; Janssens, W.; Miravittles, M. Chronic Obstructive Pulmonary Disease. *Lancet* **2012**, *379* (9823), 1341–1351.
- (102) Johnson, M. Molecular Mechanisms of B2-Adrenergic Receptor Function, Response, and Regulation. *J. Allergy Clin. Immunol.* **2006**, *117* (1), 18–24.
- (103) Santus, P.; Radovanovic, D.; Paggiaro, P.; Papi, A.; Sanduzzi, A.; Scichilone, N.; Braido, F. Why Use Long Acting Bronchodilators in Chronic Obstructive Lung Diseases? An Extensive Review on Formoterol and Salmeterol. *Eur. J. Intern. Med.* **2015**, *26* (6), 379–384.
- (104) Ralph Lardau, Basil Achilladelis, Alexander Scriabine, R. L. *Pharmaceutical Innovation: Revolutionizing Human Health (The Chemical Heritage Foundation Series in Innovation and Entrepreneurship)*; Chemical Heritage Foundation (1999), 1999.
- (105) Kane SP. The Top 300 of 2019 <https://clincalc.com/DrugStats/Top300Drugs.aspx> (accessed Sep 8, 2019).
- (106) Henderson Jr., W. R.; Banerjee, E. R.; Chi, E. Y. Differential Effects of (S)- and (R)-Enantiomers of Albuterol in a Mouse Asthma Model. *J. Allergy Clin. Immunol.* **2005**, *116* (2), 332–340.
- (107) DHAND, R.; GOODE, M.; REID, R.; FINK, J. B.; FAHEY, P. J.; TOBIN, M. J. Preferential Pulmonary Retention of (S)-Albuterol after Inhalation of Racemic Albuterol. *Am. J. Respir. Crit. Care Med.* **1999**, *160* (4), 1136–1141.
- (108) Barnes, P. J. Treatment with (R)-Albuterol Has No Advantage over Racemic Albuterol. *Am. J. Respir. Crit. Care Med.* **2006**, *174* (9), 969–972.
- (109) Page, C. P.; Morley, J. Contrasting Properties of Albuterol Stereoisomers☆☆☆. *J. Allergy*

- Clin. Immunol.* **1999**, *104* (2), S31–S41.
- (110) Anderson, G. P.; Lindén, A.; Rabe, K. F. Why Are Long-Acting Beta-Adrenoceptor Agonists Long-Acting? *Eur. Respir. J.* **1994**, *7* (3), 569–578.
- (111) Prentice, B.; Jaffe, A.; Thomas, P. S. Antimuscarinics. In *Compendium of Inflammatory Diseases*; Springer Basel: Basel, 2016; pp 101–105.
- (112) Bartow, R. A.; Brogden, R. N. Formoterol. An Update of Its Pharmacological Properties and Therapeutic Efficacy in the Management of Asthma. *Drugs* **1998**, *55* (2), 303–322.
- (113) Lötvall, J. Pharmacological Similarities and Differences between B2-Agonists. *Respir. Med.* **2001**, *95*, S7–S11.
- (114) Beeh, K. M.; Beier, J. The Short, the Long and the “Ultra-Long”: Why Duration of Bronchodilator Action Matters in Chronic Obstructive Pulmonary Disease. *Adv. Ther.* **2010**, *27* (3), 150–159.
- (115) Scarlett-Ferguson, H. Adrenergic Drugs. *Clin. Drug Ther. Can. Pract. Second Ed.* **2011**, 277–291.
- (116) Eglen, R. M. Muscarinic Receptor Subtypes in Neuronal and Non-Neuronal Cholinergic Function. *Auton. Autacoid Pharmacol.* **2006**, *26* (3), 219–233.
- (117) Gosens, R.; Gross, N. The Mode of Action of Anticholinergics in Asthma. *Eur. Respir. J.* **2018**, *52* (4), 1701247.
- (118) Qin, K.; Dong, C.; Wu, G.; Lambert, N. A. Inactive-State Preassembly of Gq-Coupled Receptors and Gq Heterotrimers. *Nat. Chem. Biol.* **2011**, *7* (10), 740–747.
- (119) Viniol, C.; Vogelmeier, C. F. Exacerbations of COPD. *Eur. Respir. Rev.* **2018**, *27* (147), 170103.
- (120) Wess, J.; Eglen, R. M.; Gautam, D. Muscarinic Acetylcholine Receptors: Mutant Mice Provide New Insights for Drug Development. *Nat. Rev. Drug Discov.* **2007**, *6* (9), 721–733.
- (121) Barnes, P. J. Muscarinic Receptor Subtypes in Airways. *Life Sci.* **1993**, *52* (5–6), 521–527.
- (122) Grandhi, R. K.; AbdElsayed, A. Anticholinergics. In *Pharmacology in Clinical Neurosciences*; Springer Singapore: Singapore, 2020; pp 165–171.
- (123) Saternos, H. C.; Almarghalani, D. A.; Gibson, H. M.; Meqdad, M. A.; Antypas, R. B.; Lingireddy, A.; AbouAlaiwi, W. A. Distribution and Function of the Muscarinic Receptor Subtypes in the Cardiovascular System. *Physiol. Genomics* **2018**, *50* (1), 1–9.
- (124) Mastrodicasa, M. A.; Droege, C. A.; Mulhall, A. M.; Ernst, N. E.; Panos, R. J.; Zafar, M. A. Long Acting Muscarinic Antagonists for the Treatment of Chronic Obstructive Pulmonary Disease: A Review of Current and Developing Drugs. *Expert Opin. Investig. Drugs* **2017**, *26* (2), 161–174.
- (125) IPRATROPIUM BROMIDE <https://bnf.nice.org.uk/drug/ipratropium-bromide.html> (accessed May 4, 2020).
- (126) Price, D.; Fromer, L.; Kaplan, A.; van der Molen, T.; Román-Rodríguez, M. Is There a Rationale and Role for Long-Acting Anticholinergic Bronchodilators in Asthma? *npj Prim. Care Respir. Med.* **2014**, *24* (1), 14023.
- (127) Matera, M. G.; Calzetta, L.; Ora, J.; Rogliani, P.; Cazzola, M. Pharmacokinetic/Pharmacodynamic Approaches to Drug Delivery Design for Inhalation Drugs. *Expert Opin. Drug Deliv.* **2021**, *18* (7), 891–906.
- (128) Pakes, G. E.; Brogden, R. N.; Heel, R. C.; Speight, T. M.; Avery, G. S. Ipratropium Bromide. *Drugs* **2012**, *20* (4), 237–266.
- (129) Leusch, A.; Eichhorn, B.; Müller, G.; Rominger, K.-L. Pharmacokinetics and Tissue Distribution of the Anticholinergics Tiotropium and Ipratropium in the Rat and Dog.

- Biopharm. Drug Dispos.* **2019**, 22 (5), 199–212.
- (130) KOUMIS, T.; SAMUEL, S. Tiotropium Bromide: A New Long-Acting Bronchodilator for the Treatment of Chronic Obstructive Pulmonary Disease. *Clin. Ther.* **2005**, 27 (4), 377–392.
- (131) Keam, S. J.; Keating, G. M. Tiotropium Bromide. *Treat. Respir. Med.* **2004**, 3 (4), 247–268.
- (132) Barnes, P. J. Tiotropium Bromide. *Expert Opin. Investig. Drugs* **2001**, 10 (4), 733–740.
- (133) de Luise, C.; Lanes, S. F.; Jacobsen, J.; Pedersen, L.; Sørensen, H. T. Cardiovascular and Respiratory Hospitalizations and Mortality among Users of Tiotropium in Denmark. *Eur. J. Epidemiol.* **2007**, 22 (4), 267–272.
- (134) Beasley, R.; Singh, S.; Loke, Y. K.; Enright, P.; Furberg, C. D. Call for Worldwide Withdrawal of Tiotropium Respimat Mist Inhaler. *BMJ* **2012**, 345 (7884).
- (135) Bateman, E. D. Tiotropium Respimat Increases the Risk of Mortality: Con. *Eur. Respir. J.* **2013**, 42 (3), 590–593.
- (136) Sentellas, S.; Ramos, I.; Albertí, J.; Salvà, M.; Antón, F.; Miralpeix, M.; Beleta, J.; Gavaldà, A. Aclidinium Bromide, a New, Long-Acting, Inhaled Muscarinic Antagonist: In Vitro Plasma Inactivation and Pharmacological Activity of Its Main Metabolites. *Eur. J. Pharm. Sci.* **2010**, 39 (5), 283–290.
- (137) Gavaldà, A.; Miralpeix, M.; Ramos, I.; Otal, R.; Carreño, C.; Viñals, M.; Doménech, T.; Carcasona, C.; Reyes, B.; Vilella, D.; et al. Characterization of Aclidinium Bromide, a Novel Inhaled Muscarinic Antagonist, with Long Duration of Action and a Favorable Pharmacological Profile. *J. Pharmacol. Exp. Ther.* **2009**, 331 (2), 740–751.
- (138) Motte, S. de la; Beier, J.; Schmid, K.; Pascual, S.; Jansat, J. M.; Gil, E. G. Pharmacokinetics and Safety of Aclidinium Bromide in Younger and Elderly Patients with Chronic Obstructive Pulmonary Disease. *Int. J. Clin. Pharmacol. Ther.* **2012**, 50 (06), 403–412.
- (139) Rogliani, P.; Calzetta, L.; Ora, J.; Lipsi, R.; Segreti, A.; Matera, M. G.; Cazzola, M. Pharmacological Assessment of the Onset of Action of Aclidinium and Glycopyrronium versus Tiotropium in COPD Patients and Human Isolated Bronchi. *Eur. J. Pharmacol.* **2015**, 761, 383–390.
- (140) Barnes, P. J. Theophylline. *Am. J. Respir. Crit. Care Med.* **2013**, 188 (8), 901–906.
- (141) Rabe, K. F.; Magnussen, H.; Dent, G. Theophylline and Selective PDE Inhibitors as Bronchodilators and Smooth Muscle Relaxants. *Eur. Respir. J.* **1995**, 8 (4), 637–642.
- (142) Banner, K. H.; Page, C. P. Theophylline and Selective Phosphodiesterase Inhibitors as Anti-Inflammatory Drugs in the Treatment of Bronchial Asthma. *Eur. Respir. J.* **1995**, 8 (6), 996–1000.
- (143) Ramamoorthy, S.; Cidlowski, J. A. Corticosteroids. *Rheum. Dis. Clin. North Am.* **2016**, 42 (1), 15–31.
- (144) Adcock, I. M. Glucocorticoid Pathways in Chronic Obstructive Pulmonary Disease Therapy. *Proc. Am. Thorac. Soc.* **2005**, 2 (4), 313–319.
- (145) Adcock, I. M. Glucocorticoids: New Mechanisms and Future Agents. *Curr. Allergy Asthma Rep.* **2003**, 3 (3), 249–257.
- (146) Anzueto, A. Impact of Exacerbations on COPD. *Eur. Respir. Rev.* **2010**, 19 (116), 113–118.
- (147) Foster, J. M.; Usherwood, T.; Smith, L.; Sawyer, S. M.; Xuan, W.; Rand, C. S.; Reddel, H. K. Inhaler Reminders Improve Adherence with Controller Treatment in Primary Care Patients with Asthma. *J. Allergy Clin. Immunol.* **2014**, 134 (6), 1260-1268.e3.
- (148) Rand, C.; Bilderback, A.; Schiller, K.; Edelman, J. M.; Hustad, C. M.; Zeiger, R. S. Adherence with Montelukast or Fluticasone in a Long-Term Clinical Trial: Results from the Mild Asthma Montelukast Versus Inhaled Corticosteroid Trial. *J. Allergy Clin. Immunol.* **2007**, 119 (4), 916–923.

- (149) Stanford, R. H.; Shah, M. B.; D'Souza, A. O.; Dhamane, A. D.; Schatz, M. Short-Acting β -Agonist Use and Its Ability to Predict Future Asthma-Related Outcomes. *Ann. Allergy, Asthma Immunol.* **2012**, *109* (6), 403–407.
- (150) O'Byrne, P. M.; FitzGerald, J. M.; Bateman, E. D.; Barnes, P. J.; Zhong, N.; Keen, C.; Jorup, C.; Lamarca, R.; Ivanov, S.; Reddel, H. K. Inhaled Combined Budesonide–Formoterol as Needed in Mild Asthma. *N. Engl. J. Med.* **2018**, *378* (20), 1865–1876.
- (151) Bateman, E. D.; Reddel, H. K.; O'Byrne, P. M.; Barnes, P. J.; Zhong, N.; Keen, C.; Jorup, C.; Lamarca, R.; Siwek-Posluszna, A.; FitzGerald, J. M. As-Needed Budesonide–Formoterol versus Maintenance Budesonide in Mild Asthma. *N. Engl. J. Med.* **2018**, *378* (20), 1877–1887.
- (152) Selent, J.; Brandt, W.; Pamperin, D.; Göber, B. Enantiomeric N-Methyl-4-Piperidyl Benzilates as Muscarinic Receptor Ligands: Radioligand Binding Studies and Docking Studies to Models of the Three Muscarinic Receptors M1, M2 and M3. *Bioorg. Med. Chem.* **2006**, *14* (6), 1729–1736.
- (153) Walther, R.; Rautio, J.; Zelikin, A. N. Prodrugs in Medicinal Chemistry and Enzyme Prodrug Therapies. *Adv. Drug Deliv. Rev.* **2017**, *118*, 65–77.
- (154) Huttunen, K. M.; Raunio, H.; Rautio, J. Prodrugs—from Serendipity to Rational Design. *Pharmacol. Rev.* **2011**, *63* (3), 750–771.
- (155) Beaumont, K.; Webster, R.; Gardner, I.; Dack, K. Design of Ester Prodrugs to Enhance Oral Absorption of Poorly Permeable Compounds: Challenges to the Discovery Scientist. *Curr. Drug Metab.* **2003**, *4* (6), 461–485.
- (156) Choi-Sledeski, Y. M.; Wermuth, C. G. Designing Prodrugs and Bioprecursors. In *The Practice of Medicinal Chemistry*; Elsevier, 2015; pp 657–696.
- (157) Fleisher, D.; Bong, R.; Stewart, B. H. Improved Oral Drug Delivery: Solubility Limitations Overcome by the Use of Prodrugs. *Adv. Drug Deliv. Rev.* **1996**, *19* (2), 115–130.
- (158) Rybak, J. M.; Roberts, K. Tedizolid Phosphate: A Next-Generation Oxazolidinone. *Infect. Dis. Ther.* **2015**, *4* (1), 1–14.
- (159) *Prodrugs*; Stella, V. J., Borchardt, R. T., Hageman, M. J., Oliyai, R., Maag, H., Tilley, J. W., Eds.; Springer New York: New York, NY, 2007.
- (160) Chandrasekaran, S.; Al-Ghananeem, A. M.; Riggs, R. M.; Crooks, P. A. Synthesis and Stability of Two Indomethacin Prodrugs. *Bioorg. Med. Chem. Lett.* **2006**, *16* (7), 1874–1879.
- (161) Helen Chan, O.; Stewart, B. H. Physicochemical and Drug-Delivery Considerations for Oral Drug Bioavailability. *Drug Discov. Today* **1996**, *1* (11), 461–473.
- (162) Beauchamp, L. M.; Orr, G. F.; de Miranda, P.; Bumette, T.; Krenitsky, T. A. Amino Acid Ester Prodrugs of Acyclovir. *Antivir. Chem. Chemother.* **1992**, *3* (3), 157–164.
- (163) Balimane, P. V.; Tamai, I.; Guo, A.; Nakanishi, T.; Kitada, H.; Leibach, F. H.; Tsuji, A.; Sinko, P. J. Direct Evidence for Peptide Transporter (PepT1)-Mediated Uptake of a Nonpeptide Prodrug, Valacyclovir. *Biochem. Biophys. Res. Commun.* **1998**, *250* (2), 246–251.
- (164) Murakami, E.; Tolstykh, T.; Bao, H.; Niu, C.; Steuer, H. M. M.; Bao, D.; Chang, W.; Espiritu, C.; Bansal, S.; Lam, A. M.; et al. Mechanism of Activation of PSI-7851 and Its Diastereoisomer PSI-7977. *J. Biol. Chem.* **2010**, *285* (45), 34337–34347.
- (165) MISSALE, C.; NASH, S. R.; ROBINSON, S. W.; JABER, M.; CARON, M. G. Dopamine Receptors: From Structure to Function. *Physiol. Rev.* **1998**, *78* (1), 189–225.
- (166) del Amo, E. M.; Urtti, A.; Yliperttula, M. Pharmacokinetic Role of L-Type Amino Acid Transporters LAT1 and LAT2. *Eur. J. Pharm. Sci.* **2008**, *35* (3), 161–174.
- (167) Nyberg, L.; Rosenborg, J.; Weibull, E.; Jönsson, S.; Kennedy, B.-M.; Nilsson, M. Pharmacokinetics of Bambuterol in Healthy Subjects. *Br. J. Clin. Pharmacol.* **2002**, *45* (5),

471–478.

- (168) Rosenborg, J.; Larsson, P.; Nyberg, L. Pharmacokinetics of Bambuterol during Oral Administration of Plain Tablets and Solution to Healthy Adults. *Br. J. Clin. Pharmacol.* **2001**, *49* (3), 199–206.
- (169) Singh, G.; Kesar, S.; Sambyal, A.; Grover, S. Role of Bambuterol in the Management of Bronchial Asthma. *Indian J. Respir. Care* **2019**, *8* (1), 27.
- (170) Lundqvist, T.; Bredenberg, S. Pharmaceutical Development. In *Drug Discovery and Development*; Elsevier, 2013; pp 227–238.
- (171) Forrest, M. L.; Yáñez, J. A.; Remsberg, C. M.; Ohgami, Y.; Kwon, G. S.; Davies, N. M. Paclitaxel Prodrugs with Sustained Release and High Solubility in Poly(Ethylene Glycol)-b-Poly(ϵ -Caprolactone) Micelle Nanocarriers: Pharmacokinetic Disposition, Tolerability, and Cytotoxicity. *Pharm. Res.* **2008**, *25* (1), 194–206.
- (172) Vig, B. S.; Huttunen, K. M.; Laine, K.; Rautio, J. Amino Acids as Promoiety in Prodrug Design and Development. *Adv. Drug Deliv. Rev.* **2013**, *65* (10), 1370–1385.
- (173) Pennick. Absorption of Lisdexamfetamine Dimesylate and Its Enzymatic Conversion to D-Amphetamine. *Neuropsychiatr. Dis. Treat.* **2010**, 317.
- (174) Elia, J.; Easley, C.; Kirkpatrick, P. Lisdexamfetamine Dimesylate. *Nat. Rev. Drug Discov.* **2007**, *6* (5), 343–344.
- (175) Zheng, X.; Polli, J. E. Synthesis and in Vitro Evaluation of Potential Sustained Release Prodrugs via Targeting ASBT. *Int. J. Pharm.* **2010**, *396* (1–2), 111–118.
- (176) Ryrfeldt, A.; Andersson, P.; Edsbäcker, S.; Tönnesson, M.; Davies, D.; Pauwels, R. Pharmacokinetics and Metabolism of Budesonide, a Selective Glucocorticoid. *Eur. J. Respir. Dis. Suppl.* **1982**, *122*, 86–95.
- (177) Sovani, M. P.; Whale, C. I.; Osborne, J.; Cooper, S.; Mortimer, K.; Ekström, T.; Tattersfield, A. E.; Harrison, T. W. Poor Adherence with Inhaled Corticosteroids for Asthma: Can Using a Single Inhaler Containing Budesonide and Formoterol Help? *Br. J. Gen. Pract.* **2008**, *58* (546), 37–43.
- (178) Waters, R. C.; Hochhaus, G. Characterization of a Dextran-Budesonide Prodrug for Inhalation Therapy. *Eur. J. Pharm. Sci.* **2019**, *129*, 58–67.
- (179) Sinha, V. R.; Kumria, R. Colonic Drug Delivery: Prodrug Approach. *Pharm. Res.* **2001**, *18* (5), 557–564.
- (180) Channick, R.; Voswinkel; Rubin, L.; Vultaggio. Inhaled Treprostinil: A Therapeutic Review. *Drug Des. Devel. Ther.* **2012**, 19.
- (181) Ruan, C.-H.; Dixon, R. A. F.; Willerson, J. T.; Ruan, K.-H. Prostacyclin Therapy for Pulmonary Arterial Hypertension. *Texas Hear. Inst. J.* **2010**, *37* (4), 391–399.
- (182) Chapman, R. W.; Corboz, M. R.; Malinin, V. S.; Plaunt, A. J.; Konicek, D. M.; Li, Z.; Perkins, W. R. An Overview of the Biology of a Long-Acting Inhaled Treprostinil Prodrug. *Pulm. Pharmacol. Ther.* **2020**, *65*, 102002.
- (183) Leifer, F.; Konicek, D.; Chen, K.-J.; Plaunt, A.; Salvail, D.; Laurent, C.; Corboz, M.; Li, Z.; Chapman, R.; Perkins, W.; et al. Inhaled Treprostinil-Prodrug Lipid Nanoparticle Formulations Provide Long-Acting Pulmonary Vasodilation. *Drug Res. (Stuttg.)* **2018**, *68* (11), 605–614.
- (184) Vladimir Malinin, Zhili Li, Richard Chapman, Franziska Leifer, Donna Omiatek, Jane Ong, Dan Salvail, Charles Laurent, W. P. Treprostinil Pharmacokinetics in Rats Are Extended Using Inhaled Prodrug Formulations. *Eur. Respir. J.* **2014**, *44*, 2367.
- (185) Reynolds, N. A.; Scott, L. J. Ciclesonide. *Drugs* **2004**, *64* (5), 511–519.
- (186) Deeks, E. D.; Perry, C. M. Ciclesonide. *Drugs* **2008**, *68* (12), 1741–1770.

- (187) Ciclesonide. In *Meyler's Side Effects of Drugs*; Elsevier, 2016; pp 292–294.
- (188) Tejani-Butt, S. M.; Luthin, G. R.; Wolfe, B. B.; Brunswick, D. J. N-Substituted Derivatives of 4-Piperidinyl Benzilate: Affinities for Brain Muscarinic Acetylcholine Receptors. *Life Sci.* **1990**, *47* (10), 841–848.
- (189) XU, R.; SIM, M.-K.; GO, M.-L. Synthesis, Antimuscarinic Activity and Quantitative Structure-Activity Relationship (QSAR) of Tropinyl and Piperidinyl Esters. *Chem. Pharm. Bull. (Tokyo)*. **1998**, *46* (2), 231–241.
- (190) Jaiswal, N.; Lambrecht, G.; Mutschler, E.; Tacke, R.; Malik, K. U. Pharmacological Characterization of the Vascular Muscarinic Receptors Mediating Relaxation and Contraction in Rabbit Aorta. *J. Pharmacol. Exp. Ther.* **1991**, *258* (3), 842–850.
- (191) Sim, M. K.; Lim, B. C. Presence of an Endothelial Esterase in the Rat Aorta: Effects on the Actions of Ester and Non-Ester Muscarinic Antagonists. *Endothelium* **1993**, *1* (2), 109–114.
- (192) Kaiser, C.; Audia, V. H.; Carter, J. P.; McPherson, D. W.; Waid, P. P.; Lowe, V. C.; Noronha-Blob, L. Synthesis and Antimuscarinic Activity of Some 1-Cycloalkyl-1-Hydroxy-1-Phenyl-3-(4-Substituted Piperazinyl)-2-Propanones and Related Compounds. *J. Med. Chem.* **1993**, *36* (5), 610–616.
- (193) Liu, H.; Hofmann, J.; Fish, I.; Schaake, B.; Eitel, K.; Bartuschat, A.; Kaindl, J.; Rampp, H.; Banerjee, A.; Hübner, H.; et al. Structure-Guided Development of Selective M3 Muscarinic Acetylcholine Receptor Antagonists. *Proc. Natl. Acad. Sci.* **2018**, *115* (47), 12046–12050.
- (194) Liu, R.; Zhang, Y.; Zhao, X.; Agarwal, A.; Mueller, L. J.; Feng, P. PH-Responsive Nanogated Ensemble Based on Gold-Capped Mesoporous Silica through an Acid-Labile Acetal Linker. *J. Am. Chem. Soc.* **2010**, *132* (5), 1500–1501.
- (195) Jia, Y.; Fei, J.; Cui, Y.; Yang, Y.; Gao, L.; Li, J. PH-Responsive Polysaccharide Microcapsules through Covalent Bonding Assembly. *Chem. Commun.* **2011**, *47* (4), 1175–1177.
- (196) Kolakowski, R. V.; Haelsig, K. T.; Emmerton, K. K.; Leiske, C. I.; Miyamoto, J. B.; Cochran, J. H.; Lyon, R. P.; Senter, P. D.; Jeffrey, S. C. The Methylene Alkoxy Carbamate Self-Immolative Unit: Utilization for the Targeted Delivery of Alcohol-Containing Payloads with Antibody-Drug Conjugates. *Angew. Chemie Int. Ed.* **2016**, *55* (28), 7948–7951.
- (197) Oishi, M.; Nagasaki, Y.; Itaka, K.; Nishiyama, N.; Kataoka, K. Lactosylated Poly(Ethylene Glycol)-SiRNA Conjugate through Acid-Labile β -Thiopropionate Linkage to Construct PH-Sensitive Polyion Complex Micelles Achieving Enhanced Gene Silencing in Hepatoma Cells. *J. Am. Chem. Soc.* **2005**, *127* (6), 1624–1625.
- (198) Qiao, Z.-Y.; Zhang, R.; Du, F.-S.; Liang, D.-H.; Li, Z.-C. Multi-Responsive Nanogels Containing Motifs of Ortho Ester, Oligo(Ethylene Glycol) and Disulfide Linkage as Carriers of Hydrophobic Anti-Cancer Drugs. *J. Control. Release* **2011**, *152* (1), 57–66.
- (199) Patel, V. F.; Hardin, J. N.; Mastro, J. M.; Law, K. L.; Zimmermann, J. L.; Ehlhardt, W. J.; Woodland, J. M.; Starling, J. J. Novel Acid Labile COL1 Trityl-Linked Difluoronucleoside Immunoconjugates: Synthesis, Characterization, and Biological Activity 1. *Bioconjug. Chem.* **1996**, *7* (4), 497–510.
- (200) Pahal, P.; Hashmi, M. F.; Sharma, S. *Chronic Obstructive Pulmonary Disease Compensatory Measure*; 2020.
- (201) Edwards, S. L. Pathophysiology of Acid Base Balance: The Theory Practice Relationship. *Intensive Crit. Care Nurs.* **2008**, *24* (1), 28–40.
- (202) Feron, V. J.; Til, H. P.; de Vrijer, F.; Woutersen, R. A.; Cassee, F. R.; van Bladeren, P. J. Aldehydes: Occurrence, Carcinogenic Potential, Mechanism of Action and Risk Assessment. *Mutat. Res. Toxicol.* **1991**, *259* (3–4), 363–385.
- (203) de Rooij, J. F. M.; Hazeleger, G. W.; Burgers, P. M. J.; van Boom, J. H. Neighbouring Group Participation in the Unblocking of Phosphotriesters of Nucleic Acids. *Nucleic Acids Res.*

- 1979**, 6 (6), 2237–2259.
- (204) Toniolo, C.; Crisma, M.; Formaggio, F.; Peggion, C. Control of Peptide Conformation by the Thorpe-Ingold Effect (C[?]-Tetrasubstitution). *Biopolymers* **2001**, 60 (6), 396–419.
- (205) Chavan, S. R.; Gavale, K. S.; Kamble, K. M.; Pingale, S. S.; Dhavale, D. D. Gem-Disubstituent Effect in Rate Acceleration of Intramolecular Alkyne-Azide Cycloaddition Reaction. *Tetrahedron* **2017**, 73 (4), 365–372.
- (206) Bettens, F. L.; Bettens, R. P. A.; Brown, R. D.; Godfrey, P. D. The Microwave Spectrum, Structure, and Ring-Puckering of the Cyclic Dipeptide Diketopiperazine. *J. Am. Chem. Soc.* **2000**, 122 (24), 5856–5860.
- (207) Hirst, J. D.; Persson, B. J. Ab Initio Calculations of the Vibrational and Electronic Spectra of Diketopiperazine. *J. Phys. Chem. A* **1998**, 102 (38), 7519–7524.
- (208) Okkenhaug, K. Signaling by the Phosphoinositide 3-Kinase Family in Immune Cells. *Annu. Rev. Immunol.* **2013**, 31 (1), 675–704.
- (209) Gross, N. J.; Barnes, P. J. New Therapies for Asthma and Chronic Obstructive Pulmonary Disease. *Am. J. Respir. Crit. Care Med.* **2017**, 195 (2), 159–166.
- (210) So, L.; Fruman, D. A. PI3K Signalling in B- and T-Lymphocytes: New Developments and Therapeutic Advances. *Biochem. J.* **2012**, 442 (3), 465–481.
- (211) Hawkins, P. T.; Stephens, L. R. PI3K Signalling in Inflammation. *Biochim. Biophys. Acta - Mol. Cell Biol. Lipids* **2015**, 1851 (6), 882–897.
- (212) Fung-Leung, W.-P. Phosphoinositide 3-Kinase Delta (PI3K δ) in Leukocyte Signaling and Function. *Cell. Signal.* **2011**, 23 (4), 603–608.
- (213) Thorpe, L. M.; Yuzugullu, H.; Zhao, J. J. PI3K in Cancer: Divergent Roles of Isoforms, Modes of Activation and Therapeutic Targeting. *Nat. Rev. Cancer* **2015**, 15 (1), 7–24.
- (214) Li, H.; Wu, X.; Hou, S.; Malek, M.; Kielkowska, A.; Noh, E.; Makondo, K. J.; Du, Q.; Wilkins, J. A.; Johnston, J. B.; et al. Phosphatidylinositol-3,4-Bisphosphate and Its Binding Protein Lamellipodin Regulate Chemotaxis of Malignant B Lymphocytes. *J. Immunol.* **2016**, 196 (2), 586–595.
- (215) Banham-Hall, E. The Therapeutic Potential for PI3K Inhibitors in Autoimmune Rheumatic Diseases. *Open Rheumatol. J.* **2012**, 6 (1), 245–258.
- (216) Foster, J. G.; Blunt, M. D.; Carter, E.; Ward, S. G. Inhibition of PI3K Signaling Spurs New Therapeutic Opportunities in Inflammatory/Autoimmune Diseases and Hematological Malignancies. *Pharmacol. Rev.* **2012**, 64 (4), 1027–1054.
- (217) Knight, Z. A.; Shokat, K. M. Chemically Targeting the PI3K Family. *Biochem. Soc. Trans.* **2007**, 35 (2), 245–249.
- (218) Berndt, A.; Miller, S.; Williams, O.; Le, D. D.; Houseman, B. T.; Pacold, J. I.; Gorrec, F.; Hon, W.-C.; Ren, P.; Liu, Y.; et al. The P110 δ Structure: Mechanisms for Selectivity and Potency of New PI(3)K Inhibitors. *Nat. Chem. Biol.* **2010**, 6 (2), 117–124.
- (219) Moradi, S.; Jarrahi, E.; Ahmadi, A.; Salimian, J.; Karimi, M.; Zarei, A.; Azimzadeh Jamalkandi, S.; Ghanei, M. PI3K Signalling in Chronic Obstructive Pulmonary Disease and Opportunities for Therapy. *J. Pathol.* **2021**, 254 (5), 505–518.
- (220) Chung, K. F.; Adcock, I. M. Multifaceted Mechanisms in COPD: Inflammation, Immunity, and Tissue Repair and Destruction. *Eur. Respir. J.* **2008**, 31 (6), 1334–1356.
- (221) Stark, A.-K.; Srisankharajah, S.; Hessel, E. M.; Okkenhaug, K. PI3K Inhibitors in Inflammation, Autoimmunity and Cancer. *Curr. Opin. Pharmacol.* **2015**, 23, 82–91.
- (222) Ghigo, A.; Damilano, F.; Braccini, L.; Hirsch, E. PI3K Inhibition in Inflammation: Toward Tailored Therapies for Specific Diseases. *BioEssays* **2010**, 32 (3), 185–196.

- (223) Dinarello, C. A. Anti-Inflammatory Agents: Present and Future. *Cell* **2010**, *140* (6), 935–950.
- (224) Lee, K. S.; Lee, H. K.; Hayflick, J. S.; Lee, Y. C.; Puri, K. D. Inhibition of Phosphoinositide 3-kinase δ Attenuates Allergic Airway Inflammation and Hyperresponsiveness in Murine Asthma Model. *FASEB J.* **2006**, *20* (3), 455–465.
- (225) Sadhu, C.; Dick, K.; Tino, W. T.; Staunton, D. E. Selective Role of PI3K δ in Neutrophil Inflammatory Responses. *Biochem. Biophys. Res. Commun.* **2003**, *308* (4), 764–769.
- (226) Down, K.; Amour, A.; Baldwin, I. R.; Cooper, A. W. J.; Deakin, A. M.; Felton, L. M.; Guntrip, S. B.; Hardy, C.; Harrison, Z. A.; Jones, K. L.; et al. Optimization of Novel Indazoles as Highly Potent and Selective Inhibitors of Phosphoinositide 3-Kinase δ for the Treatment of Respiratory Disease. *J. Med. Chem.* **2015**, *58* (18), 7381–7399.
- (227) Aronov, A. M. Common Pharmacophores for Uncharged Human Ether-a-Go-Go-Related Gene (HERG) Blockers. *J. Med. Chem.* **2006**, *49* (23), 6917–6921.
- (228) Weng, M.; Lee, H.-W.; Park, S.-H.; Hu, Y.; Wang, H.-T.; Chen, L.-C.; Rom, W. N.; Huang, W. C.; Lepor, H.; Wu, X.-R.; et al. Aldehydes Are the Predominant Forces Inducing DNA Damage and Inhibiting DNA Repair in Tobacco Smoke Carcinogenesis. *Proc. Natl. Acad. Sci.* **2018**, *115* (27), E6152–E6161.
- (229) BALDWIN IAN ROBERT [GB]; DOWN KENNETH DAVID [GB]; FAULDER PAUL [GB]; GAINES SIMON [GB]; HAMBLIN JULIE NICOLE [GB]; JONES KATHERINE LOUISE [GB]; LE JOELLE [GB]; LUNNISS CHRISTOPHER JAMES [GB]; PARR NIGEL JAMES [GB]; RITCHIE TIMOTHY JOHN [GB]; SMETHURST CHR, Y. 4-CARBOXAMIDE INDAZOLE DERIVATIVES USEFUL AS INHIBITORS OF P13-KINASES, 2009.
- (230) Schwehm, C.; Kellam, B.; Garces, A. E.; Hill, S. J.; Kindon, N. D.; Bradshaw, T. D.; Li, J.; Macdonald, S. J. F.; Rowedder, J. E.; Stoddart, L. A.; et al. Design and Elaboration of a Tractable Tricyclic Scaffold To Synthesize Druglike Inhibitors of Dipeptidyl Peptidase-4 (DPP-4), Antagonists of the C–C Chemokine Receptor Type 5 (CCR5), and Highly Potent and Selective Phosphoinositol-3 Kinase δ (PI3K δ) Inhib. *J. Med. Chem.* **2017**, *60* (4), 1534–1554.
- (231) Catalano, J. G.; Gudmundsson, K. S.; Svolto, A.; Boggs, S. D.; Miller, J. F.; Spaltenstein, A.; Thomson, M.; Wheelan, P.; Minick, D. J.; Phelps, D. P.; et al. Synthesis of a Novel Tricyclic 1,2,3,4,4a,5,6,10b-Octahydro-1,10-Phenanthroline Ring System and CXCR4 Antagonists with Potent Activity against HIV-1. *Bioorg. Med. Chem. Lett.* **2010**, *20* (7), 2186–2190.
- (232) Garces, A. E.; Al-Hayali, M.; Lee, J. B.; Li, J.; Gershkovich, P.; Bradshaw, T. D.; Stocks, M. J. Codrug Approach for the Potential Treatment of EML4-ALK Positive Lung Cancer. *ACS Med. Chem. Lett.* **2020**, *11* (3), 316–321.
- (233) Wu, L.; Li, X.; Ling, Y.; Huang, C.; Jia, N. Morpholine Derivative-Functionalized Carbon Dots-Based Fluorescent Probe for Highly Selective Lysosomal Imaging in Living Cells. *ACS Appl. Mater. Interfaces* **2017**, *9* (34), 28222–28232.
- (234) Yapici, N. B.; Bi, Y.; Li, P.; Chen, X.; Yan, X.; Mandalapu, S. R.; Faucett, M.; Jockusch, S.; Ju, J.; Gibson, K. M.; et al. Highly Stable and Sensitive Fluorescent Probes (LysoProbes) for Lysosomal Labeling and Tracking. *Sci. Rep.* **2015**, *5* (1), 8576.
- (235) Daniel, W. A.; Wójcikowski, J. Contribution of Lysosomal Trapping to the Total Tissue Uptake of Psychotropic Drugs. *Pharmacol. Toxicol.* **1997**, *80* (2), 62–68.
- (236) Poole, B.; Ohkuma, S. Effect of Weak Bases on the Intralysosomal pH in Mouse Peritoneal Macrophages. *J. Cell Biol.* **1981**, *90* (3), 665–669.
- (237) Funk, R. S.; Krise, J. P. Cationic Amphiphilic Drugs Cause a Marked Expansion of Apparent Lysosomal Volume: Implications for an Intracellular Distribution-Based Drug Interaction. *Mol. Pharm.* **2012**, *9* (5), 1384–1395.
- (238) Hein, L.; Lüllmann-rauch, R.; Mohr, K. Human Accumulation Potential of Xenobiotics: Potential of Catamphiphilic Drugs to Promote Their Accumulation via Inducing Lipidosis or

- Mucopolysaccharidosis. *Xenobiotica* **1990**, 20 (11), 1259–1267.
- (239) Anderson, N.; Borlak, J. Drug-Induced Phospholipidosis. *FEBS Lett.* **2006**, 580 (23), 5533–5540.
- (240) Reasor, M. J.; Kacew, S. Drug-Induced Phospholipidosis: Are There Functional Consequences? *Exp. Biol. Med.* **2001**, 226 (9), 825–830.
- (241) Daniel, W. A.; Bickel, M. H.; Honegger, U. E. The Contribution of Lysosomal Trapping in the Uptake of Desipramine and Chloroquine by Different Tissues. *Pharmacol. Toxicol.* **1995**, 77 (6), 402–406.
- (242) Bäckström, E.; Boger, E.; Lundqvist, A.; Hammarlund-Udenaes, M.; Fridén, M. Lung Retention by Lysosomal Trapping of Inhaled Drugs Can Be Predicted In Vitro With Lung Slices. *J. Pharm. Sci.* **2016**, 105 (11), 3432–3439.
- (243) Lichtman, J. W.; Conchello, J.-A. Fluorescence Microscopy. *Nat. Methods* **2005**, 2 (12), 910–919.
- (244) Bernard Valeur. *Molecular Fluorescence: Principles and Applications*; Wiley-VCH Verlag GmbH, 2001.
- (245) Fogel, J. L.; Thein, T. Z. T.; Mariani, F. V. Use of LysoTracker to Detect Programmed Cell Death in Embryos and Differentiating Embryonic Stem Cells. *J. Vis. Exp.* **2012**, No. 68.
- (246) Svendsen, C.; Spurgeon, D. .; Hankard, P. .; Weeks, J. . A Review of Lysosomal Membrane Stability Measured by Neutral Red Retention: Is It a Workable Earthworm Biomarker? *Ecotoxicol. Environ. Saf.* **2004**, 57 (1), 20–29.
- (247) Kazmi, F.; Hensley, T.; Pope, C.; Funk, R. S.; Loewen, G. J.; Buckley, D. B.; Parkinson, A. Lysosomal Sequestration (Trapping) of Lipophilic Amine (Cationic Amphiphilic) Drugs in Immortalized Human Hepatocytes (Fa2N-4 Cells). *Drug Metab. Dispos.* **2013**, 41 (4), 897–905.
- (248) Nemes, Z.; Dietz, R.; Lüth, J. B.; Gomba, S.; Hackenthal, E.; Gross, F. The Pharmacological Relevance of Vital Staining with Neutral Red. *Experientia* **1979**, 35 (11), 1475–1476.
- (249) Winckler, J. [Vital Staining of Lysosomes and Other Cell Organelles of the Rat with Neutral Red (Author's Transl)]. *Prog. Histochem. Cytochem.* **1974**, 6 (3), 1–91.
- (250) Dubyak, G. R. Ion Homeostasis, Channels, and Transporters: An Update on Cellular Mechanisms. *Adv. Physiol. Educ.* **2004**, 28 (4), 143–154.
- (251) Chan, J.; Dodani, S. C.; Chang, C. J. Reaction-Based Small-Molecule Fluorescent Probes for Chemosensitive Bioimaging. *Nat. Chem.* **2012**, 4 (12), 973–984.
- (252) Zorov, D. B.; Kobrinsky, E.; Juhaszova, M.; Sollott, S. J. Examining Intracellular Organelle Function Using Fluorescent Probes. *Circ. Res.* **2004**, 95 (3), 239–252.
- (253) Dong, H.-Q.; Wei, T.-B.; Ma, X.-Q.; Yang, Q.-Y.; Zhang, Y.-F.; Sun, Y.-J.; Shi, B.-B.; Yao, H.; Zhang, Y.-M.; Lin, Q. 1,8-Naphthalimide-Based Fluorescent Chemosensors: Recent Advances and Perspectives. *J. Mater. Chem. C* **2020**, 8 (39), 13501–13529.
- (254) Yu, H.; Guo, Y.; Zhu, W.; Havener, K.; Zheng, X. Recent Advances in 1,8-Naphthalimide-Based Small-Molecule Fluorescent Probes for Organelles Imaging and Tracking in Living Cells. *Coord. Chem. Rev.* **2021**, 444, 214019.
- (255) Li, X.; Hou, J.; Peng, C.; Chen, L.; Liu, W.; Liu, Y. A 1,8-Naphthalimide-Based Fluorescent Probe for Selective and Sensitive Detection of Peroxynitrite and Its Applications in Living Cell Imaging. *RSC Adv.* **2017**, 7 (54), 34287–34292.
- (256) Yu, H.; Xiao, Y.; Jin, L. A Lysosome-Targetable and Two-Photon Fluorescent Probe for Monitoring Endogenous and Exogenous Nitric Oxide in Living Cells. *J. Am. Chem. Soc.* **2012**, 134 (42), 17486–17489.
- (257) Liu, T.; Xu, Z.; Spring, D. R.; Cui, J. A Lysosome-Targetable Fluorescent Probe for Imaging

- Hydrogen Sulfide in Living Cells. *Org. Lett.* **2013**, *15* (9), 2310–2313.
- (258) Dombkowski, R. A.; Russell, M. J.; Olson, K. R. Hydrogen Sulfide as an Endogenous Regulator of Vascular Smooth Muscle Tone in Trout. *Am. J. Physiol. Integr. Comp. Physiol.* **2004**, *286* (4), R678–R685.
- (259) Qian, Y.; Karpus, J.; Kabil, O.; Zhang, S.-Y.; Zhu, H.-L.; Banerjee, R.; Zhao, J.; He, C. Selective Fluorescent Probes for Live-Cell Monitoring of Sulphide. *Nat. Commun.* **2011**, *2* (1), 495.
- (260) Schmitt, M. V.; Lienau, P.; Fricker, G.; Reichel, A. Quantitation of Lysosomal Trapping of Basic Lipophilic Compounds Using In Vitro Assays and In Silico Predictions Based on the Determination of the Full PH Profile of the Endo-/Lysosomal System in Rat Hepatocytes. *Drug Metab. Dispos.* **2019**, *47* (1), 49–57.
- (261) Schindelin, J.; Arganda-Carreras, I.; Frise, E.; Kaynig, V.; Longair, M.; Pietzsch, T.; Preibisch, S.; Rueden, C.; Saalfeld, S.; Schmid, B.; et al. Fiji: An Open-Source Platform for Biological-Image Analysis. *Nat. Methods* **2012**, *9* (7), 676–682.